主論文

INFLUENCE OF LOADING RATE AND SHEAR-DISPLACEMENT MAGNITUDE ON THE PORE PRESSURE GENERATION AT SLIDING SURFACE

by

Dmitri A. VANKOV

A Thesis submitted to the

Department of Earth and Planetary Science

Graduate School of Science, Kyoto University.

In partial fulfillment of the requirements for the

Degree of Doctor of Science.

December, 1999

TABLE OF CONTENTS

ABSTRACT

Landslide prevention and mitigation are very important tasks for maintaining public safety and property. Among various types of landslides, these of liquefaction nature are the most dangerous and catastrophic ones. The mass of liquefied soil often moves at the speed of several meters per second and leaves no time for people to escape. In order to prevent such calamities, studying of mechanism of earthquake-induced landslides and affecting factors, are extremely important.

Nearly always, landslides of the liquefaction nature are triggered by earthquakes. Seismic shaking produces cyclic conditions at the potential sliding surface. Loading frequency and amplitude of cyclic loading are very important parameters, which describe cyclic loading conditions.

In the presents Thesis, basic study on the influence of the rate of loading and the magnitude of the shear displacement on the pore pressure generation at sliding surface have been carried out. Ring shear apparatus, which is very suitable for reproducing stress-deformation conditions at the sliding surface, was employed as primary apparatus. In parallel, series of triaxial compression tests were conducted in order to compare obtained results. A sandy soil, which belongs to the Osaka Formation, widely distributed in Kansai area was used as a sample.

Dependency of the pore pressure generation on the frequency of loading and deformation rate was examined by conducting series of undrained stress-controlled tests and deformation-controlled tests using the ring shear apparatus and the triaxial compression apparatus. The sandy soil, which belongs to the Osaka Formation was used as a sample. Test results were analyzed from the standpoint of an energy approach.

Cyclic shear-stress-controlled ring shear tests demonstrated that as the frequency of loading increases, the total dissipated energy required to liquefaction substantially decreases, however shear-displacement-controlled tests showed that if amplitude shear displacement was constant, the dissipated energy required for liquefaction was independent on the loading frequency. Therefore, it was found that the apparent effect of loading frequency was caused by different amplitudes of the shear displacement during testing, because the dissipated energy depends on shear resistance and shear displacement. Large shear displacement amplitude was result of long period of loading during low-frequency tests. When the sample was subjected to the large amplitude of the shear displacement, while shear resistance still remained,

large amount of energy should have dissipated due to plastic deformations in the extent of large shear displacement.

Data obtained by the cyclic stress-controlled triaxial compression tests showed that as the loading frequency increased, the total dissipated energy required to liquefaction decreased. The mechanism of this effect is similar to that of the shear-stress-controlled ring shear test.

It was found that tests with the shear displacement amplitude around 0.5mm consumed the minimum amount of dissipated energy for liquefaction of the sample. An increase of the shear displacement amplitude from 0.50mm, led to energy consumption due to plastic deformations and, therefore, increase in the total dissipated energy required to liquefaction; the shear displacement amplitude smaller than 0.5mm was, probably, not so effective to cause volume shrinkage and pore pressure generation.

The magnitude of shear displacement profoundly affected the effectiveness of the excess pore pressure build up. It was found that, within the range of shear displacement around 0.5mm, the relation between pore pressure increment and shear displacement amplitude (parameter $r_u/\Delta l_{max}$) has its peak value. The deviation of the shear displacement from that value leads to decreasing of the parameter.

In monotonic tests (constant-speed ring shear test and constant-axial-strain-rate triaxial tests), the deformation rate did not affect the pore pressure generation and energy dissipation in the investigated soils. It was confirmed that the mechanism of pore pressure generation in the ring shear tests, which simulates sliding surface, is very different from that of triaxial compression test; stage of "the negative dilatancy due to grain crushing" was observed only in the ring shear tests.

The total shear displacement required to liquefy the normally consolidated specimen under cyclic conditions was substantially smaller, than that of constant-deformation-rate shearing, because the change of the direction of loading had significant effect on the pore pressure generation.

CHAPTER I

Introduction

1-1. GOALS AND OBJECTIVES OF THIS STUDY

The earliest known case of a major landslide resulting from soil liquefaction induced by an earthquake was probably the destruction of Helice about 400 years BC (Seed 1968). It stated that "...during a disastrous winter night, a strange thing happened in central Greece, Helice, a great and prosperous town on the north coast of Pelloponnesus, was engulfed by the waves after being levelled by a great earthquake. Not a single soul survived.... The next day two thousand men hastened to the spot to bury the dead, but they found none, for the people of Helice had been buried under the ruins and subsequently carried to the bottom of the sea where they now lie". Helice was located on deltaic deposits of alluvial sand about a mile and half from the coast. The city is now completely covered and no trace of it exists.

On 17th January 1995, at 5:47 in the morning a devastating earthquake measuring 7.2 on the Richter scale hit the southern Hyogo Prefecture, Japan. Strong motions caused ground failures such as landslides and liquefaction at many locations. The Kobe port area was heavily damaged due to liquefaction of sandy ground. A rapid landslide, named subsequently the "Nikawa landslide", occurred in Nishinomya City and killed 34 people.

The soil behavior under dynamic loading has become a widely investigated topic during the last decades of this century (Seed & Lee, 1966; Seed & Idriss, 1971; Martin & Finn, 1975; Casagrande, 1976; Castro & Poulos, 1977; Peck, 1979; McRoberts & Sladen, 1992). At first scientific activities in this field were stimulated by the disastrous consequences of liquefaction of sands during some large earthquakes such as the Niigata earthquake (Japan, 1964), and the Chilean earthquake (1960). Since numerous studies have been carried out by different researchers all over the world. Many different methods and techniques for the

determination of the liquefaction potential of sands were developed. However, liquefaction in the Kobe portal area, triggered by the Hyogo-ken Nanbu earthquake (Japan, 1995) clearly demonstrated that these previous studies were insufficient to enable the interpretation of such phenomena.

Analysis of slope failures, which occurred during the Hyogo-ken Nanbu earthquake introduced some new and presently not clearly explained phenomena. Kamai (1995) and Sassa (1996) reported ground failures in very gentle sloping residential areas. These failures could not be explained by traditional slope stability analysis because of the almost complete absence of the shear stress. They must have been caused mostly by vibration, and in case of basic laboratory study it is reasonable to apply reversal cyclic loading without any initial shear stress.

The nature of soil liquefaction is well known. If a sample of saturated sand is subjected to cyclic loading conditions, it may remain stable for a certain number of cycles, though pore pressure in the sample build up progressively, and then suddenly lose all its strength with the accompanying development of pore water pressure equal the applied confining pressure. This substantial loss of strength, the characteristic of sand to undergo displacements without exhibiting resistance is known as liquefaction.

It should be noted that liquefaction of soil occurs not only under cyclic loading but under monotonic loading as well. For example, the Gamahara Torrent debris flow was induced by a retrogressive landslide, which loaded the torrent deposits at the foot of the slope. These deposits were loose and saturated, and being hit by the mass of the initial landslide, turned into a liquefied state and formed the debris flow (Sassa et al. 1997).

It is clear that landslides formed by liquefaction are the most dangerous and catastrophic ones. The mass of liquefied soil often moves at speeds of several meters per second, leaving no time for people to escape.

The load can be applied at different rates. For cyclic loading it is termed "frequency" and has the dimension of the quantity of cycles per time unit. For monotonic loading the rate of loading is measured by shear speed. There are some studies on the influence of the frequency of loading on the liquefaction behavior of soils. Much less is known about pore pressure generation under monotonic loading. However, recent investigations in the Landslide Section of DPRI (Kyoto University, Japan) have focused on this aspect (Wang 1998, Okada 1999).

It should be added that most of previous researchers studied features of liquefaction occurrence in a soil massif. Meanwhile, for landslide triggering it is enough if a sandy lens located on the potential sliding surface will liquefy. In such a case a landslide will occur, while all sliding block remains intact. Note that loading conditions at sliding surface are rather different from those in soil massif, in which the landslide occurs. The loading conditions on the sliding surface can be simulated very well by means of ring shear apparatus, because the direct shear state provided by the ring shear apparatus corresponds to these conditions.

Review of previous studies (Chapter 1.2) shows that there is no generally accepted opinion on the issue whether the frequency of loading has an influence on the shear behavior or not. Extensive studies have been conducted about the behavior of soils under cyclic loading, however conclusions about role of frequency have the nature of empirical statements. It appears that a reasonable explanation of mechanism for whether the frequency of loading has an influence on the character of liquefaction of soils has yet to be proposed.

It often happens in scientific work that during the study of one phenomenon, investigation of another one becomes necessary. Usage of an energy approach for analyzing the influence of loading frequency on the liquefaction of sandy soil lead to the idea that the amplitude of the shear displacement might have a significant role in the process of energy consumption at the sliding surface. Additional experiments have been conducted in order to verify this idea.

Summarizing all mentioned above, the following scientific targets were set up:

- Does the process of pore pressure generation depend on frequency of loading?
- Does the process of pore pressure generation depend on rate or magnitude of deformation?
- What are the features of the mechanism of the pore pressure generation at sliding surface?

The present thesis is an modest attempt to clarify these problems.

1-2. REVIEW OF PREVIOUS STUDIES

There are two general types of loading in soil mechanics: cyclic loading and monotonic loading. Cyclic loading means that value and (or) direction of the load applied to a soil repeatedly changes with time. Monotonic loading, therefore, is when the load is gradually increase with time.

Rigorous search was conducted on available literature for reports of previous studies on the influence of rate of monotone loading on pore pressure generation. While there are reports about the undrained behavior of soils under monotonic loading (Castro, 1975; Castro & Poulos, 1977; Sassa, 1985; Sassa et al., 1985; Vaid & Thomas, 1995), it seems, that no special attention to the influence of the rate of loading on pore pressure generation was paid. The possible explanation of this fact could be that with exception of ring shear apparatus, all other conventional types of testing devices (e.g. triaxial apparatus, simple shear apparatus, box shear device) have a very limited range of shear displacement, usually about first millimeters or even less. Therefore, it is rather difficult to calculate shear speed precisely, since the shear displacement is very small. Influence of the shear speed on the strength parameters of soils or granular materials were investigated (as reviewed by Fukuoka, 1991), however conditions were always drained. Only recently, some data appeared (Wang 1998, Okada 1999)

On the other hand several researchers have reported results from studies of the influence of loading frequency in cyclic behavior of various types of soils.

Peacock & Seed (1968) studied sand liquefaction under cyclic loading simple shear condition. Clean, uniform sand from Monterey, California was used as the specimen. To determine the effect of frequency on cyclic behavior of sand they carried out tests with frequencies of 1/6, 2 and 4 cycles per second. The relative density of samples was 50% and confining pressure was 5 kg/cm^2. The results of their tests are represented on the Fig. 1-2-1. From this figure it can be seen that apparently, for frequencies of 1 and 2 cycles per second the form of the relationship between the peak pulsating shear stress and the number of stress cycles required to

cause initial liquefaction or failure is essentially the same. Although data are limited, the form of this relationship is apparently the same for the other two frequencies of 1/6 and 4 cycles per second. The fact that the positions of the curves in Fig. 2-2 show no particular sequence with respect to frequency suggests, on their opinion, that the influence of frequency on the location of each curve is due to some small but random error in the test data. Furthermore, in the stress range causing liquefaction to occur at a low number of cycles, the test data show only small variation due to frequency effects. For stresses causing failure in 10 cycles the result for all frequencies within the range investigated fall within ±10% of the mean, with no special order prevailing, indicating the effect of frequency variation is small.

Drnevich (1972) used resonant column apparatus to study the undrained cyclic shear of saturated sand. His tests were performed on Ottawa silica sand with different values of confining pressure and relative density. He concluded, that "...quasistatic tests (frequency 1/10 Hz) cause the effective confining pressure to decrease much more quickly than in resonant tests (frequency 30 Hz to 100 Hz). However, there is very little frequency dependence for frequencies between 30 Hz and 100 Hz. Although Peacock & Seed (1968) show little effect of frequency between 1.6 Hz and 4 Hz, straining at higher frequencies such as beneath machine foundations may exhibit behaviour different than predicted by quasistatic tests."

Wong et al. (1975) conducted research of cyclic loading liquefaction of gravelly soils. In the conclusions they stated that "The effect of frequency of stress applications, within the range of 20 cycle/min to 1 cycle/min, on the stress conditions causing initial liquefaction or given strain conditions in specimens of saturated sand was negligibly small". Their paper also contains the illustration of that conclusion (Fig. 1-2-2). These researchers employed triaxial testing device using the Monterey sand at a relative density of 60% as a sample.

Vankov (1997) found that with increasing of the frequency of loading, the total dissipated energy required for liquefaction of a coarse-grain sandy soil substantially decrease. Meanwhile, the number of cycles required to liquefaction is practically independent of loading frequency. That study was conducted by means of dynamic loading ring shear apparatus.

A very wide range of information available about the influence of frequency on cyclic behavior in cohesion soils. The following examples are the most demonstrative and clear.

Extensive review of frequency influence on shear strength characteristics was conducted by Wood (1982). Below are some extracts from his paper.

" Thiers and Seed (1969) show that doubling the frequency from 1 Hz to 2 Hz increases considerably the number of cycles to failure for cyclic simple shear test on San Francisco Bay mud. Sherif and Wu (1971) show that in general increasing the frequency from 1 Hz to 2 Hz has little effect on the permanent and cyclic strains and pore pressure. They investigated Seattle clays by triaxial apparatus. Andersen (1975) reports cyclic stress-controlled simple shear test on the Drammen clay and also concluded that changing of frequency of loading from 0.1 Hz to 0.05 Hz has no significant effect on the number of cycles required to reach a cyclic strain amplitude of $\pm$ 3% at any overconsolidation ratio. Brewer (1975) shows that for frequency range 0.01-4 Hz, the lower the frequency, in general the higher the strain for cyclic triaxial tests on kaolinite."

As summary Wood wrote that "…sand being a relatively permeable material, relying no obviously time-depending bonding, might be expected to show little sensitivity to rate of testing." However, about clays: "It seems likely that the effect of frequency is greater for more plastic clays, and intuitively it seems reasonable that slower cycles give the clay, as a viscous material, more time to follow the applied load and are likely to produce greater strains and greater pore pressure".

Lin et al. (1996) concluded that "…for the torsional shear test, the simplified spring-damping model can be used to interpret testing results when excitation frequency is smaller than about 20 Hz and the shear modulus is not too small. However, when frequency increases, the inertia effect becomes significant, and the continuum model would be more appropriate for interpreting testing results…The damping ratio obtained from laboratory cyclic test should be used with caution, and should not be extended into frequency range much different from the range of frequency tested."

Voznesensky (1998) analyzed the dynamic behavior of sand, silt, and clay using unit dissipated energy. He stated that frequency of loading has no effect on the dynamic stability of soil, other testing conditions being equal. His tests were conducted by triaxial apparatus. However, he pointed out that "Frequency of loading

itself cannot influence the soil strength and determines only the conditions of energy consumption." (Voznesensky & Nordal, 1999)

Wang & Sassa (1998) after conducting several ring shear tests with different sands and sandy soils concluded that higher frequency causes the excess pore pressure generate more quickly.

It can be seen that many scientists have touched on the problem of whether the frequency of loading has an effect on cyclic shear strength of soils or not. Different experimental techniques were employed. Various soils were tested. And it appears that there is no generally accepted opinion on this issue. On the other hand, it could be noted that conclusions about role of frequency have nature of empirical statements. It also appears that reasonable explanation of mechanism whether frequency of loading has an influence on the character of liquefaction of soils is yet to be proposed.

CHAPTER 2

Experimental Apparatuses and Sample Preparation

2-1. RING SHEAR APPARATUS

Ring shear apparatus is not a common piece of equipment for determination of the dynamic properties of a soil, especially in comparison with triaxial or simple shear devices. However, if appropriately designed, a ring shear apparatus can become a powerful tool for solving of a broad range of engineering geological problems.

The principal difference between ring shear apparatus, and the above-mentioned devices, is that the sample is subjected to direct shear conditions and a shear plane is predetermined. The stress distribution in such case is very close to the stress conditions within the sliding surface of landslide. It is also should be noted, that in ring shear apparatus, the value of shear displacement is unlimited. Hence, for studying the behavior of geotechnical parameters during motion the ring shear apparatus is the most suitable device. In conventional ring shear apparatus, an annular donut-like specimen (Fig. 2-1-1) subjected to normal stress is confined laterally, and ultimately caused to rupture on a plane of relative rotary motion, the so-called shear plane. The total normal stress and shear stress being transmitted through the soil across the shear plane are precisely known. The inner diameter of the sample is sufficiently large compared to the outer diameter for uncertainties arising from assumed non-uniform stress distribution across the shear plane to be reduced to an acceptable level. The lower half of the sample is carried on a rotating table driven by a shear motor. The upper half of the sample is reacted via an arm against one or pair of fixed proving rings (transducers) that measure the shear load. The shortcomings of ring shear apparatus were stated (Bishop et al. 1971) as follows:

- it failed to satisfy criteria of the simplicity of construction and operation;
- difficulties of maintaining a small but adequate clearance between the two pairs of metal rings.

Let us add also some new requirements such as:

- in order to investigate pore pressure generation before or after failure the possibility of undrained testing should be provided;
- for studying of the earthquake-induced landslides it is necessary to reproduce conditions of cyclic loading for both normal and shear stresses;
- for wider application of the ring shear apparatus, shear stress control test as well as constant speed control test should be provided.

All factors mentioned above were carefully considered and consequently embodied by Sassa and his colleagues during designing new ring shear apparatuses: DPRI-3 in 1992, DPRI-4 in 1995, and both DPRI-5 and DPRI-6 in 1996. The main parameters are presented in the Table 2-1-1(Vankov & Sassa, 1998).

Table 2-1-1. *The most important features of new ring shear apparatuses.*

Parameter	DPRI-3	DPRI-4	DPRI-5	DPRI-6
Shear box				
-inner diameter (mm)	210	210	120	250
-outer diameter (mm)	310	290	180	350
Maximal normal stress (MPa)	0.5	3.0	2.0	3.0
Maximum shear speed (cm/sec)	30	18	10	224
Resolution of gap control system (mm)	0.001	0.001	0.001	0.001
Maximum data acquisition rate (readings/second)	12	200	200	200
Maximum frequency of loading (Hz)	0.5	5	5	3
Possibility of undrained test	yes	yes	Yes	yes
Possibility of reproducing of monitored earthquake record by shear stress and normal stress	no	yes	Yes	yes
Automatic safeguard and alarm system for mishandling	no	no	Yes	yes

The principal scheme of new ring shear apparatus (DPRI-4) is drawn in the Figure 2-1-2. The sample (S) confined between pairs of upper and lower confining rings (UCR and LCR respectively), is loaded normally through annular loading platens by a hydraulic oil piston (OP1). The lower half of the shear box is rotatable in both directions, driven by a servomotor through transmission system. The upper confining rings are fixed with the cap plate (CP) which is sustained through two shear stress transducers (SST). Drainage is obtained by means of two channels: from the upper part of sample, water can go out through the porous metal (PM) screwed to the loading plate (LP) and then through the hollow columns, and from the bottom of sample through a porous metal (PM) screwed to bottom of the shear box. For the

prevention of slip between the sample and the porous metal 60 sharpened radial steel fins 2.0 mm thick, projecting 5.0 mm and extending the full width of sample were provided on the loading plate (LP) and on the bottom of the shear box. The rubber edges are located between the upper and the lower confining rings and designed to prevent leakage of the sample or water during consolidation or shearing. A constant contact force between rubber edges and the upper confining rings was provided in the range of 170-250 kgf. Before the each test they were covered by Teflon spray three times to decrease friction between them. In addition, for undrained tests vacuum silicon grease is used. A very sensitive gap control transducer (GC) monitors the gap between the upper and lower confining rings.

The normal stress is applied by means of hydraulic or pneumatic (DPRI-3) piston. There are two principal schemes of measuring of the applied normal stress, as illustrated in the Figure 2-1-3. The differences between them are determined by quantity of load cells used for monitoring of the normal stress. In the one-load cell model (Figure 3A), the load cell for normal stress (VL) monitors the normal stress acting upward on the shear surface plus the constant contact pressure between rubber edges. The oil piston (OP1) is free from the hanging frame (FR) during the test. The oil piston (OP1) automatically controls the normal stress acting on the shear surface through the feedback signal from the load cell (VL) and the control signal given by the personal computer. The gap control oil piston (OP2) automatically controls the position of cap plate (CP), namely the rubber edge pressure through the feedback signal from the gap sensor (GS in the Figure 2-1-2) with precision of 0.001 mm. This one-load cell model exists on the DPRI-4.

The other (DPRI-3, DPRI-5 and DPRI-6) apparatuses have two-load cell scheme for monitoring the normal stress. On these apparatuses the oil piston (OP1) is fixed on the frame (FR) and a upper load cell (VL1) is inserted between loading plate and oil piston. Another load cell (VL2) monitors the side friction plus the self-weight of the cap plate (CP). Load difference (VL1-VL2) gives the value of the normal stress working on the shear surface plus the constant rubber edge pressure. There is no fundamental difference between two schemes, except whether the side friction is separately measured or automatically cancelled.

Torque is applied by servomotor rotatable in both directions through the system of driving belts to the torque converter (TC) and then through the gear box (GB) to the drive gear (DG) connected with gears to the lower half of the shear box.

When the torque is applied the sample (S) reacts via cap plate (CP) against a pair of fixed shear stress transducers (SST) that measure tangential load. Shear displacement is measured by a transducer (SDT) connected to the lower half of the shear box. Vertical displacement of the loading plate is monitored by vertical displacement transducer (VDT) fixed on the stable frame. Pore pressure can be measured by means of a pore pressure transducer (PPT) connected with the water channel (PPC), located 2 mm above the shear zone. Changing of the pore pressure at the shear surface is most interesting and important for correct understanding of shear strength parameters.

The enlarged part of sample assembly is presented in the Figure 2-1-2 (upper right corner) for clear understanding of how completely undrained conditions can be achieved with ring shear apparatus. The key role is played by rubber edges (RE) pasted on the lower confining ring (LCR) and so-called "O"-rings (OR), which are inserted into special slots in the loading plate (LP). These parts made of hard rubber prevent leakage of water from the shear box during testing.

The undrained capability of ring shear apparatus has certain limitations. Primarily it depends on how accurately the rubber edges are pasted and what pressure is assigned to the contact between upper confining rings and rubber edges (Fig. 2-1-4) by the gap control oil piston. It is also necessary to place vacuum silicon grease on the edges. This grease fills the microscopic defects in the rubber or steel and ensures a completely undrained condition. The maximum pore pressure that can be achieved in the DPRI-4 is 490 kPa.

Two personal computers are set for test control functions and data recording. The process of testing is controlled by the operating computer. The test could be either shear torque controlled, shear speed controlled or shear displacement controlled. The cyclic mode is available for shear torque control and displacement control tests. Normal stress is applied independently from shear load. The resolution of transducers sending data to be recorded by recording computer, for DPRI-4 are given in the Table 2-1-2.

Such resolution is enough for the recording of test parameters with necessary accuracy. Generally, the sandy samples are used in tests. It should be noticed that, because of large size of sample box, conducting of tests with clayey samples is rather difficult, since consolidation takes a long time. For example, sample with bentonite clay was consolidated only after 30 days.

Since the upper and lower confining rings are in contact with each other by mediation of the rubber edges, the value of the shear resistance obtained via shear resistance transducers includes shear resistance of sample itself as well as shear resistance of rubber edges. For this purpose the shear resistance of rubber edges should be obtained before test with empty (for tests with dry samples) or filled with water (for saturated tests) shear box. Then, during data processing, this value should

Table 2-1-2. *Resolution of transducers (DPRI-4)*

Parameter	Resolution
Normal stress (kPa)	2.5
Shear torque (kPa)	1.0
Shear resistance (kPa)	1.0
Pore pressure (kPa)	0.5
Vertical displacement of loading plate(mm)	0.05
Shear displacement (mm)	0.02

be subtracted from the total shear resistance. Because of the high sensitivity and preciseness of the gap control (GC) transducer, this value is practically the same during all test procedure and should not lead to any miscalculations.

One of the most important parameters of each apparatus is its productivity, i.e. time required for conducting the test. This is greatly depends on the test program or type of sample used, however, as mentioned above, the "criteria of the simplicity of construction and operation " should be considered very seriously. For example, to conduct one undrained test on a sandy sample with full saturation by DPRI-4, requires from 12 to 36 hours, depends on how rapidly saturation is obtained. Considering the mass of the dry sample (approximately 3.5 kg), advances in testing program and precision of recorded data, this test duration is reasonable.

2-2. TRIAXIAL COMPRESSION APPARATUS

Triaxial compression apparatus is, probably, the most common equipment for the determination of the mechanical properties of a soil. This device correctly simulates stress condition of soil element in massif.

Cylindrical sample of studied soil is first subjected to a confining pressure σ_c, which equally stresses all surfaces of the sample. Then the axial stress is increased $\Delta\sigma_a$ until the sample fails. Since there are no shearing stresses on the sides of the cylindrical sample, the axial stress $\sigma_c+\Delta\sigma_a$ and the confining stress σ_c are the major and minor principal stresses σ_1 and σ_3 respectively. The increment of axial stress, $\Delta\sigma_a=\sigma_1-\sigma_3$, is the deviator stress.

The size of sample depends on nature of studied soil. For example for testing clays and fine uniform sands, a sample about 38 mm in diameter and from 75 to 100 mm in length is rather common. However, with increasing of coarse particles in the soil the size of sample also increases. It should be noted, that accordingly to Sen-Vinan's principle the length of the sample should be at least two times greater than diameter.

The principal scheme of triaxial compression apparatus, which was used in present study, is drawn in the Fig. 2-2-1. A cylindrical sample, with initial diameter and height of 95-96 mm and 198-199 mm respectively, is surrounded by rubber membrane which is secured to pedestal and top-loading platen. To prevent undesirable deformations of cohesionless sample a full vacuum was applied to the upper and lower drainage lines. Once chamber was filled with de-aired water, the line connecting chamber with water tank was closed and line from chamber volume control cylinder was opened. This allows measurement of chamber volume at any moment of the test, which is crucially important for calculating actual density of the sample prior testing.

The chamber pressure is controlled by a transducer (CPT) located in the lower part of the chamber. The vertical displacement of top-loading platen measured

by a vertical displacement transducer (VDT). Both, CPT and VDT are servo controlled in order to conduct stress or strain controlled tests. Pore pressure is monitored by two transducers: upper (UPPT) and lower (LPPT). The average of value of the pore pressure is used for further calculations. The resolutions of transducers are shown in Table 2-2-1.

Table 2-2-1. *Resolution of transducers (triaxial compression apparatus)*

Parameter	Resolution
Axial pressure (kPa)	0.745
Chamber pressure (kPa)	0.490
Pore pressure (kPa)	0.490
Vertical displacement of top-loading platen (mm)	0.05-0.10 mm

During stress controlled tests, the axial stress is created by an oil piston located on the top of the movable frame. This oil piston is enabled to provide monotone loading and cyclic loading modes. Axial load during strain controlled test could be applied either by the oil piston or lifting motor. The latter located inside of basement of the apparatus. However, cyclic strain controlled tests can be done only by the oil piston, because of the feedback connection.

The test program is firstly loaded into control computer, which via AD board is connected with the servoamplifier control unit. Once the test program had been loaded, the execution of the test proceeds automatically. A recording computer collects all data from transducers, with data acquisition rate up to 200 readings per second.

2-3. SAMPLE PROPERTIES

The soil used in this investigation was a coarse-grain sandy soil belonging to Middle-Upper Subgroup of the Plio-Pleistocene Osaka Group (Osaka Formation) widely distributed in the Kansai Area. The Osaka Group consists of loose sediments made of gravel, sand and clay, and is dividable into three subgroups, Lower, Middle and the Upper. Lower Subgroup is clearly distinguished from the other due to absence of marine deposits. Differences between the Middle and the Upper subgroups are not so clear. Geomorphologically the Osaka Group forms hilly lands and uplifting. These deposits assumed to be overconsolidated

The sampling site was at the headscarp of Takarazuka Landslide, triggered by the Hyogo-ken Nanbu earthquake, January 17, 1995. That landslide was described in detail by Sassa et al., 1996. The depth of the sampling point was about 4 meters. Totally more than 1000 kg of soil were taken by excavating machine.

Grain-size distribution analysis was provided by sieve method, duration of shaking of the sieve column was 45-50 minutes and mass of sample about 850 g. Test was repeated four times to obtaining reliable data. Determination of the minimal and maximal density was performed by Russian standard method (Trofimov & Korolev, 1993), where procedure for determination of the minimal density is the same as in ASTM method, but in case of maximal density without using mechanical vibrator, only shocking the tank containing the sample with a wooden stick. Results of the grain-size distribution analysis and basic physical properties are summarized in the Table 2-3-1.

Because no chemical dispergation of the sample during grain-size distribution analysis was performed, probably more correctly will be use term "aggregate-size distribution". However the total percentage content of the faction with a diameter less than 0.074mm is about two percent, so the appearance of silt and clay particles could be neglected.

The mineral composition analysis had been carried out visually and shows that investigated soil mostly consisted of quartz and feldspar, probably albite. Both

of these minerals being interacted with water are chemically not active (Sergeev, 1983).

Table 2-3-1. *Basic characteristics of specimen*

Particle content (%)							C_U	D_r (max)	D_r (min)	G_s (g/cm^3)
>2.00 mm	2.00- 0.84 mm	0.84- 0.42 mm	0.42- 0.25 mm	0.20- 0.105 mm	0.105- 0.074 mm	<0.074 mm				
12	36	33	7	8	2	2	5.55	1.44	1.20	2.61

C_U: coefficient of uniformity; D_r (max) & D_r (min): maximum and minimum relative density, respectively; G_s : relative density.

The procedure for preparation of sample for the tests was as follows. Because the Osaka Formation includes some clay layers, at first, sandy soil was separated from the clayey blocks. Then sandy soil was dried at the temperature of 105°C during 48 hours. It was removed from the stove and cooled. After that soils were dispergated by means of rubber hammer and sieved through the sieve with diameter 4.00mm. The sieved soil was used for the test. Samples were kept in hermetically closed metal boxes for preserving them from hygroscopic moisturizing. It was important to keep samples dried for correct calculations of basic physical parameters, such as dry density, void ratio and degree of saturation.

2-4. SAMPLE PREPARATION

There are numerous studies, which demonstrate the importance of careful evaluation of the experimental procedure, because of its tremendous effect on the results of an investigation (Silver & Park, 1975). The utmost important factor is sample preparation for the undrained testing. There are several methods of sample preparations for laboratory experiments. Comprehensive investigation on the influence of sample preparation methods on the undrained strength of the sand, has been done by Mulilis et al. (1977). That study considered various forms of sample preparation (pluviation; high & low frequency vibrations of samples formed in different number of layers; rodding and tamping of dry and moist soil). It was concluded that:

1. The weakest samples were those formed by pluviating the soil through air, and the strongest were those formed by vibrating the soil in a moist condition.

2. The slopes of the curves for samples formed by moist tamping, moist rodding and moist vibratory compaction are similar, yet distinctly different from those for samples formed by pluvial and vibratory compaction.

3. The orientations of the induced vibrations had apparently no significant effect on the cyclic strength.

4. The variation of frequency of vibrations had about 7-10% effect on the cyclic stress ratio required to cause both initial liquefaction and ±2.5% axial strain in 10 cycles; the samples prepared by the low frequency were somewhat stronger than those prepared by high frequency.

5. Samples that were prepared in seven 1 in. layers were about 3% stronger than samples prepared in one 7 in. layer; again this is well within the scatter of the results

6. All samples formed in a dry condition by vibratory compaction were stronger than samples prepared by pluvial compaction.

7. The size of the compaction foot had about 10% effect on the cyclic stress ratio required to cause both initial liquefaction and ±2.5% axial strain in 10 cycles; samples prepared by moist tamping (1.4 in. diam) were somewhat stronger than those prepared by mist rodding (3/8 in. diam).

8. Samples formed by dry rodding had about the same strength as those formed by frequency vibrations at 4 cycles, about the same strength as those formed by pluviation through the water at 10 cycles, and about the same strength as those formed by pluviation through the air at 100 cycles.

9. The effect of forming samples in a moist condition was to increase the dynamic strength of the soil.

Considering all mentioned above, it was decided that, for present study, dry pluviation through the air is most suitable method of sample preparation, since it forms the weakest samples. Therefore, pore pressure measurement should be easier, than in cases of more dense samples.

Another extremely important aspect is saturation of the samples. Pore pressure buildup in the soil due to application of external loading depends on several factors. However, from the practical point of view the most crucial one is saturation. In case of a soil, which is poorly saturated, reliable pore pressure measurement is virtually impossible. For correct evaluation of pore pressure behavior under cyclic loading a sample should be fully saturated. In order to control the saturation researchers usually use two parameters - degree of saturation (S), and parameter of pore pressure response (B).

Degree of saturation (S) is determined as:

$$S = V_w / V_v \qquad\qquad [2.4.1]$$

where: V_w is volume of water in the voids and V_v is volume of voids. S=0, when soil is completely dry and S=1 when fully saturated.

Parameter of pore pressure response (B) was introduced by Skempton (1954) for triaxial compression test:

$$\Delta u = B(\Delta\sigma_3 + A(\Delta\sigma_1 - \Delta\sigma_3)) \qquad\qquad [2.4.2]$$

where: A and B: pore pressure parameters, Δu: is increment of pore pressure, $\Delta\sigma_1$ and $\Delta\sigma_3$: are increments of principal stresses. Traditionally this equation is used in a more simple way as follows:

$$B=\Delta u/\Delta\sigma_3 \qquad\qquad [2.4.3]$$

Sassa et al. (1985) suggested that B-parameter in the direct shear state can be defined as:

$$B_D=\Delta u/\Delta\sigma \qquad\qquad [2.4.4]$$

The B parameter is considered as more informative and accurate for estimation degree of saturation than S. However, it can be seen that B-parameter does not have any relation to soil characteristics. Later, Black and Lee (1973) derived the following equation to relating B and S:

$$S = \frac{1 - Z(1 - B)}{1 - ZQ} \qquad\qquad [2.4.5]$$

The four items in that equation are defined as

$$Q = Bn_i \frac{C_w}{C_d} \qquad\qquad [2.4.6]$$

$$Z = \frac{Y}{D} \qquad\qquad [2.4.7]$$

$$Y = C_d \frac{\Delta\sigma_3}{n_i} \qquad\qquad [2.4.8]$$

$$D = 1 - \frac{P_i}{P_i + B\Delta\sigma_3} \qquad\qquad [2.4.9]$$

The terms n_i, $\Delta\sigma_3$, C_w and C_d have the usual meaning, i.e., initial porosity, change in cell pressure, compressibility of water and compressibility of soil structure, respectively.

Comparison of theoretical data with experimental observations showed that saturation of soil strongly depends on its density. For example, for Ottawa sand at 100% relative density, saturation degree, of 100%, 99.5% and 99% correspond to B parameter of 0.9877, 0.69 and 0.51, respectively (Black & Lee, 1973). Therefore, it

is absolutely unacceptable to study of pore pressure generation in dense sandy soil with pore pressure response value less than 0.95.

In Fig. 2-4-1 the experimental relation between saturation degree and B parameter, compiled from different sources (Sassa, 1988; Black & Lee, 1973) is presented. All studies were conducted on samples from triaxial apparatus. The following soils were investigated:

- Clayey soil taken from site of the Jizukiyama landslide. Void ratio is fluctuates from 0.84 to 1.04.
- Sandy soil taken from torrent deposits of the Denjo river.
- Ottawa sand at 100% relative density.

It can be seen that the curves for sandy soil and the Ottawa sand are rather similar. On the other hand, they are quite different from clayey soil. This difference could be explained by differences in compressibility of these soils. The compressibility of sand and sandy soil are close to each other, while non-overconsolidated clayey is more compressible. Since in this case the investigated soil is sandy with some gravel faction and almost absence of silt and clay particles, it is assumed that relation of the degree of saturation to the pore pressure response parameter is generally similar to that of the Ottawa sand and the Denjo river soil.

Complete saturation is conventionally accomplished by increasing the back pressure to an certain amount and then waiting until pore pressure response parameter indicates that saturation had been achieved. Using of back pressure is common in soil testing. The increments of back pressure in the sample and confining pressure are applying simultaneously in order to keep the effective stresses constant. Generally speaking, the back pressure method is based on the following two principles:

- Terzaghi's effective stress principle in soils - at present, this principle is usually defined as, if the forces applied on the soil skeleton (effective stresses) bare the same, then the soil exhibits the completely identical mechanical properties no matter how much the pore pressure is;
- Henry's law about dissolution of air in water and Boyle's law in classic physic. In other words, under the same temperature, the volume of air and the value of pressure existing on the water is constant.

The another sensitive aspect is the time of checking saturation degree, i.e. before or after consolidation of the sample. Measurement of pore pressure response before consolidation is rather common among geotechnical researchers (Drnevich, 1972; Ladd, 1977; Mulilis et al., 1977; Novak & Kim, 1981;Towhata & Ishihara, 1985; Figueroa et al., 1994; Boulanger, 1995;Hatanaka et al.,1997). It was established by preliminary tests that in both triaxial and ring shear apparatus pore pressure response parameters after consolidation are substantially less than before consolidation. For example one test conducted by triaxial apparatus indicated that although before consolidation B parameter was 0.95, after 40 minutes of consolidation under 200 kPa confining pressure it was reduced to only 0.36. Attempts to increase this value were not successful. It is certain, that the sample was getting denser due to consolidation and it's stiffness increased and to the same degree of saturation pore pressure response should decreased (Black & Lee, 1973).

Considering all mentioned above the following procedure for saturation of samples and control of pore pressure response was adopted.

1. Before setting the sample, shear box (ring shear apparatus) and rubber membrane (triaxial apparatus) was filled by CO_2 gas.

2. Dry sample was pluviated into shear box or rubber membrane.

3. Once sample is assembled, full vacuum was applied to upper and lower drainage lines until absolute pressure within the sample's voids became 10-12 kPa.

4. CO_2 gas was applied through lower drainage line until absolute pressure within the sample voids became 100-105 kPa.

5. Full vacuum to the top drainage line was applied until absolute pressure dropped to 10-12 kPa.

6. Steps 4-5 were repeated three times.

7. After that upper drainage line was opened to allow CO_2 gas to bleed from the sample for 10-15 min. During this time a reservoir with gas was attached to the lower drainage line.

8. The lower drainage line was connected to the tank containing de-aired water and water was allowed to inflow under low (5-6 kPa) pressure into the sample until it will not come out of upper drainage line.

9. Upper drainage line was closed.

10. 120 kPa confining pressure and 105-107 kPa back pressure was applied until the B value was not less than 0.95.

11. 305 kPa confining pressure was applied until the sample consolidated.

12. The B parameter was checked again. In case of B<0.95 test was delayed until it will reach desirable value.

CHAPTER 3

Testing Procedure

3-1. TESTS BY RING SHEAR APPARATUS

3-1-1. Cyclic Shear-Torque-Controlled Tests

This series of ring shear test were conducted in order to investigate the mechanism of earthquake-induced landslides on almost flat sloped, triggered by the Hyogoken-Nanbu earthquake 17 January 1995. Behavior of sandy soil under cyclic loading with different frequencies of loading was studied (Vankov & Sassa, 2000).

After the sample had been consolidated and saturated, the reversible cyclic shear stress with a given loading frequency was applied. In addition to normally consolidated samples (tests No.1-6), samples with overconsolidation ratio 1.91-2.14(tests No. 7-12) and 2.58-2.94(tests No.13-18) were tested. No initial shear stress was provided. The values of loading frequency of 0.01, 0.05, 0.1, 0.5, 1.0 and 2.0 Hz were used. The latter two values of frequency (1.0 and 2.0 Hz) can be found in almost all earthquakes. Values of 0.01, 0.05, 0.1 and 0.5 Hz were included in order to extend range of data. Totally 18 experiments have been conducted on this stage of investigation.

The initial effective normal stress and the amplitude of shear stress was kept constant for all tests (No.1-18), equal to 187-230 kPa and 56-63 kPa respectively. (Note that in the test No.2 the sample failed on the first cycle, and therefore, sustained only 50 kPa of the shear stress). This corresponds to a peak seismic acceleration of about 238-330 gal assuming only horizontal direction of shaking on the horizontal ground, which is relatively strong level of seismic acceleration. During the Hyogo-ken Nanbu earthquake, such values of acceleration were recorded at 10-50 km distance from the assumed fault line causing the earthquake (Sassa et al., 1995, after Irikura, 1996). All drainage lines were closed beforehand to ensure the undrained condition of the experiment. The test conditions are summarized in Table 3-1-1.

In this paper, liquefaction was regarded to have occurred when the pore pressure reached 95% or more of the normal stress through a full cycle of loading.

This is in contrast to the point of initial liquefaction (cyclic mobility) where the pore pressure equals to the normal stress only at its maximum value during a loading cycle (Castro, 1975). This determination of liquefaction was chosen because landslides in Kobe area took place in very gentle slopes, so the initial shear stress was very small. Under such conditions, movements of these slopes is unlikely to proceed in the state of initial liquefaction. At the point of liquefaction there was no further increase in the pore water pressure. After the sample reached the liquefaction state, the test was terminated.

Table 3-1-1. *Parameters of shear torque controlled cyclic loading tests*

Test No	σ_{con} (kPa)	OCR	f, (Hz)	σ (kPa)	u_0 (kPa)	σ'_0 (kPa)	$\Delta\tau_{max}$ (kPa)	e	B_D
1	220	1.00	0.01	326	106	220	61	0.77	0.95
2	213	1.00	0.05	282	69	213	50	0.74	0.95
3	201	1.00	0.10	285	84	201	61	0.75	0.98
4	210	1.00	0.50	295	85	210	56	0.72	0.96
5	206	1.00	1.00	309	103	206	59	0.71	0.97
6	199	1.00	2.00	307	108	199	57	0.67	0.96
7	400	1.95	0.01	269	64	205	59	0.73	0.95
8	400	1.96	0.05	293	89	204	59	0.74	0.96
9	400	2.08	0.10	306	114	192	62	0.73	0.98
10	400	2.14	0.50	324	137	187	63	0.74	0.95
11	400	1.93	1.00	304	97	207	60	0.70	0.95
12	400	1.91	2.00	308	99	209	61	0.69	0.95
13	600	2.58	0.01	280	47	233	59	0.73	0.96
14	600	2.64	0.05	296	69	227	58	0.71	0.97
15	600	2.65	0.10	303	77	226	61	0.70	0.95
16	600	2.83	0.50	310	98	212	61	0.68	0.96
17	600	2.93	1.00	299	94	205	63	0.69	0.95
18	600	2.94	2.00	307	103	204	61	0.67	0.97

σ_{con}: normal stress during consolidation, f: loading frequency; σ: total normal stress during test, u_0: initial pore pressure, σ'_0: initial effective normal stress, $\Delta\tau_{max}$-amplitude of the shear stress, e: void ratio during test, B_D: pore pressure parameter in direct shear state.

3-1-2. Cyclic Shear-Displacement-Controlled Tests

A series of shear displacement controlled loading tests (No.19-33) was conducted in order to:

- assess the frequency effect on pore pressure build up during cyclic loading with very small values of shear displacements;
- verify the tendencies of the soil behavior, which have been revealed after torque controlled shear tests;
- reveal the influence of the amplitude of the shear displacement on the energy dissipation.

Totally 15 tests were carried out (Vankov & Sassa, 1999). The parameters of shear displacement controlled cyclic loading tests are summarized in the Table 3-1-2.

The values of applied loading frequency were in the range of 0.005-0.50 Hz. Unfortunately, even with such powerful servomotor, as is installed on the DPRI-4, it was impossible to apply higher frequency.

The specimens were slightly denser than during shear torque controlled cyclic loading tests. The values of the effective normal stress were kept around 200 kPa in order to maintain the same stress conditions as with the shear torque controlled cyclic loading tests.

Table 3-1-2. *Parameters of shear displacement controlled cyclic loading tests*

Test No	F (Hz)	Δl_{max} (mm)	σ (kPa)	u_0 (kPa)	σ'_0 (kPa)	e	B_D
19	0.01	0.50	247	47	200	0.68	0.95
20	0.02	0.49	250	50	200	0.68	0.97
21	0.04	0.49	249	57	192	0.67	1.00
22	0.08	0.49	258	63	195	0.66	0.97
23	0.20	0.50	243	39	204	0.67	0.95
24	0.30	0.46	249	47	202	0.67	0.96
25	0.50	0.38	258	56	202	0.67	1.00
26	0.02	0.97	182	0	182	0.58	0.95
27	0.01	2.42	164	0	164	0.60	0.95
28	0.01	7.25	193	0	193	0.59	0.96
29	0.05	0.08	191	0	191	0.62	0.95
30	0.05	0.10	194	0	194	0.61	0.98
31	0.05	0.25	193	0	193	0.62	0.98
32	0.005	89.00	191	0	191	0.63	0.99
33	0.10(0.02)	0.03(0.06)	192	0	192	0.65	0.98

f: loading frequency, Δl_{max}: amplitude of shear displacement, σ: total normal stress during test, u_0:initial pore pressure, σ'_0:initial effective normal stress, e: void ratio, B_D: pore pressure parameter in direct shear state.

In the test No.32 the amplitude of the shear displacement was 89mm. Since the shear displacement transducer has capacity of only 20mm, it was impossible to obtain a feedback signal for such amplitude. The amplitude of the shear displacement was controlled manually. Due to that, wave shape was changed from sinusoidal to triangle.

3-1-3. Monotonic Constant-Shear-Speed Tests

The previous series of ring shear tests were conducted in order to understand basic mechanism of pore pressure generation during cyclic loading stage. However, once the landslide mass starts moving downward, the type of loading turns from cyclic to monotone one. In other words, during this stage, the shear speed, not the

frequency, is main rate parameter. Thus, several monotonic constant-shear-speed tests (No.34-37) were carried out. Test properties are presented in Tab. 3-1-3.

Table 3-1-3. *Parameters of constant speed shear tests*

Test No	v (mm/sec)	τ_p (kPa)	σ (kPa)	u_0 (kPa)	σ'_0 (kPa)	e	B_D
34	0.25	65	249	49	200	0.60	0.97
35	0.40	68	246	45	201	0.67	0.95
36	0.54	67	258	56	202	0.68	0.95
37	8.00	66	252	52	200	0.69	0.95

v: shear speed, τ_p: peak shear resistance, σ: total normal stress during test, u_0: initial pore pressure, σ'_0: initial effective normal stress, e: void ratio, B_D: pore pressure parameter in direct shear state.

Totally 4 experiment have been conducted. The higher relative density in the test No.34 was produced by different method of sample preparation (dry tamping), in order to evaluate the combined effect of the soil density and shear speed on the pore pressure generation.

3-2. TESTS BY TRIAXIAL COMPRESSION APPARATUS

3-2-1. Cyclic Stress-Controlled Tests

Triaxial testing is a very common method of studying of soil behavior. It is widely believed that stress conditions produced by the triaxial apparatus are most similar to those in real ones. Since the ring shear apparatus is not a very popular testing device it was crucial to reproduce similar stress condition by some common device, in order to verify truthfulness of data obtained by the ring shear testing. Test parameters are summarized in Table 3-2-1. Totally 5 tests (No.38-42) have been conducted.

Table 3-2-1. *Parameters of cyclic stress-controlled tests*

Test No	f, (Hz)	σ_3 (kPa)	u_0 (kPa)	$\sigma_3{'}_0$ (kPa)	$\Delta\sigma_{d\ max}$ (kPa)	e	B
38	0.05	298	98	200	74	0.65	0.95
39	0.10	302	102	200	74	0.62	0.96
40	0.50	303	103	200	73	0.64	0.95
41	1.00	299	99	200	73	0.64	0.95
42	2.00	298	98	200	73	0.63	0.95

f: loading frequency, σ_3: total confining pressure during test, u_0:initial pore pressure, $\sigma_3{'}_0$:initial effective confining pressure , $\Delta\sigma_{d\ max}$: amplitude of deviator stress; e: void ratio, **B**: pore pressure parameter.

It should be noted, that stress conditions created by the triaxial apparatus are not completely the same to those of the ring shear ones. The effective stress path for the triaxial apparatus is described in **p'- q** (p'=$(\sigma_1+\sigma_3)$/2-u q=$(\sigma_1-\sigma_3)$/2), while for the ring shear it is σ'- τ coordinate system. Strictly speaking, **p'**is not equal to σ', and **q** is not equal to τ. However, it seems to be the most accurate approximation.

A very important point is whether the confining pressure should be changed during testing or not. The effective stress path diagram for the ring shear tests described in previous section of the thesis, as well as effective stress path diagrams for triaxial test are presented in Fig. 3-2-1. Point A is the initial point for a cycle of loading. Points B and C correspond to peak values of shear amplitude during the same cycle of loading. It can be seen that in order to reproduce the effective stress path of the ring shear test by triaxial apparatus the scheme "Triaxial test 1" should be adopted. In such case, confining pressure (σ_3) should decrease to the same value as

axial pressure (σ_1) is increased and opposite. However, Seed & Lee (1966) stated that "…effects of reduction of all-around confining pressure are well-known. It would simply reduce the pore-water pressure in the saturated sample without causing any change in effective stresses in the sample. Because the deformation of the sample is caused only by changes in the effective stress, the deformations of the specimen would be the same whether the change of confining pressure was made or not". Since this pioneering work, such approach has been adopted by almost all scientists involved in soil dynamic testing. All triaxial tests conducted in the frame of the present thesis were conducted without changing of confining pressure (σ_3), as it shown in Fig. 3-2-1 (Triaxial test 2).

Analogous to ring shear cyclic tests, once the pore pressure reached level of the 95% of the initial effective confining pressure and didn't show any signs of an alteration the test was terminated.

3-2-2. Monotonic Constant-Strain-Rate Tests

Parameters of constant strain rate triaxial compression tests are presented in Table 3-2-2. Totally 4 tests (No.43-46) have been conducted. The sample in triaxial apparatus is approximately 200 mm before testing, therefore the deformation rate in these test (from No1 to No5) was 0.04, 0.20, 0.40, and 2.04 mm/sec.

Table 3-2-2. *Parameters of monotonic constant-strain-rate tests*

Test No	Strain rate (/sec)	σ_3 (kPa)	u_0 (kPa)	$\sigma_3{'}_0$ (kPa)	e	B
43	0.0002	310	110	200	0.62	0.96
44	0.0010	306	107	199	0.62	0.96
45	0.0020	306	107	199	0.61	0.96
46	0.0102	296	98	198	0.63	0.95

σ_3: total confining pressure during test, u_0: initial pore pressure, $\sigma_3{'}_0$: initial effective confining pressure, e: void ratio, B: pore pressure parameter.

All tests have been carried out with constant confining pressure. After axial deformation of the specimen reached approximately 5cm, which corresponds to 0.25 strain the test was terminated.

CHAPTER 4

Test Results

4-1. RING SHEAR TESTS

4-1-1. Cyclic Shear Tests

The results of cyclic ring shear tests are presented in Appendix 1 (tests 1-33). Each test is described by means of two plots. The first plot shows behavior of total normal stress, shear resistance, shear displacement and pore pressure versus time. The second graph indicates effective stress path, i.e. shear resistance versus effective normal stress.

The sample was considered to be in a liquefaction state, when pore pressure reached 0.95 of the total normal stress. Thus effective normal stress becomes almost zero and shear resistance should be almost zero too. However, in some cases shear resistance sometimes does not completely reach a zero value. The reason to explain this phenomena is that of the total shear resistance measured by shear stress transducers consists of shear resistance of sample and resistance of rubber edges between upper and lower halves of the shear box. The friction between the edges is not a constant value and can fluctuate within ±5 kPa whereas shear stress transducers are able to measure with a preciseness of about 1.5 kPa. Usually rubber edge resistance was about 20-22 kPa and this value was used in our calculations. In some tests, probably due to imperfectly covering the surface of rubber edges with teflon spray small defects occurred and shear resistance of rubber edges increased.

It is should be mentioned that for shear torque controlled tests, the form of curve of shear displacement at it's peak area is a little bit different from an ideal sinusoidal. This is because after switching with the servomotor in working mode some initial torque, usually about 2-3 kPa, was applied automatically. This applied torque value has some bias towards the direction of initial torque. However, in the case of completely liquefied sample shear resistance is so small that this initial torque value leads to a bias of the shear displacement. At the same time when shear torque reaches it's peak amplitude and is about to change the direction value the resistance of rubber edges prevents further shear displacement. This leads to appearance of

some "flat" part of shear displacement curve around its peak amplitude value. These factors both distort the shape of the curve.

Most of the effective stress path diagrams indicates that when pore pressure reached a critical value and sample started to fail, the stress path followed along the failure envelope, but final point does not correspond to the zero value because shear resistance does not reach a zero value. The way, pore water pressure builds up is different for different OCR values. In case of OCR=1.0, pore pressure increased rapidly because of a fast soil skeleton collapse. Even in relatively high frequency tests, for instance 0.5 Hz (test No. 4) the character of accumulation of pore pressure is almost linear until sample began to fail. With increasing overconsolidation ratio the character of pore pressure accumulation changes strongly. The soil skeleton structure reacts on each phase of cycle. However, the general tendency is the same for all tests: pore water pressure built up gradually until it reached the total normal stress value and effective normal stress becomes zero. Limitations of data acquisition rate (initially maximum sampling rate of the DPRI-4 was 10 readings per second. It was improved up to 200 readings per second later on) meant parameters of tests with loading frequency 0.5 Hz were recorded at only 20 points per cycle. Hence, the stress path diagram looks a bit different from other tests. However this data acquisition rate is sufficient for solving of established problem.

It can be observed on some of the effective stress path diagrams, which are relevant to saturated tests with OCR>1.00, that effective normal stress increases when shear stress reach its peak value and decrease when shear stress is zero during the same cycle (e.g. tests No.8 & No.14). This is not a new observation; several researchers reported the same phenomena during the tests conducted by simple shear device as well as triaxial apparatus (for example Finn et al., 1970). This effect occurs because when shear stress is acting on the sample, the pore water pressure decreases, which indicates that sample has a tendency to expand. The effective normal stress increases at this time and mobilizes frictional resistance to the shear force.

For all conducted shear torque controlled as well as shear displacement controlled tests, the following common tendencies could be observed:

- As shear stress is applied, the pore pressure gradually builds up and eventually reached almost the value of the total normal stress. In other words all samples liquefied, despite the fact that some of them were almost at the peak value of the

relative density. It should be noted that dense samples are usually not susceptible to mass liquefaction, only sliding surface liquefaction is possible.

- Since in shear torque controlled tests the duration (period) of loading is inversely proportional to the loading frequency, in tests with low frequency the shear displacement at stages of loading, which corresponds to the decaying of the shear resistance, is larger than in the high-frequency test.

- For dense sample it was observed that when the pore pressure approaches to the level of the total normal stress, differences between the highest and the lowest values of the pore pressure during the same cycle are substantial. This state corresponds to state of "cyclic mobility" (Castro 1975). However, as the loading proceeded this state was transformed into the liquefaction state, when the pore pressure did not change at any stage of loading.

- In the effective stress path diagrams the trajectory of the effective stress path moves cyclically leftward until it reaches the failure line. From this moment the trajectory follows along the failure line. This behavior was practically the same for all cyclic tests. The only exception was test No2 (OCR=1.00, f=0.05 Hz), in which sample failed on a purely liquefaction state and effective stress path trajectory reached the failure line only at the end.

4-1-2. Monotonic Shear Tests

The results of constant speed ring shear tests are presented in Appendix 1 (tests 34-37). Each test is described by means of two graphs. First graph shows behavior of total normal stress, shear resistance, and pore pressure versus shear displacement. Second graph indicates effective stress path, i.e. shear resistance versus effective normal stress.

From the first diagram it can be seen, that pore pressure quickly built up and reached level of about 78% of initial effective normal stress during very first millimeters of the shear displacement. After that the pore pressure slightly decreased due to sample dilatancy, and then increased again but with much lower rate than before. Therefore, the process of the pore pressure generation could be divided into two stages. The pore pressure during the stage with a rapid build up, is generated from the radical rearrangement and subsidence of soil particles, which lead to volume shrinkage, and, in turn, in the undrained condition to transferring effective stresses into neutral ones. However, since the sample is in quite a dense state, the

volume shrinkage is limited and not enough to bring the sample to liquefaction. Moreover, as it was noted above, after some shear displacement certain dilatancy takes place. During the second stage with low rate of pore pressure build up volume shrinkage is very small, in comparison with the first stage. It proceeds mostly because of grain crushing and comminution at the shear zone.

This type of behavior is quite similar for all other constant speed ring shear tests conducted.

4-2. TRIAXIAL COMPRESSION TESTS

4-2-1. Cyclic Compression Tests

The results of triaxial stress controlled cyclic loading tests are presented in Appendix 1 (tests 38-42). Each test is described by means of two graphs. The first graph shows behavior of confining pressure, axial pressure, deviator stress, strain, and pore pressure versus time. The second graph show the effective stress path, i.e. *p-q* diagram, where $p'=(\sigma_1+\sigma_3)/2-u$ and $q=(\sigma_1-\sigma_3)/2$.

The stress conditions created by triaxial apparatus are different from those of the ring shear apparatus. The results of tests could not be compared directly, because of this. However, since the triaxial apparatus is the most common device for determination of stress-strain behavior of soils, the obtained test results are very important.

During triaxial stress controlled cyclic tests the total confining pressure was kept constant. The axial pressure was cyclically changed. It can be seen from the time series that as axial pressure was applied to a sample the pore pressure gradually built up and subsequently reached the value of the total confining pressure. When the average pore pressure during full cycle of loading was not less than 0.95 of total confining pressure sample liquefaction state was assumed.

The trajectory of the effective stress path in the diagrams, looks very similar to that of ring shear tests. However, for the tests with frequency values of 0.50, 1.00, and 2.00 Hz (tests No. 40, 41, and 42) the internal friction angle during extension phase appeared to be somewhat less than during compression phase.

The absolute magnitude of the axial strain is dependent on the frequency of loading in the same manner, and probably for the same reason as in ring shear testing. The bias of the strain happens because of different sample strength exhibited in extension and compression phases. In our time series diagrams, positive strain corresponds to compression, and negative to extension of the specimen. Since the cohesionless soil almost does not resist to the extension forces, the negative strains should be produced more easily than positive ones.

During low frequency (0.05 and 0.10 Hz) the so-called "necking" effect was observed (tests No. 38 and 39). This effect occurs due to large extension strains of the specimen, when pore pressure is already quite high, usually more than 0.70 of the total confining pressure. In the mentioned tests (No.38 and 39), the capacity of the axial displacement transducer was exceeded during extension phases of cyclic loading. Obviously, this effect has nothing to do with real soil conditions during cyclic loading, however other tests (No. 40, 41, and 42) were not affected by necking, because of small strain values. It should be noted, that because of undrained conditions the volume of sample was virtually constant.

4-2-2. Monotonic Compression Tests

The results of triaxial constant strain rate tests are presented in Appendix 1 (tests 43-46). Each test is described by means of two graphs. The first graph shows behavior of confining pressure, axial pressure, deviator stress, and pore pressure versus strain. The second graph shows the effective stress path, i.e. *p-q* diagram, where $p'=(\sigma_1+\sigma_3)/2-u$ and $q=(\sigma_1-\sigma_3)/2$.

Pore pressure generation in constant strain rate triaxial test is different from that in constant shear speed ring shear tests. However, in relation to triaxial cyclic tests there are some very similar observations.

As vertical stress was applied to the specimen, pore pressure gradually built up, and the trajectory of the effective stress path moved leftward, which indicates pore pressure generation. During this stage of loading, the specimen structure undergoes contraction. However, when the trajectory reached the failure envelope, its direction changed from leftward to right-upward. The change of the direction occurred because the specimen can not be contracted any more, however as axial loading proceeded, the specimen started to dilate, which lead to decrease of the pore pressure.

It should be noted, that in the triaxial constant strain rate tests none of the samples reached liquefaction state irrespective to the rate of loading. A similar tendency has been observed during ring shear testing.

CHAPTER 5

Analysis of Experimental Data

5-1. An Energy Approach

The energy approach is relatively new method for evaluating pore pressure generation in soils. The first detailed work on this subject was conducted by Nemat-Nasser & Shakooh (1979). These authors presented "...a unified theory for the densification and liquefaction of cohesionless sand. The theory is based on the observation that densification of sand involves rearrangement of its grains and hence an expenditure of a certain amount of energy, which increases as void ratio, approaches its minimum value. If the saturated sand is undrained and is subjected to a fixed confining pressure, the tendency toward densification induced by cyclic shearing results in an increase in the pore water pressure, and therefore a decrease in the frictional and contact forces that exist at the interface between adjacent sand particles". Nemat-Nasser & Shakooh's study led to the idea that the energy required to change the volume (in drained condition) or pore pressure (in undrained condition) is related to the dissipated energy per volume calculated from the hysteresis loop.

Towhata & Ishihara (1985) used principally the same parameter for evaluating pore pressure behavior in undrained conditions. However, they used terms "strain energy" and "shear work" instead of dissipated energy.

Figueroa (1993), Figueroa et al. (1994), and his postgraduate student Liang et al. (1995) carried out a comprehensive study on applicability of the energy principles to the liquefaction phenomena. They stated that: "Apart from using the fundamental concept that a definite amount of energy is associated with the onset of liquefaction of an undrained deposit during dynamic motion, this approach is also capable of incorporating non-uniform loading. "

Voznesensky (1994) suggested that "dynamic instability of any soil and rock is based on one unique mechanism-their ability to accumulate from cycle to cycle a certain part of undissipated energy".

Potentially, the energy approach is very promising, because it describes the liquefaction phenomenon as an energy process. Since many liquefaction cases occur during an earthquake, it seems very attractive goal to incorporate the energy characteristics of earthquake with the energy characteristics of the liquefaction potential of soils.

Certain steps in this direction have been done by Davis & Berrill (1982), Moroto & Tanoue (1989), Law et al. (1990), and Trifunac (1995). A quintessential parts of the proposed method was summarized as: "The total radiated energy is related to the earthquake magnitude via the Gutenberg and Richter relationship. The portion of arriving energy, which is dissipated at the site, is assumed to depend upon the standard penetration resistance and the initial effective overburden stress. We determine the relationship between standard penetration value and energy dissipation by examination of historical records of earthquake induced liquefaction. Once the dissipated energy has been estimated, the increase in pore pressure follows directly." (Davis & Berrill, 1982).

Therefore, the energy approach can be very useful in evaluating the liquefaction potential of a soil. The energy required for liquefaction can be found for almost any conventional cyclic laboratory test. Compared with other existing empirical methods of analysis, the energy approach has several advantages. The most important among them are (Voznesensky & Nordal, 1999):

- Dissipated energy is directly related to the intensity of dynamic loading.
- It is not necessary to decompose the shear stress history to find equivalent number of uniform cycles for selected stress or strain levels.
- It is practically independent of the load waveform and since there is no need to model a complicated random stress history in laboratory experiments, a simple sinusoidal pattern of loading could be used in all cases.
- It is generally independent of the type of testing device, which facilitates the comparison of the results obtained in different laboratories.

It seems that unique and common terminology for energy principles have yet to be developed. In the present Thesis, the term "dissipated energy" will be referred to the energy-per-unit-volume (for cases with a dimensionless deformation parameter), or energy-per-unit-shear-plane (for cases in which deformation has the dimension of length). This dissipated energy can be denoted as:

$$W\left(J/m^3\right) = \sum_{i=1}^{n-1} \frac{1}{2}\left(\tau_i + \tau_{i+1}\right)\left(\gamma_{i+1} - \gamma_i\right) \qquad [5.1.1]$$

$$W\left(J/m^2\right) = \sum_{i=1}^{n-1} \frac{1}{2}\left(\tau_i + \tau_{i+1}\right)\left(l_{i+1} - l_i\right) \qquad [5.1.2]$$

Where γ: is shear strain; τ: is shear resistance; l: is shear displacement; n: is number of points recorded. In other words the energy dissipated during one cycle of loading can be represented by the area of hysteresis loop; in the case of constant-speed-shear test total dissipated energy can be represented by the area under the shear stress-shear displacement line (Fig. 5-1-1). Equation (5.1.2) is essentially mathematical formulae for calculating these areas for the tests carried out by the ring shear apparatus.

The accuracy of calculations strongly depends on the number of points recorded during a cycle of loading. In the present study, data acquisition rate was not less than 50 points per cycle.

It is necessary to underline that the energy "dissipated in the soil" and not "dissipated by the soil". Let us imagine the situation, when the energy dissipated in the soil is zero, for cyclic ring shear test. Obviously, as it follows from Eq. 5.1.2 it will be if:

a) Shear resistance is zero (shearing water, for instance);

b) Plastic shear displacement is zero.

The latter case needs some explanation. As it was mentioned above, dissipated energy is proportional to the area of hysteresis loop. If the deformation has only an elastic nature, there will be no hysteresis loop, but just straight line with zero area. Therefore, the dissipated energy, considering the whole cycle, will be also zero.

The energy consumption due to viscoelastic behavior is unlikely in sandy soil. Accordingly to Mitchell (1993) such type of behavior is characteristic for the plastic clays with high organic content. For clear sands there is so-called vibroviscosity (Sergeev, 1983), which can be observed for sands vibrated with large (about 0.8-1.0g) accelerations. Since in the tests conducted the acceleration values were substantially less (0.24-0.33g), there is no reason to expect the effect of vibroviscosity.

The total dissipated energy will be used in the Thesis as one of the most important parameters, for evaluation of character of the pore pressure generation during undrained loading.

5-2. Mechanism of Energy Consumption at the Sliding Surface

5-2-1 Cyclic Shear State

In Fig. 5-2-1 the dependency of number of cycles required to liquefaction (N) plotted against loading frequency (f) values for the shear-stress controlled ring shear test. It is observed that for overconsolidated samples, the N is practically independent on the loading frequency. However, the tests on samples with OCR=1.00 indicate as N increases f increases as well. On the other hand, there are rather large fluctuations of obtained values of N from their mean value. For example, for samples with the OCR=2.58-2.94 (test No.13-18) the minimum and maximum N differs almost twice 12 (test No.17) and 23 cycles (test No. 16). Peacock & Seed (1968), concluded that "...in the stress range causing liquefaction to occur at low number of cycles, the tests data show only small variations due to frequency effects". Meanwhile, in Fig. 5-2-2 modified data obtained from these authors are plotted. Since these researchers used triaxial compression testing equipment and different samples, it is difficult to make direct comparison. However, it can be readily seen that for the highest level of the peak pulsating shear stress (30-40 kPa) the tendency observed by Peacock & Seed is somewhat similar to that of normally consolidated samples in our stress-controlled ring shear tests, with the amplitude of the shear stress of 65-70 kPa.

For the same loading frequency samples with the higher OCR required more cycles to liquefy. This is very reasonable, because overconsolidation produces an increase of density as well as amount of contacts between soil particles. This transformation of the soil structure improves its stability against dynamic loading.

Data from the shear-displacement-controlled ring shear tests (No.19-33) show that number of cycles required to liquefaction is practically constant for the frequency range of 0.01-0.20 Hz (Fig. 5-2-3). All samples, being normally consolidated, liquefied after 4-5 cycles of loading (tests No. 19-23) with only one

after six cycles (test No.19). The values of the shear displacement amplitude for these tests (No.19-23) were 0.49-0.50mm. Further, it will be shown later that shear displacement amplitude has significant influence on the number of cycles required to liquefaction.

It was mentioned above that the ring shear apparatus is not common equipment for soil mechanics laboratories, though it is very suitable for studying landslides. In order to compare tests result on Osaka Formation sandy soil obtained by ring shear apparatus with other studies, several tests with different frequencies of loading were performed by triaxial compression apparatus. Data obtained by triaxial compression cyclic stress-controlled tests added even more controversy. Accordingly to Wong et al. (1975) "...the effect of frequency on the results of cyclic loading tests is negligibly small". Their data after being modified and compared with ours (Fig. 5-2-4) show an almost opposite tendency. On the other hand it should be noted that Wong et al. conducted tests with only two different frequencies. Data obtained during this study shows that the increase in the number of cycles required for liquefaction with increase of the loading frequency is similar to that of stress-controlled ring shear tests on the normally consolidated samples.

Therefore, the effect of the frequency of loading on the number of cycles required to liquefaction is not clear. This suggests that the widely used criteria N has certain shortcomings, and is not always reliable. Indeed, direct comparison between our data and those of other researchers is impossible because the stress level, the samples, and the apparatus are different. However, even when analyzing not the absolute values but only the trends sometimes opposite results are produced. In such a situation, another approach of analysis is needed. The energy approach is a possible solution.

The total dissipated energy required to liquefaction (W) is very important parameter, which is closely related to the pore pressure build-up, as it was shown in the section 5-1. Therefore, it is necessary to assess the process of pore pressure generation from the standpoint of the energy approach.

In Fig. 5-2-5 values of the total dissipated energy required for liquefaction are plotted against loading frequency for shear-stress-controlled ring shear tests. It can be clearly seen, that as the loading frequency increases, the total dissipated energy required for liquefaction substantially decreases. This is true for all OCR levels. Among the same frequency values, samples with higher OCR dissipated more energy

to liquefy. This is because overconsolidated samples exhibit higher shear resistance, as it was explained above.

The observation that the W required to liquefaction increases with loading frequency is very interesting and needs careful analysis to understand. As was mentioned above the dissipated energy during shearing depends on the shear displacement and shear resistance. Therefore, the total dissipated energy is proportional to the total shear displacement during shearing. The principle of the calculation of the total shear displacement during cyclic loading is illustrated in Fig. 5-2-6. Accordingly, the total shear displacement during cyclic loading can be defined as:

$$l_t = 4\ l_{max}$$

Where Δl_{max} is amplitude of the shear displacement during one cycle of loading

The amplitude of the shear displacement and therefore the total shear displacement is directly affected by the loading frequency in shear-stress-controlled tests. In Fig. 5-2-7 the effective stress path of test with f=0.01 Hz (test No.1) is presented. It can be observed, that until the stress path reached the failure line, a relatively small shear displacement occurred (8.24 mm) and low amount of W (112 J/m^2) was dissipated. This is because the shear resistance was greater than the applied shear stress. As the excess pore pressure gradually built-up, the shear resistance was reduced and eventually the stress path reached the failure line. At this point the shear stress was larger than the shear resistance and the shear displacement progressed. The stress point moved along the failure line. Since the period of loading is long, a large shear displacement occurs. During this stage of loading the sample undergoes one-directional shearing. Accordingly to concept of the sliding-surface liquefaction (Sassa, 1996), during one-directional shearing the excess pore pressure is generated mostly due to grain crushing and comminuting of the shear zone. The process of grain crushing requires a large amount of the energy to be dissipated. Indeed, during this stage the excess pore pressure ratio increased by only 0.2, while total shear displacement and dissipated energy increased 40.92mm and 706 J/m^2, respectively (Fig. 5-2-7). However, tests No. 5, with higher frequency-1.00 (Fig. 5-2-8) demonstrate rather different behavior. The period of loading is 100 times shorter than in the previous test (No.1), and the shear stress was the same, therefore duration of the one-directional shearing was much shorter. Thus grain crushing was less, and

pore pressure was generated mostly because of volume shrinkage due to process of particle rearrangement. The total shear displacement required for liquefaction was much smaller, than in a test with f=0.01 Hz (No.1) and the total dissipated energy was also less.

All shear-stress-controlled ring shear tests are in line with this mechanism, which is clearly seen in Fig. 5-2-9. On the other hand, it is clear that this tendency can not be expressed by simple straight line, because there must be some minimum value of the total shear displacement required for liquefaction. The first small signs of a changing of the shape of the curve can be observed in Fig. 5-2-9 around frequency values of 1.00-2.00 Hz. However, the present ring shear apparatus does not allow to conduct the tests with a further increase in loading frequency, with the same shear stress level. Therefore, additional experiments, which can reveal influence of the total shear displacement required for liquefaction, are necessary.

Data, which were calculated on the basis of the cyclic triaxial compression stress-controlled tests (Fig. 5-2-10), are in very good agreement with those of shear-stress-controlled tests. Apparently, it is because of similarity between the loading schemes in both experiments. Again, as the loading frequency increases, the total dissipated energy required to liquefaction drastically decreases. Fig. 5-2-10 contains three sets of data. Two of them represents values of the W calculated up to the points when excess pore pressure ratio (r_u) reaches 0.50 and 0.95, respectively. The latter value indicates the liquefaction of the sample. The third set of points stands for total axial displacement required to liquefaction. Deformation of a sample, in tests with f=0.05 and f=0.10 Hz, was affected by "necking", during which the sample undergoes large extension deformations. In these tests, the magnitude of the extension deformations exceeded transducer's capacity, therefore the true deformation could not be measured correctly, and W could not be calculated accurately. In order to cope with this problem, the total dissipated energy was calculated up to the point, where deformations are still small. This approach was proposed by Casagrande (1976). From Fig. 5-2-10 it can be seen that both lines correlate well with each other, therefore the proposed approach appears to be correct.

Note that the absolute values for the total dissipated energy required for liquefaction are different for cyclic shear-stress-controlled ring shear tests and cyclic stress-controlled triaxial compression tests. In case of ring shear test the dissipated energy is measured in J/m^2, while in triaxial tests in J/m^3. Therefore it is difficult to

make any certain conclusions about absolute values of the total dissipated energy required to liquefaction.

In Fig. 5-2-11 and Fig. 5-2-12 values of the total shear displacement and total dissipated energy required for liquefaction, for shear-stress-controlled and shear-displacement-controlled ring shear tests, respectively, are plotted with respect to the loading frequency. It is interesting that for both types of test, values of W and the l_t converge at around 1-2 Hz. It is possible that a level of dissipated energy of 100-150 J/m^2 is the minimum level of the dissipated energy required for liquefaction for the given samples, under the given condition. In an analogous manner, the total shear displacement of 8-10 mm seems to be necessary for liquefaction.

This proposition was examined, and results of the examination are presented in the section 5-3.

5-2-2 Monotonic Shear State

Cyclic loading is not only the factor, which may trigger a landslide disaster. Rapid loading of monotone nature can cause mass liquefaction of a torrent deposit (Sassa, 1985; Sassa et al., 1985). The Gamahara debris flow in 1996 was triggered by fall of failed mass of soil onto the torrent deposits (Sassa, 1997).

When a failed mass starts to move, a high pore pressure can be generated either by mass liquefaction or sliding surface liquefaction. It is not clear yet, whether the velocity of the moving mass has some relation to the pore pressure generation or not. Therefore, certain experiments were required.

Four monotonic constant-shear-speed ring shear tests were carried out with different shear speed values. Pattern of the pore pressure generation in these tests are presented in Fig. 5-2-13. From the beginning of a test, a pore pressure of about $r_u=0.70$ was generated, while shear displacement was 2-3mm. During this first stage of shearing the pore pressure was generated generally due to particle rearrangement, which in the undrained conditions leads to a pore pressure rise. Then, small decrease of excess pore pressure ratio was observed. This drop of pore pressure is typical for non-loose samples of Osaka Formation, and was rigorously analyzed by Wang (1998) in his PhD Thesis. This stage was named "initial positive dilatancy". When this stage was over, the pore pressure rose again, but at a much lower rate. This is because the pore pressure is generated due to grain crushing and comminuting of the

shear zone. The final pore pressure ratio depends on the magnitude of the shear displacement. For Osaka Formation sandy soil it usually takes about 10 meters of the shear displacement to reach an excess pore pressure ratio of about 0.90. Within the range of 100mm of the shear displacement, results from all tests seem to be very similar to each other. It can be observed, that in the test with highest shear speed, the rate of pore pressure generation was slightly lower than in other tests. Probably this effect was due to delay in the pore pressure measurement system, resulting from the high-speed shearing.

The mechanism of the accumulation of the dissipated energy during monotonic shearing (Fig. 5-2-14) can be divided into two stages. At first stage, when particle rearrangement occurs, a relatively small amount of energy is dissipated. Due to particle rearrangement, the pore pressure increases and shear resistance decreases. The first stage ends when pore pressure reaches its peak value before reducing due to dilatancy. As the sample starts to dilate, the second stage begins. Here the increment in pore pressure is not sufficient for complete loss of shear resistance, hence some part of the shear resistance still remains. Further shearing leads to constant energy dissipation due to plastic deformations. Pore pressure rise in the second stage occurs as a result of grain crushing and comminuting of the shear zone.

Data obtained by constant-strain-rate triaxial compression tests are in good agreement with that of ring shear ones. In Fig. 5-2-15 excess pore pressure ratios of tests with different strain rates are plotted against strain. From this figure it appears that there is no obvious dependence of r_u on the strain rate. However, it should be noted that the mechanism of the pore pressure generation in the triaxial test is very different from that of the ring shear test. Pore pressure increases with an increment of the axial strain of 0.05 (10mm), and starts to decrease gradually without further increase. It indicates a principal difference between pore pressure generation in a triaxial compression and the ring shear tests. The grain crushing is very unlikely to occur in the triaxial compression test, while in the ring shear it is important cause of pore pressure generation during one-directional shearing, if the sample is not loose.

Fig. 5-2-16 shows the accumulation of the dissipated energy with respect to the axial strain. Again, for all tests with different strain rates there are no significant differences in the energy dissipation. The shape of the curves are rather similar to that obtained by ring shear tests. Comparison of absolute values is rather problematic, however, because of the different dimensions of obtained energy.

It can be summarized that in the constant-speed ring shear tests as well as in constant-strain-rate triaxial tests, the character of the pore pressure generation and the values of the dissipated energy are irrelevant to the rate of loading. However, the mechanism of the pore pressure generation in the monotonic constant-shear-speed ring shear tests is principally different from that of the monotonic triaxial compression test.

5-3. Optimal Shear Amplitude for the Pore Pressure Generation

It was shown in the section 5-2, that there is some minimum level of the dissipated energy required to liquefy a given soil under given conditions. It was also concluded that since the shear resistance of the sample limited by the failure line, the shear displacement is the very important factor for energy dissipation. Therefore, an examination of the dependency of the dissipated energy on the shear displacement is required.

In Fig. 5-3-1 the dependence of the total dissipated energy required for liquefaction on the shear displacement amplitude (Δl_{max}) is presented. It can be observed that when the values of the shear displacement amplitude are close to 0.50mm, minimum value of dissipated energy (approximately 100 J/m^2) is dissipated until the sample liquefy. The further increase of the Δl_{max} produces an increment of the total dissipated energy; decrease of the Δl_{max} also leads to the raise of the total dissipated energy required for liquefaction.

As to number of cycles required to liquefaction (Fig. 5-3-2) the tendency is completely different. Samples tested with Δl_{max} larger than 2.5 mm liquefied at the very first cycle. Decrease of the Δl_{max} lead to a rapid growth in the number of cycles.

Possible explanation of the mechanism of energy dissipation presented in Fig. 5-3-3. It is suggested, that there the energy, which is transmitted to the soil can be spent in two ways, namely for pore pressure generation and plastic deformations. The very minimum level of the energy required to produce pore pressure equal to the total normal stress (for the ring shear case) can be expressed as:

$$W_{liq} = \sigma \times \Delta h_{liq} \tag{5.3.1}$$

$$\Delta h_{liq} = f(n, C_w, C_m) \tag{5.3.2}$$

Where σ: is total normal stress, and Δh_{liq} change of sample height, which can be expressed as a function of porosity (n), compressibility of pore water (C_w), and compressibility of soil minerals (C_m). This minimum level of the energy is schematically repressented by the dotted line, because current precision of the

apparatus does not allow accurate calculations. Above this dotted line virtually all energy is spent for plastic deformations and not for the pore pressure generation.

The fundamental difference of cyclic loading from monotone loading (from our research) is the change in the direction of the shear stress. During cyclic loading, the shear stress changes its direction twice per each cycle, while in monotone loading, the direction of the shear stress is constant. Change of direction of shearing has tremendous effect on the volume shrinkage tendency. In Fig. 5-3-4 a time series of a large-amplitude test (Δl_{max}=7.25mm) is presented. It can be clearly seen, that at the moment of stress reversal (peaks of the shear displacement curve), the pore pressure "jumps" with a subsequent decrease during the shearing process. This is because change in the shear stress direction causes soil structure to undergo major structural reshuffle, because acting shear stress is almost zero, and soil particles try to find the position with a minimum potential energy. This lead to volume shrinkage and pore pressure generation.

From the results of the constant-speed ring shear tests we can say that normally consolidated samples of the Osaka Formation with void ratio of 0.67-0.69 can not be liquefied within a relatively small (<100 mm) range of the shear displacement. It was also established that, in these tests, the peak pore pressure was generated at a level of about 2mm shear displacement (Fig.5-2-13), up to the stage of the initial negative dilatancy. Further increase of the pore pressure occurs due to extensive grain crushing, but the extensive grain crushing process consumes a large amount of dissipated energy, because after the initial pore pressure build-up, the shear resistance still remains, and shear displacement progresses. However, in shear-displacement-controlled cyclic ring shear tests the first quarter of the first cycle is very similar to the constant-speed shear tests. Therefore, the shear-displacement-controlled cyclic ring shear tests with a Δl_{max} of more than 0.5mm consumes more energy.

However, decrease of the Δl_{max} from the mentioned value (0.5mm) also leads to an increase of the total dissipated energy required for liquefaction. When the amplitude of the shear displacement is very small (<0.5mm), the structural rearrangements are limited because the soil particles can not be moved from their initial positions. Under such conditions the energy is spent on small local deformations and overcoming friction forces between adjacent particles. The volume shrinkage in such circumstances is induced mostly by slow and gradual comminution

of particles, while the structure itself does not undergo any significant reshuffle. Note, that tests with Δl_{max}=0.03mm failed to produce liquefaction after 6000 cycles. The excess pore pressure ratio was only 0.44, while accumulated dissipated energy reached 2376 J/m^2. It is difficult to simulate precisely, how many cycles, and how much energy to be dissipate, will be necessary to liquefy that sample with such small shear displacement amplitude. Therefore, the point which corresponds to Δl_{max}=0.03mm in Fig. 5-3-1 has an upward arrow. On the other hand, when in the same test the shear displacement amplitude was increased to 0.06mm, the excess pore pressure ratio reached 0.94 after 1253 cycles. Total dissipated energy was 3268 J/m^2. Probably, if we had used the latter shear displacement amplitude from the beginning of the test, the value of the W would be lower, so the point, which corresponds to Δl_{max}=0.06mm in Fig. 5-3-1 has a downward arrow.

All mentioned above lead us to the idea that there must be some level of the shear displacement, which has maximum effect on the pore pressure generation. Since most of the absolute value of the excess pore pressure is generated during first cycles of loading, it is interesting to analyze how pore pressure generation depends on the magnitude of the shear displacement in the first quarter cycle, i,e. when the sample still "fresh". For this purpose parameter $r_u/\Delta l_{max}$ (r_u is the excess pore pressure, and Δl_{max} is shear displacement amplitude) was computed. In Fig.5-3-5 this parameter is plotted with respect to the shear displacement amplitude for the shear-displacement-controlled tests. It is obvious that parameter $r_u/\Delta l_{max}$ has a peak around the 0.5mm of the shear displacement amplitude. This fact provides a reasonable explanation, as to why the minimum energy is dissipated for liquefaction, when the shear displacement amplitude is about 0.5mm. Deviation of the shear displacement amplitude from the 0.5mm value leads to a drastic decrease of the parameter $r_u/\Delta l_{max}$.

Since the excess pore pressure ratio has its upper limit of 1.00, the parameter r_u/l_t, calculated for each 0.25 of the first two cycles, decreases as the cyclic test proceeds (Fig. 5-3-6). The mechanism of this effect is, probably, as follows. Due to pore pressure generation, the effective stresses between angular soil particles of the Osaka Formation are reduced. Therefore, each new cycle of loading has less impact on the soil structure than the previous one, until the sample reaches liquefaction.

However, the value of 0.5mm of the shear displacement should not be taken as universal optimal shear displacement for the pore pressure generation. On contrary, such value is probably most effective for the rather specific type of the

sample, namely coarse grain sandy soil, which belongs to the Osaka Formation. For soils with different grain-size distribution, angularity, and mineral composition, optimal shear displacement for pore pressure generation is probably different from 0.5mm. It is rather difficult to suggest reasonable explanation on the matter why such shear displacement amplitude (0.5mm) was so effective for pore pressure generation. Verification of this suggestion requires additional testing of different soils.

CHAPTER 6

Conclusions

1. Dependency of the pore pressure generation on the frequency of loading and deformation rate was examined by conducting a series of undrained stress-controlled tests and deformation-controlled tests using the ring shear apparatus and the triaxial compression apparatus. Sandy soil, belonging to the Osaka Formation was used as the sample. Test results were analyzed from the standpoint of an energy approach.

2. Cyclic shear-stress-controlled ring shear tests demonstrated that as the frequency of loading increases, the total dissipated energy required to liquefaction substantially decreases, however shear-displacement-controlled tests showed that if amplitude shear displacement was constant, the dissipated energy required for liquefaction was independent on the loading frequency. Therefore, it was found that the apparent effect of loading frequency was caused by different amplitudes of the shear displacement during testing, because the dissipated energy depends on shear resistance and shear displacement. Large shear displacement amplitude was result of a long period of loading during low-frequency tests. When the sample was subjected to the large amplitude of the shear displacement, while shear resistance remained, large amount of energy should have dissipated due to plastic deformations in the extent of large shear displacement.

3. Data obtained by the cyclic stress-controlled triaxial compression tests showed that as the loading frequency increased, the total dissipated energy required to liquefaction decreased. The mechanism of this effect is similar to that of the shear-stress-controlled ring shear test.

4. It was found that tests with a shear displacement amplitude around 0.5mm consumed the minimum amount of dissipated energy for liquefaction of the sample. An increase of the shear displacement amplitude from 0.5mm, led to increased energy consumption due to plastic deformations and, therefore, increases in the total dissipated energy required to liquefaction; the shear displacement amplitudes smaller than 0.5mm were, probably, not so effective to cause volume shrinkage and pore pressure generation.

5. The magnitude of shear displacement profoundly affected the effectiveness of the excess pore pressure build up. It was found that, within the range of shear displacement of around 0.5mm, the relation between pore pressure increment and shear displacement amplitude (parameter $r_u/\Delta l_{max}$), for studied soil, has its peak value. The deviation of the shear displacement from 0.5mm led to decreases of the parameter.

6. In monotonic tests (constant-speed ring shear test and constant-axial-strain-rate triaxial tests), the deformation rate did not affect the pore pressure generation and energy dissipation in the investigated soils. It was confirmed that the mechanism of pore pressure generation in the ring shear tests, which simulates a sliding surface, is very different from that of triaxial compression test; the stage of "the negative dilatancy due to grain crushing" was observed only in the ring shear tests.

7. The total shear displacement required to liquefy the normally consolidated specimen under cyclic conditions was substantially smaller, than that of constant-deformation-rate shearing, because the change of the direction of loading had significant effect on the pore pressure generation.

Contents of this Thesis are based on papers as follows:

1. Vankov, D.A., Sassa, K.(1998): Dynamic Testing of Soils by Ring Shear Apparatus. *Proceedings of 8th Congress of IAEG*, September 21-25, Vancouver, Canada, BALKEMA, Vol. 1, pp.485-492

2. Vankov, D.A., Sassa, K.(1999):Dependence of Pore Pressure generation on Frequency of Loading at Sliding Surface. *Proceedings of the International Symposium on Slope Stability Engineering-IS-SHIKOKU'99*, BALKEMA, Vol.1, pp.601-606

3. Vankov, D.A., Sassa, K.(2000) Mechanism of Earthquake-Induced Landslides at Almost Flat-Slopes by Means of Ring Shear Apparatus. Accepted for publication by the *Journal of Natural Disaster Science*, Vol. 21, No.1, (in press).

ACKNOWLEDGEMENTS

REFERENCES

1. Bishop, A.W., Green, G.E, Garga, V.K., Andresen, A., Brown, J.D. (1971): A New Ring-Shear Apparatus and its Application to the Measurement of Residual Strength. *Geotechnique*, Vol. 21, No.4, pp.243-328.

2. Black, D.K, Lee, K.L. (1973): Saturating Laboratory Samples by Back Pressure. *Journal of the Soil Mechanics and Foundation Engineering Division, Proceedings ASCE*, Vol. 99, No. SM1, January, pp.75-93.

3. Boulanger, R.W., Seed, R.B. (1995): Liquefaction of Sand under Bidirectional Monotonic and Cyclic Loading. *Journal of Geotechnical Engineering Division*, Vol.121, p.870-878.

4. Castro, G. (1975): Liquefaction and Cyclic Mobility of Saturated Sands. *Journal of Geotechnical Engineering, ASCE*, Vol.101, No. 1, pp.551-569.

5. Castro, G., Poulos, S.J. (1977): Factors Affecting Liquefaction and Cyclic Mobility. *Journal of Geotechnical Engineering, ASCE*, Vol.103, pp.501-516.

6. Casagrande, A. (1976): Liquefaction and Cyclic Deformation of Sands. A Critical Review. *Harvard Soil Mechanic Series*, No 88.

7. Davis, R.O., Berrill, J.B.(1982): Energy Dissipation and Seismic Liquefaction in Sands. *Journal of Earthquake Engineering and Structural Dynamics*, Vol.10, pp.59-68.

8. Definition of Terms Related to Liquefaction (1978). By the Committee on Soil Dynamics of the Geotechnical Engineering Division, ASCE. *Journal of the Geotechnical Engineering Division, Proceedings ASCE*, Vol.104, No.GT9, pp.1197-1200.

9. Drnevich, V.P. (1972): Undrained Cyclic Shear of Saturated Sand. *Journal of Soil Mechanics and Foundation Engineering, ASCE*, No. SM8, Vol. 98, pp. 807-825.

10. Figueroa, J.L. (1993): Unit Energy Level Associated with Pore Pressure Development during Liquefaction. In the book *"Soil Dynamics and Earthquake Engineering"*, edited by Cakmak, A.S.& Brebbia, C.A. Computational Mechanics Publications, Southampton, Boston, pp.413-427.

11. Figueroa, J.L., Saada, A.S., Liang, L., Dahisaria, N.M (1994): Evaluation of Soil Liquefaction by Energy Principles. *Journal of Geotechnical Engineering*, Vol. 120, No.9, pp.1554-1569.

12. Finn, L.W.D., Bransby, P.L., Pickering, D.J.(1970): Effect of Strain History on Liquefaction of the Sand. *Journal of Soil Mechanics and Foundation Engineering, ASCE*, No. SM6, Vol. 96, pp. 1917-1934.

13. Fukuoka, H. (1991): Variation of the Friction Angle of Granular Materials in the High-Speed-High-Stress Ring Shear Apparatus. *Bulletin of the Disaster Prevention Research Institute, Kyoto University*, Vol.41 (offprint).

14. *Gruntovedenie* (1983): Under edition of Sergeev, E.,M., Moscow University Press. (in Russian)

15. Hatanaka, M., Uchida, A., Ohara, J. (1997): Liquefaction characteristics of a gravelly fill liquefied during the 1995 Hyogo-ken Nanbu earthquake. *Soils and Foundations*, Vol. 37, No.3, pp. 107-115.

16. Irikura, K. (1996): Strong ground motionof the Hyogoken-Nanbu earthquake and the fault model. The Great Hanshin-Awaji Earthquake Disaster-for the Disaster Prevention Research. DPRI, Kyoto University, pp.81-98 (in Japanese).

17. Kamai, T. (1995): Landslides in Hanshin Urban Region Caused by 1995 Hyogoken-Nanbu Earthquake, Japan. *Landslide News*, No. 9, pp.12-13.

18. Ladd, R.S. (1977): Specimen Preparation and Cyclic Stability of Sands. *Journal of Geotechnical Engineering Division, Proceedings of ASCE*, Vol.103, No.GT6, pp.535-547.

19. Landslides Investigation and Mitigation (1996): *Special report 247 by Transportation Research Board of National Research Council of U.S.A*. Edited by Turner A.K., Schuster R.L. National Academy Press, Washington, D.C.

20. Law, K.T., Cao, Y.L., He, G.N.(1990): An Energy Approach for Assessing Seismic Liquefaction Potential. *Canadian Geotechnical Journal*, Vol.27, pp.320-329.

21. Liang, L., Figueroa, L.J., Saada, A.S.(1995): Liquefaction under Random Loading: Unit Energy Approach. *Journal of Geotechnical Engineering ASCE, Vol. 121, No 11*, pp.776-781.

22. Lin, M.L., Huang, T.H., You, J.C. (1996): The Effect of Frequency on Damping Properties of Sand. *Soil Dynamics and Earthquake Engineering.* 15, pp.269-278

23. Martin, G.R., Finn, L.W.D. (1975): Fundamentals of Liquefaction under Cyclic Loading. *Journal of Geotechnical Engineering Division, Proceedings of ASCE*, Vol.101, No.GT5, pp.423-438.

24. McRoberts, E.C., Sladen, J.A.(1992): Observation on Static and Cyclic Sand Liquefaction Methodologies. *Canadian Geotechnical Journal, 29*, pp. 650-665.

25. Mitchell, J.K.(1993): Fundamentals of Soil Behaviour. The Second Edition. John Wiley&Sons.

26. Moroto, N., Tanoue, Y. (1989): Liquefaction Potential of Sandy Ground from an Energy Considerations. *Proceedings of the 5th Intl. Conference on Soil Dynamics*

and Earthquake Engineering. Computational Mechanics Publications, Southampton, Boston, pp.21-25.

27. Mulilis, J.P., Seed, H.B., Chan, C.K., Mitchell, J.K., Arulanandan, K. (1977): Effects of Sample Preparation on Sand Liquefaction. *Journal of Geotechnical Engineering Division, Proceedings of ASCE*, Vol.103, No.GT2, pp.91-108

28. Nemat-Nasser S, Shakooh A. (1979): A Unified Approach to Densification and Liquefaction of Cohesionless Sand in Cyclic Shearing. *Canadian Geotechnical Journal, 16(4),* pp. 659-678.

29. Novak, M., Kim, T.C. (1981): Resonant Column Technique for Dynamic Testing of Cohesive Soils. *Canadian Geotechnical Journal*, Vol. 18, pp. 448-455.

30. Okada, Y. (1999): An Experimental Study on the Liquidization of Sandy Soils. *Master Thesis*, the Division of Earth and Planetary Science, Graduate School of Science, Kyoto University.

31. Peacock, W.H. and Seed, B.H (1968*):* Sand Liquefaction under Cyclic Loading Simple Shear Condition. *Journal of Geotechnical Engineering ASCE* No. SM3, Vol. 94, pp. 689-708.

32. Peck, R.(1979): Liquefaction Potential: Science Versus Practice. *Journal of Geotechnical Engineering ASCE* No. ST3, Vol. 105, pp. 393-398.

33. Trofimov, V.T., Korolev, V.A. (1993): Practicum po Gruntovedeniyu. Moscow State University Press, 390 pages, (in Russian).

34. Sassa, K.(1985): The Mechanisms of Debris Flows. *Proceedings XI International Conference on Soil Mechanics and Foundation Engineering*, San Francisco, Vol.3, pp.1173-1176.

35. Sassa, K. (1988): Motion of Landslides and Debris Flows-Prediction of Hazard Area. *Report for grant-in-aid for scientific research by the Japanese Ministry of Education Science and Culture (project No. 61480062).*

36. Sassa, K. (1996): Prediction of Earthquake Induced Landslides. *Proceedings of the 7th International Symposium on Landslides*, Trondheim, Norway, "Landslides", Balkema, Vol.1, pp.115-132.

37. Sassa, K., Fukuoka, H., Scarascia-Mugnozza, G. and Evans, S. (1996): Earthquake-Induced Landslides: Distribution, Motion and Mechanisms. Special Issue for the Hyogoken-Nanbu earthquake. *Soils and Foundations*, pp.53-64.

38. Sassa, K., Fukuoka, H., Scarascia-Mugnozza, G., Irikura, K., Okimura, T. (1995): Landslide Triggered by the Hyogoken-Nanbu Earthquake, 1) The Hyogoken-Nanbu Earthquake and the Distribution of Triggered Landslides. *Landslide News*, No. 9, pp.2-5.

39. Sassa, K., Fukuoka, H., Wang, F.W.(1997): Gamahara Torrent Debris Flow on 6 December 1996, Japan. Possible Mechanism of the Debris Flow. *Landslide News* No10, pp.6-9.

40. Sassa, K., Kaibori, M., Kitera, N (1985): Liquefaction and Undrained Shear of the Torrent Deposits as the Cause of Debris Flows. *Proceedings of the International Symposium on Erosion, Debris Flows and Disaster Prevention*, Tsukuba, Japan, pp.231-236.

41. Seed, H.B. (1968): Landslide during Earthquakes due to Soil Liquefaction. *Journal of Soil Mechanics and Foundations Division, Proceedings ASCE*, Vol.94, NoSM5, pp. 1055-1121.

42. Seed, H.B., Lee, K. (1966): Liquefaction of Saturated Sands during Cyclic Loading. *Journal of the Soil Mechanics and Foundation Division, Proceedings ASCE*. Vol.92, NoSM6, pp.105-134.

43. Seed, H.B., Idriss, I.M. (1971): Simplified Procedure for Evaluating Soil Liquefaction Potential. . *Journal of the Soil Mechanics and Foundation Division, Proceedings ASCE*. Vol.97, NoSM9, pp.1249-1273.

44. Sergeev, E.M.(1983): *Gruntovedenie*, Moscow University Press, 390 pages, (in Russian)

45. Silver, M.L., Park, T.K. (1975): Testing Procedure Effect on Dynamic Soil Behaviour. *Journal of the Soil Mechanics and Foundation Division, Proceedings ASCE*. Vol.101-2, NoGT105, pp.1061-1083.

46. Skempton, A.W. (1954): The Pore Pressure Coefficients A and B. *Geotechnique*, No 4(4), pp.143-147.

47. Towhata, I., Ishihara, K. (1985): Shear Work and Pore Water Pressure in Undrained Shear. *Soils and Foundations*, Vol. 25, No.3, pp. 73-84.

48. Trifunac, M.D. (1995): Empirical Criteria for Liquefaction in Sands via Standard Penetration Test and Seismic Wave Energy. *Soil Dynamics and Earthquake Engineering*, 14, pp.419-426.

49. Trofimov, V.T., Korolev, V.A. (1993): Practicum po Gruntovedeniyu. Moscow State University Press, 390 pages, (in Russian).

50. Vaid, Y.P., Thomas, J. (1995): Liquefaction and Postliquefaction Behaviour of Sand. *Journal of Geotechnical Engineering ASCE*, No. 2, Vol. 121, pp. 163-173.

51. Vankov, D.A. (1997): Behaviour of Dry and Saturated Sandy Soil Subjected to Different Frequencies of Loading. *Master Thesis*, Dept. of Earth and Planetary Science, Fac. of Science, Kyoto University.

52. Vankov, D.A., Sassa, K. (1998): Dynamic Testing of Soils by Ring Shear Apparatus. *Proceedings of 8th Congress of IAEG, Vancouver, Canada, Balkema, Vol.1* pp.485-492.

53. Vankov, D.A., Sassa, K. (1999): Dependence of Pore Pressure Generation on Frequency of Loading at Sliding Surface. . *Proceedings of the International Symposium on Slope Stability Engineering,* Vol.1, pp.601-606.

54. Vankov, D.A., Sassa, K.() Mechanism of Earthquake-Induced Landslides at Almost Flat-Slopes by Means of Ring Shear Apparatus. Accepted for publication by the *Journal of Natural Disaster Science*, Vol. 21, No.1.

55. Voznesensky, E.A. (1994): Dynamic Instability of Soils and Rocks. *Proceedings of 7th Congress of IAEG*, Lisboa, Portugal. BALKEMA, offprint, pp.683-692.

56. Voznesensky, E.A. (1998): An Energy Approach to Dynamic Instabilty of Soils. *Proceedings of the Second International Conference On Environmental Management (ICEM 2),* Australia, Vol.2, pp.1011-1018.

57. Voznesensky, E.A., Nordal, S. (1999): Dynamic Instability of Clays: an Energy Approach. *Soil Dynamics and Earthquake Engineering*, 18, pp.125-133.

58. Wang, F. (1998): An Experimental Study on Grain Crushing and Excess Pore Pressure Generation during Shearing of Sandy Soil. *Doctor Thesis*, the Division of Earth and Planetary Science, Graduate School of Science, Kyoto University.

59. Wang, F., Sassa, K. (1998): Ring–Shear Test on Sliding Surface Liquefaction Behaviour of Sandy Soils. *Reprint from the Annuals of the DPRI, Kyoto University*, No41, B-1, pp.245-260.

60. Wong, R.T., Seed, H.B., Chan, C.K. (1975): Cyclic Loading Liquefaction of Gravelly Soils. *Journal of Soil Mechanics and Foundation Engineering, ASCE,* No. ST6, Vol. 101, pp. 571-583.

61. Wood D. M. (1982): Laboratory investigation of the behaviour of soils under cyclic loading: a review. In the book "*Soil Mechanics-Transient and Cyclic Loads*", edited by Pande and Zienkevich, pp. 513-582.

FIGURE CAPTIONS

Fig. 1-2-1
Influence of frequency on undrained strength of loose Monterrey sand under cyclic loading-simple shear conditions (after Peacock & Seed, 1968)

Fig. 1-2-2
Effect of frequency on cyclic stresses causing initial liquefaction of Monterrey sand (after Wong. et al., 1975)

Fig. 2-1-1
Stresses applied to ring shear sample.
σ :normal stress; τ : shear stress.

Fig. 2-1-2
Principal scheme of ring shear apparatus (DPRI-4) with enlarged sample assembly part.(see text for comments)

Fig. 2-1-3
Normal stress control systems: with one load cell (A) and two load cells (B). (See text for comments)

Fig. 2-1-4
Undrained shear box (section of half part)

Fig. 2-2-1
Principal scheme of triaxial compression apparatus with auxiliary units

Fig. 2-4-1
Relationship between degree of saturation and pore pressure parameter (after Sassa, 1988; Black & Lee, 1973)

Fig. 3-2-1
Stress path mechanism for ring shear test and triaxial compression tests. σ :normal stress, σ_1 : axial stress; σ_3 : confining stress; τ : shear stress.
$p=(\sigma_1+\sigma_2)/2$; $q=(\sigma_1-\sigma_2)/2$

Fig. 5-1-1
The energy (W) dissipated during constant-shear-speed shearing (a), and cyclic loading (b)

Fig. 5-2-1.
Number of cycles required to liquefaction (N) versus loading frequency (f) for differently overconsolidated samples (torque-controlled ring shear tests). Constant shear torque amplitude (56-63 kPa) for all tests. Void ratios are 0.67-0.77 (OCR=1.00), 0.69-0.74 (OCR=1.91-2.14), and 0.67-0.73 (OCR=2.58-2.94).

Fig. 5-2-2
Number of cycles required to liquefaction (N) versus loading frequency (f) for different levels of cyclic stress. (Simple shear test, Monterey sand). Modified from Peacock & Seed (1968)

Fig. 5-2-3.
Number of cycles (N), total dissipated energy (W), and total shear displacement required for liquefaction versus loading frequency (f) for normally consolidated samples. Shear-displacement-controlled ring shear tests. Amplitudes of the shear displacement are 0.49-0.50mm. Void ratios are 0.66-0.68.

Fig. 5-2-4
Number of cycles required to liquefaction (N) versus loading frequency (f) for diffrent levels of deviator stress. Triaxial stress-controlled tests. Constant deviator stress amplitude (73-74 kPa). Void ratios are 0.62-0.65. Compared with modified data of Wong et al. Seed ,1975. (Triaxial test, Monterey sand).

Fig. 5-2-5
Dependence of the total dissipated energy required for liquefaction (W) on the loading frequency (f) for differently overconsolidated samples. Torque-controlled ring shear tests. Constant shear torque amplitude (56-63 kPa) for all tests. Void ratios are 0.67-0.77 (OCR=1.00), 0.69-0.74 (OCR=1.91-2.14), and 0.67-0.73 (OCR=2.58-2.94).

Fig. 5-2-6
Principle of calculations of the total shear displacement during cyclic loading.

Fig. 5-2-7
Effective stress path of shear-stress-controlled ring shear test (OCR=1.00, f=0.01 Hz, e=0.75)

Fig. 5-2-8
Effective stress path of shear-stress-controlled ring shear test (OCR=1.00, f=1.00 Hz, e=0.73)

Fig. 5-2-9
Total shear displacement(l_t) required for liquefaction versus loading frequency (f) for differently overconsolidated samples. Torque-controlled ring shear tests. Constant shear torque amplitude (56-63 kPa) for all tests. Void ratios are 0.67-0.77 (OCR=1.00), 0.69-0.74 (OCR=1.91-2.14), and 0.67-0.73 (OCR=2.58-2.94).

Fig. 5-2-10
Total axial displacement (h_t) and total dissipated energy (W, required for r_u=0.50 and for liquefaction, versus loading frequency (f) for normally consolidated samples Triaxial stress-controlled tests. Constant deviator stress amplitude (73-74 kPa). Void ratios are 0.62-0.65.

Fig. 5-2-11

Comparison of the total shear displacements (l_t) required for liquefaction, for shear-torque-controlled ($\Delta\tau_{max}$=56-61 kPa; e=0.67-0.77) and shear-displacement-controlled ring shear tests (Δl_{max}=0.49-0.50mm, e=0.66-0.68). All samples are normally consolidated.

Fig. 5-2-12

Comparison of the total dissipated energy (W) required for liquefaction for shear-torque-controlled ($\Delta\tau_{max}$=56-61 kPa; e=0.67-0.77) and shear-displacement-controlled ring shear tests (Δl_{max}=0.49-0.50mm, e=0.66-0.68). All samples are normally consolidated.

Fig.5-2-13

Excess pore pressure ratio(r_u) versus shear displacement(l). Monotonic constant-shear-speed ring test. Normally consolidated samples. Void ratios are 0.60-0.69.

Fig.5-2-14

Accumulated dissipated energy during shearing (W) versus shear displacement (l). Monotonic constant-shear-speed test. Normally consolidated samples. Void ratios are 0.67-0.69.

Fig. 5-2-15

Excess pore pressure ratio (r_u) versus strain. Monotonic constant-strain-rate triaxial compression test. Normally consolidated samples. Void ratios are 0.61-0.63

Fig. 5-2-16

Accumulated dissipated energy (W) versus strain. Monotonic constant-strain-rate triaxial compression test. Normally consolidated samples. Void ratios are 0.61-0.63.

Fig. 5-3-1

Dependence of the total dissipated energy (W) required for liquefaction on the shear displacement amplitude (Δl_{max}) in the shear-displacement-controlled test. Loading frequencies are 0.005-0.5 Hz; Void ratios are 0.58-0.68.See text for comments.

Fig. 5-3-2

Dependence of the number of cycles required for liquefaction on the shear displacement amplitude (Δl_{max}) in the shear-displacement-controlled test. Loading frequencies are 0.005-0.5 Hz; Void ratios are 0.58-0.68.See text for comments.

Fig. 5-3-3

Mechanism of spending of the energy (W) required for liquefaction in the shear-displacement-controlled test. Loading frequencies are 0.005-0.5 Hz; Void ratios are 0.58-0.68. See text for comments.

Fig. 5-3-4

Time series of the shear-displacement-controlled ring shear tests. f=0.01 Hz; Δl_{max}=7.25mm; e=0.59;

Fig. 5-3-5

Dependence of the r_u/l_{max} parameter on the shear displacement amplitude (l_{max}), in the shear-displacement-controlled test. Loading frequencies are 0.005-0.5 Hz; Void ratios are 0.58-0.68.

Fig. 5-3-6

Effectiveness of the excess pore pressure generation (r_u/l_t) during the first and the second cycles (N) in the shear-displacement-controlled test. Loading frequencies are 0.005-0.5 Hz; Void ratios are 0.58-0.68

Fig. 1-2-1

Influence of frequency on undrained strength of loose Monterrey sand under cyclic loading-simple shear conditions (after Peacock & Seed, 1968)

Fig. 1-2-2

Effect of frequency on cyclic stresses causing initial liquefaction of Monterrey sand (after Wong et al., 1975)

Fig. 2-1-1
Stresses applied to ring shear sample.
σ :normal stress; τ : shear stress.

Fig. 2-1-2

Principal scheme of ring shear apparatus (DPRI-4) with enlarged sample assembly part.
(see text for comments)

Fig. 2-1-3
Normal stress control systems: with one load cell (A) and two load cells (B).
(see text for comments)

Fig. 2-1-4
Undrained shear box (section of half part)

Upper drainage line

Valve

Bolt

Cap plate

"O"-rings

Loading Plate

Porous metal

Filter paper

Pore pressure transducer

Metal filters

Sample

Rubber edge

Felt cloth filter

Filter paper

Lower drainage line

Porous metal

Valve

Fig. 2-2-1

Principal scheme of triaxial compression apparatus with auxiliary units

Fig. 2-4-1

Relationship between degree of saturation and pore pressure parameter
(after Sassa, 1988; Black & Lee, 1973)

Fig. 3-2-1

Stress path mechanism for ring shear test and triaxial compression tests. σ :normal stress, σ₁ : axial stress; σ₃ : confining stress; τ : shear stress.

$p=(\sigma_1+\sigma_2)/2$; $q=(\sigma_1-\sigma_2)/2$

Fig. 5-1-1

The energy (W) dissipated during constant-shear-speed shearing (a), and cyclic loading (b)

Fig. 5-2-1.

Number of cycles required to liquefaction (N) versus loading frequency (f) for differently overconsolidated samples (torque-controlled ring shear tests). Constant shear torque amplitude (56-63 kPa) for all tests. Void ratios are 0.67-0.77 (OCR=1.00), 0.69-0.74 (OCR=1.91-2.14), and 0.67-0.73 (OCR=2.58-2.94).

Fig. 5-2-2
Number of cycles required to liquefaction (N) versus loading frequency (f) for different levels of cyclic stress. (Simple shear test, Monterey sand). Modified from Peacock & Seed (1968)

Fig. 5-2-3.

Number of cycles (N), total dissipated energy (W), and total shear displacement required for liquefaction versus loading frequency (f) for normally consolidated samples. Shear-displacement-controlled ring shear tests. Amplitudes of the shear displacement are 0.49-0.50mm. Void ratios are 0.66-0.68.

Fig. 5-2-4

Number of cycles required to liquefaction (N) versus loading frequency (f) for diffrent levels of deviator stress. Triaxial stress-controlled tests. Constant deviator stress amplitude (73-74 kPa). Void ratios are 0.62-0.65. Compared with modified data of Wong et al., 1975. (Triaxial test, Monterey sand).

Fig. 5-2-5

Dependence of the total dissipated energy required for liquefaction (W) on the loading frequency (f) for differently overconsolidated samples. Torque-controlled ring shear tests. Constant shear torque amplitude (56-63 kPa) for all tests. Void ratios are 0.67-0.77 (OCR=1.00), 0.69-0.74 (OCR=1.91-2.14), and 0.67-0.73 (OCR=2.58-2.94).

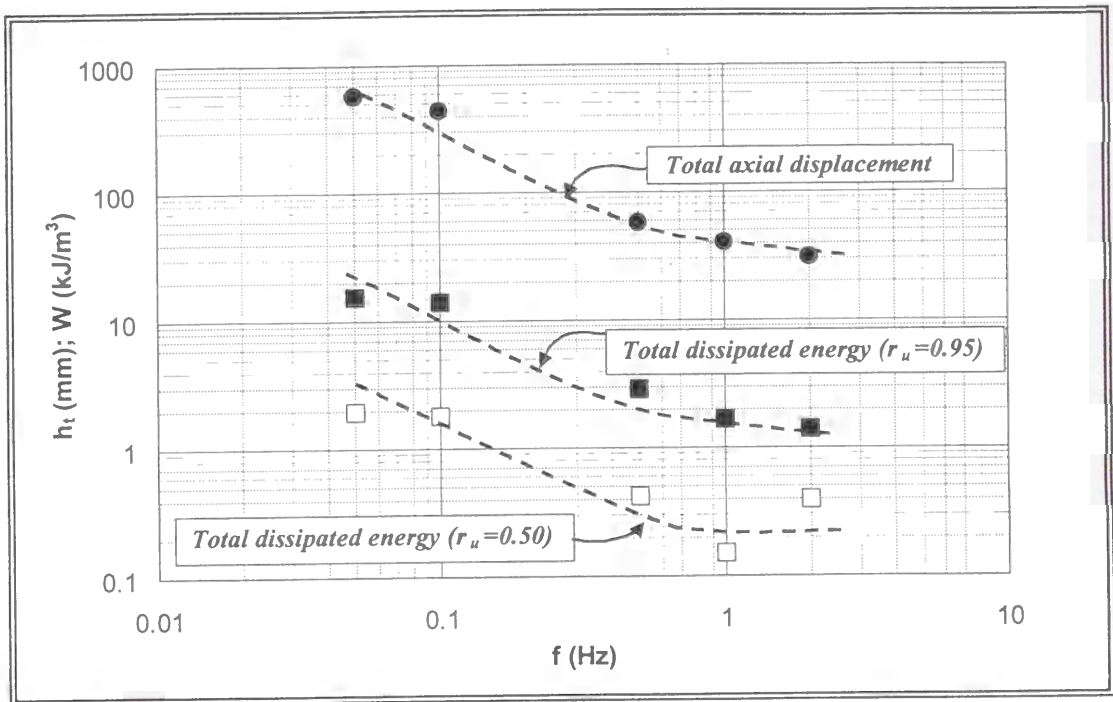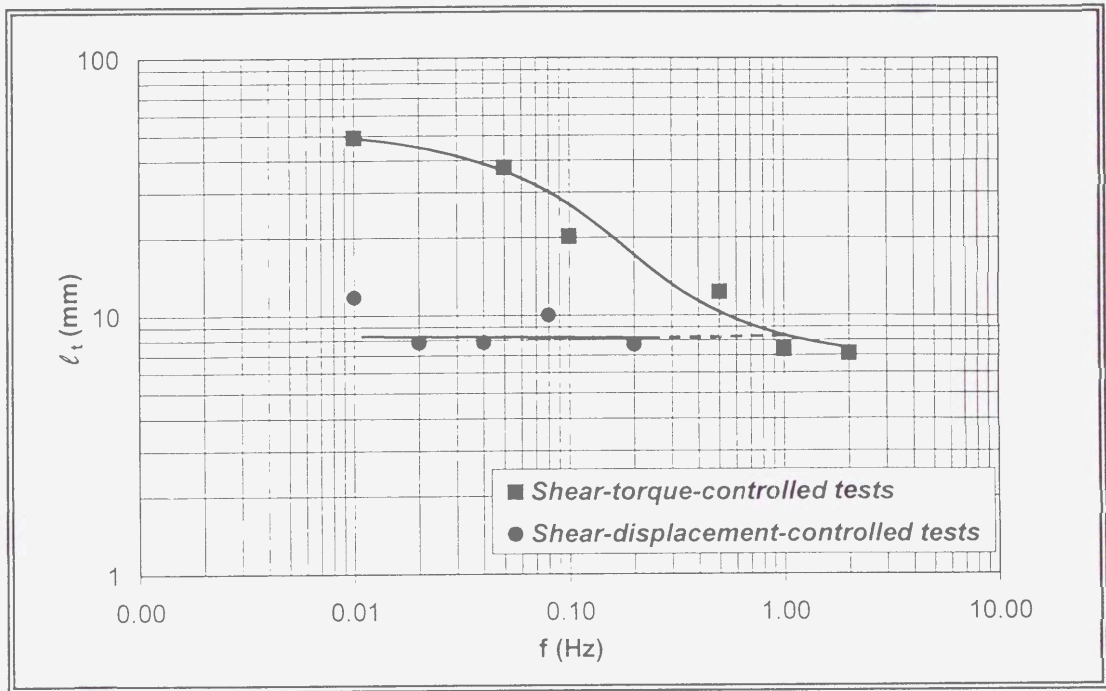**Fig. 5-2-6**

Principle of calculations of the total shear displacement during cyclic loading.

Fig. 5-2-7

Effective stress path of shear-stress-controlled ring shear test (OCR=1.00, f=0.01 Hz, e=0.75)

Fig. 5-2-8

Effective stress path of shear-stress-controlled ring shear test (OCR=1.00, f=1.00 Hz, e=0.73)

Fig. 5-2-9

Total shear displacement(l_t) required for liquefaction versus loading frequency (f) for differently overconsolidated samples. Torque-controlled ring shear tests. Constant shear torque amplitude (56-63 kPa) for all tests. Void ratios are 0.67-0.77 (OCR=1.00), 0.69-0.74 (OCR=1.91-2.14), and 0.67-0.73 (OCR=2.58-2.94).

Fig. 5-2-10

Total axial displacement (h_t) and total dissipated energy (W, required for $r_u=0.50$ and for liquefaction, versus loading frequency (f) for normally consolidated samples Triaxial stress-controlled tests. Constant deviator stress amplitude (73-74 kPa). Void ratios are 0.62-0.65.

Fig. 5-2-11

Comparison of the total shear displacements (l_t) required for liquefaction, for shear-torque-controlled ($\Delta\tau_{max}$=56-61 kPa; e=0.67-0.77) and shear-displacement-controlled ring shear tests (Δl_{max}=0.49-0.50mm, e=0.66-0.68). All samples are normally consolidated.
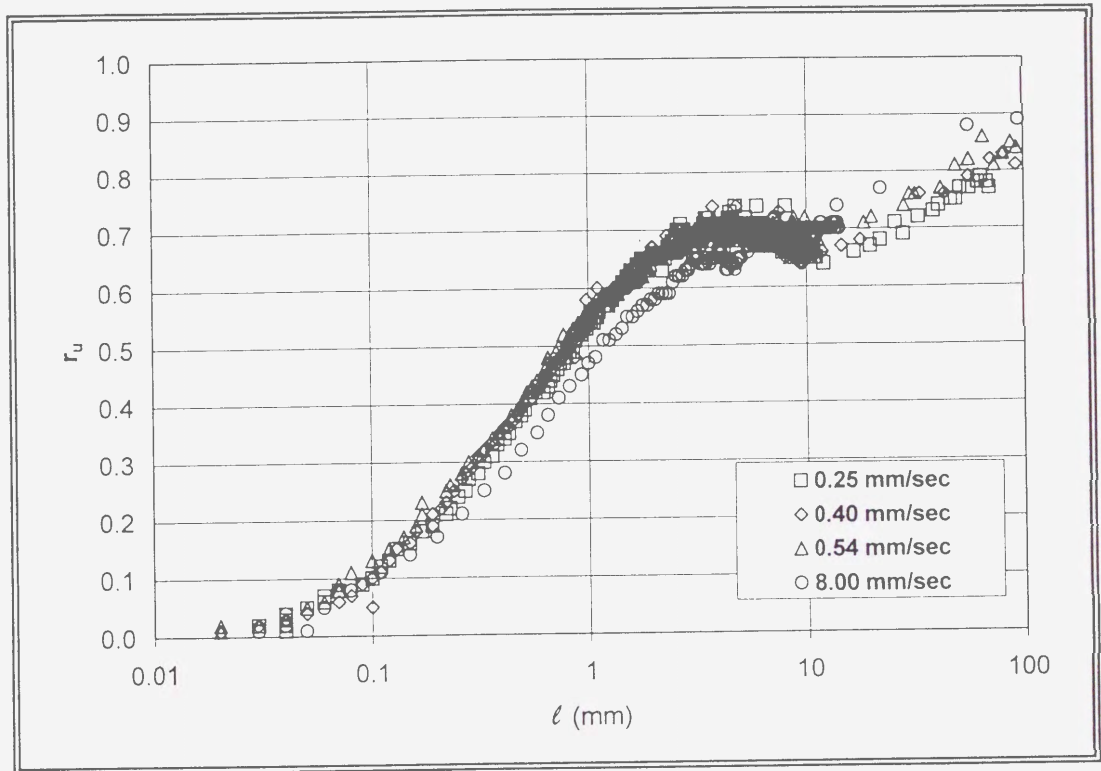
Fig. 5-2-12

Comparison of the total dissipated energy (W) required for liquefaction for shear-torque-controlled ($\Delta\tau_{max}$=56-61 kPa; e=0.67-0.77) and shear-displacement-controlled ring shear tests (Δl_{max}=0.49-0.50mm, e=0.66-0.68). All samples are normally consolidated.

Fig.5-2-13

Excess pore pressure ratio(r_u) versus shear displacement(l). Monotonic constant-shear-speed ring test. Normally consolidated samples. Void ratios are 0.60-0.69.
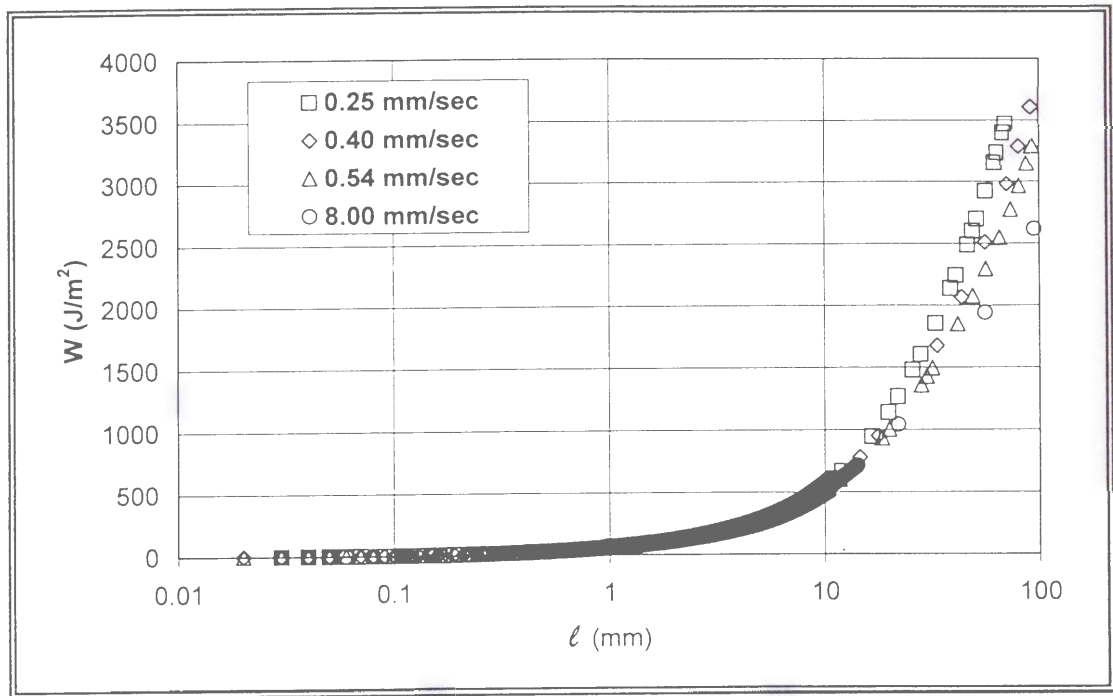
Fig.5-2-14

Accumulated dissipated energy during shearing (W) versus shear displacement (l).
Monotonic constant-shear-speed test. Normally consolidated samples. Void ratios
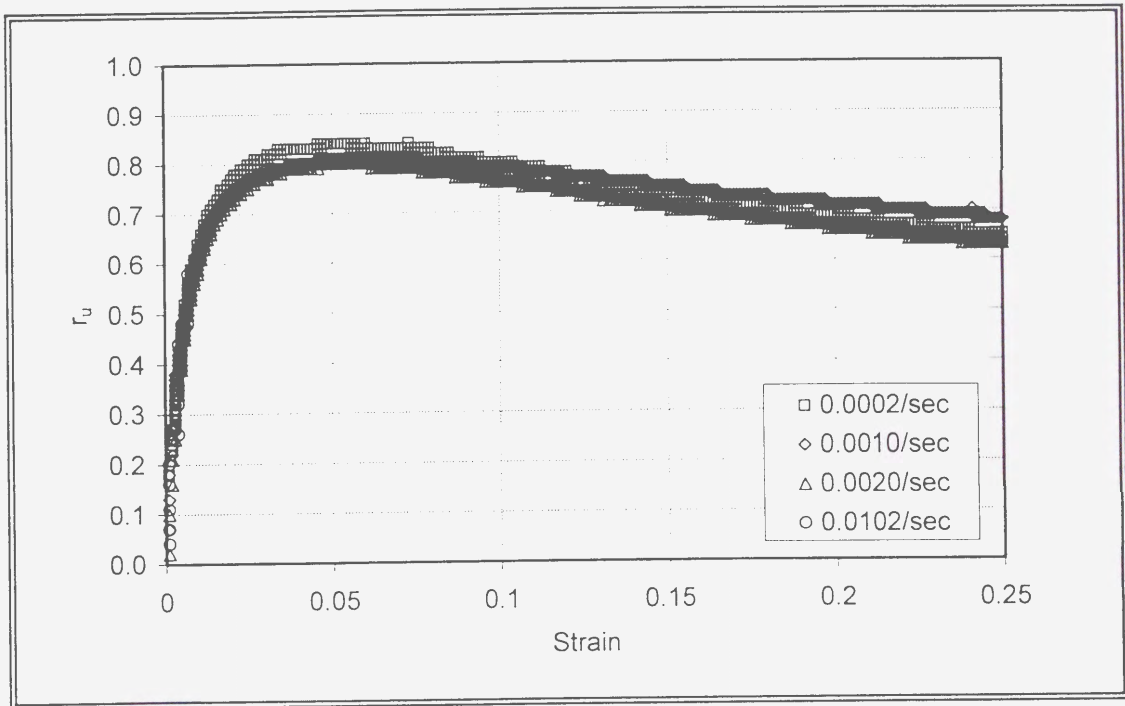*are 0.67-0.69.*

Fig. 5-2-15

Excess pore pressure ratio (r_u) versus strain. Monotonic constant-strain-rate triaxial compression test. Normally consolidated samples. Void ratios are 0.61-0.63
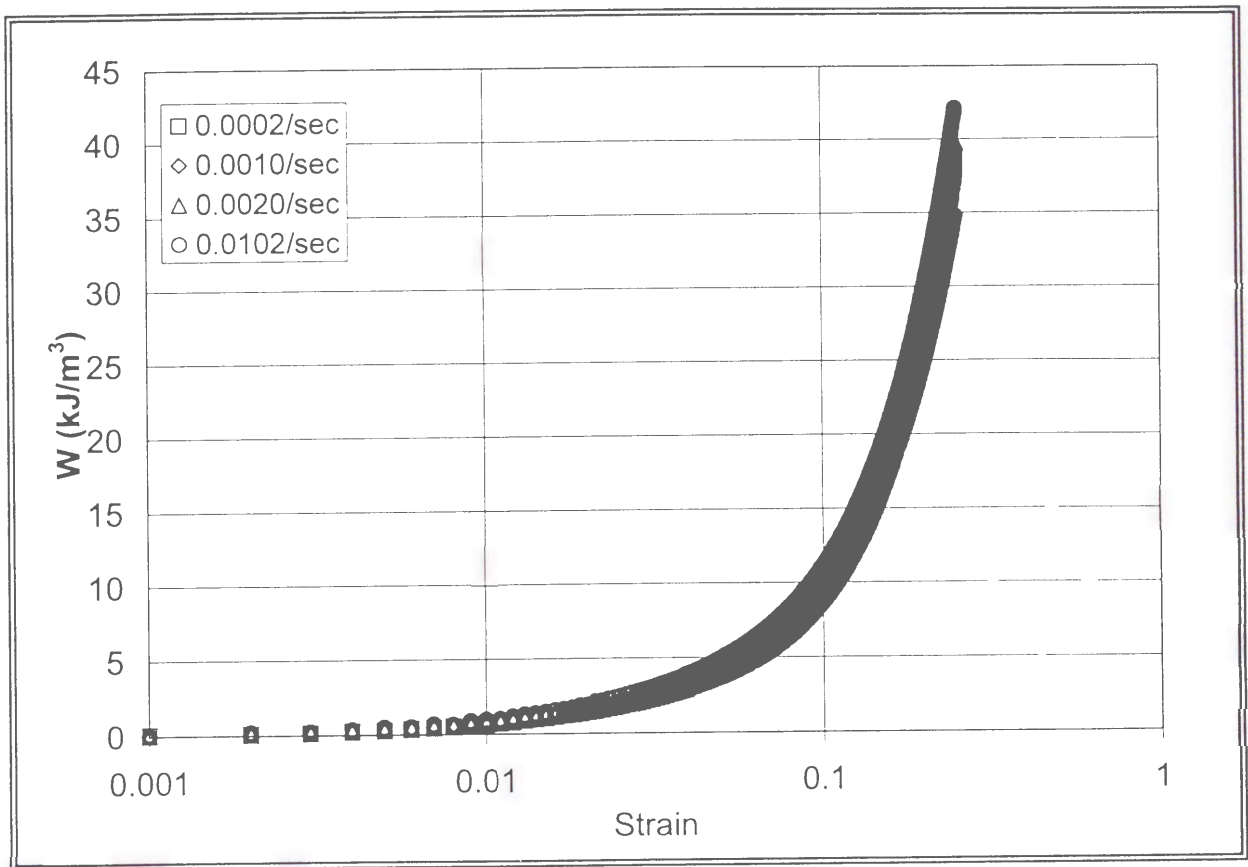
Fig. 5-2-16

Accumulated dissipated energy (W) versus strain. Monotonic constant-strain-rate triaxial compression test. Normally consolidated samples. Void ratios are 0.61-0.63.
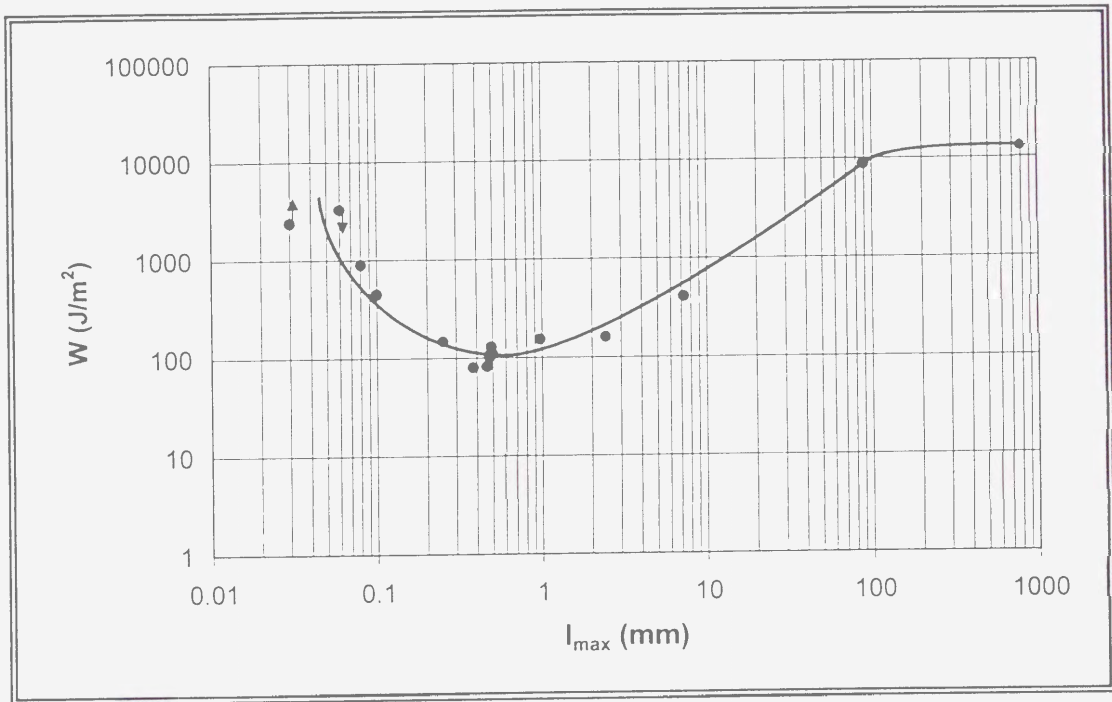
Fig. 5-3-1

Dependence of the total dissipated energy (W) required for liquefaction on the shear displacement amplitude (Δl_{max}) in the shear-displacement-controlled test. Loading frequencies are 0.005-0.5 Hz; Void ratios are 0.58-0.68.See text for comments.

Fig. 5-3-2

Dependence of the number of cycles required for liquefaction on the shear displacement amplitude (Δl_{max}) in the shear-displacement-controlled test. Loading frequencies are 0.005-0.5 Hz; Void ratios are 0.58-0.68.See text for comments.
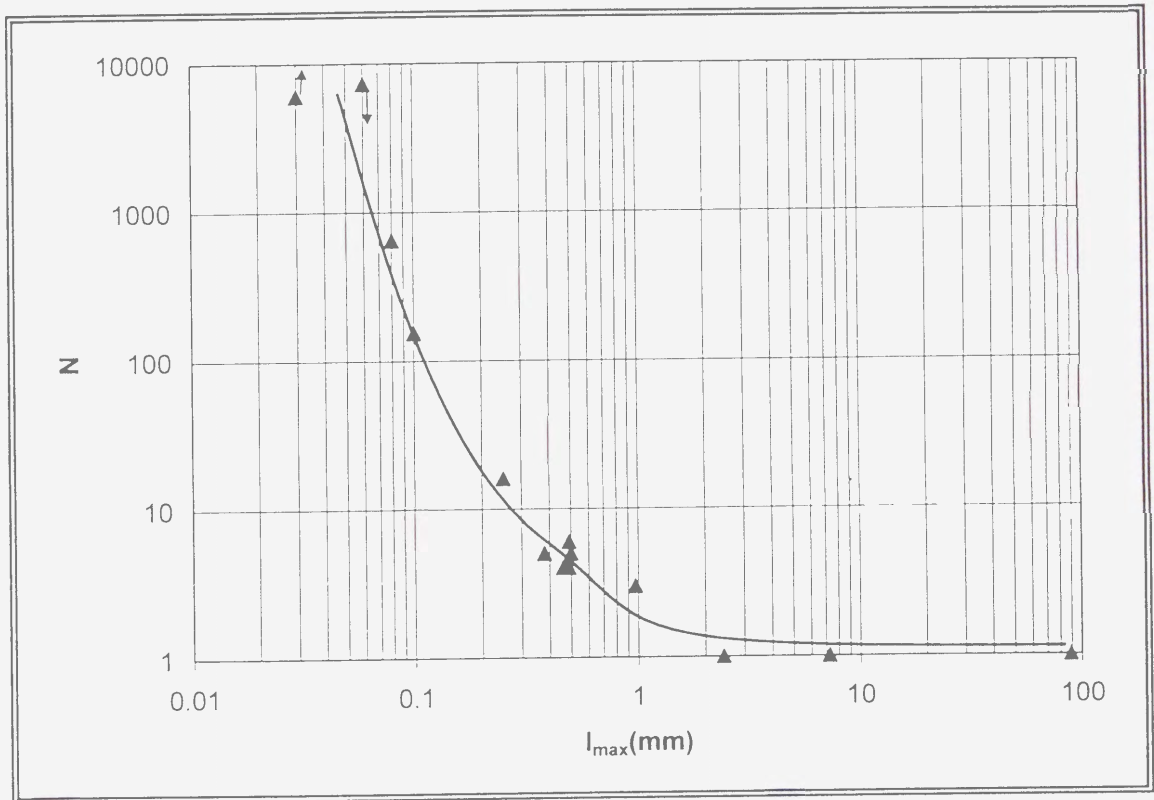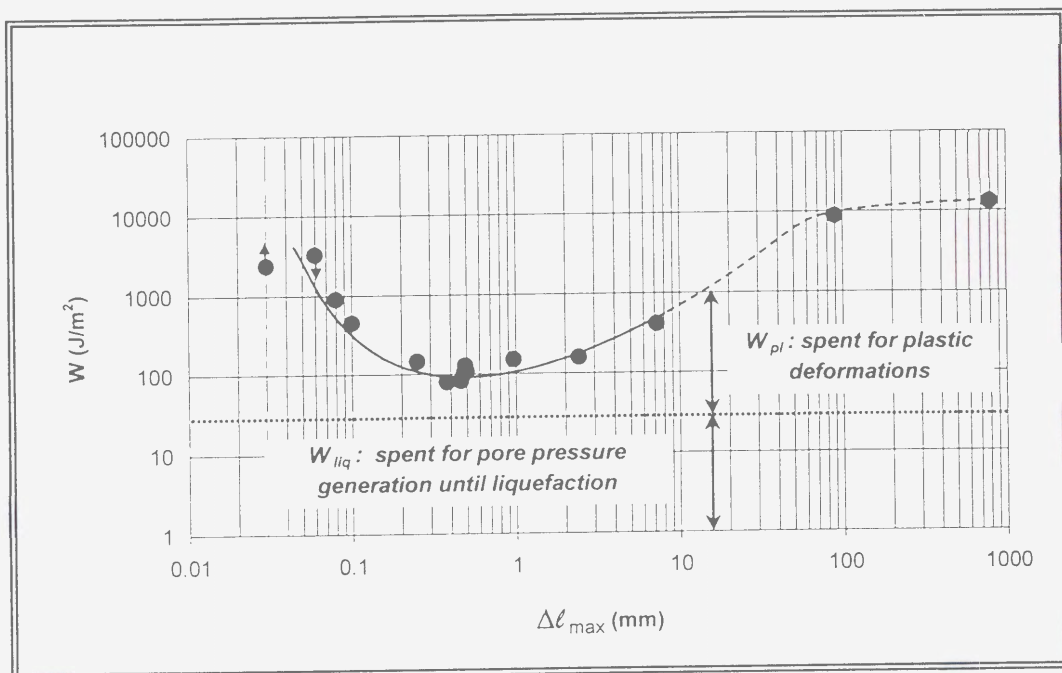
Fig. 5-3-3

Mechanism of spending of the energy (W) required for liquefaction in the shear-displacement-controlled test. Loading frequencies are 0.005-0.5 Hz; Void ratios are 0.58-0.68. See text for comments.
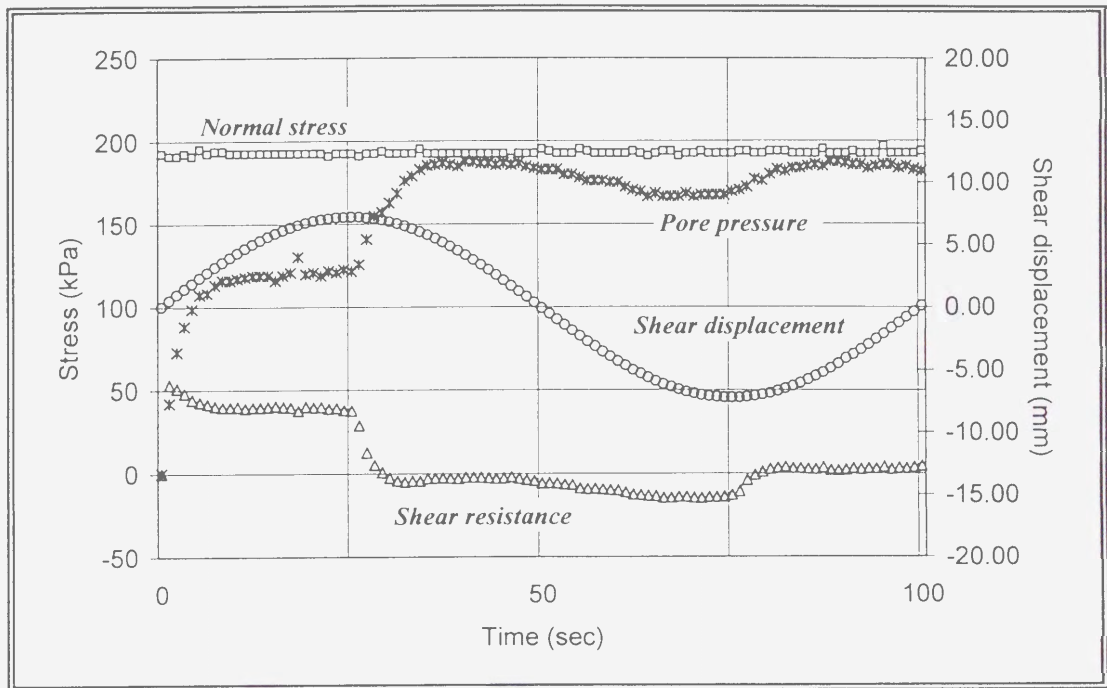
Fig. 5-3-4

Time series of the shear-displacement-controlled ring shear tests. f=0.01 Hz; Δl_{max}=7.25mm; e=0.59;
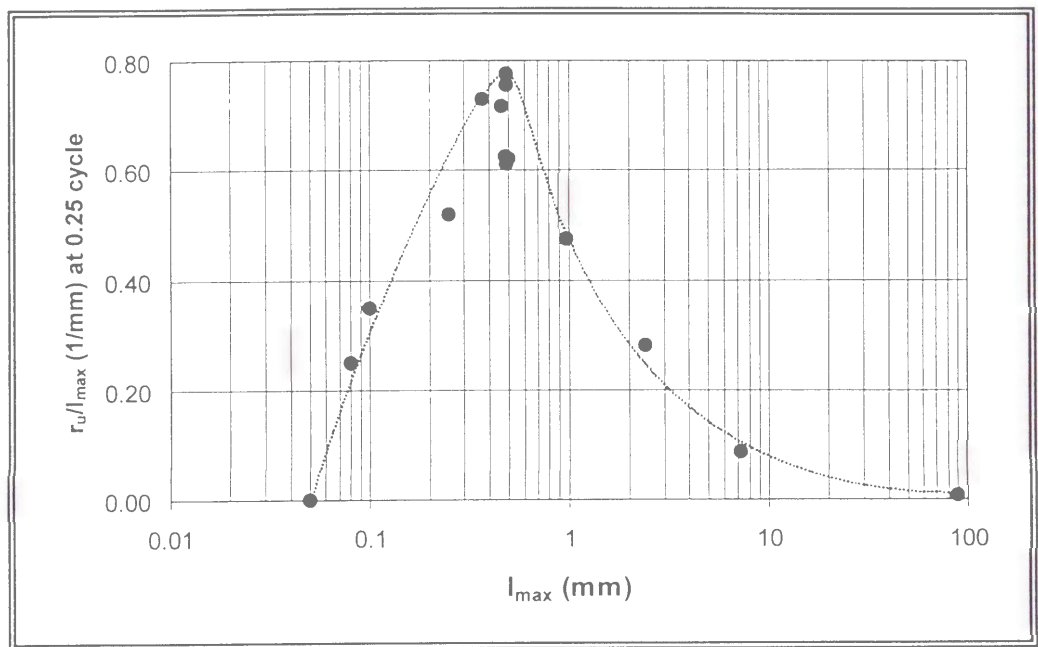
Fig. 5-3-5

Dependence of the $r_u/\Delta l_{max}$ parameter on the shear displacement amplitude (Δl_{max}), in the shear-displacement-controlled test. Loading frequencies are 0.005-0.5 Hz; Void ratios are 0.58-0.68.
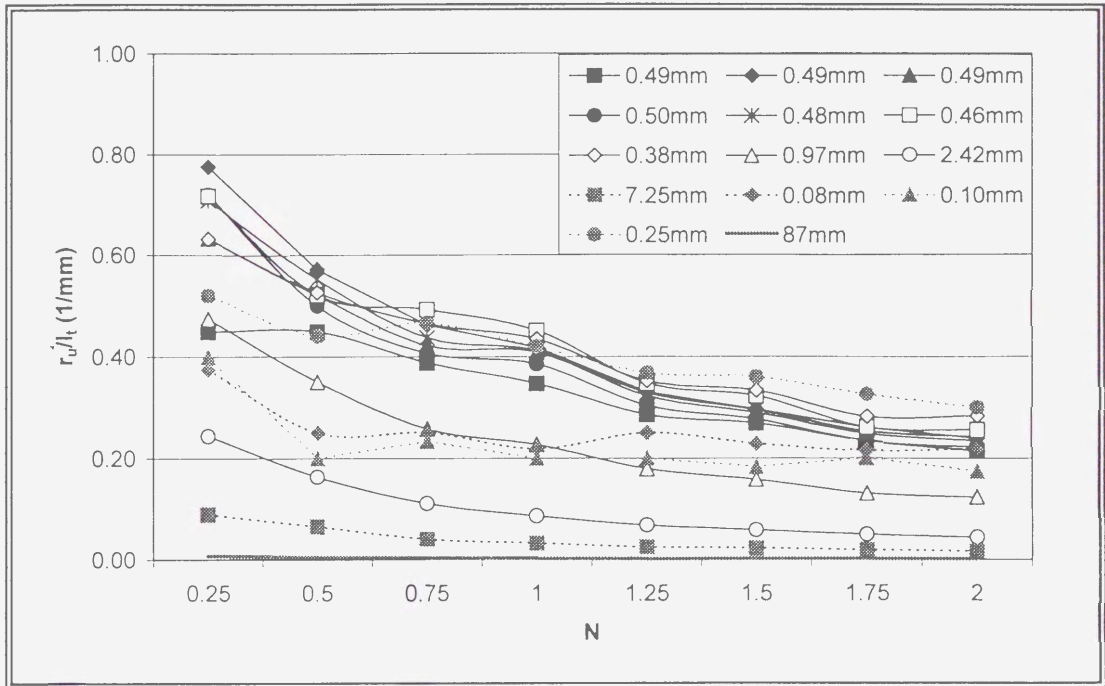
Fig. 5-3-6

Effectiveness of the excess pore pressure generation (r_u/l_t) during the first and the second cycles (N) in the shear-displacement-controlled test. Loading frequencies are 0.005-0.5 Hz; Void ratios are 0.58-0.68.

APPENDIX 1

TEST No. 1

PARAMETER	UNIT	VALUE
Apparatus		Ring shear (DPRI-4)
Test type		Cyclic shear-torque-controlled
Loading frequency	Hz	0.01
Data acquisition rate	point/cycle	1000
Void ratio		0.77
Consolidation stress (σ_{con})	kPa	220
Initial effective normal stress (σ'_{in})	kPa	220
OCR		1.00
Pore pressure coefficient B_D		0.95
Back pressure (u_0)	kPa	106

The following plots are included:

- **Plot No. 1-1**

Time series of total normal stress, shear resistance, pore pressure, and shear displacement.

- **Plot No. 1-2**

Effective stress path.

Test No.1 — Cyclic shear-torque-controlled test. OCR=1.00; f=0.01 Hz. — Plot No.1-1

Y-axis: Shear Resistance (kPa)

X-axis: Effective Normal Stress (kPa)

Test No.1   Cyclic shear-torque-controlled ring shear test. OCR=1.00. f=0.01 Hz.   Plot No.1-2

TEST No. 2

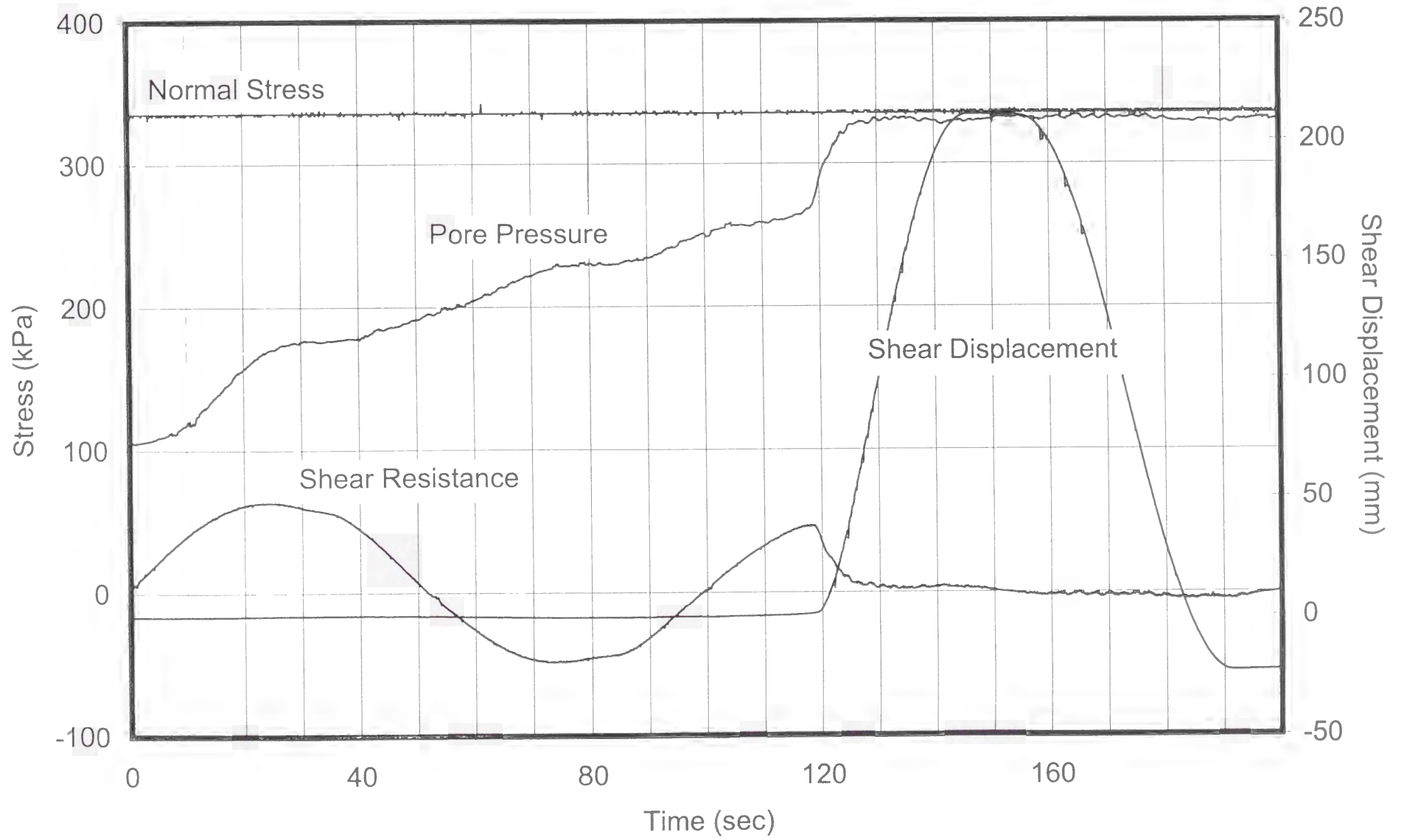| PARAMETER	UNIT	VALUE
Apparatus		Ring shear (DPRI-4)
Test type		Cyclic shear-torque-controlled
Loading frequency	Hz	0.05
Data acquisition rate	point/cycle	200
Void ratio		0.74
Consolidation stress (σ_{con})	kPa	213
Initial effective normal stress (σ'_{in})	kPa	213
OCR		1.00
Pore pressure coefficient B_D		0.95
Back pressure (u_0)	kPa	69

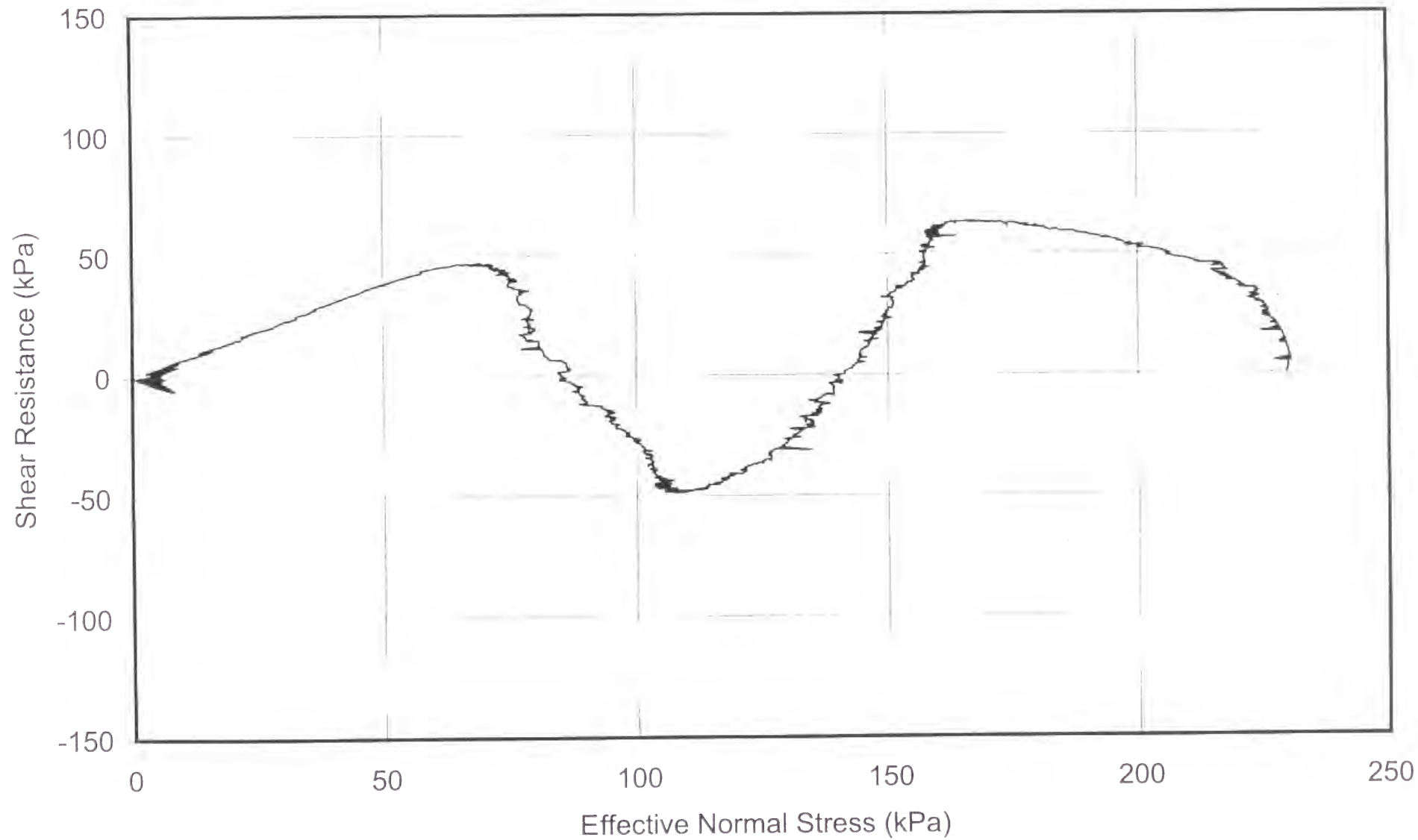**The following plots are included:**

- **Plot No. 2-1**
Time series of total normal stress, shear resistance, pore pressure, and shear displacement.

- **Plot No. 2-2**
Effective stress path.

Normal Stress

Pore Pressure

Shear Displacement

Shear Resistance

Stress (kPa)

Shear Displacement (mm)

Time (sec)

Test No.2

Cyclic shear-torque-controlled test. OCR=1.00; f=0.05 Hz.

Plot No.2-1

Cyclic shear-torque-controlled test. OCR=1.00; f=0.05 Hz.

Test No.2

Plot No.2-2

TEST No. 3

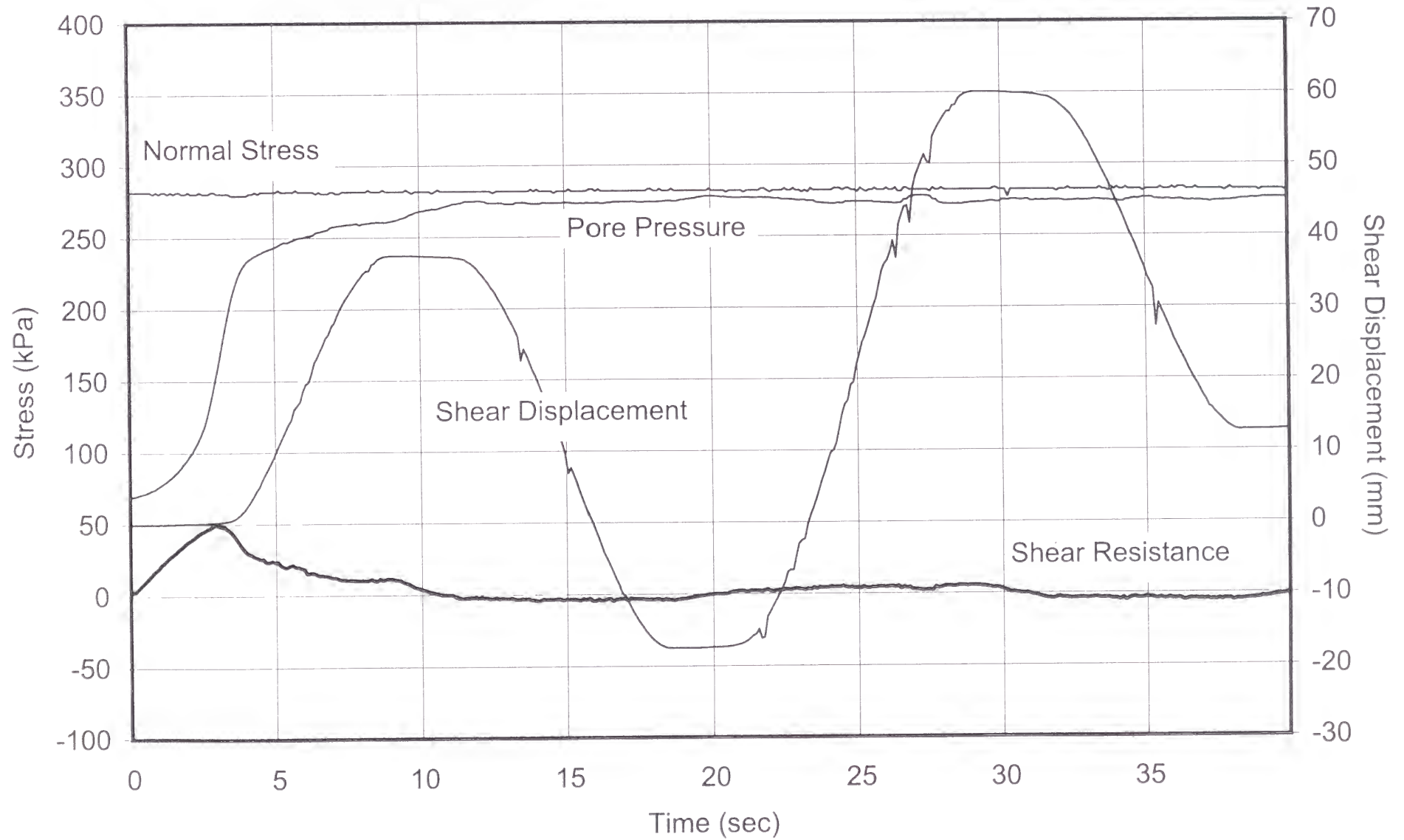| PARAMETER	UNIT	VALUE
Apparatus		Ring shear (DPRI-4)
Test type		Cyclic shear-torque-controlled
Loading frequency	Hz	0.10
Data acquisition rate	point/cycle	100
Void ratio		0.75
Consolidation stress (σ_{con})	kPa	201
Initial effective normal stress (σ'_{in})	kPa	201
OCR		1.00
Pore pressure coefficient B_D		0.98
Back pressure (u_0)	kPa	84

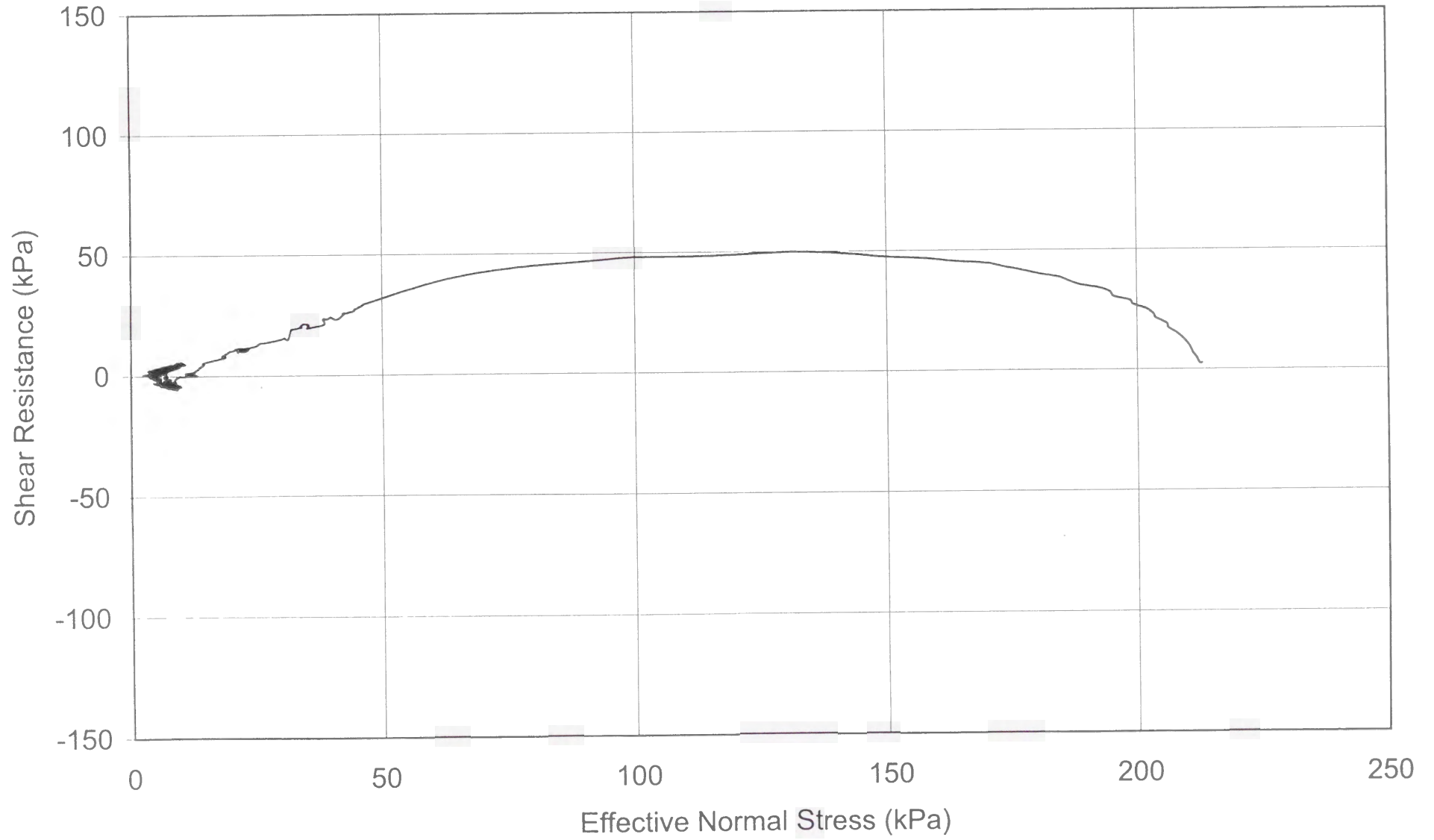**The following plots are included:**

- **Plot No. 3-1**
Time series of total normal stress, shear resistance, pore pressure, and shear displacement.

- **Plot No. 3-2**
Effective stress path.

Cyclic shear-torque-controlled test. OCR=1.00; f=0.10 Hz

Test No.3

Plot No.3-1

Cyclic shear-torque-controlled test. OCR=1.00; f=0.10 Hz.

Test No.3

Plot No.3-2

TEST No. 4

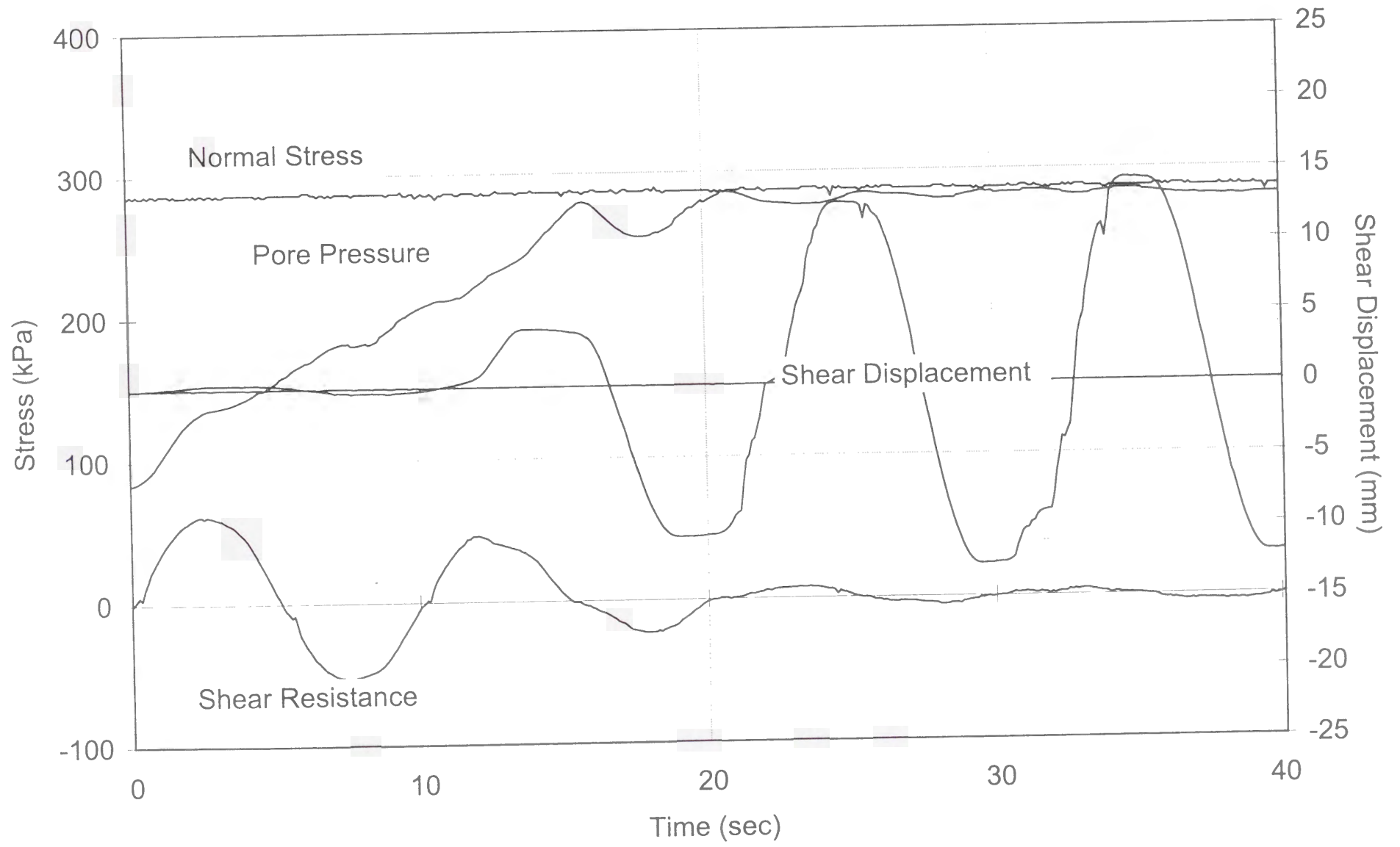| PARAMETER	UNIT	VALUE
Apparatus		Ring shear (DPRI-4)
Test type		Cyclic shear-torque-controlled
Loading frequency	Hz	0.50
Data acquisition rate	point/cycle	25
Void ratio		0.72
Consolidation stress (σ_{con})	kPa	210
Initial effective normal stress (σ'_{in})	kPa	210
OCR		1.00
Pore pressure coefficient B_D		0.96
Back pressure (u_0)	kPa	85

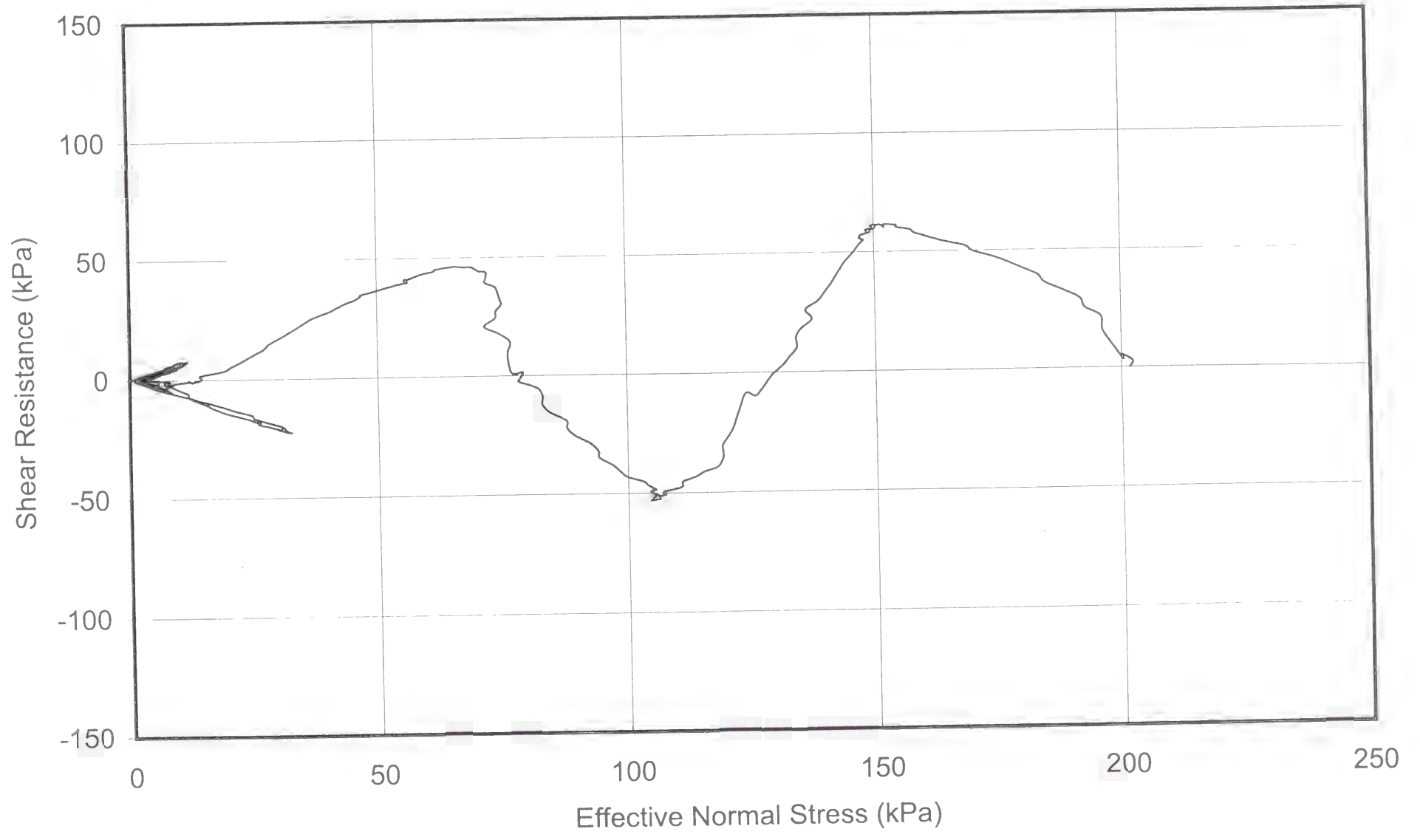## The following plots are included:

- **Plot No. 4-1**

Time series of total normal stress, shear resistance, pore pressure, and shear displacement.

- **Plot No. 4-2**

Effective stress path.

Cyclic shear-torque-controlled test. OCR=1.00; f=0.50 Hz.

Test No.4

Plot No.4-1

Cyclic shear-torque-controlled test. OCR=1.00; f=0.50 Hz.

Test No.4

Plot No.4-2

TEST No. 5

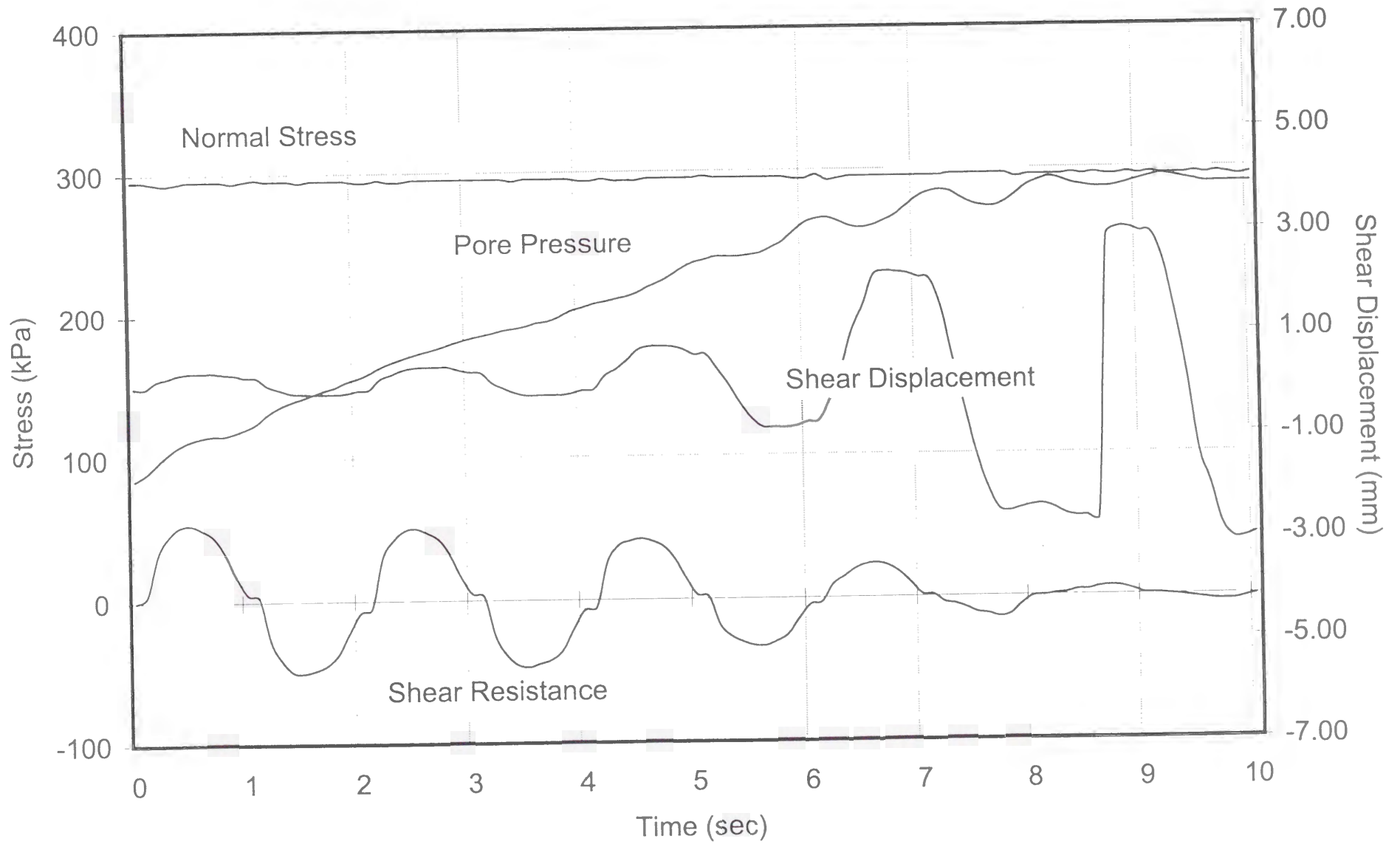| PARAMETER	UNIT	VALUE
Apparatus		Ring shear (DPRI-4)
Test type		Cyclic shear-torque-controlled
Loading frequency	Hz	1.00
Data acquisition rate	point/cycle	50
Void ratio		0.71
Consolidation stress (σ_{con})	kPa	206
Initial effective normal stress (σ'_{in})	kPa	206
OCR		1.00
Pore pressure coefficient B_D		0.97
Back pressure (u_0)	kPa	103

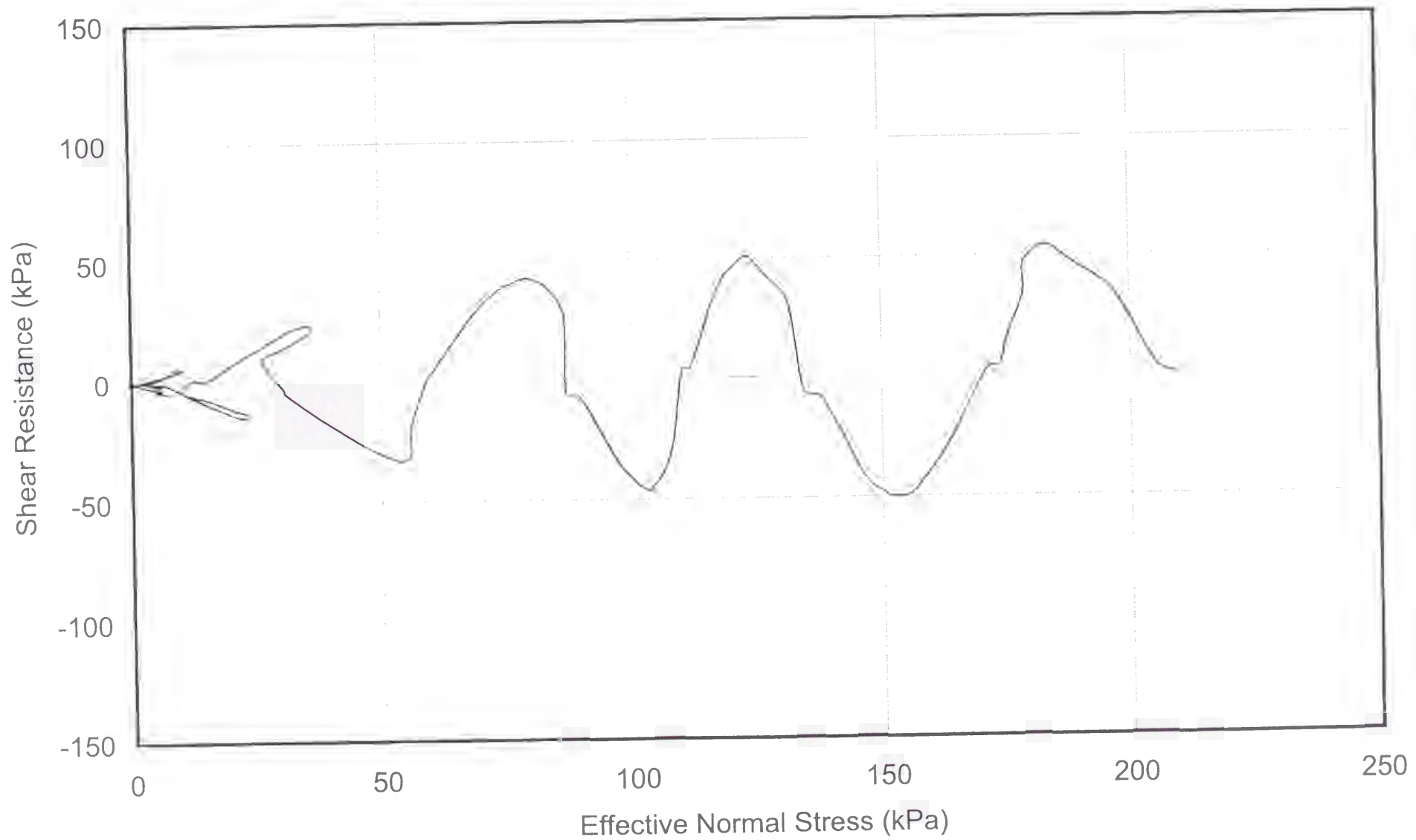The following plots are included:

- **Plot No. 5-1**
Time series of total normal stress, shear resistance, pore pressure, and shear displacement.

- **Plot No. 5-2**
Effective stress path.

Cyclic shear-torque-controlled test. OCR=1.00; f=1.00 Hz.

Test No.5

Plot No.5-1

Cyclic shear-torque-controlled test. OCR=1.00; f=1.00 Hz.

Test No.5

Plot No.5-2

TEST No. 6

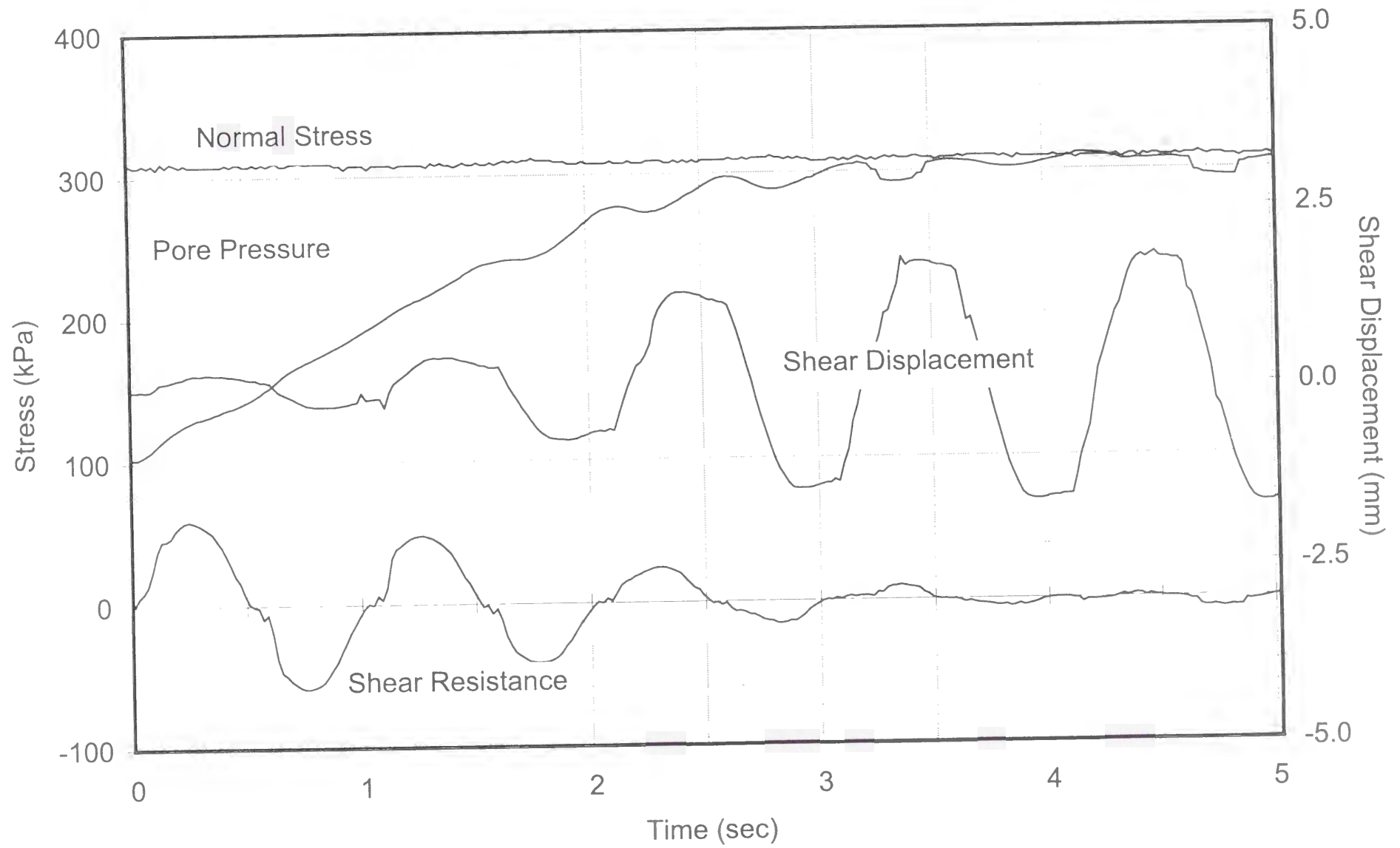| PARAMETER	UNIT	VALUE
Apparatus		Ring shear (DPRI-4)
Test type		Cyclic shear-torque-controlled
Loading frequency	Hz	2.00
Data acquisition rate	point/cycle	50
Void ratio		0.67
Consolidation stress (σ_{con})	kPa	199
Initial effective normal stress (σ'_{in})	kPa	199
OCR		1.00
Pore pressure coefficient B_D		0.96
Back pressure (u_0)	kPa	108

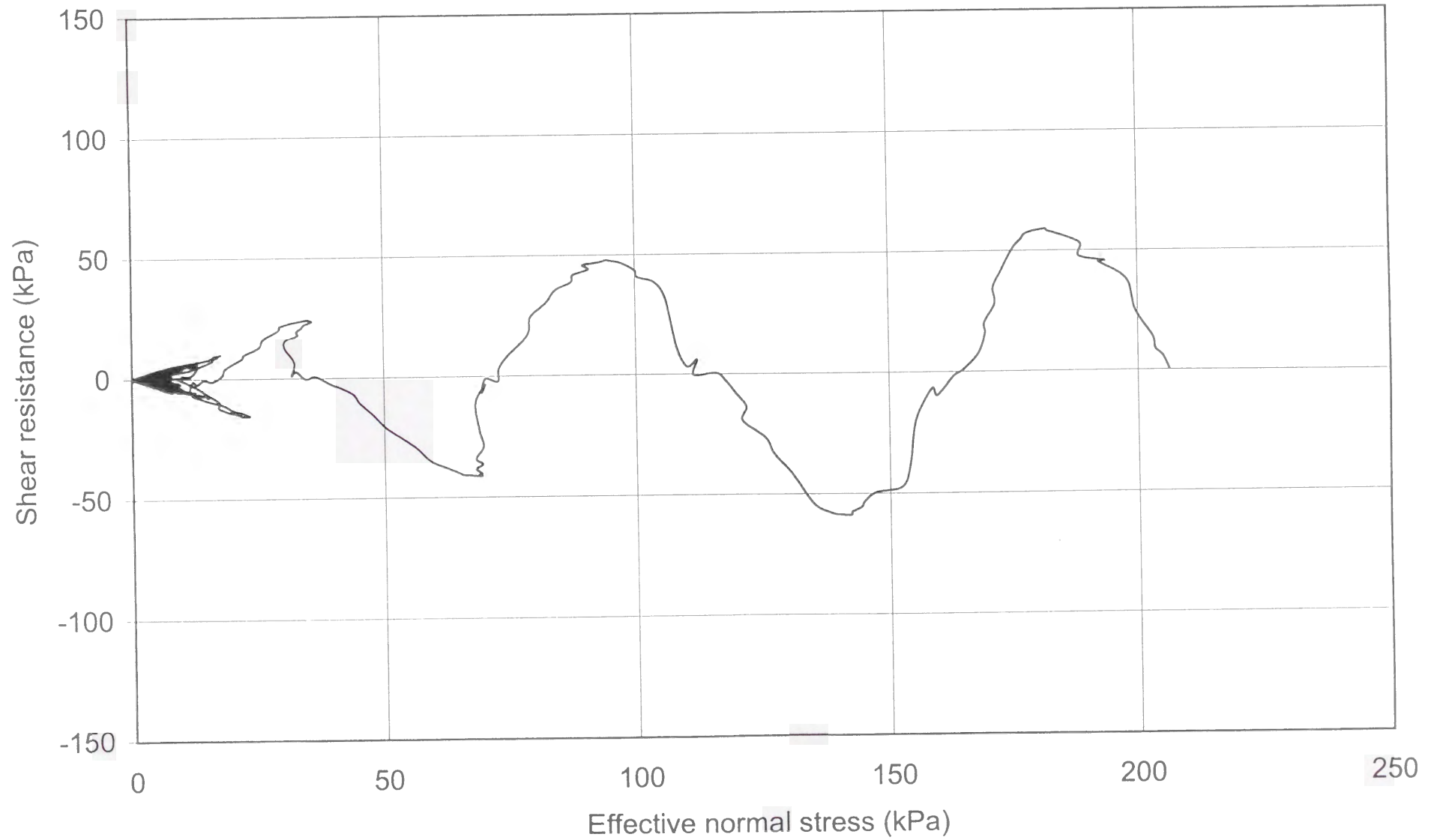The following plots are included:

- **Plot No. 6-1**

Time series of total normal stress, shear resistance, pore pressure, and shear displacement.

- **Plot No. 6-2**

Effective stress path.

Normal Stress

Pore Pressure

Shear Displacement

Shear Resistance

Test No.6 — Cyclic shear-torque-controlled test. OCR=1.00; f=2.00 Hz. — Plot No.6-1

Shear Resistance (kPa) vs Effective Normal Stress (kPa)

Test No.6

Cyclic shear-torque-controlled test. OCR=1.00; f=2.00 Hz.

Plot No.6-2

TEST No. 7

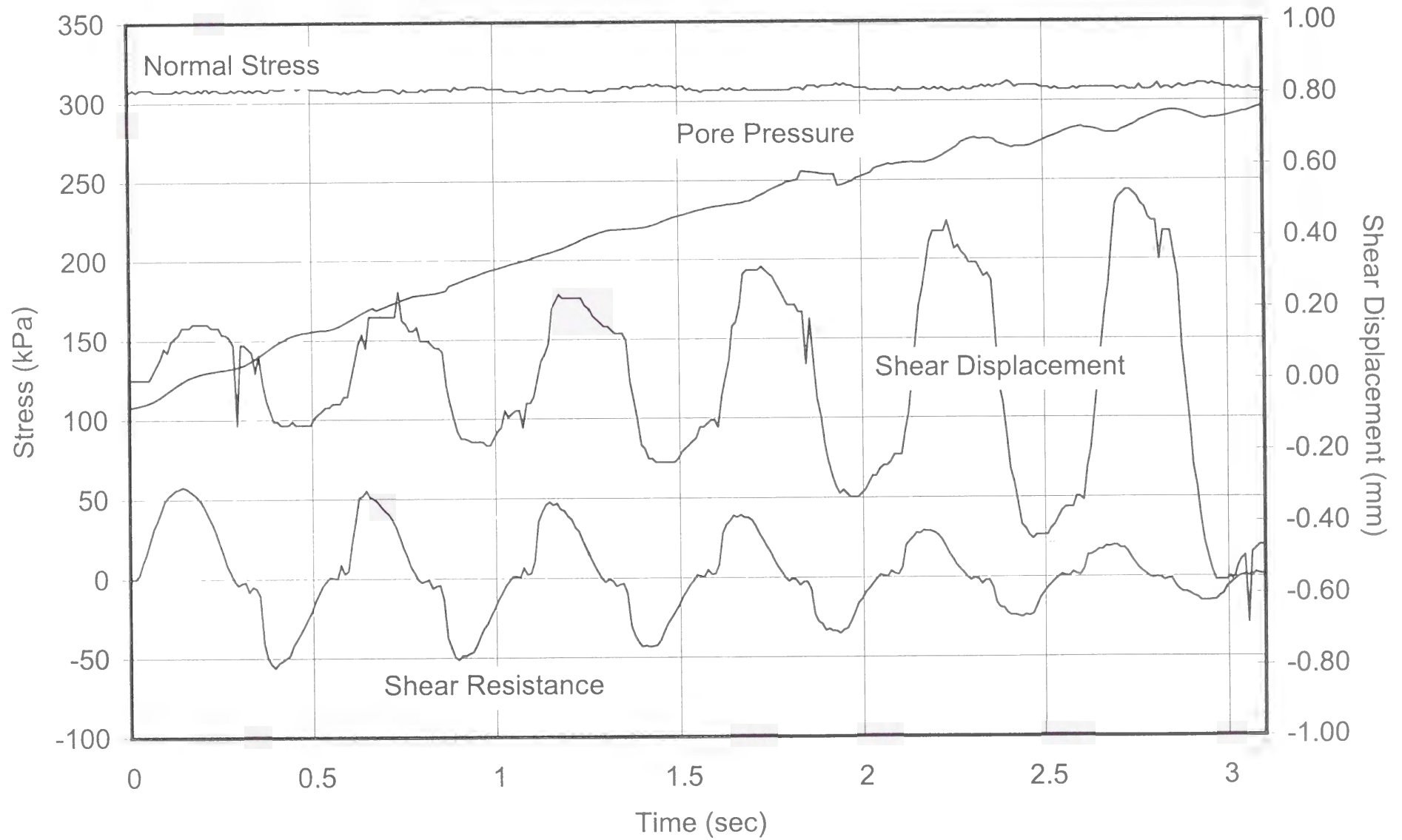| PARAMETER	UNIT	VALUE
Apparatus		Ring shear (DPRI-4)
Test type		Cyclic shear-torque-controlled
Loading frequency	Hz	0.01
Data acquisition rate	point/cycle	200
Void ratio		0.73
Consolidation stress (σ_{con})	kPa	400
Initial effective normal stress (σ'_{in})	kPa	205
OCR		1.95
Pore pressure coefficient B_D		0.95
Back pressure (u_0)	kPa	64

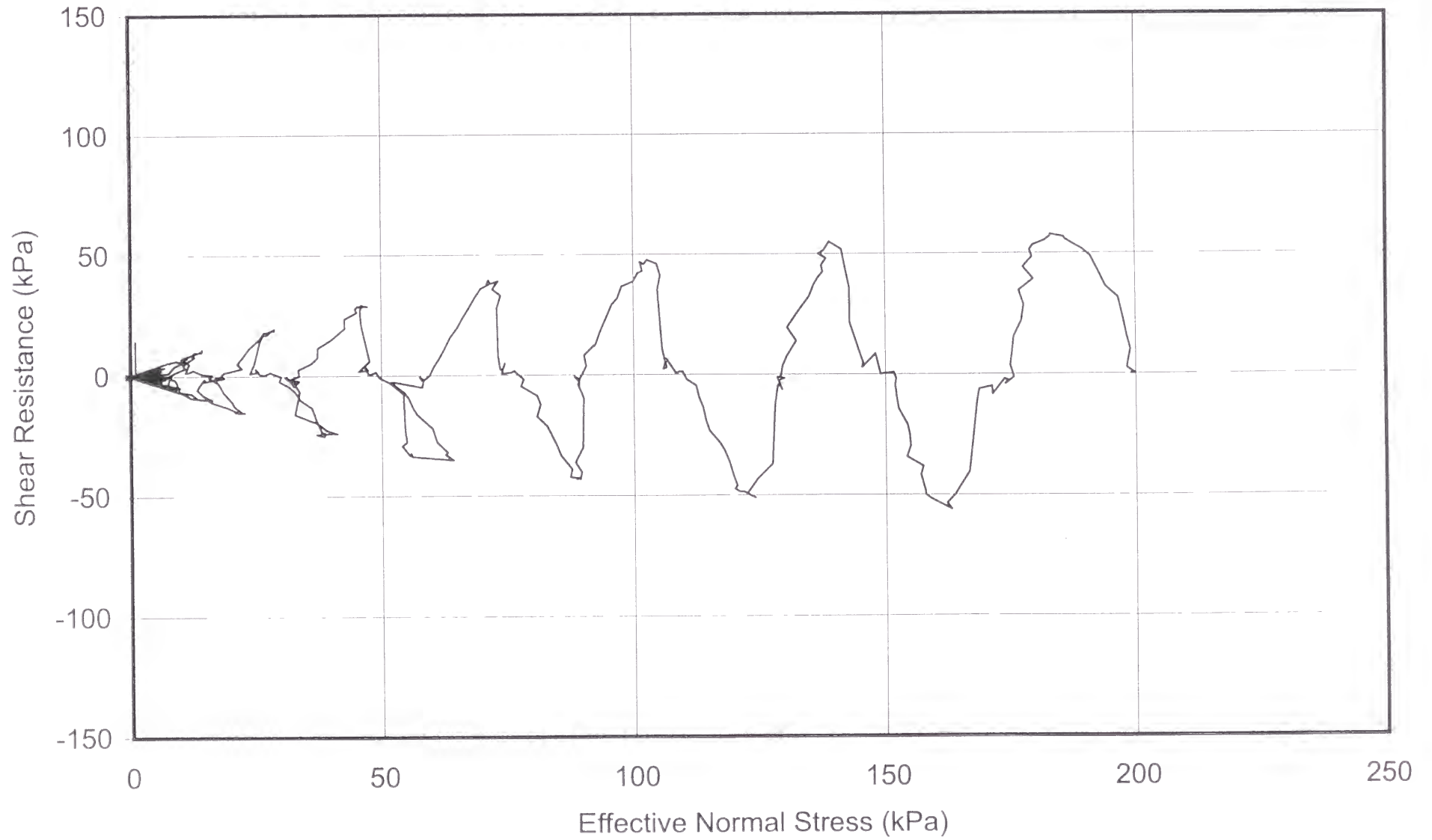The following plots are included:

- **Plot No. 7-1**
Time series of total normal stress, shear resistance, pore pressure, and shear displacement.

- **Plot No. 7-2**
Effective stress path.

Test No.7   Cyclic shear-torque-controlled test. OCR=1.95; f=0.01 Hz.   Plot No.7-1

Cyclic shear-torque-controlled test. OCR=1.95; f=0.01 Hz.

Test No.7

Plot No.7-2

TEST No. 8

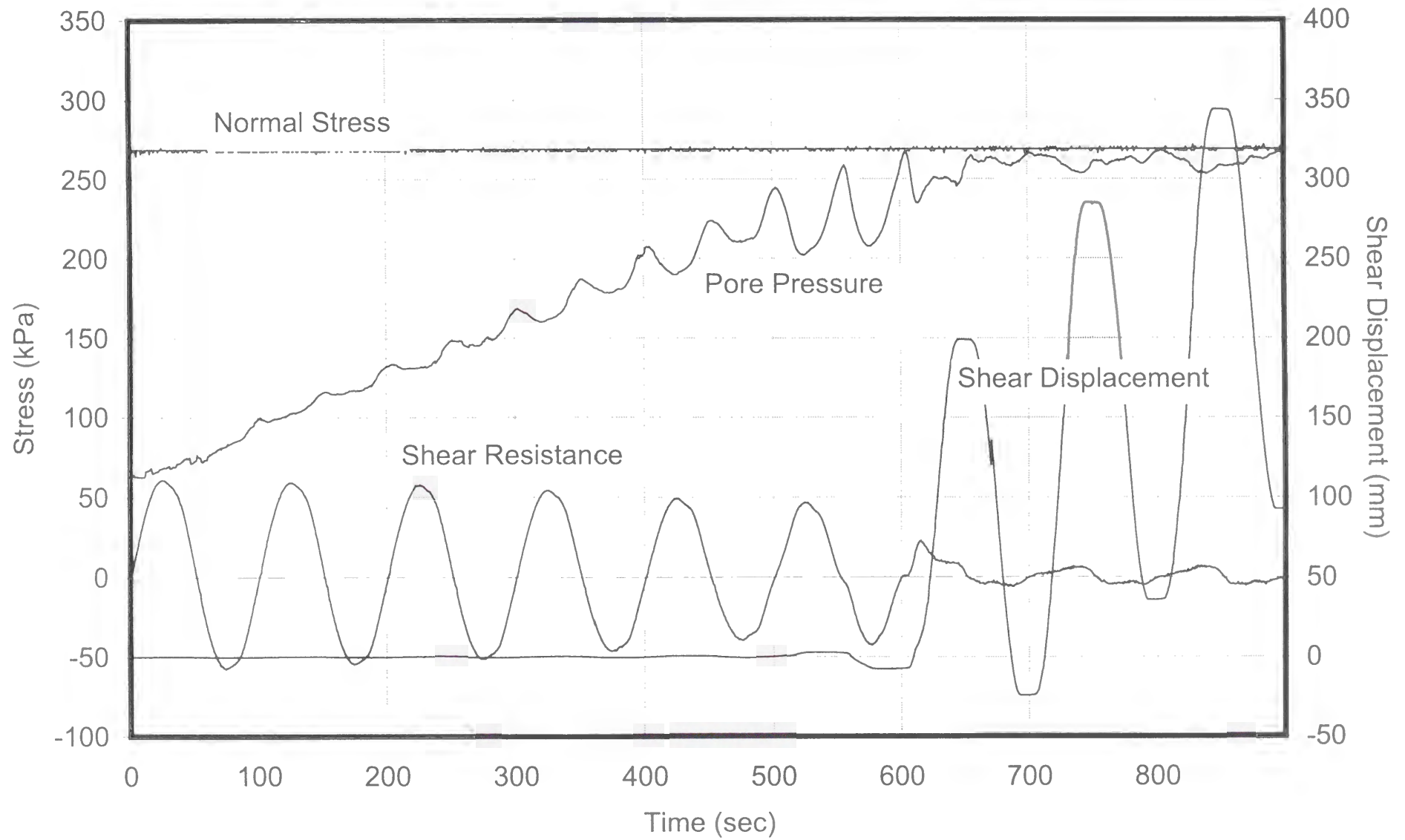| PARAMETER	UNIT	VALUE
Apparatus		Ring shear (DPRI-4)
Test type		Cyclic shear-torque-controlled
Loading frequency	Hz	0.05
Data acquisition rate	point/cycle	100
Void ratio		0.74
Consolidation stress (σ_{con})	kPa	4000
Initial effective normal stress (σ'_{in})	kPa	204
OCR		1.96
Pore pressure coefficient B_D		0.96
Back pressure (u_0)	kPa	89

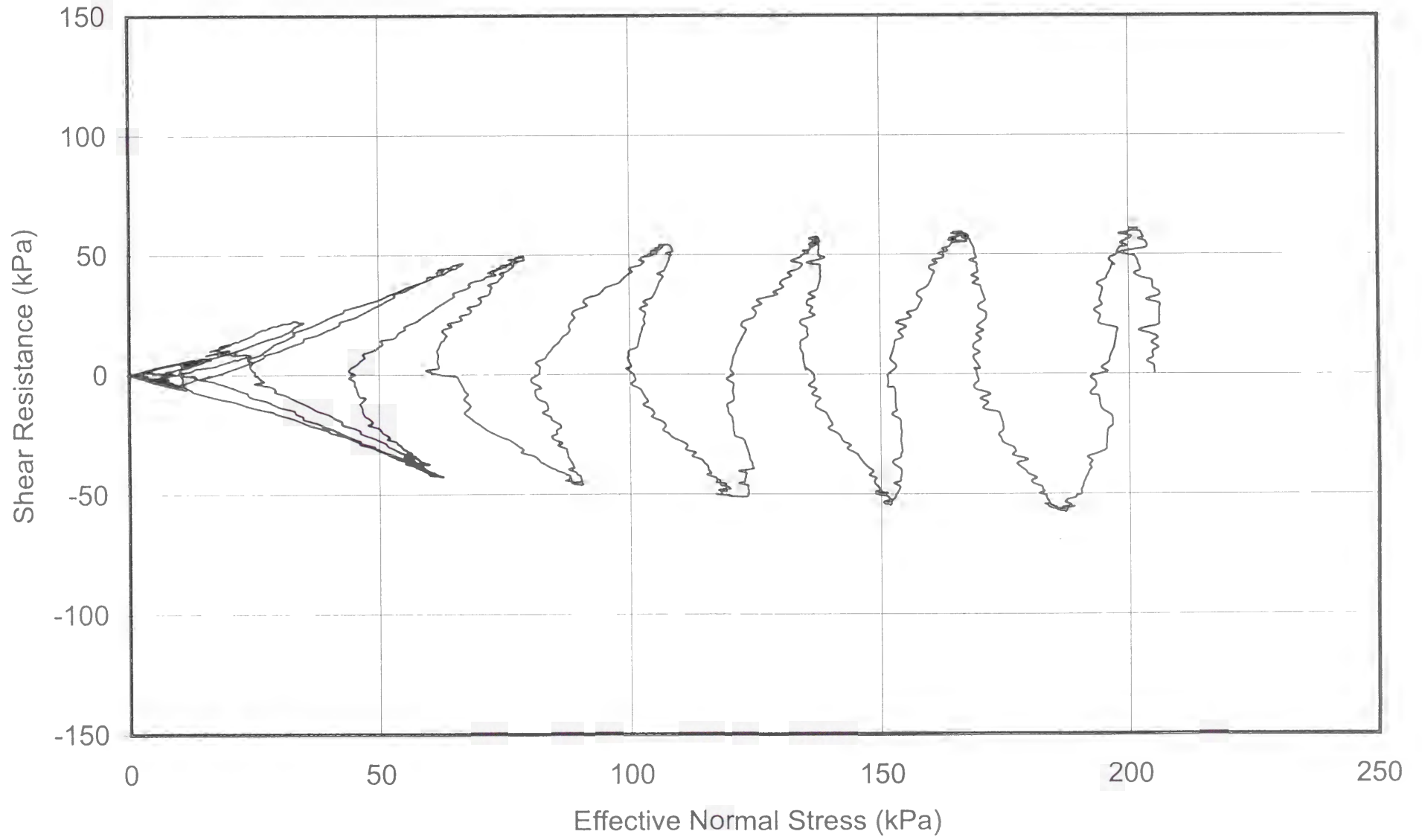The following plots are included:

- **Plot No. 8-1**

Time series of total normal stress, shear resistance, pore pressure, and shear displacement.

- **Plot No. 8-2**

Effective stress path.

Test No.8 — Cyclic shear-torque-controlled test. OCR=1.96; f=0.05 Hz. — Plot No.8-1

Shear resistance (kPa) vs Effective Normal Stress (kPa)

Test No.8

Cyclic shear-torque-controlled test. OCR=1.96; f=0.05 Hz.

Plot No.8-2

TEST No. 9

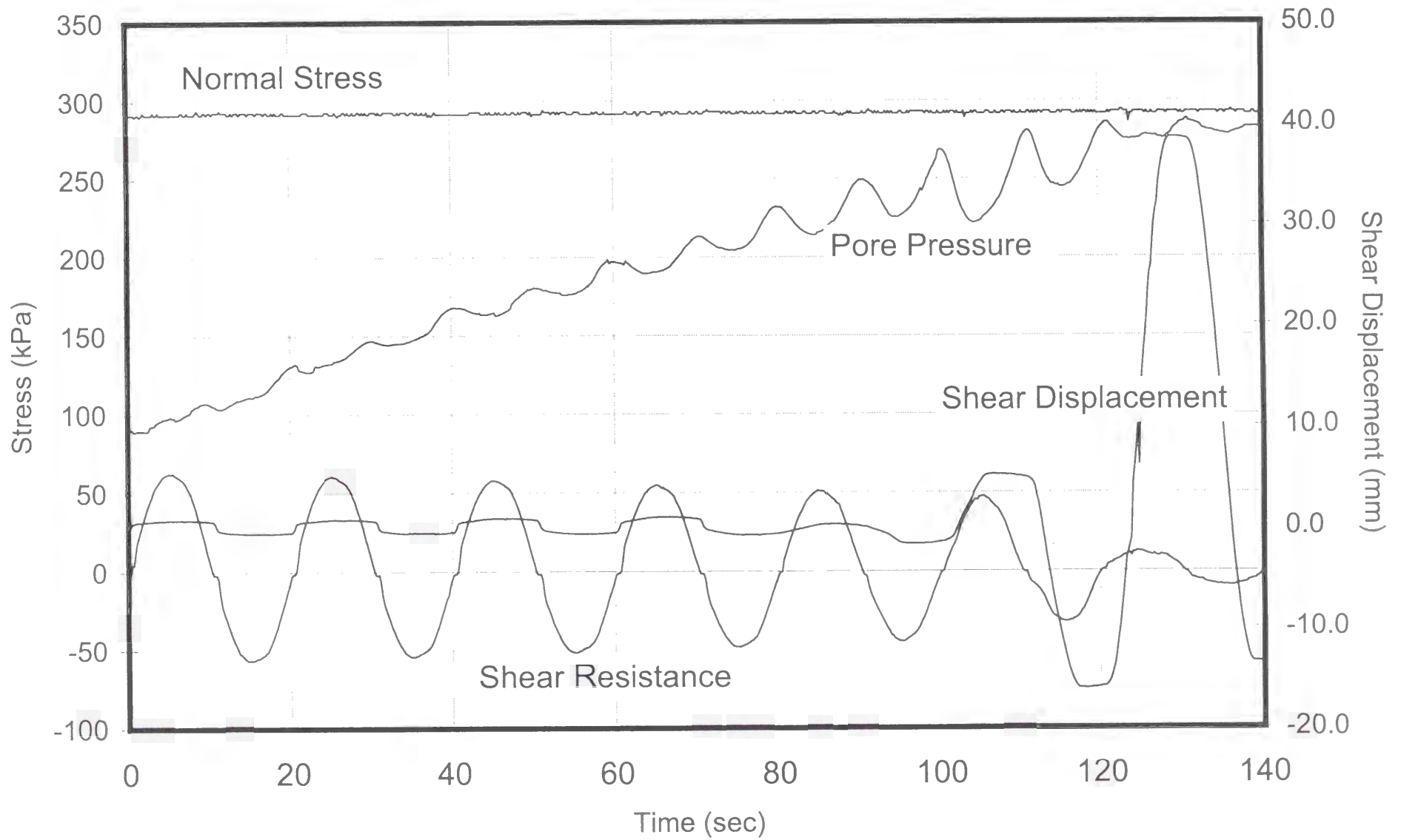| PARAMETER	UNIT	VALUE
Apparatus		Ring shear (DPRI-4)
Test type		Cyclic shear-torque-controlled
Loading frequency	Hz	0.10
Data acquisition rate	point/cycle	100
Void ratio		0.73
Consolidation stress (σ_{con})	kPa	400
Initial effective normal stress (σ'_{in})	kPa	192
OCR		2.08
Pore pressure coefficient B_D		0.98
Back pressure (u_0)	kPa	114

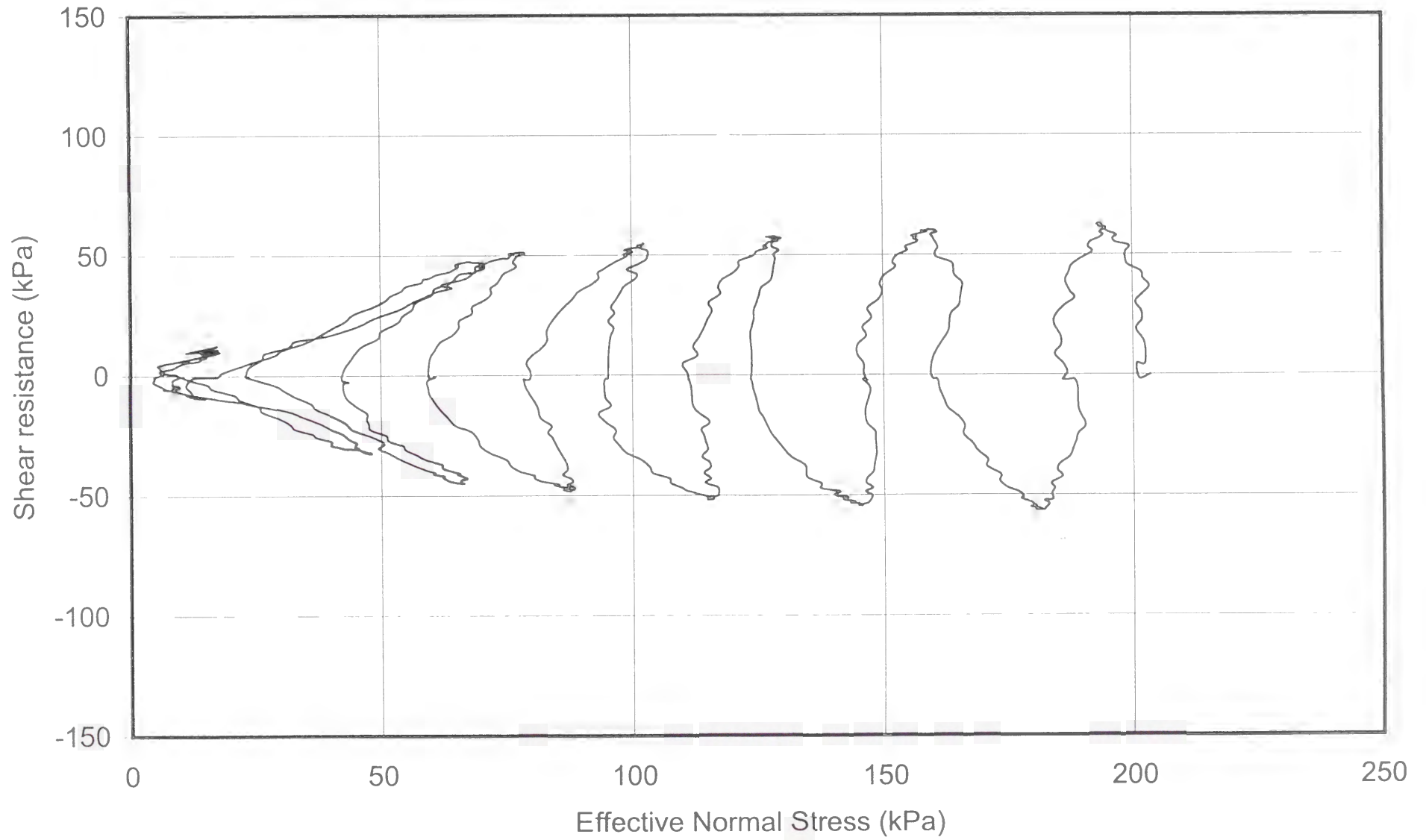The following plots are included:

- **Plot No. 9-1**

Time series of total normal stress, shear resistance, pore pressure, and shear displacement.

- **Plot No. 9-2**

Effective stress path.

Test No.9 — Cyclic shear-torque-controlled test. OCR=2.08; f=0.10 Hz. — Plot No.9-1

Test No.9

Cyclic shear-torque-controlled test. OCR=2.08; f=0.10 Hz.

Plot No.9-2

TEST No. 10

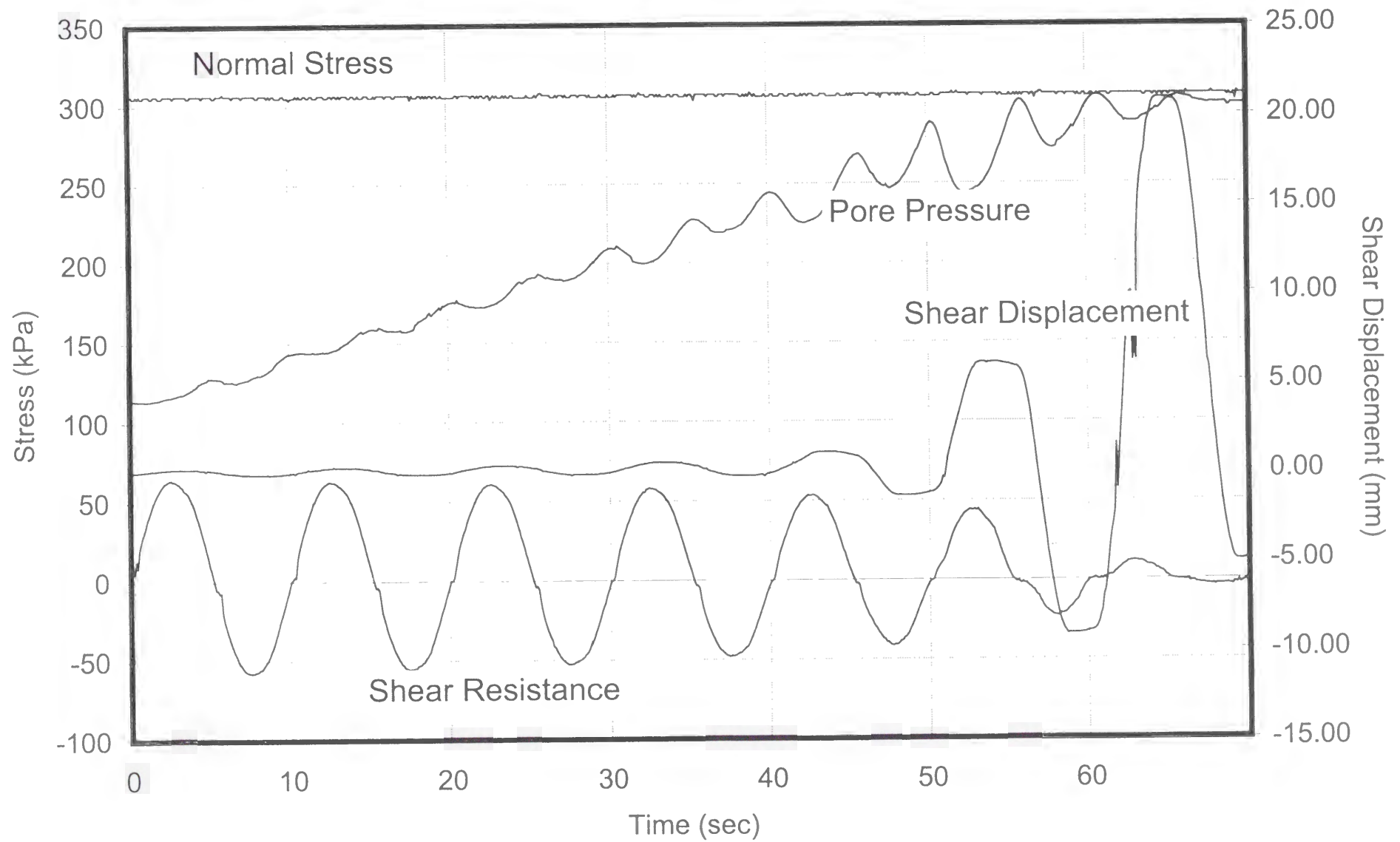| PARAMETER	UNIT	VALUE
Apparatus		Ring shear (DPRI-4)
Test type		Cyclic shear-torque-controlled
Loading frequency	Hz	0.50
Data acquisition rate	point/cycle	20
Void ratio		0.74
Consolidation stress (σ_{con})	kPa	400
Initial effective normal stress (σ'_{in})	kPa	187
OCR		2.14
Pore pressure coefficient B_D		0.95
Back pressure (u_0)	kPa	137

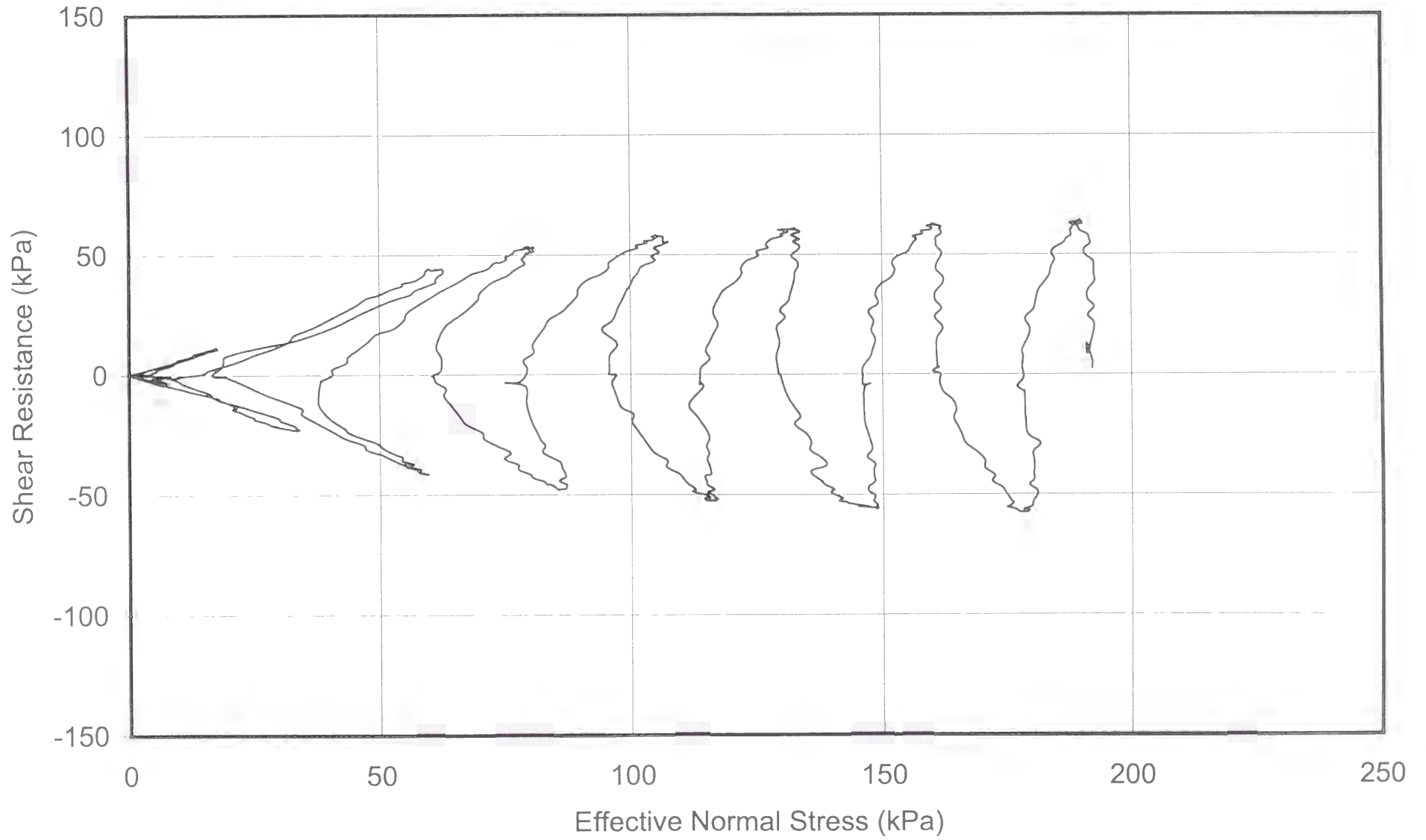The following plots are included:

- **Plot No. 10-1**
Time series of total normal stress, shear resistance, pore pressure, and shear displacement.

- **Plot No. 10-2**
Effective stress path.

Cyclic shear-torque-controlled test. OCR=2.14; f=0.50 Hz.

Test No.10

Plot No.10-1

Test No.10

Cyclic shear-torque-controlled test. OCR=2.14; f=0.50 Hz.

Plot No.10-2

TEST No. 11

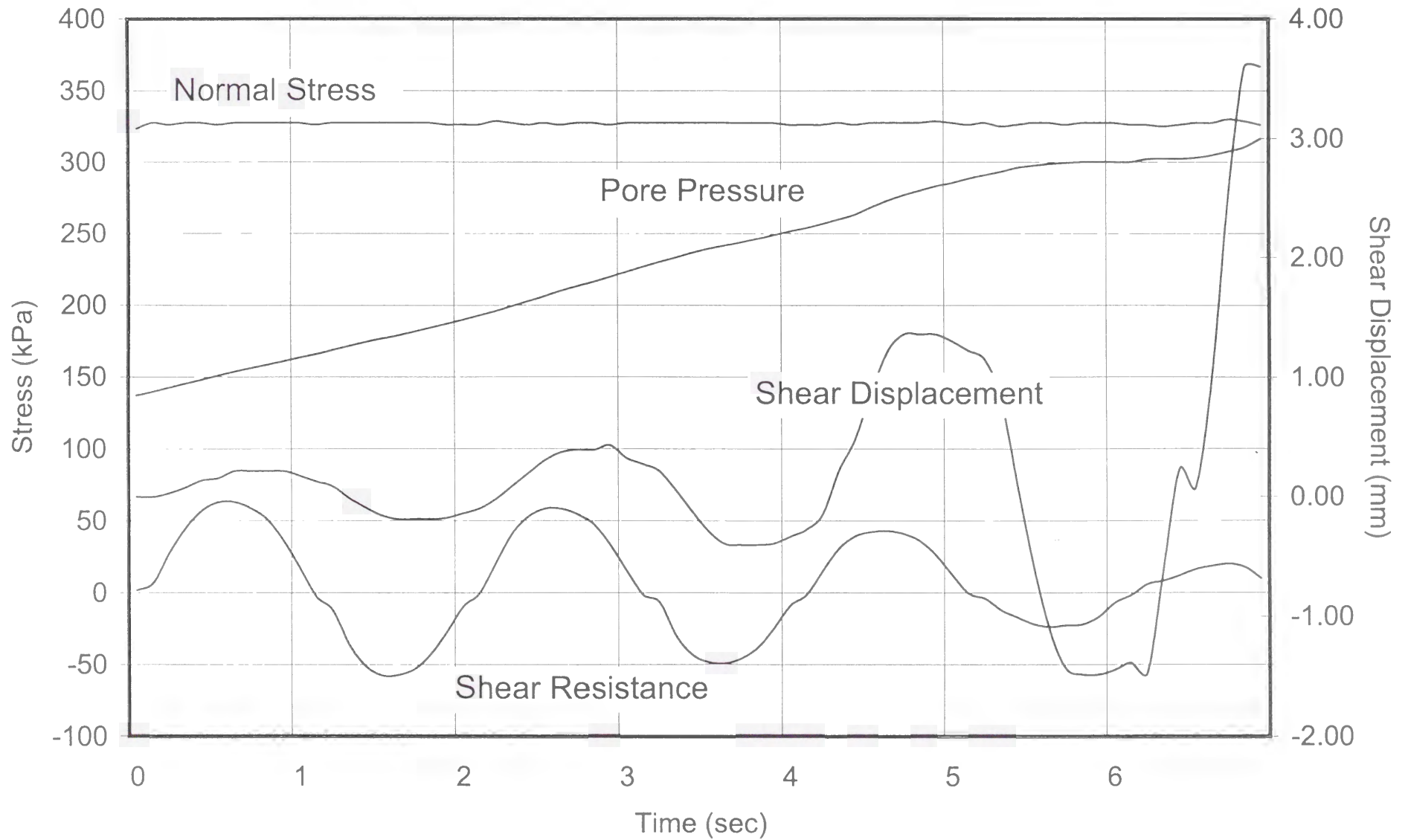| PARAMETER	UNIT	VALUE
Apparatus		Ring shear (DPRI-4)
Test type		Cyclic shear-torque-controlled
Loading frequency	Hz	1.00
Data acquisition rate	point/cycle	50
Void ratio		0.70
Consolidation stress (σ_{con})	kPa	400
Initial effective normal stress (σ'_{in})	kPa	207
OCR		1.93
Pore pressure coefficient B_D		0.95
Back pressure (u_0)	kPa	97

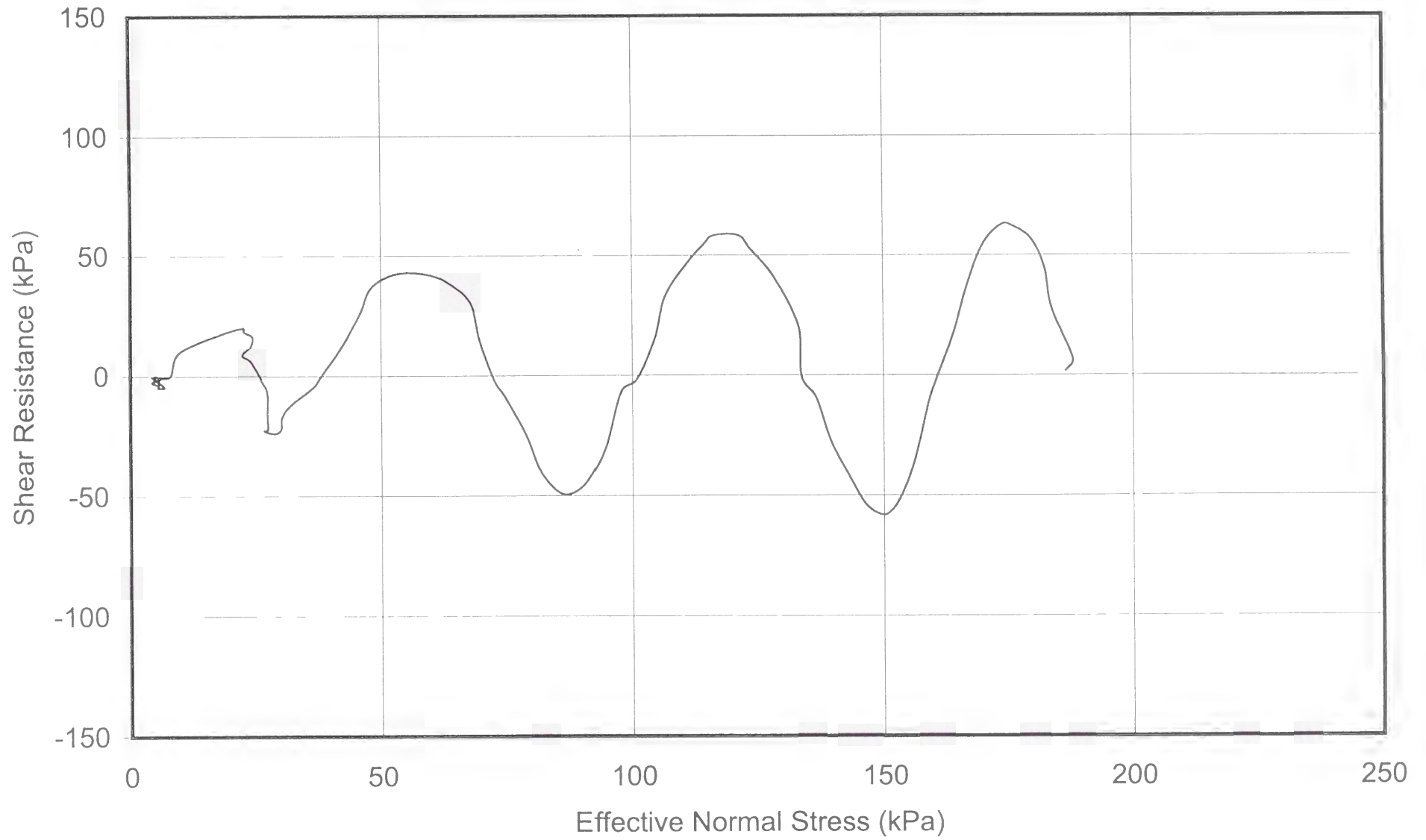The following plots are included:

- **Plot No. 11-1**
Time series of total normal stress, shear resistance, pore pressure, and shear displacement.

- **Plot No. 11-2**
Effective stress path.

Test No.11   Cyclic shear-torque-controlled test. OCR=1.93; f=1.00.   Plot No.11-1

Cyclic shear-torque-controlled test. OCR=1.93; f=1.00 Hz.

Test No.12

Plot No.11-2

TEST No. 12

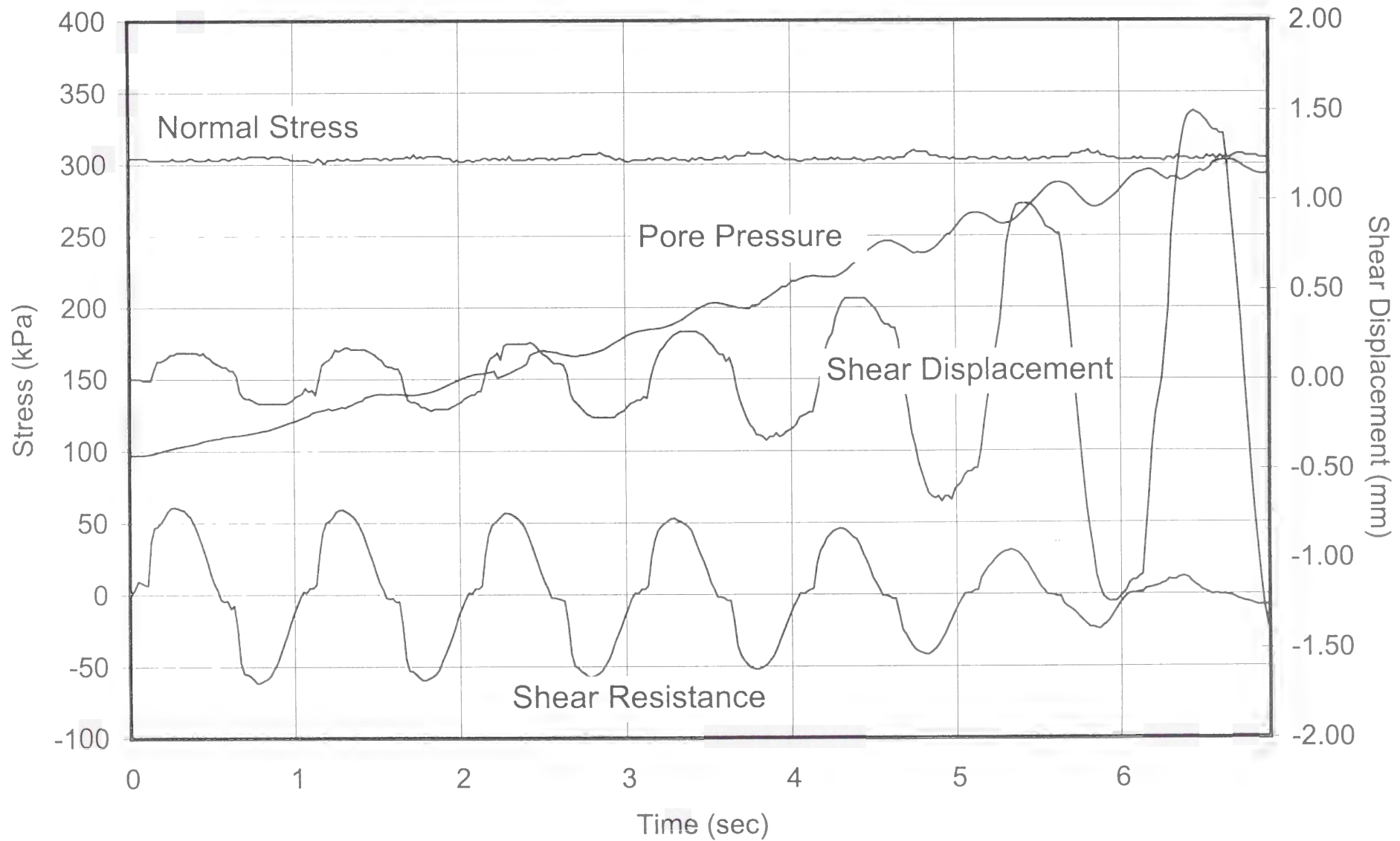| PARAMETER	UNIT	VALUE
Apparatus		Ring shear (DPRI-4)
Test type		Cyclic shear-torque-controlled
Loading frequency	Hz	2.00
Data acquisition rate	point/cycle	50
Void ratio		0.69
Consolidation stress (σ_{con})	kPa	400
Initial effective normal stress (σ'_{in})	kPa	209
OCR		1.91
Pore pressure coefficient B_D		0.95
Back pressure (u_0)	kPa	99

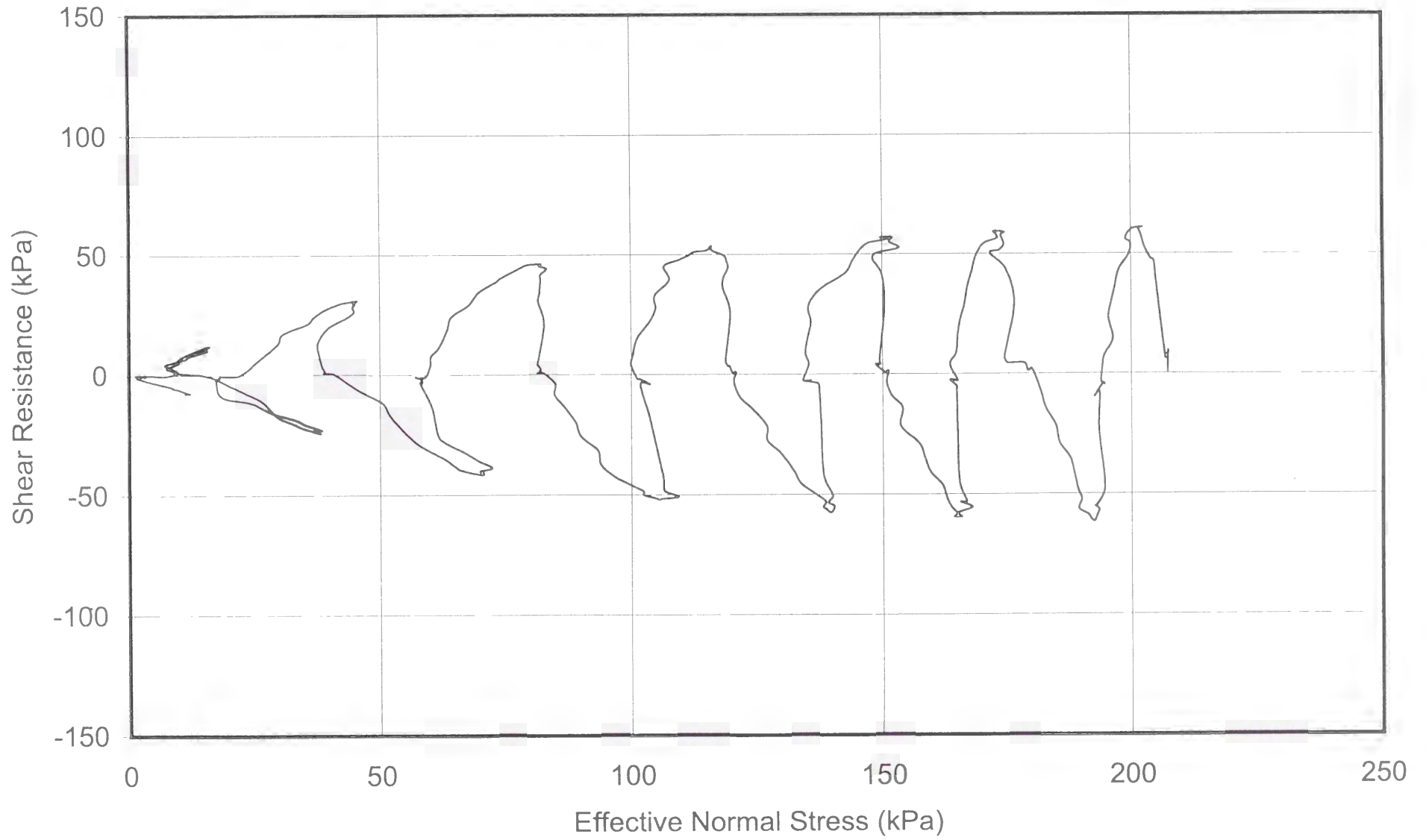The following plots are included:

- **Plot No. 12-1**
Time series of total normal stress, shear resistance, pore pressure, and shear displacement.

- **Plot No. 12-2**
Effective stress path.

Cyclic shear-torque-controlled test. OCR= 1.91; f=2.00 Hz.

Test No.12

Shear Resistance (kPa) vs Effective Normal Stress (kPa)

Cyclic shear-torque-controlled test. OCR=1.91. f=2.00 Hz;

TEST No. 13

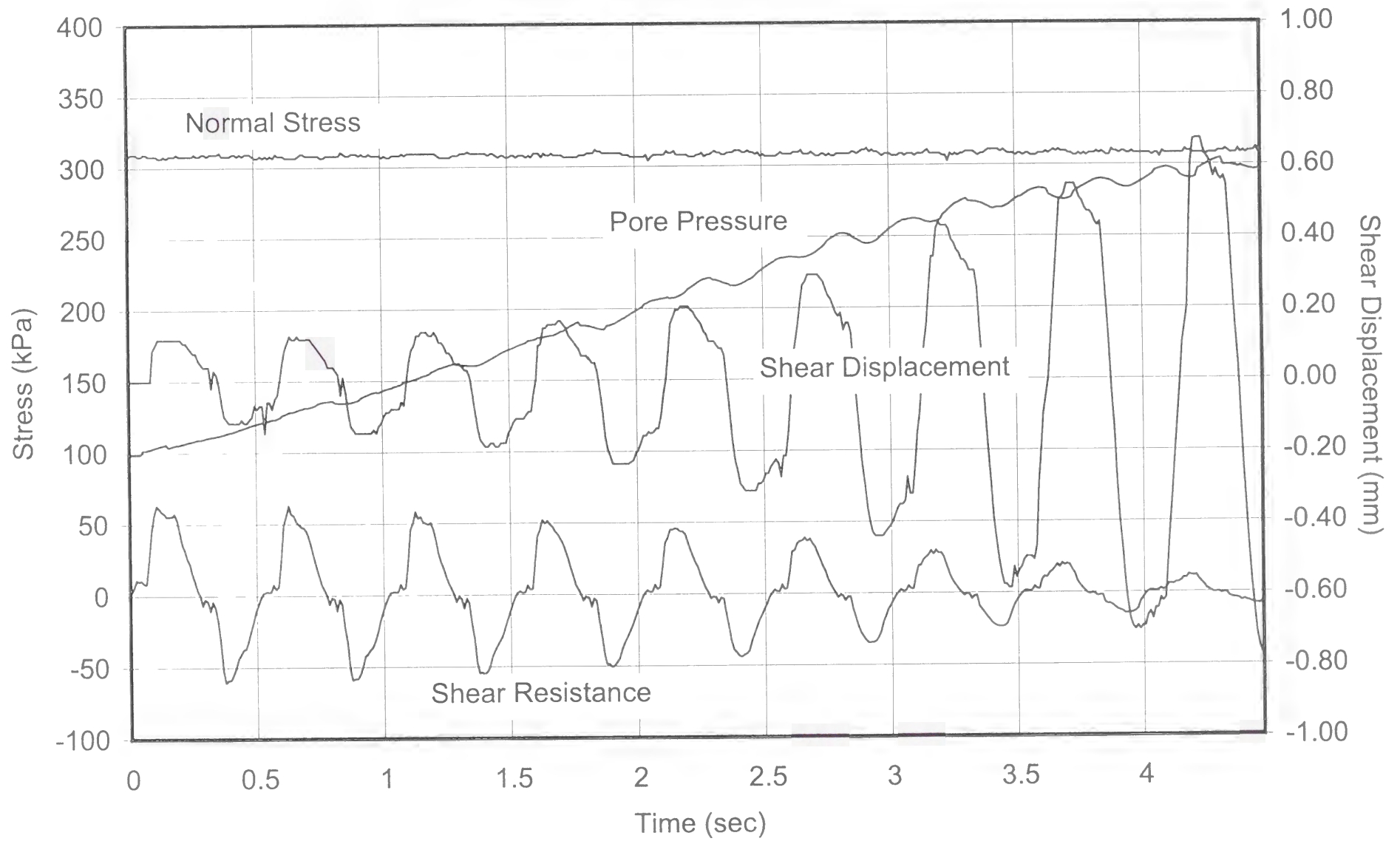| PARAMETER	UNIT	VALUE
Apparatus		Ring shear (DPRI-4)
Test type		Cyclic shear-torque-controlled
Loading frequency	Hz	0.01
Data acquisition rate	point/cycle	100
Void ratio		0.73
Consolidation stress (σ_{con})	kPa	600
Initial effective normal stress (σ'_{in})	kPa	233
OCR		2.58
Pore pressure coefficient B_D		0.96
Back pressure (u_0)	kPa	47

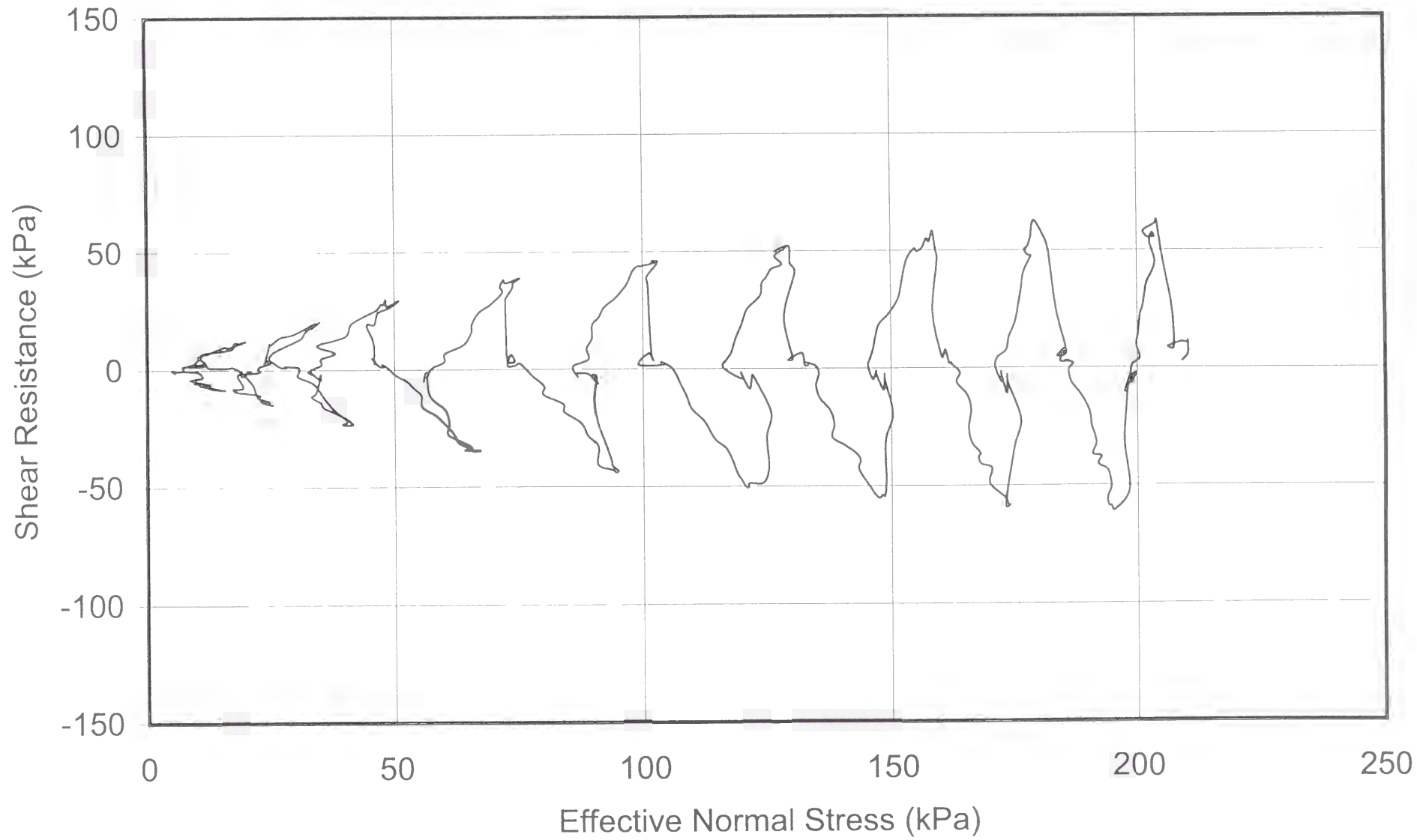**The following plots are included:**

- **Plot No. 13-1**

Time series of total normal stress, shear resistance, pore pressure, and shear displacement.

- **Plot No. 13-2**

Effective stress path.

Cyclic shear-torque-controlled test. OCR=2.58; f=0.01 Hz.

Cyclic shear-torque-controlled test. OCR=2.58; f=0.01 Hz.

Test No.13

Plot No.13-1

TEST No. 14

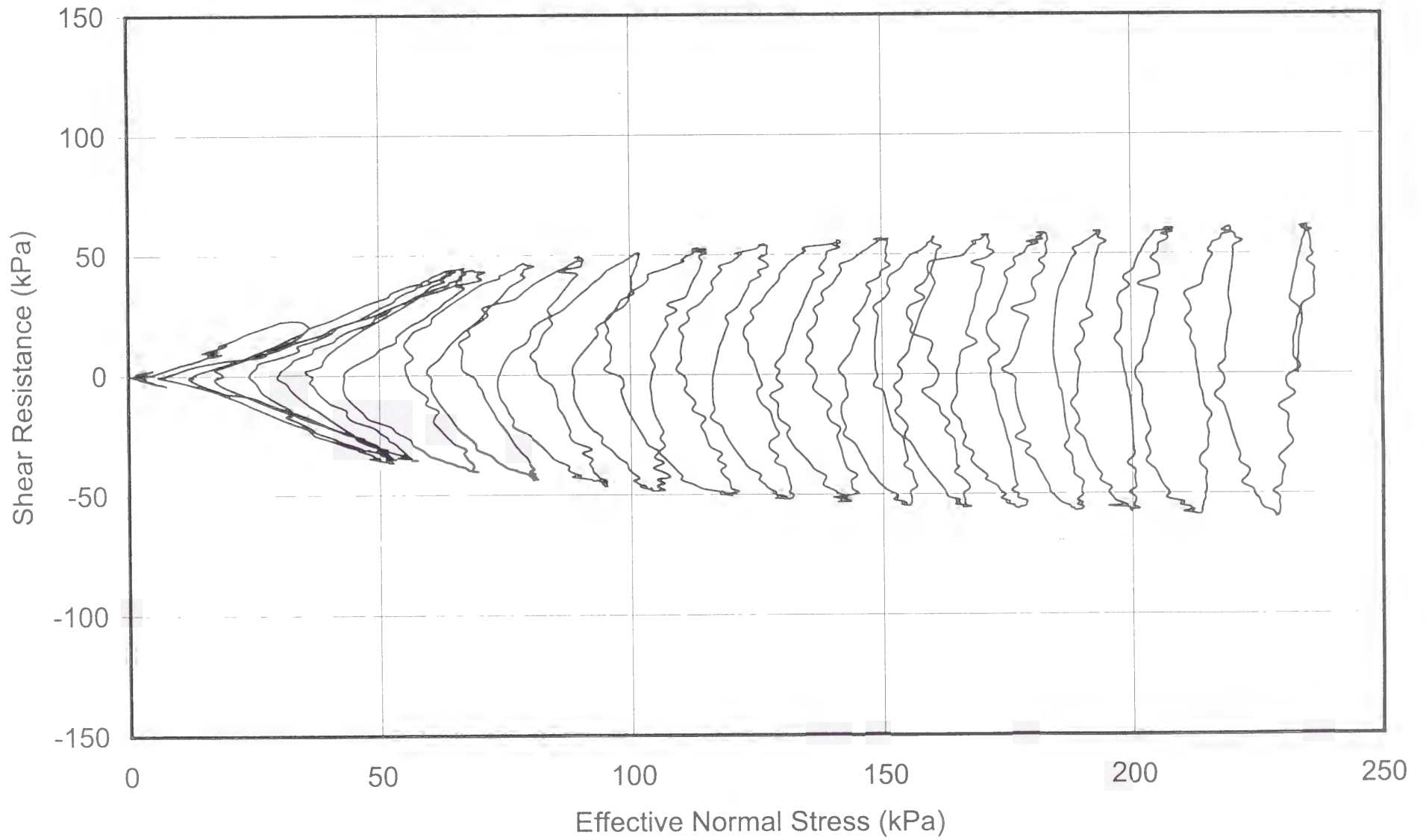| PARAMETER	UNIT	VALUE
Apparatus		Ring shear (DPRI-4)
Test type		Cyclic shear-torque-controlled
Loading frequency	Hz	0.05
Data acquisition rate	point/cycle	100
Void ratio		0.71
Consolidation stress (σ_{con})	kPa	600
Initial effective normal stress (σ'_{in})	kPa	227
OCR		2.64
Pore pressure coefficient B_D		0.97
Back pressure (u_0)	kPa	69

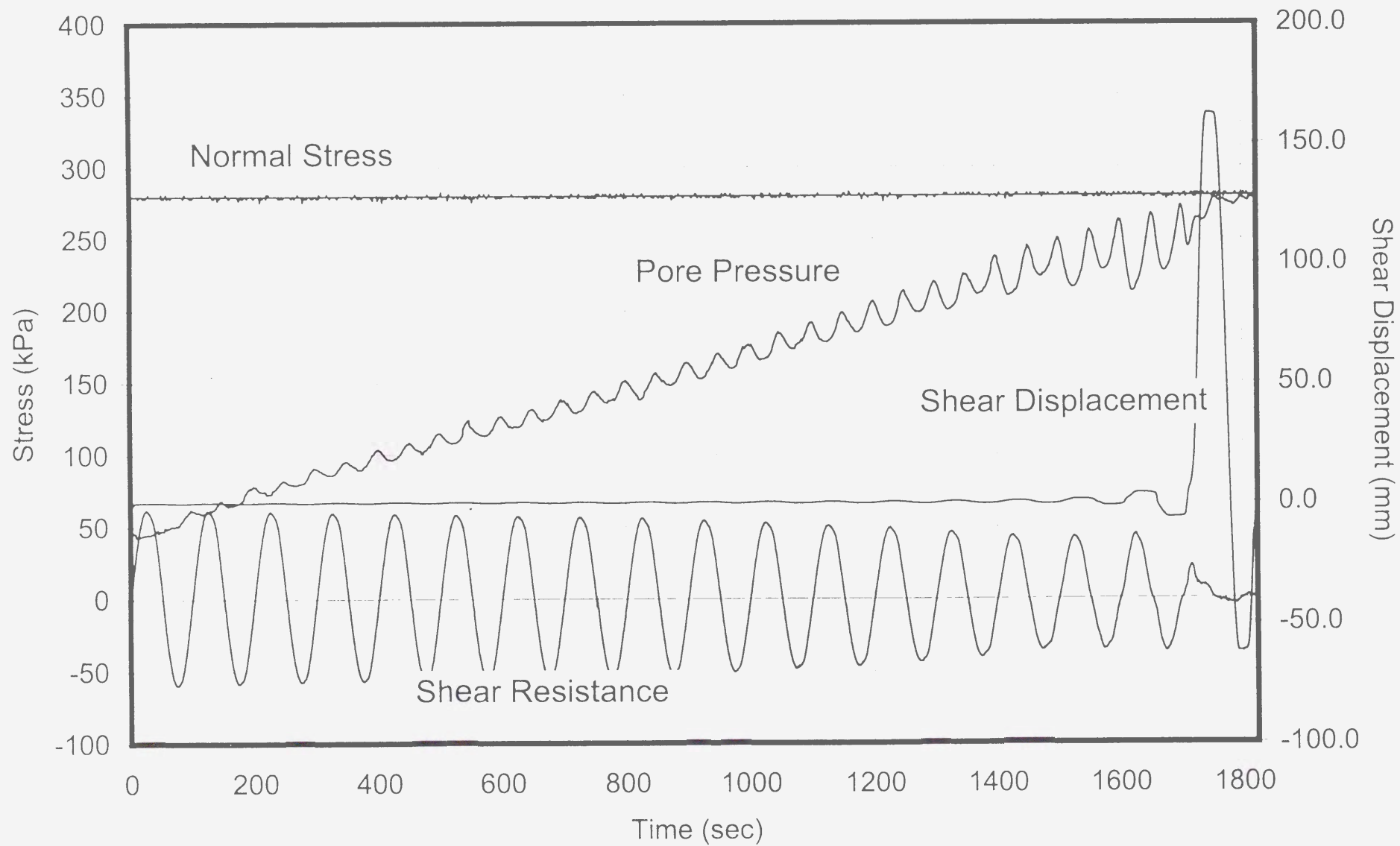The following plots are included:

- **Plot No. 14-1**
Time series of total normal stress, shear resistance, pore pressure, and shear displacement.

- **Plot No. 14-2**
Effective stress path.

Cyclic shear-torque-controlled test. OCR=2.64; f=0.05 Hz.

Test No.14

Plot No.14-1

Y axis: Shear Resistance (kPa), ranging from -150 to 150

X axis: Effective Normal Stress (kPa), ranging from 0 to 250

Test No.14

Cyclic shear-torque-controlled test. OCR=2.64; f=0.05 Hz.

Plot No.14-2

TEST No. 15

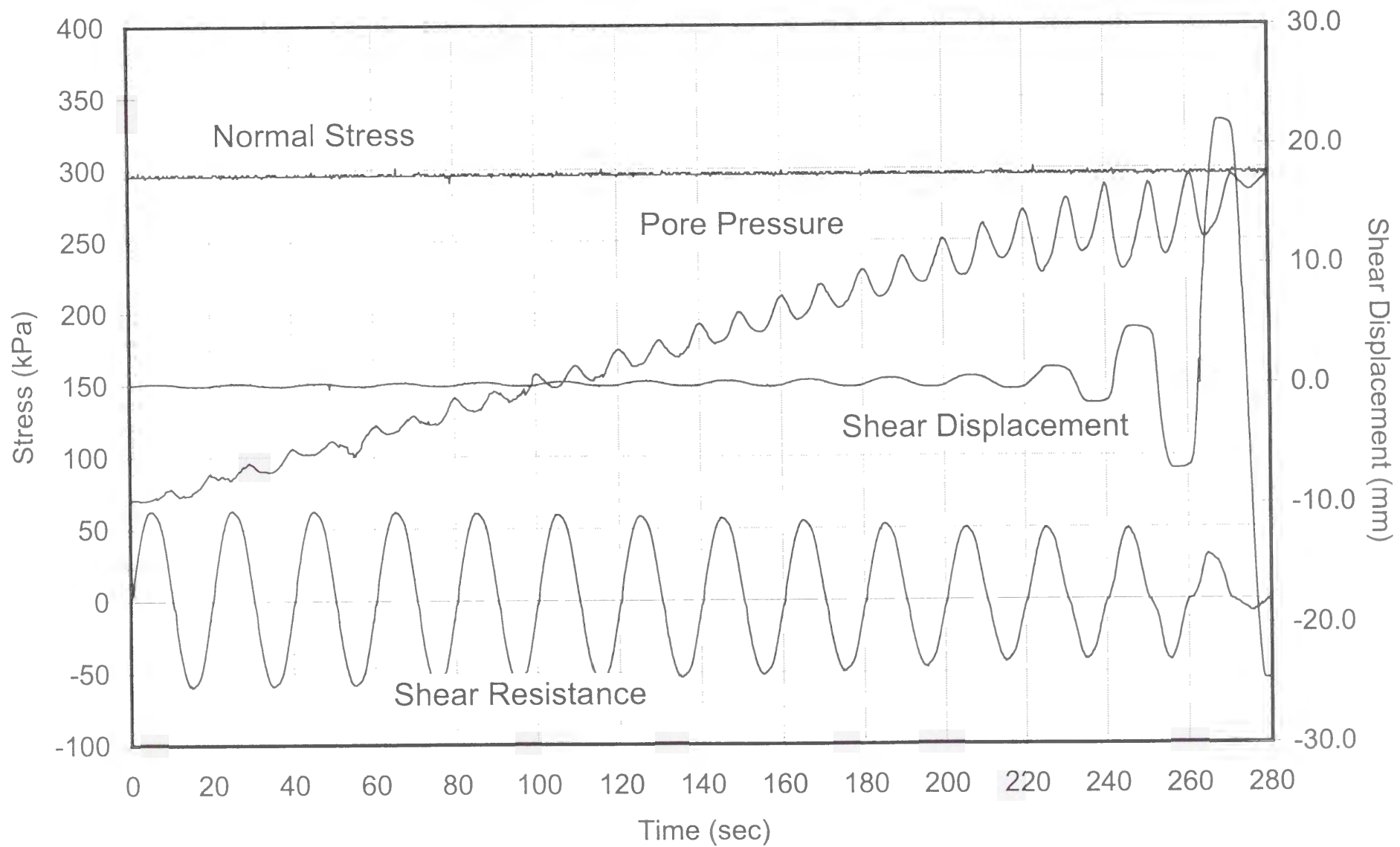| PARAMETER	UNIT	VALUE
Apparatus		Ring shear (DPRI-4)
Test type		Cyclic shear-torque-controlled
Loading frequency	Hz	0.10
Data acquisition rate	point/cycle	100
Void ratio		0.70
Consolidation stress (σ_{con})	kPa	600
Initial effective normal stress (σ'_{in})	kPa	226
OCR		2.65
Pore pressure coefficient B_D		0.95
Back pressure (u_0)	kPa	77

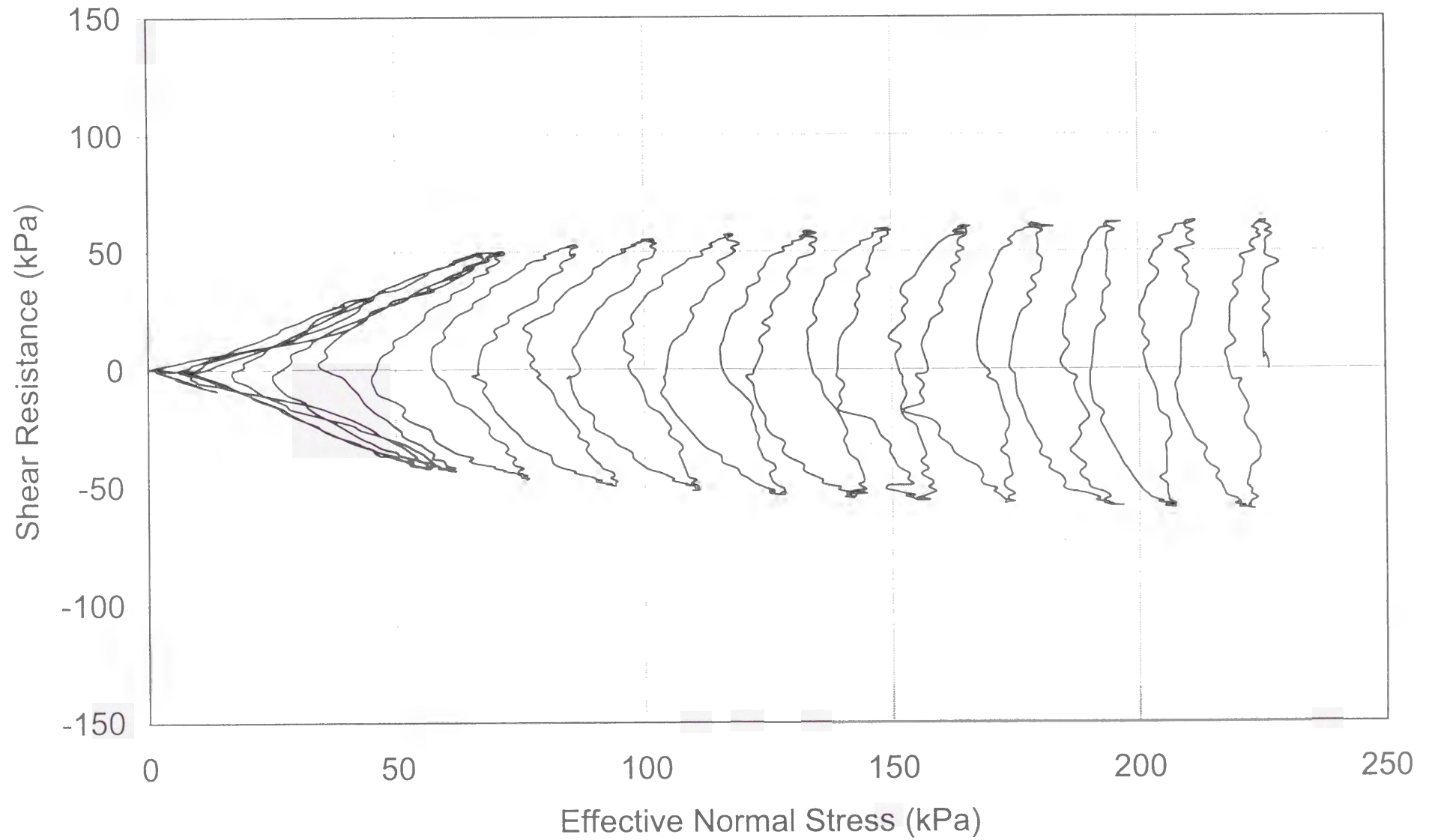The following plots are included:

- **Plot No. 15-1**

Time series of total normal stress, shear resistance, pore pressure, and shear displacement.

- **Plot No. 15-2**

Effective stress path.

Test No.15   Cyclic shear-torque-controlled test. OCR=2.65; f=0.10 Hz.   Plot No.15-1

Shear Resistance (kPa) vs Effective Normal Stress (kPa)

Test No.15

Cyclic shear-torque-controlled test. OCR=2.65; f=0.10 Hz.

Plot No.15-2

TEST No. 16

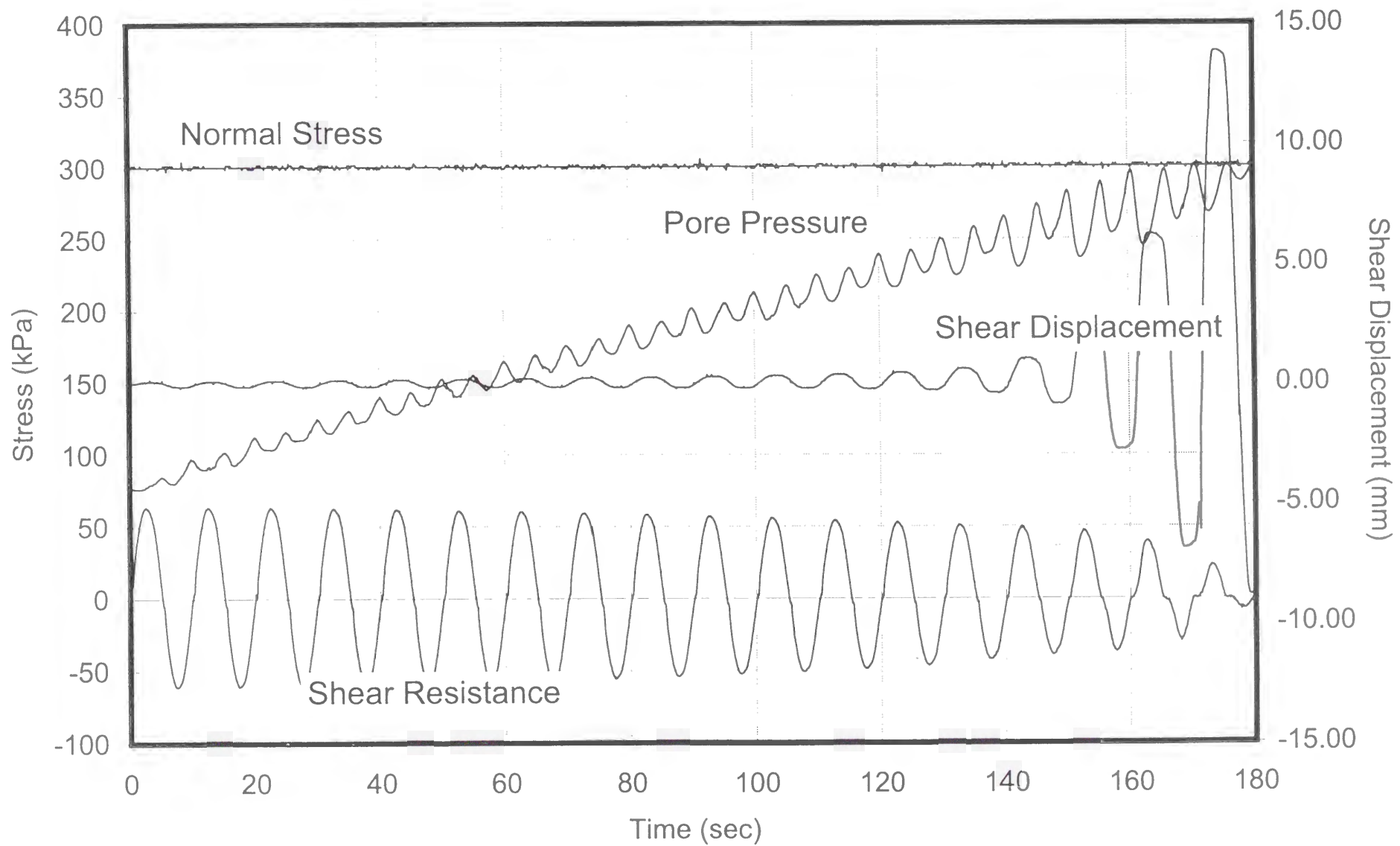| PARAMETER	UNIT	VALUE
Apparatus		Ring shear (DPRI-4)
Test type		Cyclic shear-torque-controlled
Loading frequency	Hz	0.50
Data acquisition rate	point/cycle	25
Void ratio		0.68
Consolidation stress (σ_{con})	kPa	600
Initial effective normal stress (σ'_{in})	kPa	212
OCR		2.83
Pore pressure coefficient B_D		0.96
Back pressure (u_0)	kPa	98

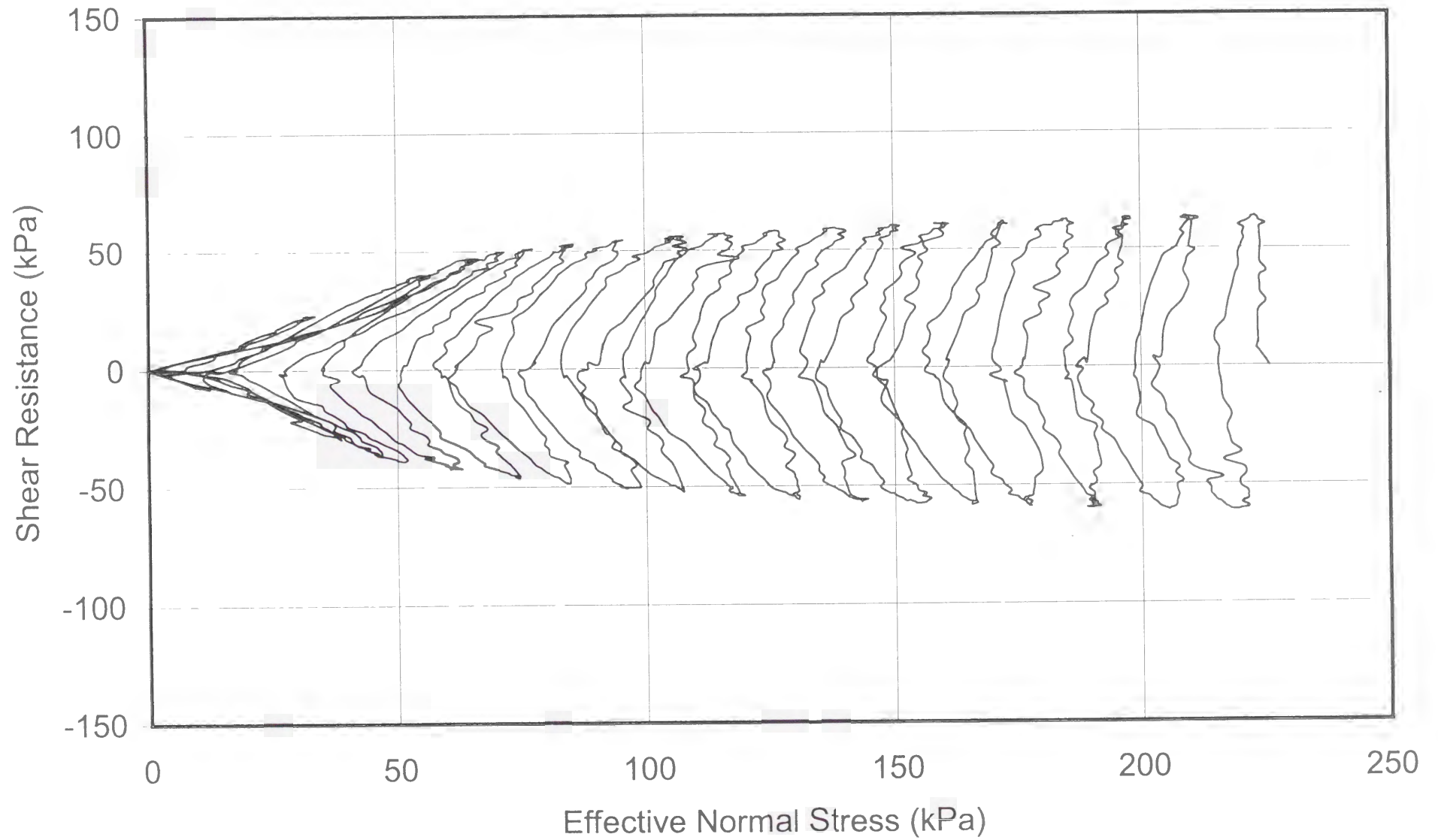The following plots are included:

- **Plot No. 16-1**

Time series of total normal stress, shear resistance, pore pressure, and shear displacement.

- **Plot No. 16-2**

Effective stress path.

Cyclic shear-torque-controlled test. OCR=2.83; f=0.50 Hz.

Test No.16

Plot No.16-1

Shear Resistance (kPa) vs Effective Normal Stress (kPa)

Test No.16

Cyclic shear-torque-controlled test. OCR=2.83; f=0.50 Hz.

Plot No.16-2

TEST No. 17

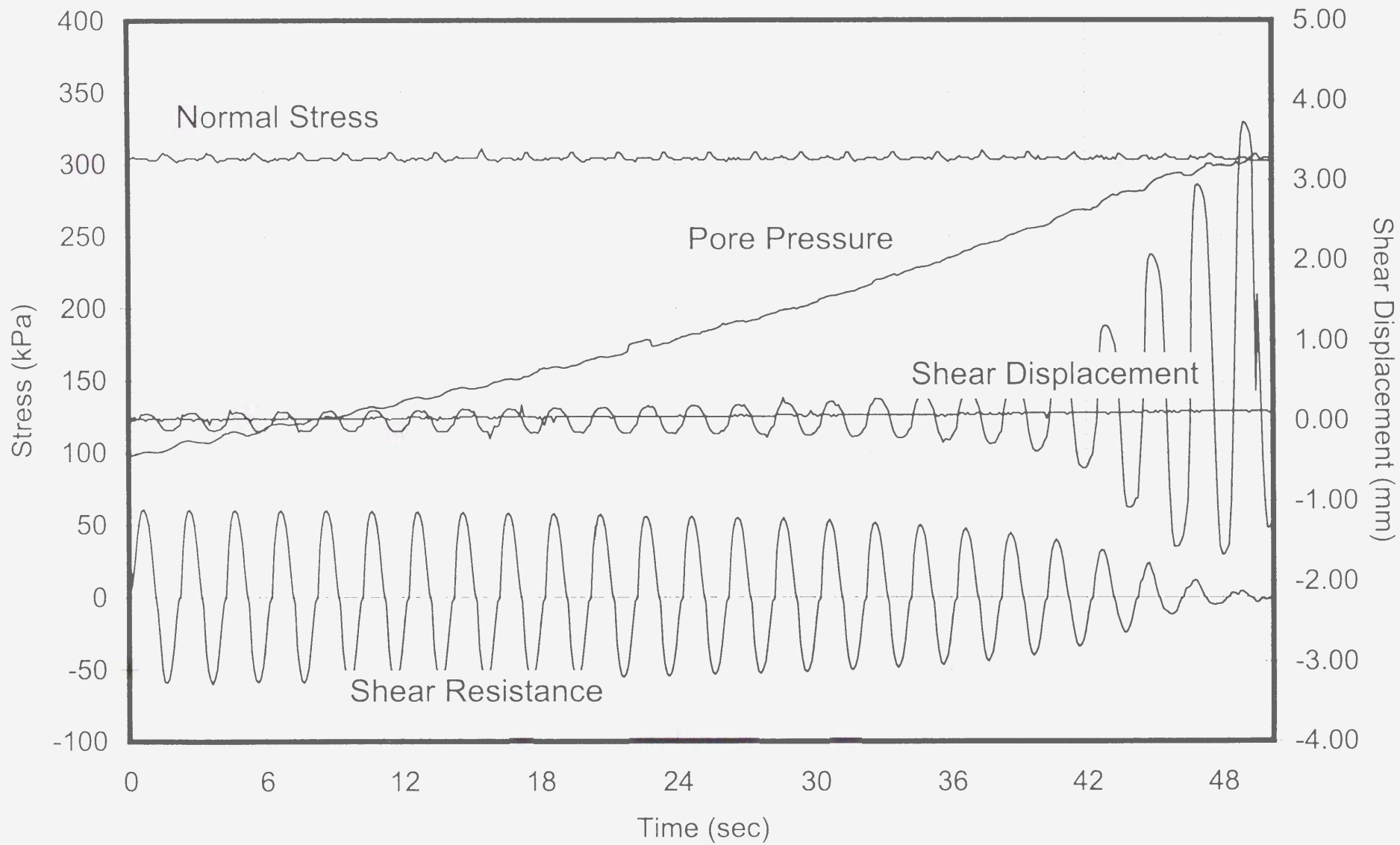| PARAMETER	UNIT	VALUE
Apparatus		Ring shear (DPRI-4)
Test type		Cyclic shear-torque-controlled
Loading frequency	Hz	1.00
Data acquisition rate	point/cycle	50
Void ratio		0.69
Consolidation stress (σ_{con})	kPa	600
Initial effective normal stress (σ'_{in})	kPa	205
OCR		2.93
Pore pressure coefficient B_D		0.95
Back pressure (u_0)	kPa	94

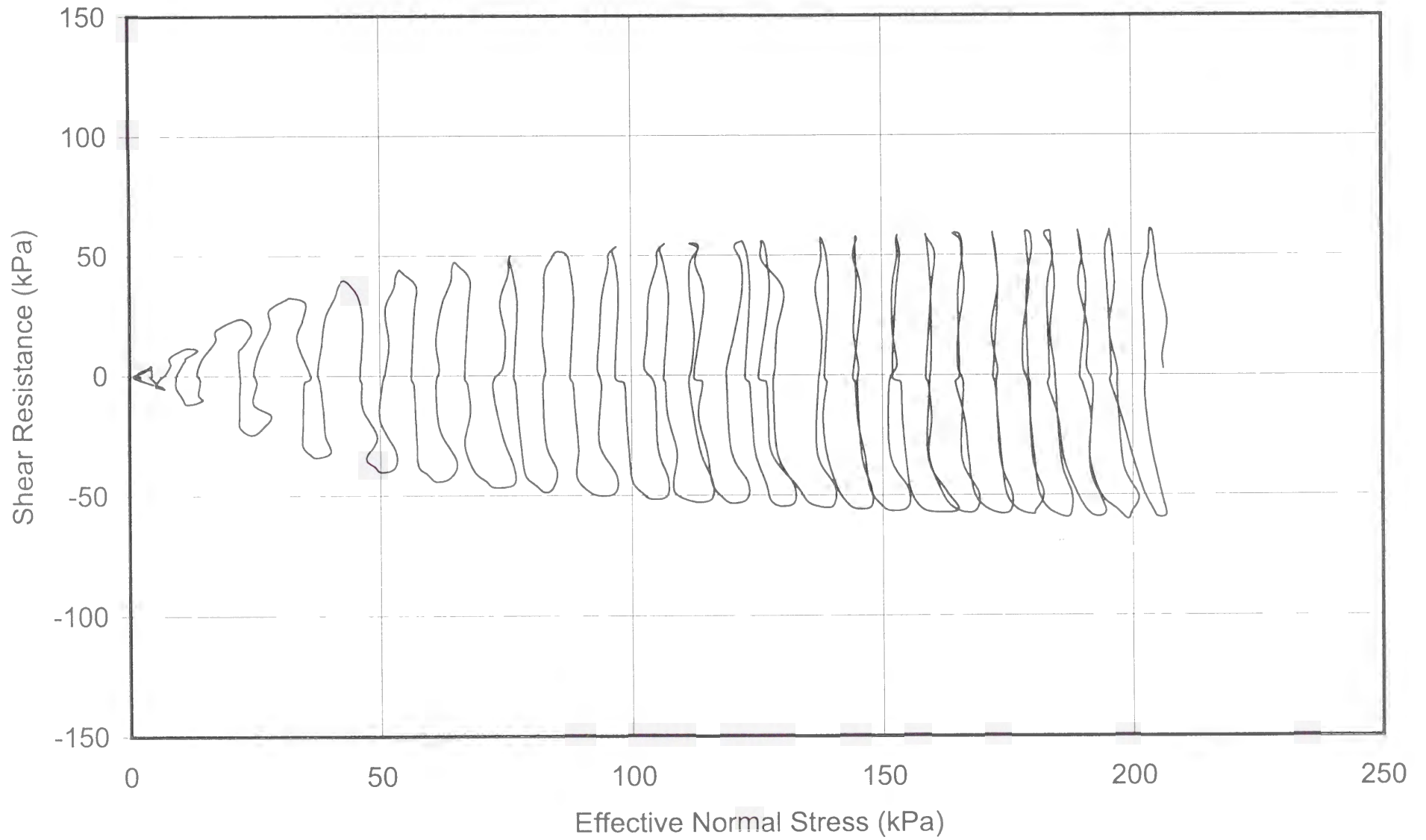**The following plots are included:**

- **Plot No. 17-1**

Time series of total normal stress, shear resistance, pore pressure, and shear displacement.

- **Plot No. 17-2**

Effective stress path.

Cyclic shear-torque-controlled test. OCR=2.93; f=1.00 Hz.

Shear Resistance (kPa) vs Effective Normal Stress (kPa)

Cyclic shear-torque-controlled test. OCR=2.90; f=1.00 Hz.

TEST No. 18

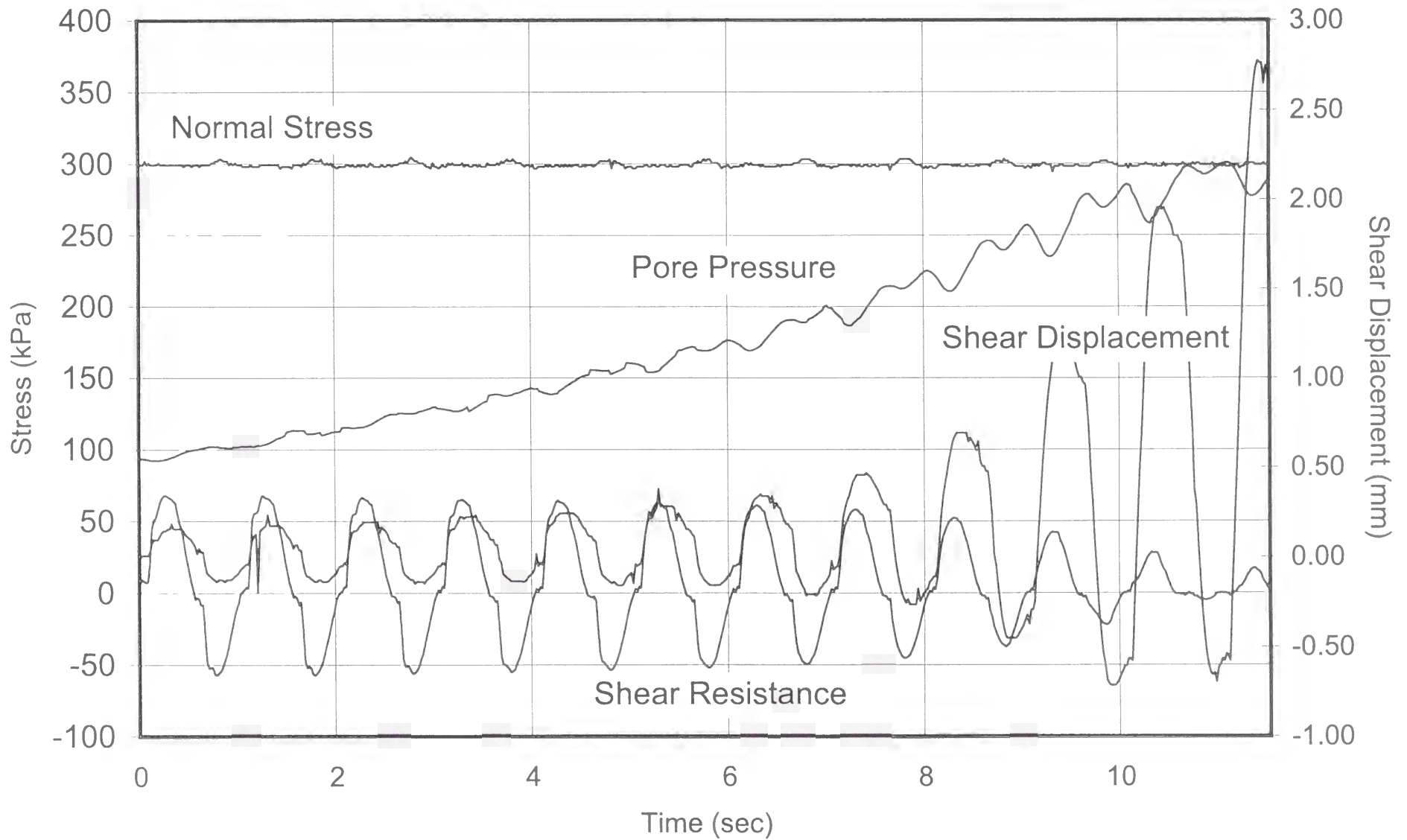| PARAMETER	UNIT	VALUE
Apparatus		Ring shear (DPRI-4)
Test type		Cyclic shear-torque-controlled
Loading frequency	Hz	2.00
Data acquisition rate	point/cycle	50
Void ratio		0.67
Consolidation stress (σ_{con})	kPa	600
Initial effective normal stress (σ'_{in})	kPa	204
OCR		2.94
Pore pressure coefficient B_D		0.97
Back pressure (u_0)	kPa	103

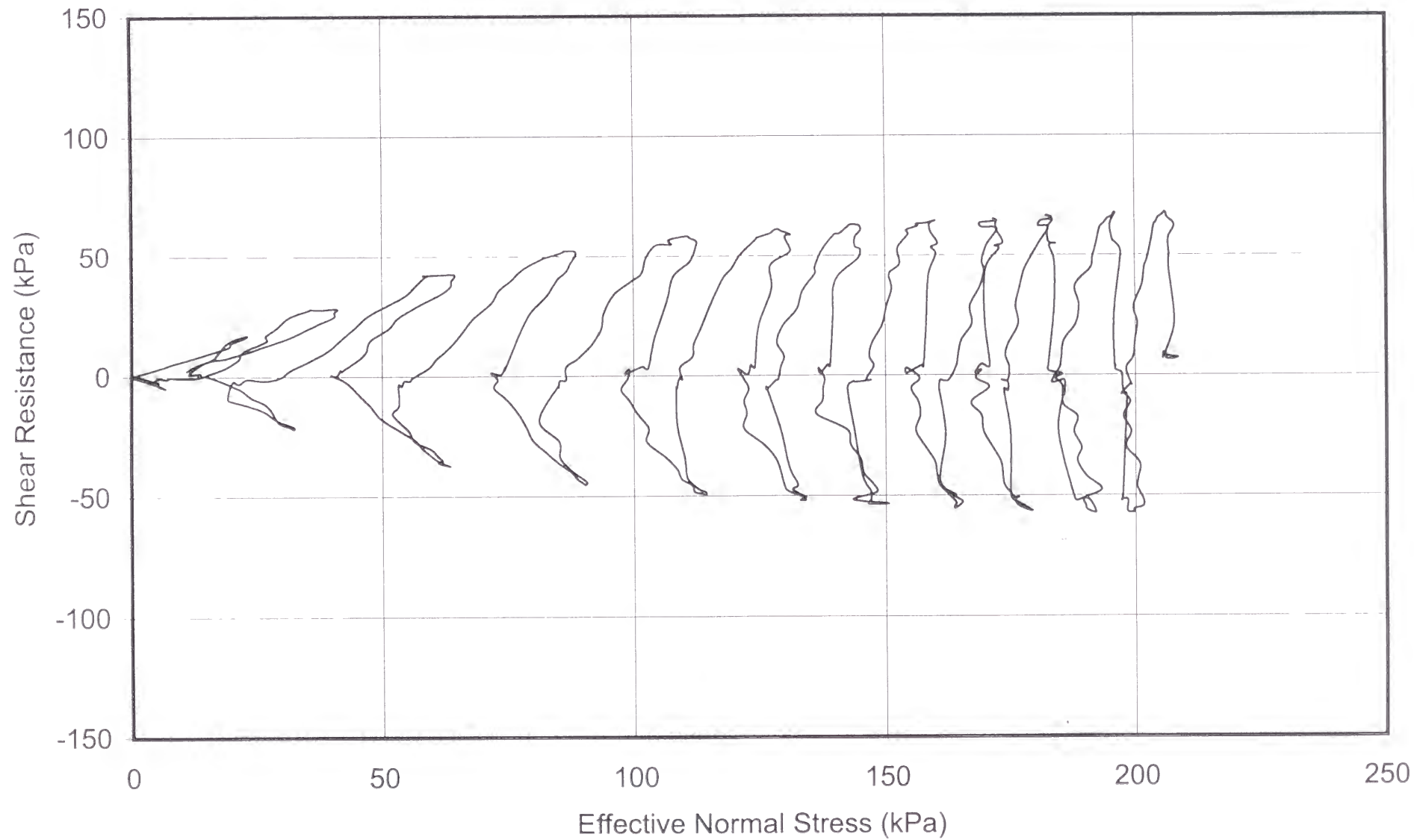## The following plots are included:

- **Plot No. 18-1**

Time series of total normal stress, shear resistance, pore pressure, and shear displacement.
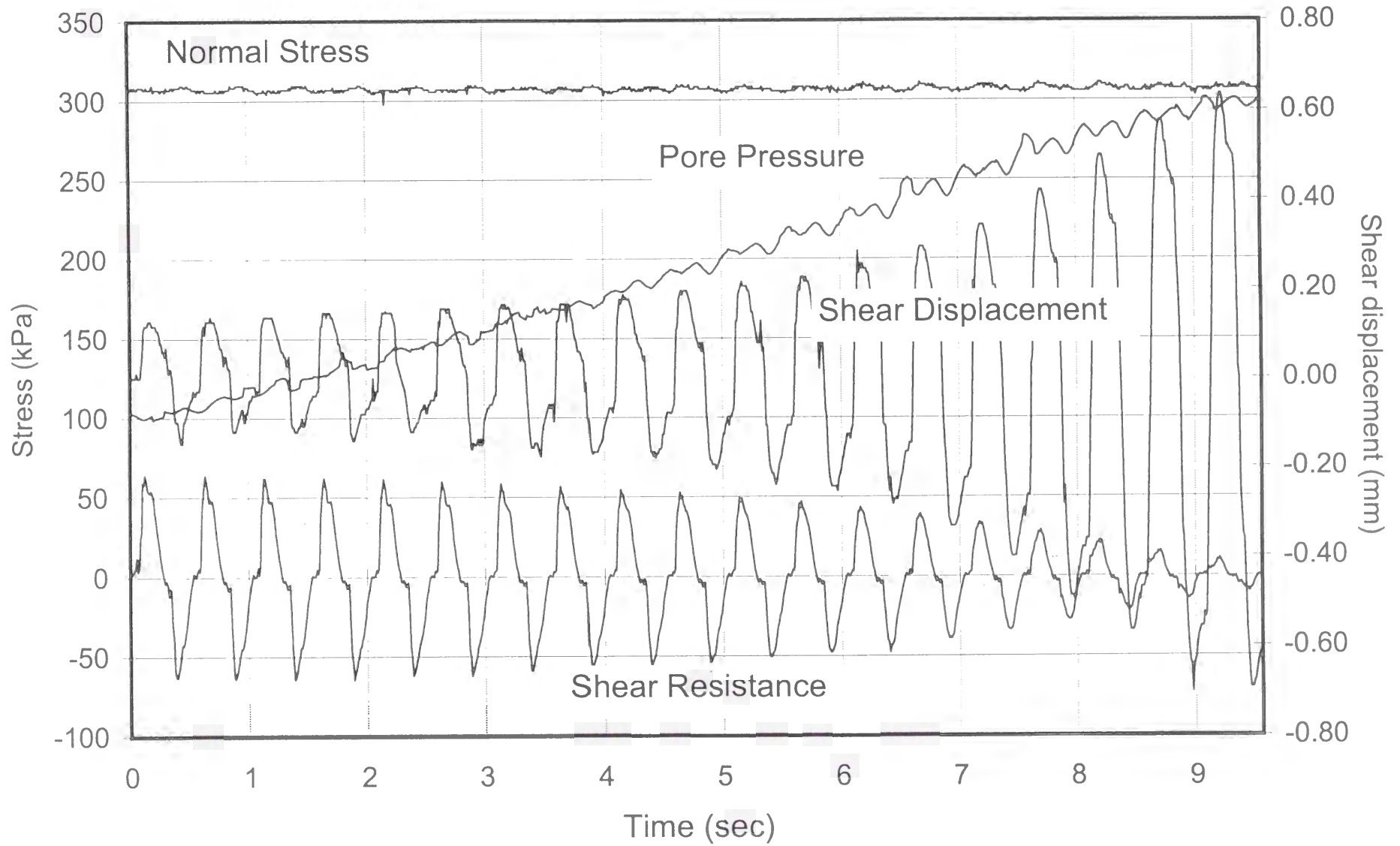
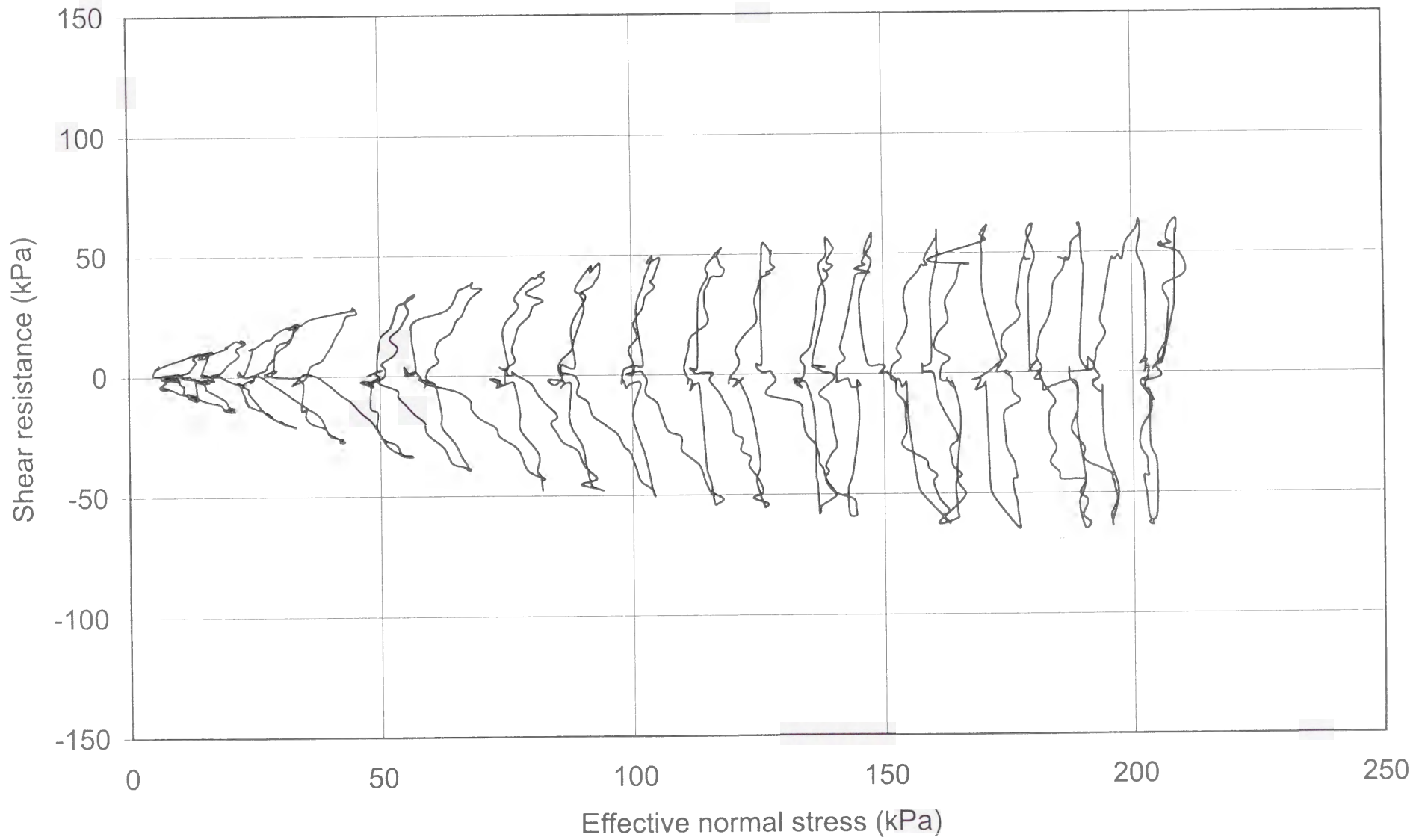- **Plot No. 18-2**

Effective stress path.

Test No.18 — Cyclic shear-torque-controlled test. OCR=2.94; f=2.00 Hz. — Plot No.18-1

Shear resistance (kPa) vs Effective normal stress (kPa)

Test No.18

Cyclic shear-torque-controlled test. OCR=2.94; f=2.00 Hz

Plot No.18-2

TEST No. 19

PARAMETER	UNIT	VALUE
Apparatus		Ring shear (DPRI-4)
Test type		Cyclic shear-displacement-controlled
Shear displacement amplitude	mm	0.50
Loading frequency	Hz	0.01
Data acquisition rate	point/cycle	200
Void ratio		0.68
Initial effective normal stress (σ'_{in})	kPa	200
Pore pressure coefficient B_D		0.95
Back pressure (u_0)	kPa	47

The following plots are included:

- **Plot No. 19-1**
Time series of total normal stress, shear resistance, pore pressure, and shear displacement.

- **Plot No. 19-2**
Effective stress path.

Normal Stress

Pore Pressure

Shear Displacement

Shear Resistance

Stress (kPa)

Shear Displacement (mm)

Time (sec)

Test No.19

Cyc shear-displacement controlled test. f=0.01 Hz; l 0.50mm.

Plot No.19-1

Test No.19

'Cyc' shear-displacement-controlled test. f=0.01 Hz; l₀ -0.50mm

Plot No.19-2

TEST No. 20

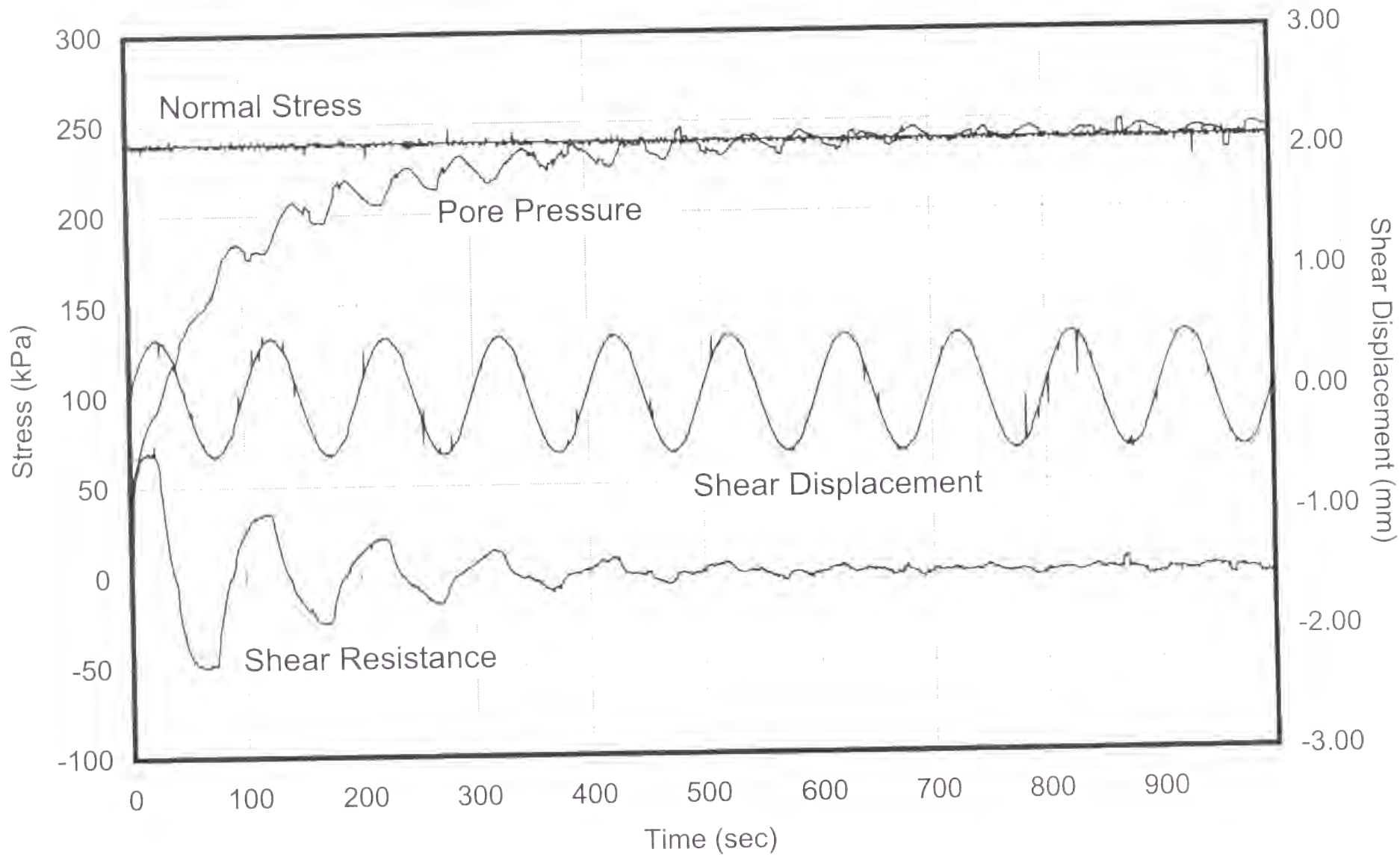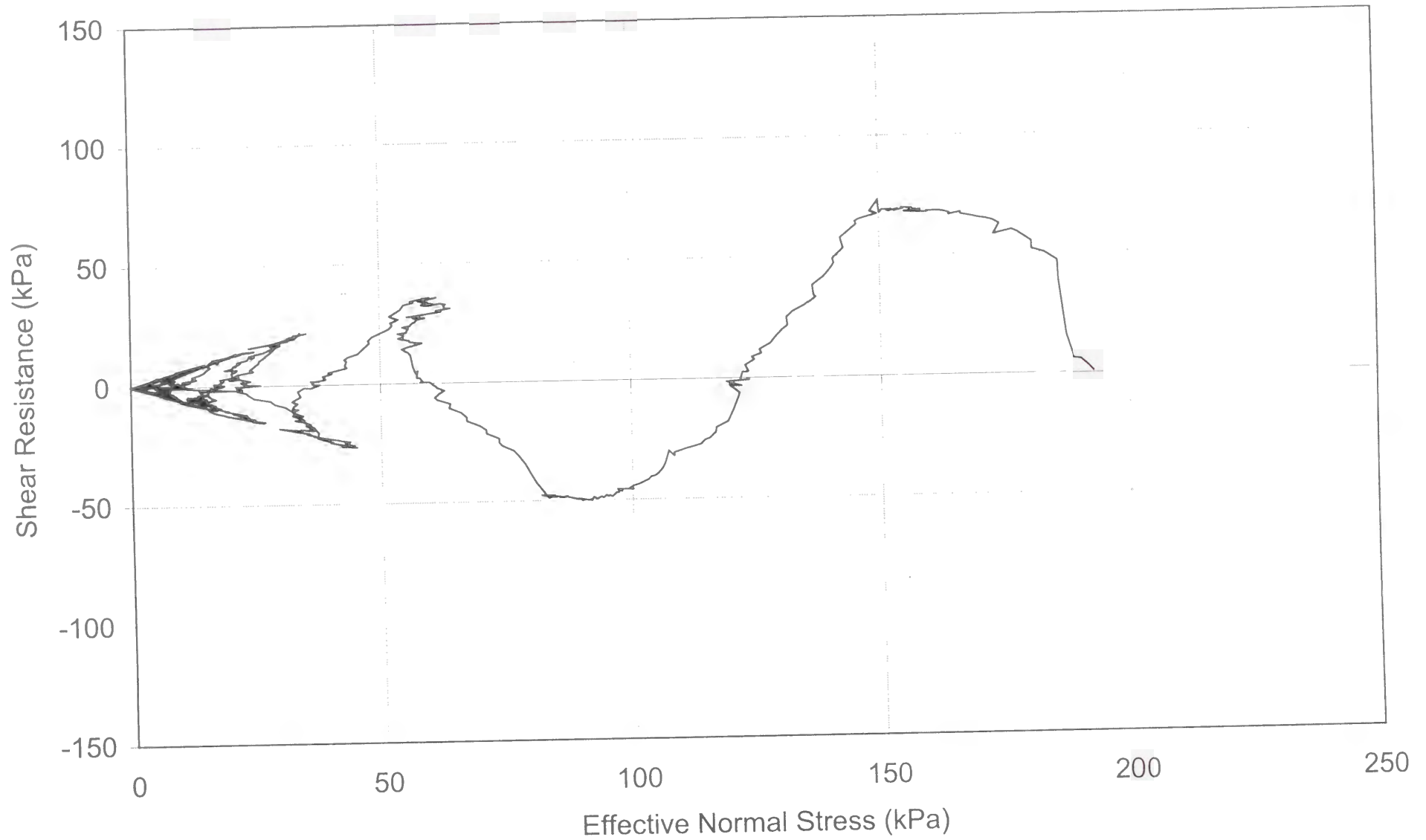| PARAMETER	UNIT	VALUE
Apparatus		Ring shear (DPRI-4)
Test type		Cyclic shear-displacement-controlled
Shear displacement amplitude	mm	0.49
Loading frequency	Hz	0.02
Data acquisition rate	point/cycle	250
Void ratio		0.68
Initial effective normal stress (σ'_{in})	kPa	200
Pore pressure coefficient B_D		0.97
Back pressure (u_0)	kPa	50

The following plots are included:
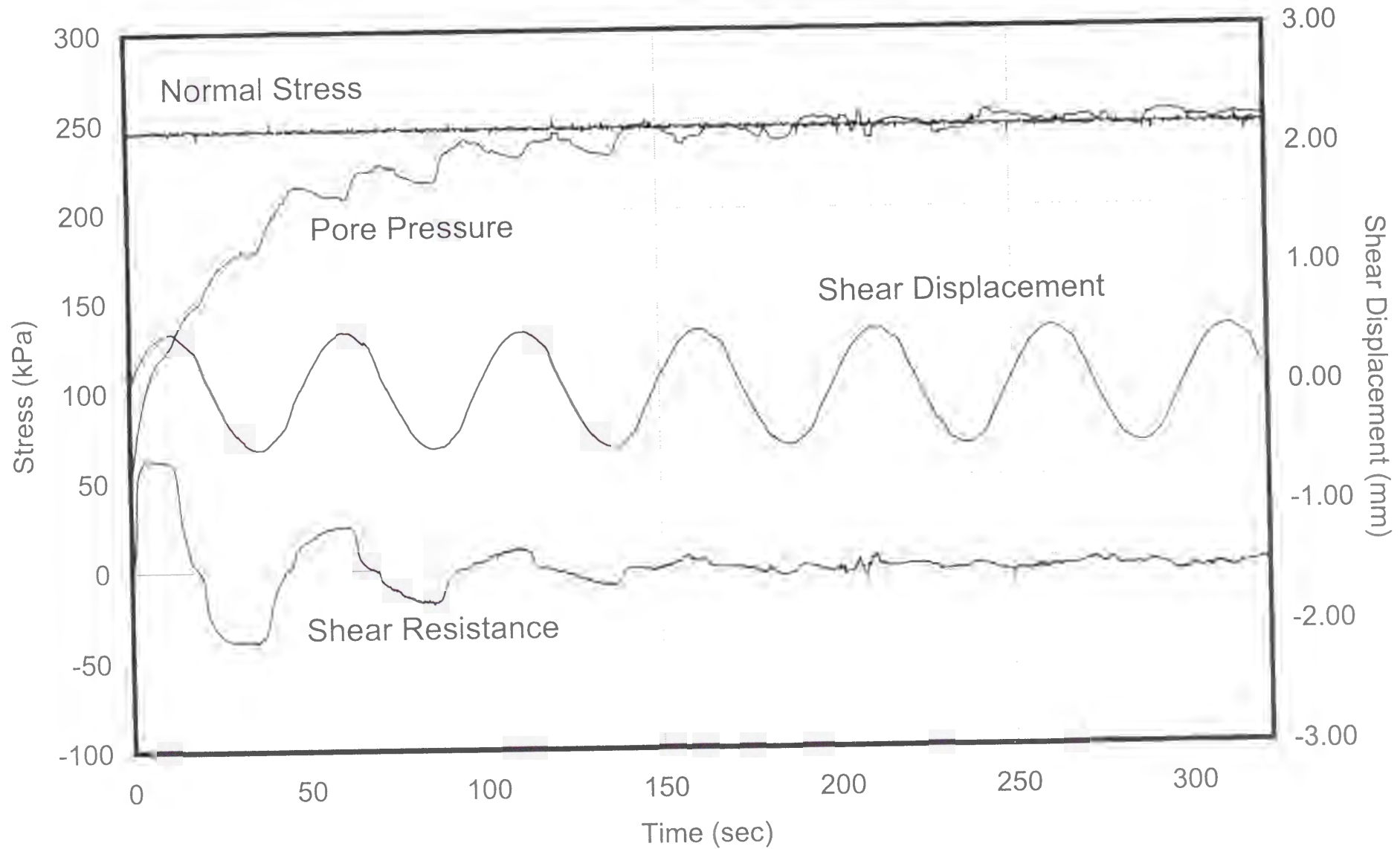
- **Plot No. 20-1**
  Time series of total normal stress, shear resistance, pore pressure, and shear displacement.

- **Plot No. 20-2**
  Effective stress path.

Normal Stress

Pore Pressure

Shear Displacement

Shear Resistance

Stress (kPa)

Shear Displacement (mm)

Time (sec)

Test No.20

Cyclic shear-displacement-controlled test. f=0.02 Hz; l_{max}=0.49mm.

Plot No.20-1

Cyclic shear displacement controlled test. f=0.02 Hz; I_{max}=0.49mm.

Test No.20

Plot No.20-2

TEST No. 21

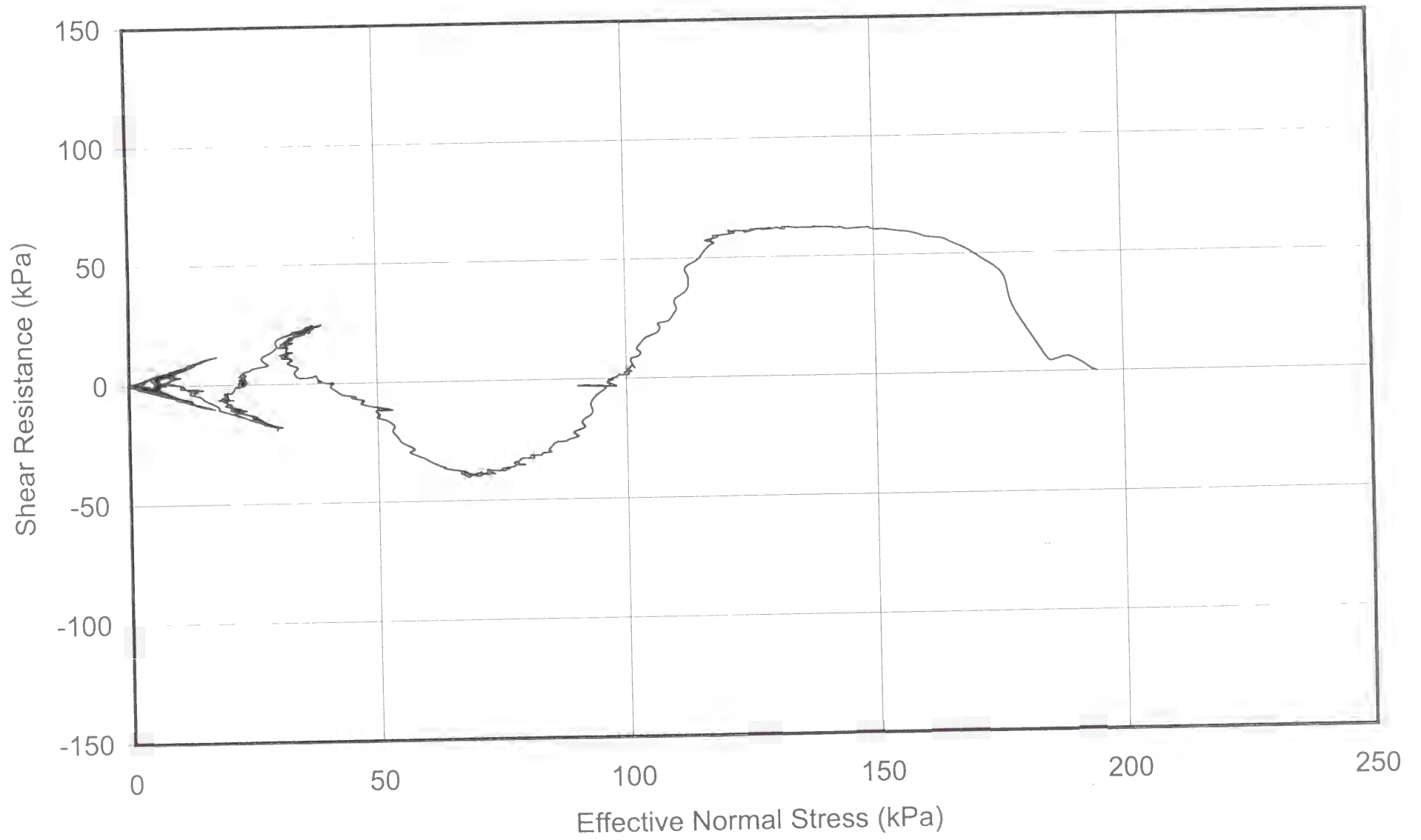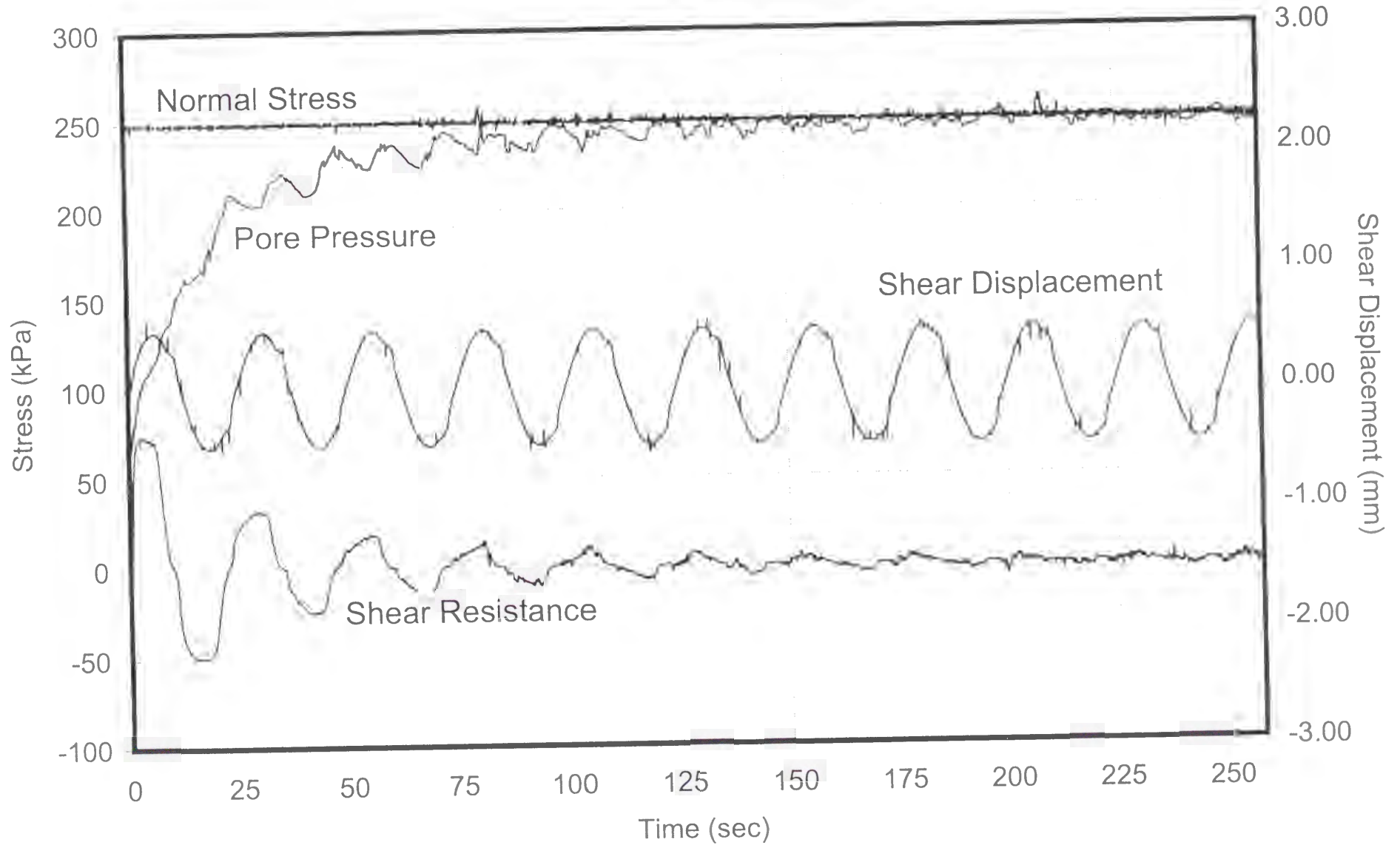| PARAMETER	UNIT	VALUE
Apparatus		Ring shear (DPRI-4)
Test type		Cyclic shear-displacement-controlled
Shear displacement amplitude	mm	0.49
Loading frequency	Hz	0.04
Data acquisition rate	point/cycle	250
Void ratio		0.67
Initial effective normal stress (σ'_{in})	kPa	192
Pore pressure coefficient B_D		1.00
Back pressure (u_0)	kPa	57

The following plots are included:

- **Plot No. 21-1**
Time series of total normal stress, shear resistance, pore pressure, and shear displacement.

- **Plot No. 21-2**
Effective stress path.

Normal Stress

Pore Pressure

Shear Displacement

Shear Resistance

Stress (kPa)

Shear Displacement (mm)

Time (sec)

Test No.21

Cyclic shear-displacement-controlled test. f=0.04 Hz; l_{max}=0.49mm.

Plot No.21-1

Cyclic shear-displacement-controlled test. f=0.04 Hz; l_{max}=0.49mm.

Test No.21

Plot No.21-2

TEST No. 22

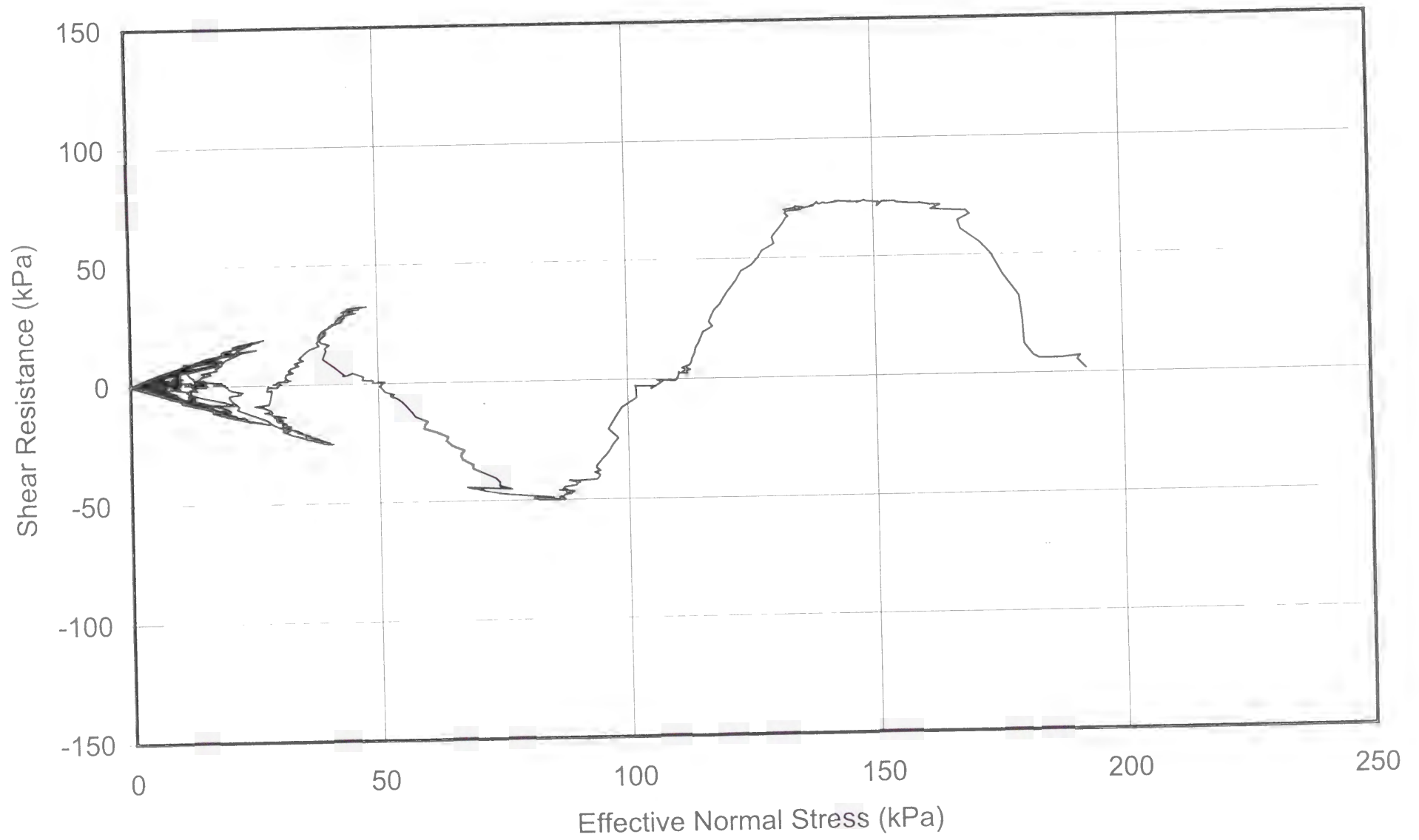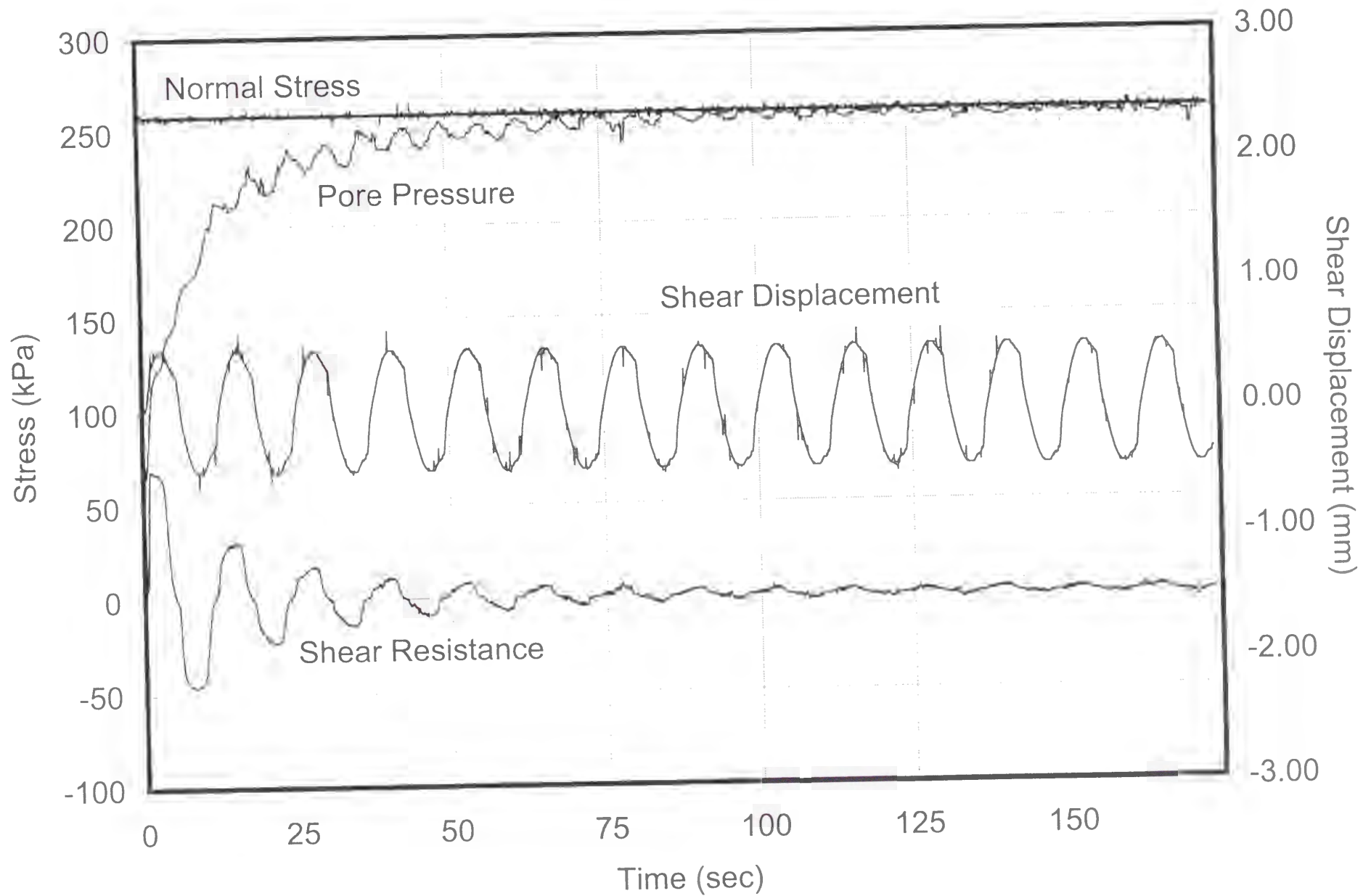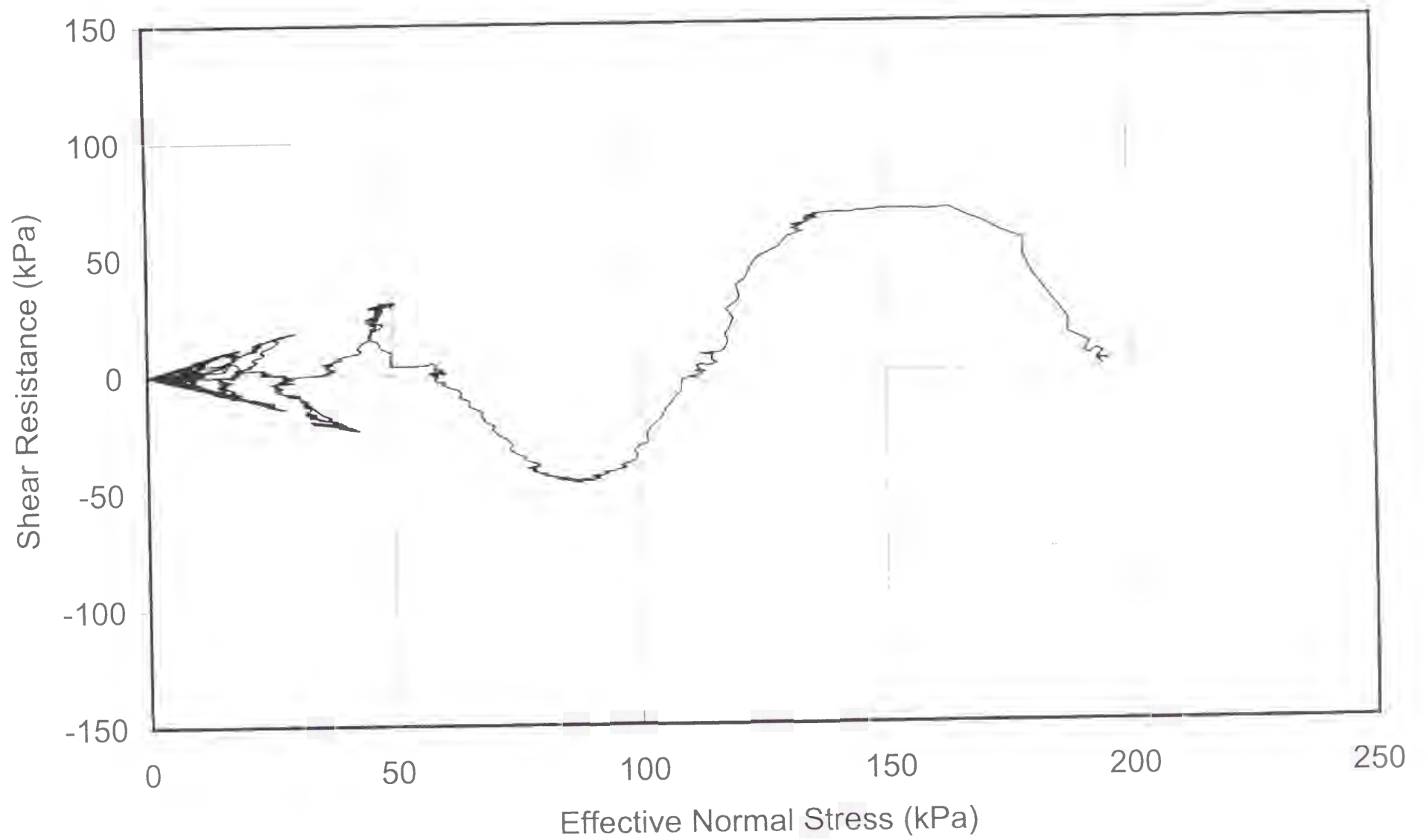| PARAMETER	UNIT	VALUE
Apparatus		Ring shear (DPRI-4)
Test type		Cyclic shear-displacement-controlled
Shear displacement amplitude	mm	0.49
Loading frequency	Hz	0.08
Data acquisition rate	point/cycle	250
Void ratio		0.66
Initial effective normal stress (σ'_{in})	kPa	195
Pore pressure coefficient B_D		0.97
Back pressure (u_0)	kPa	63

The following plots are included:

- **Plot No. 22-1**
Time series of total normal stress, shear resistance, pore pressure, and shear displacement.

- **Plot No. 22-2**
Effective stress path.

Cyclic shear displacement-controlled test. f=0.08 Hz; l$_{max}$=0.49mm.

Test No.22

Plot No.22-1

Y-axis: Shear Resistance (kPa) — 150, 100, 50, 0, -50, -100, -150

X-axis: Effective Normal Stress (kPa) — 0, 50, 100, 150, 200, 250

Test No.22

Cyclic shear-displacement-controlled test. f=0.08 Hz; l_{max}=0.49mm.

Plot No.22-2

TEST No. 23

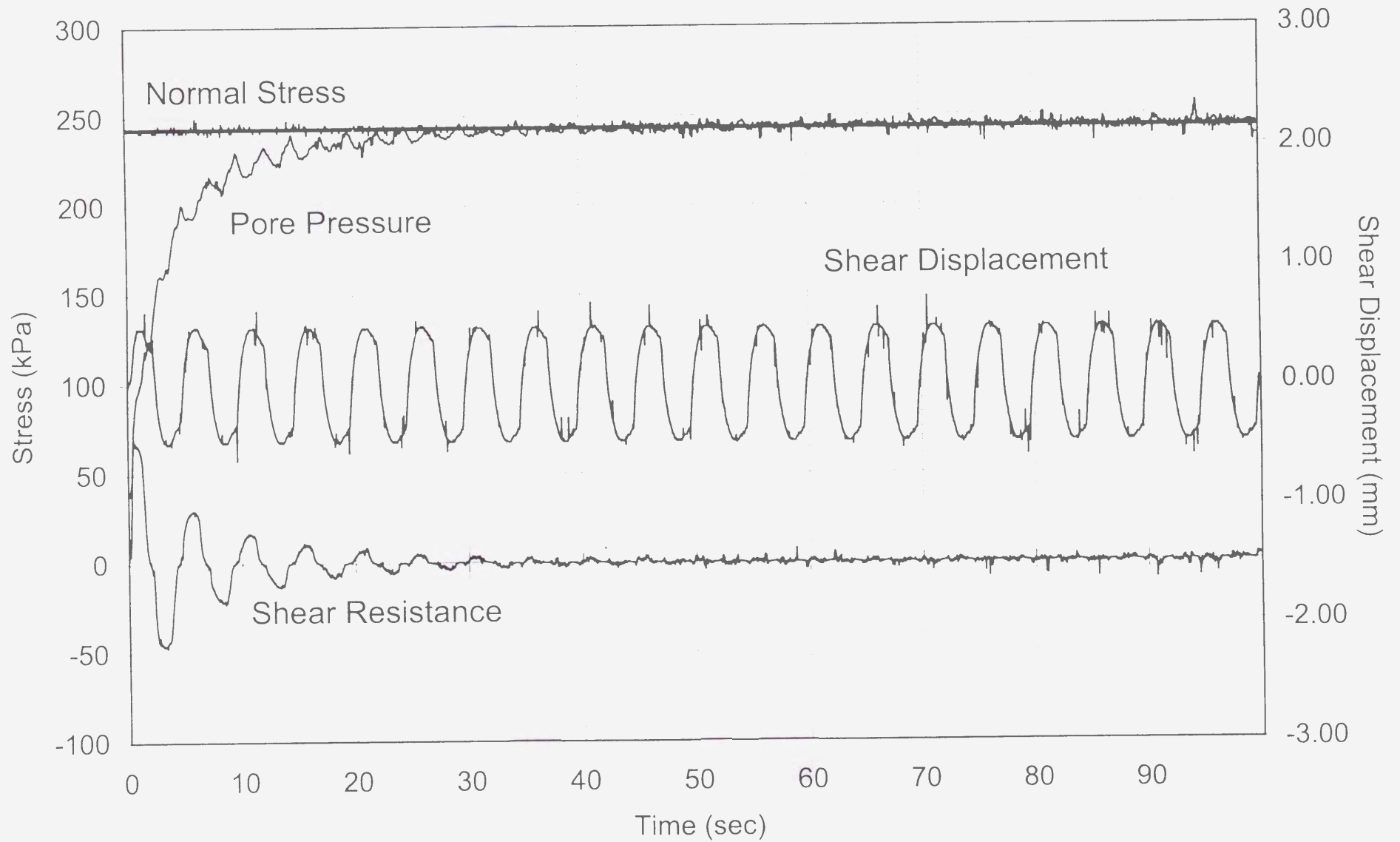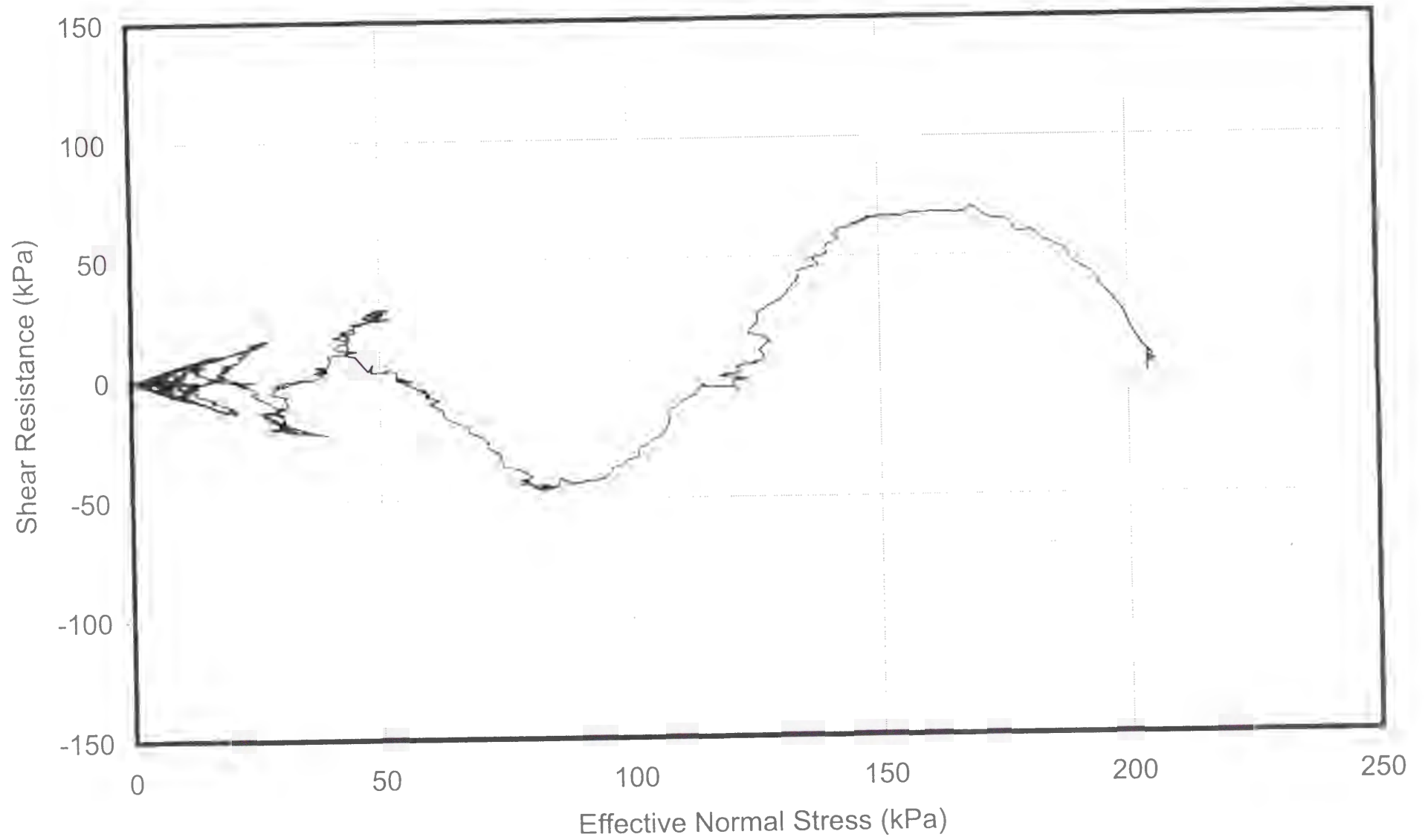| PARAMETER	UNIT	VALUE
Apparatus		Ring shear (DPRI-4)
Test type		Cyclic shear-displacement-controlled
Shear displacement amplitude	mm	0.50
Loading frequency	Hz	0.20
Data acquisition rate	point/cycle	250
Void ratio		0.67
Initial effective normal stress (σ'_{in})	kPa	204
Pore pressure coefficient B_D		0.95
Back pressure (u_0)	kPa	39

The following plots are included:

- **Plot No. 23-1**
Time series of total normal stress, shear resistance, pore pressure, and shear displacement.

- **Plot No. 23-2**
Effective stress path.

Test No.23   Cyclic shear-displacement-controlled test. f=0.20 Hz; l_{max}=0.50mm.   Plot No.23-1

Y-axis: Shear Resistance (kPa)

X-axis: Effective Normal Stress (kPa)

Cyclic shear-displacement-controlled test. f=0.20 Hz; I_{max}=0.50mm.

Test No.23

Plot No.23-2

TEST No. 24

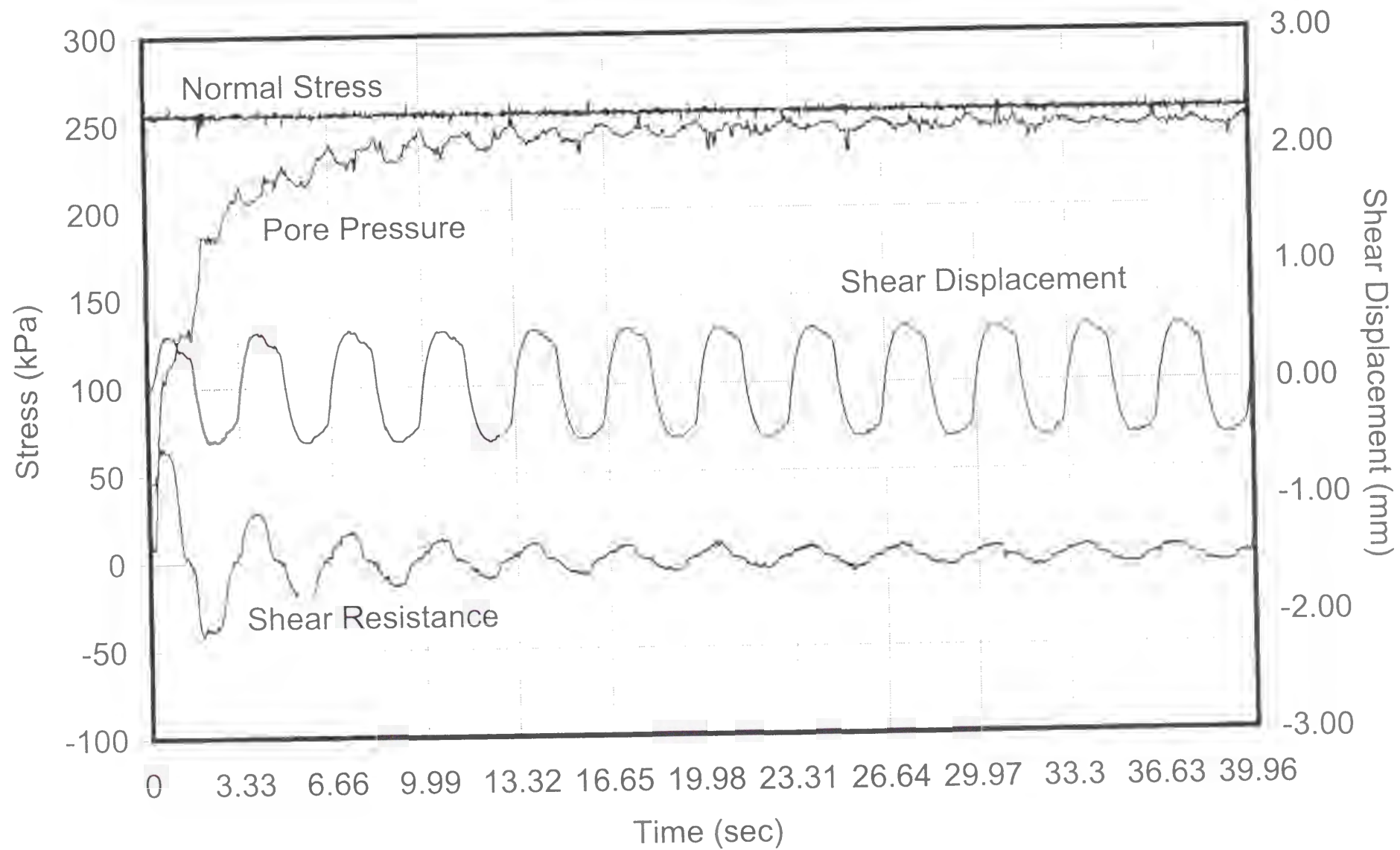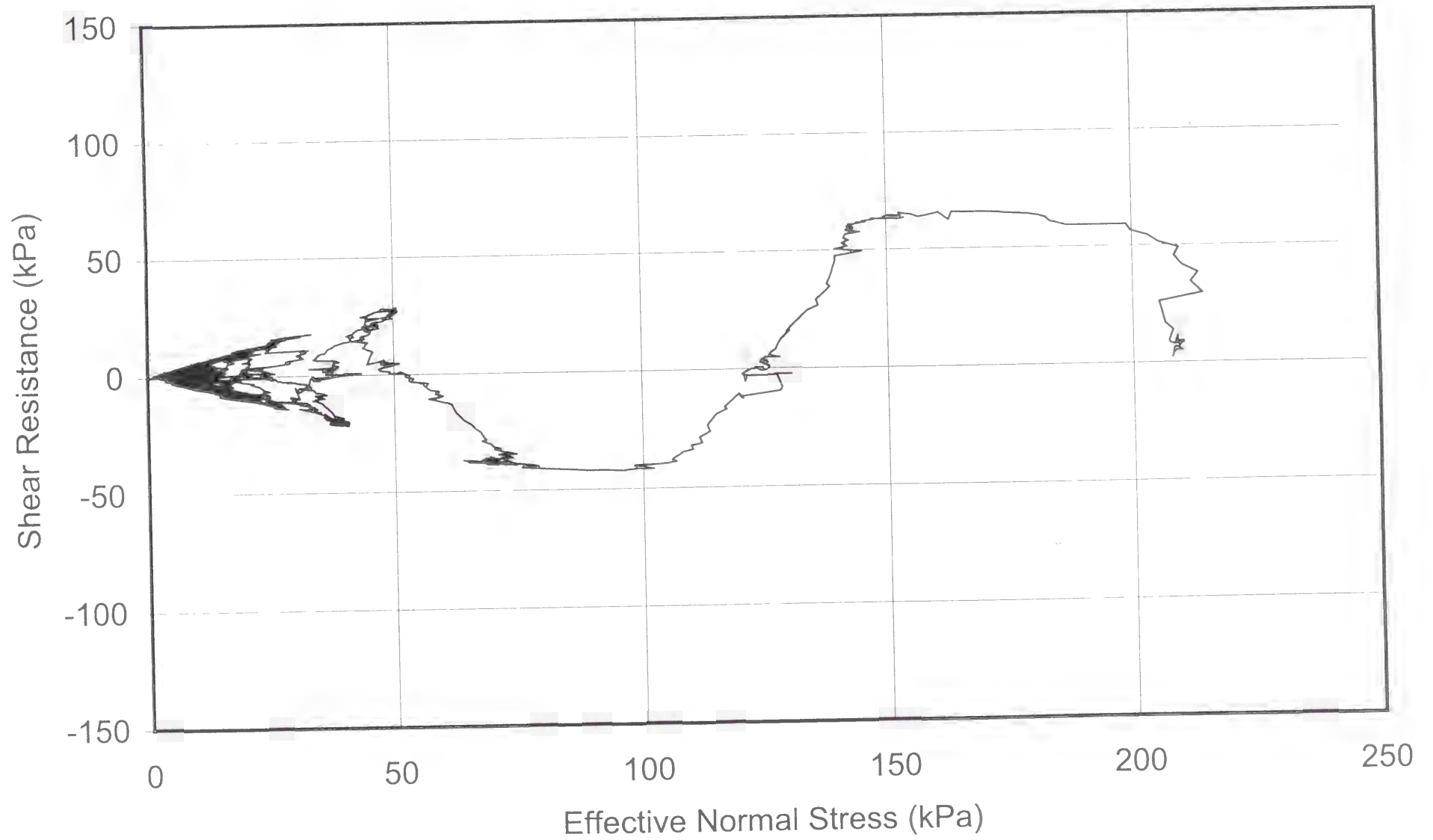| PARAMETER	UNIT	VALUE
Apparatus		Ring shear (DPRI-4)
Test type		Cyclic shear-displacement-controlled
Shear displacement amplitude	mm	0.46
Loading frequency	Hz	0.30
Data acquisition rate	point/cycle	333
Void ratio		0.67
Initial effective normal stress (σ'_{in})	kPa	202
Pore pressure coefficient B_D		0.96
Back pressure (u_0)	kPa	47

The following plots are included:

- **Plot No. 24-1**
Time series of total normal stress, shear resistance, pore pressure, and shear displacement.

- **Plot No. 24-2**
Effective stress path.

Cyclic shear-displacement-controlled test. f=0.30 Hz; I_{max}=0.46mm.

Test No.24

Cyclic shear displacement controlled test. f=0.30 Hz; I_{max}=0.46mm.

Test No.24

TEST No. 25

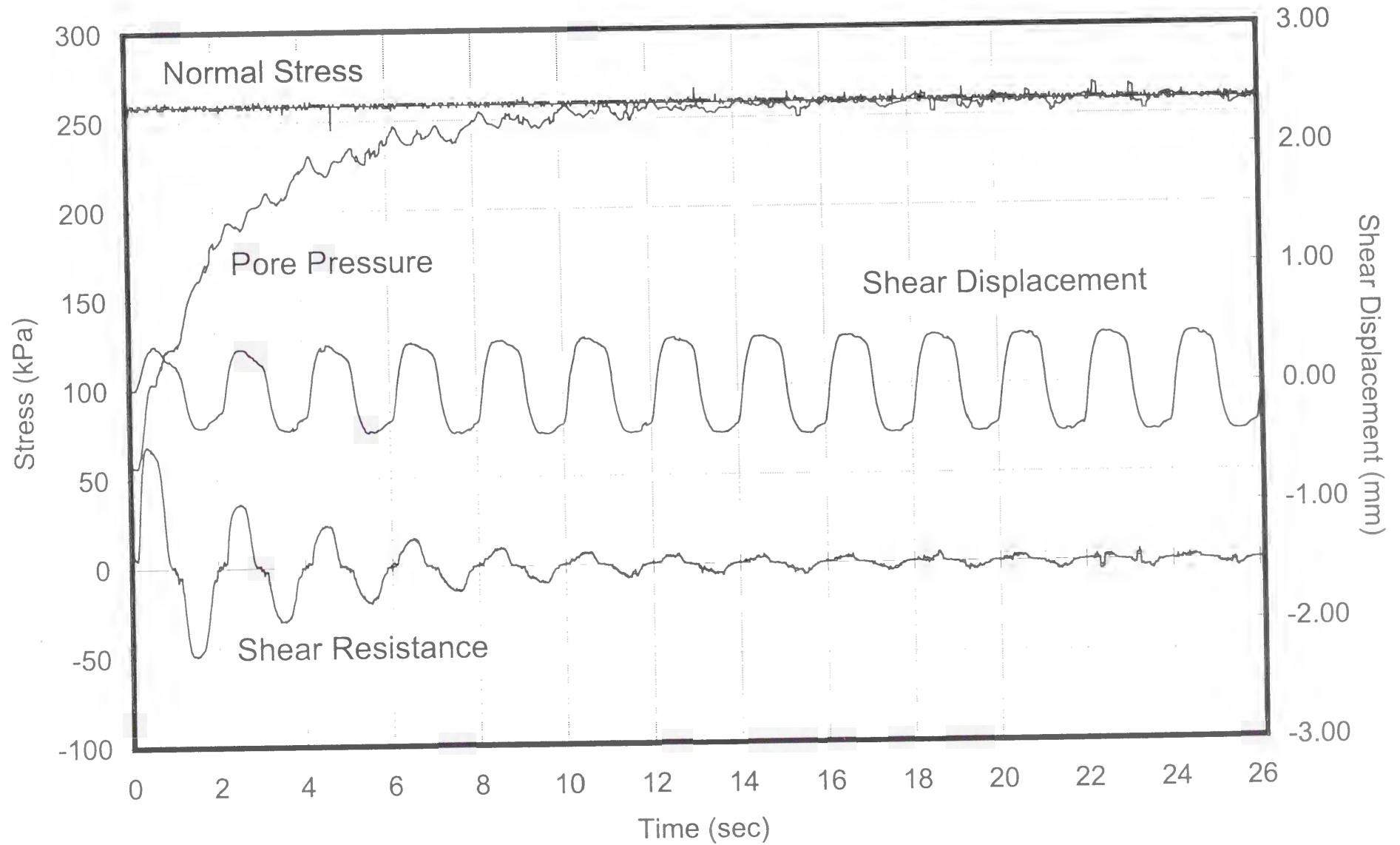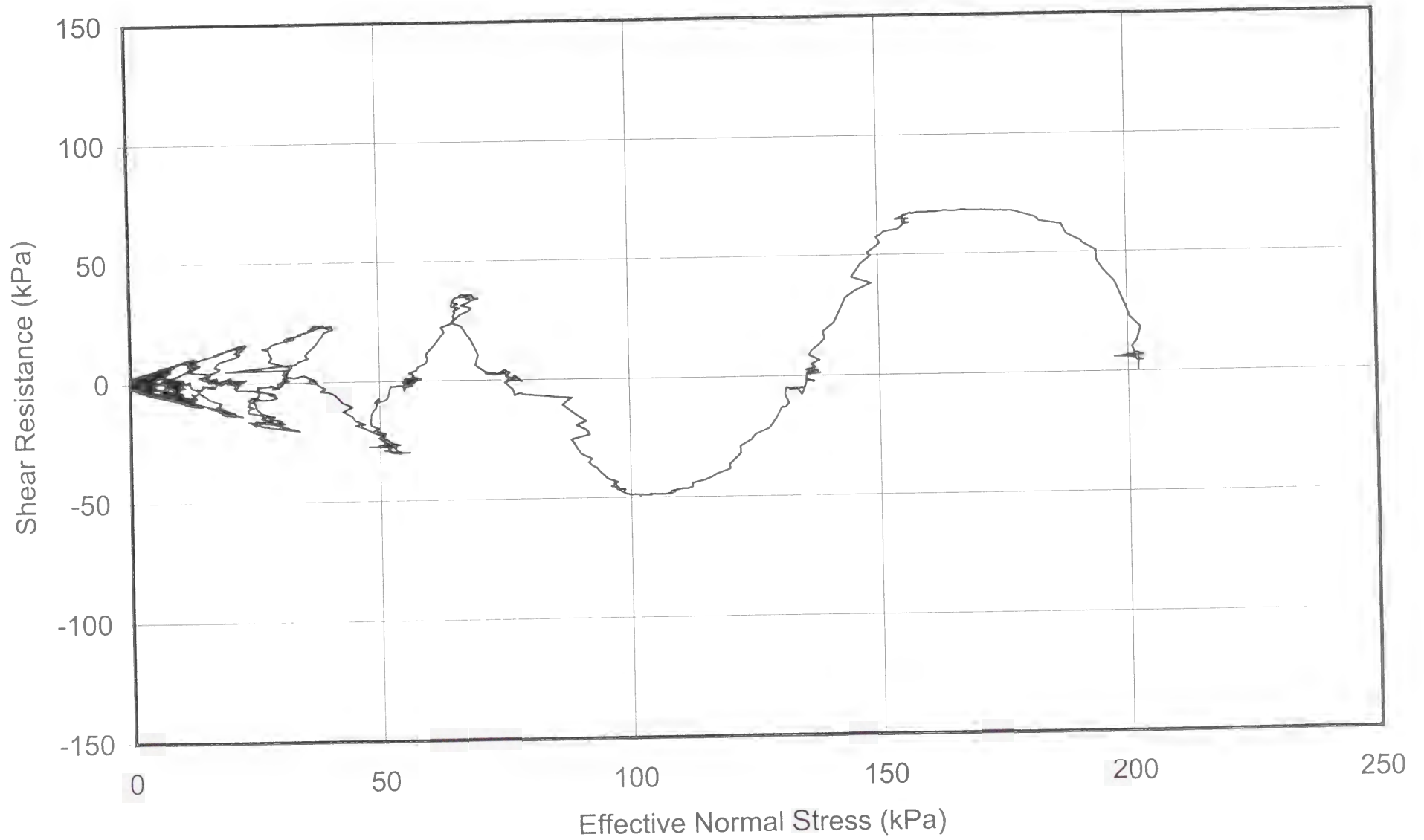| PARAMETER	UNIT	VALUE
Apparatus		Ring shear (DPRI-4)
Test type		Cyclic shear-displacement-controlled
Shear displacement amplitude	mm	0.38
Loading frequency	Hz	0.50
Data acquisition rate	point/cycle	200
Void ratio		0.67
Initial effective normal stress (σ'_{in})	kPa	202
Pore pressure coefficient B_D		1.00
Back pressure (u_0)	kPa	56

The following plots are included:

- **Plot No. 25-1**

Time series of total normal stress, shear resistance, pore pressure, and shear displacement.

- **Plot No. 25-2**

Effective stress path.

Normal Stress

Pore Pressure

Shear Displacement

Shear Resistance

Stress (kPa)

Shear Displacement (mm)

Time (sec)

Test No25

Cyclic shear-displacement-controlled test. f=0.50 Hz; l_{max}=0.38mm.

Plot No.25-1

Cyclic shear-displacement-controlled test. f=0.50 Hz; I_{max}=0.38mm

Test No.25

Plot No.25-2

TEST No. 26

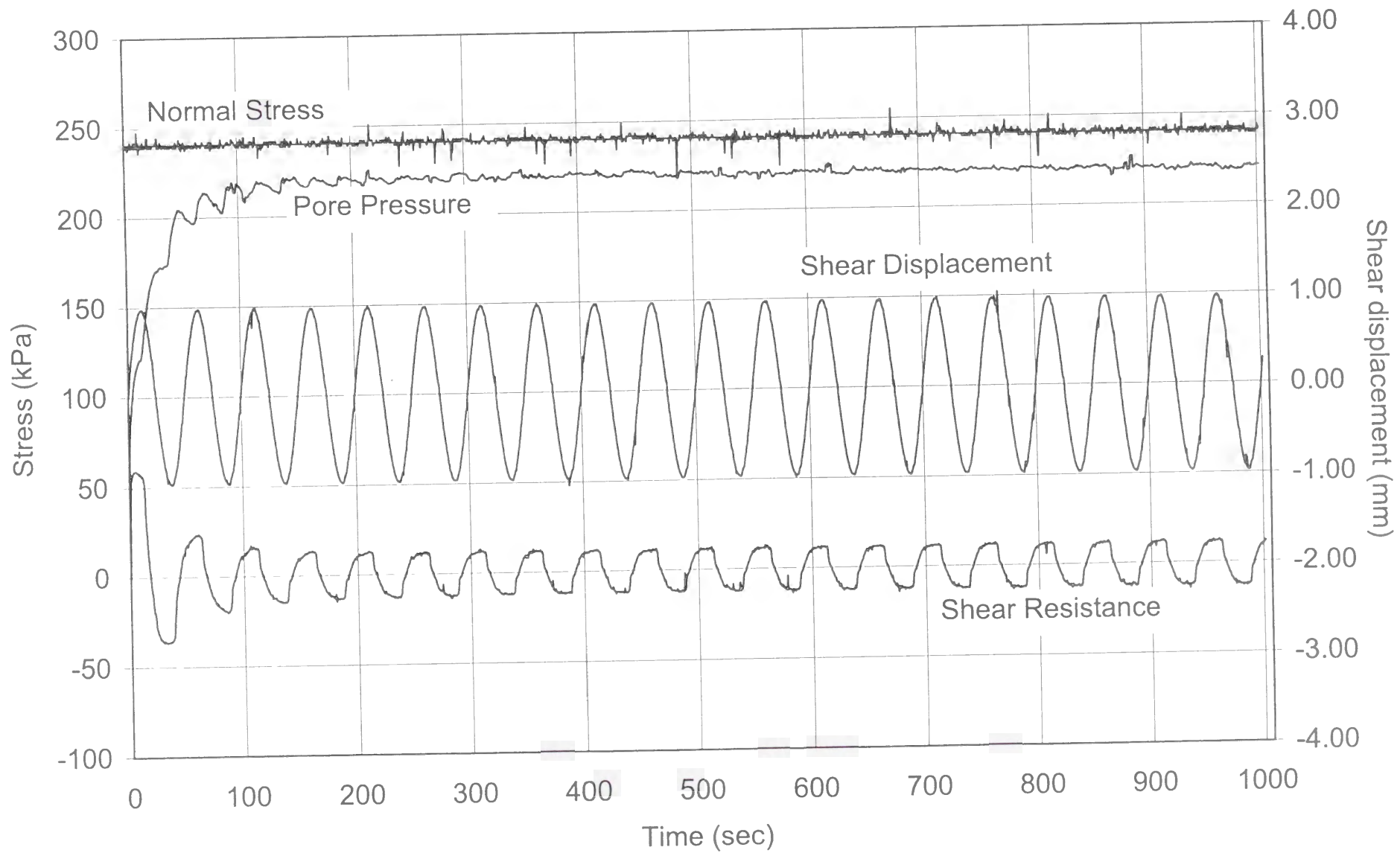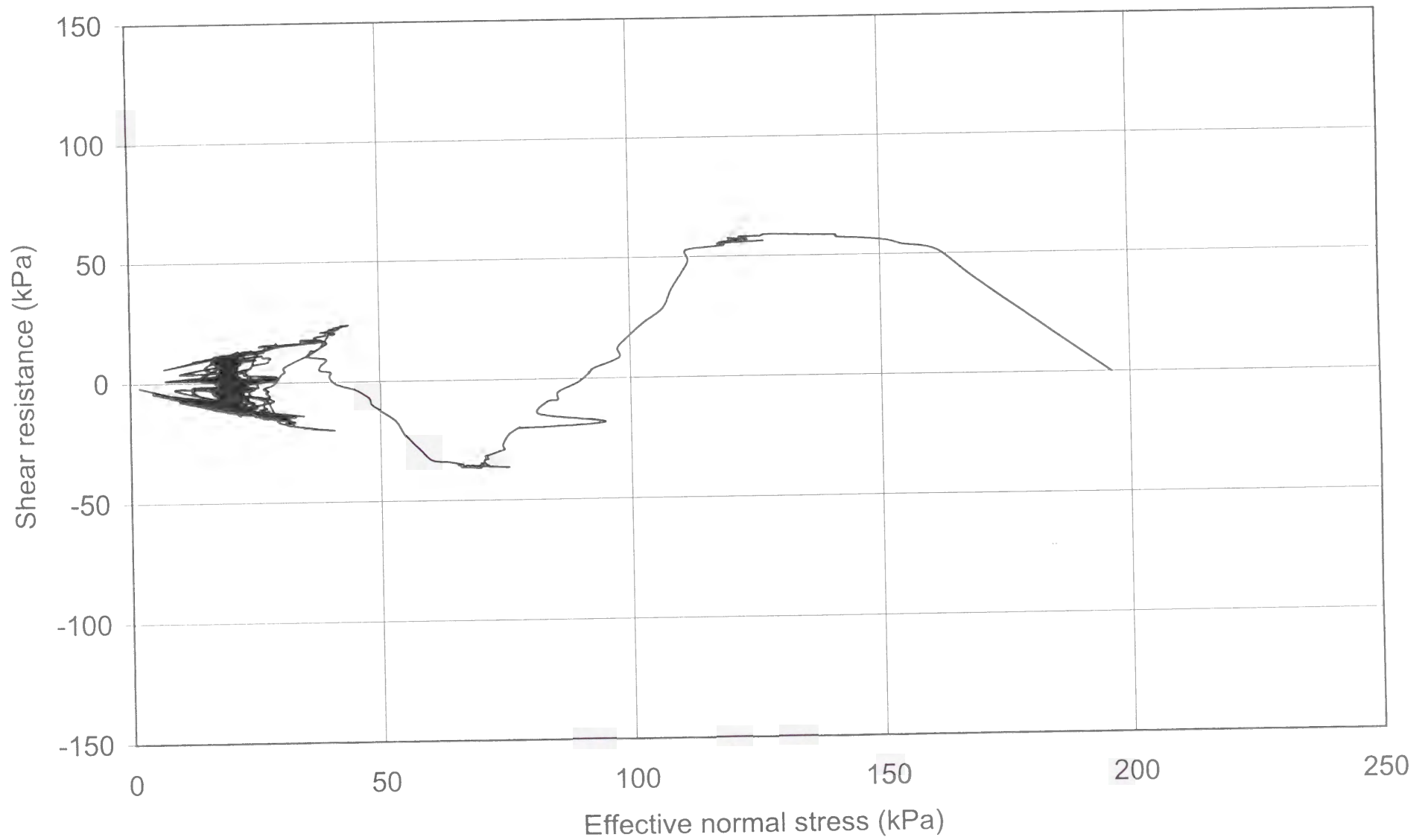| PARAMETER	UNIT	VALUE
Apparatus		Ring shear (DPRI-4)
Test type		Cyclic shear-displacement-controlled
Shear displacement amplitude	mm	0.97
Loading frequency	Hz	0.02
Data acquisition rate	point/cycle	100
Void ratio		0.58
Initial effective normal stress (σ'_{in})	kPa	182
Pore pressure coefficient B_D		0.95
Back pressure (u_0)	kPa	0

The following plots are included:

- **Plot No. 26-1**
Time series of total normal stress, shear resistance, pore pressure, and shear displacement.

- **Plot No. 26-2**
Effective stress path.

Cyclic shear-displacement-controlled test. f=0.02 Hz. l_{max}=0.97mm

Test No.26

Plot No.26-1

Cyclic shear-displacement-controlled test. f=0.02 Hz; l_{max}=0.97mm.

Test No.26

Plot No.26-2

TEST No. 27

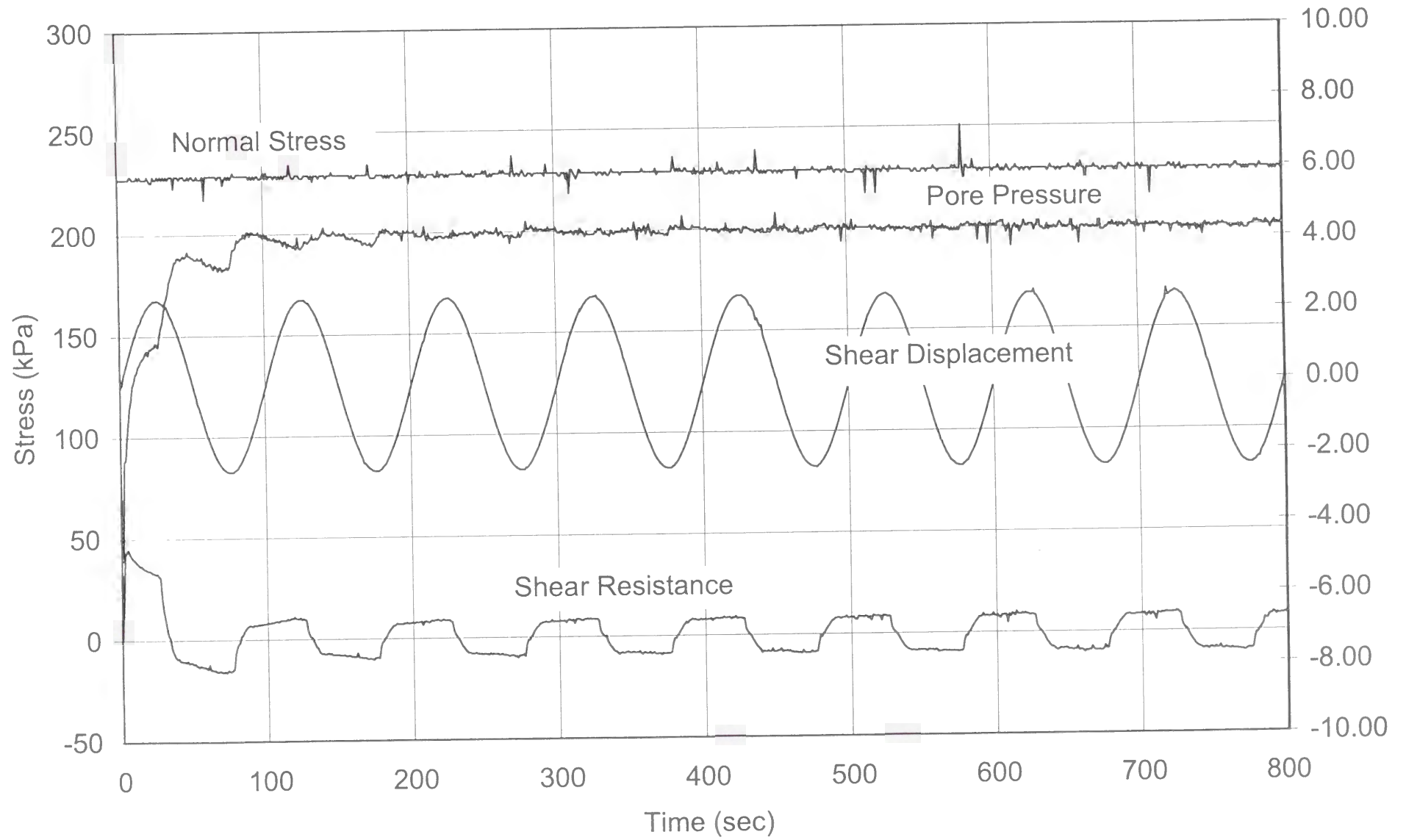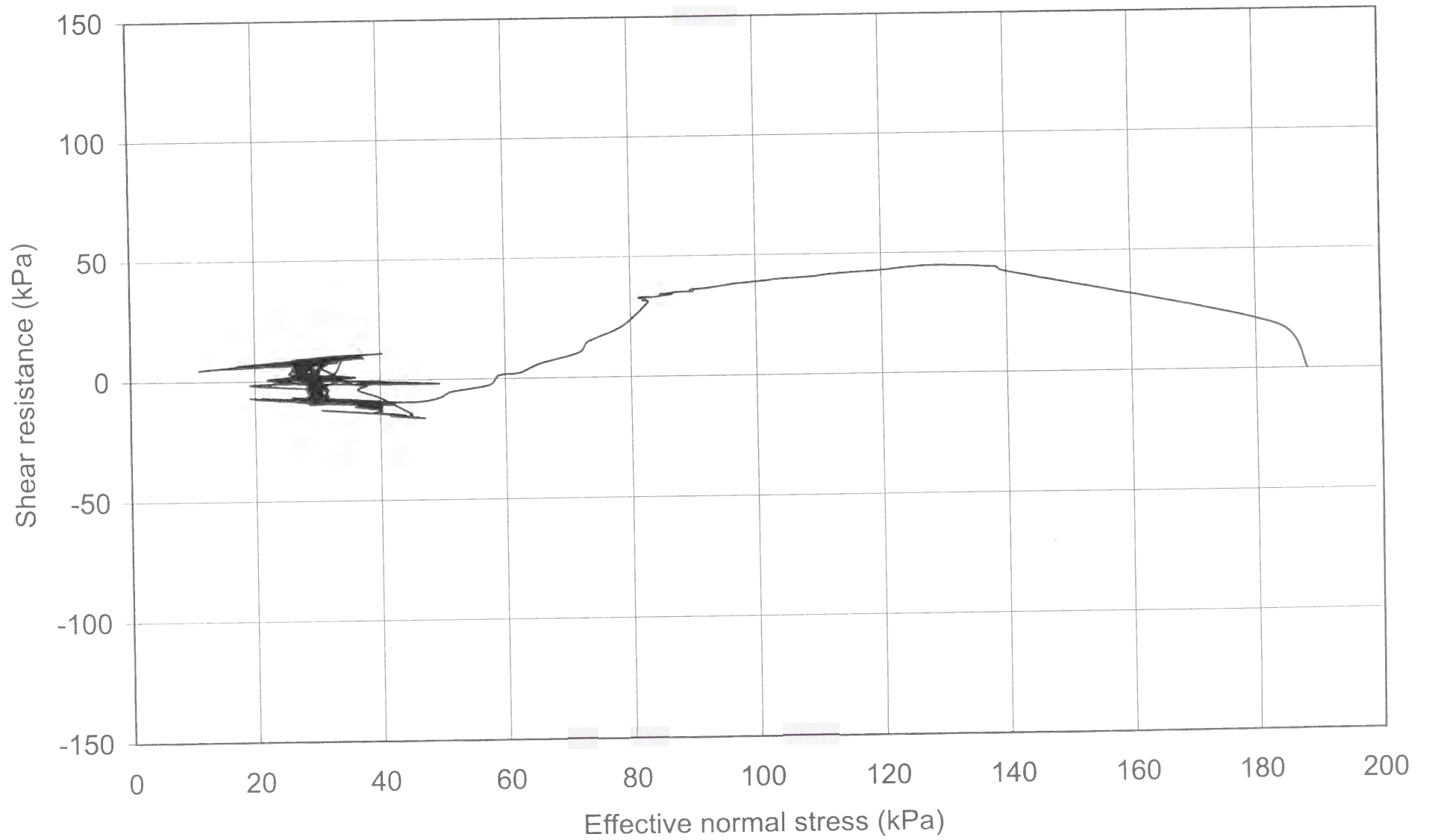| PARAMETER	UNIT	VALUE
Apparatus		Ring shear (DPRI-4)
Test type		Cyclic shear-displacement-controlled
Shear displacement amplitude	mm	2.42
Loading frequency	Hz	0.01
Data acquisition rate	point/cycle	100
Void ratio		0.60
Initial effective normal stress (σ'_{in})	kPa	164
Pore pressure coefficient B_D		0.95
Back pressure (u_0)	kPa	0

The following plots are included:

- **Plot No. 27-1**
Time series of total normal stress, shear resistance, pore pressure, and shear displacement.

- **Plot No. 27-2**
Effective stress path.

Cyclic shear-displacement-controlled test. $f=0.01$ Hz; $l_{max}=2.42$mm.

Test No.27

Plot No.27-1

Shear resistance (kPa) vs **Effective normal stress (kPa)**

Test No.27

Cyclic shear-displacement-controlled test, f=0.01 Hz; I_{max}=2.42mm.

Plot No.27-2

TEST No. 28

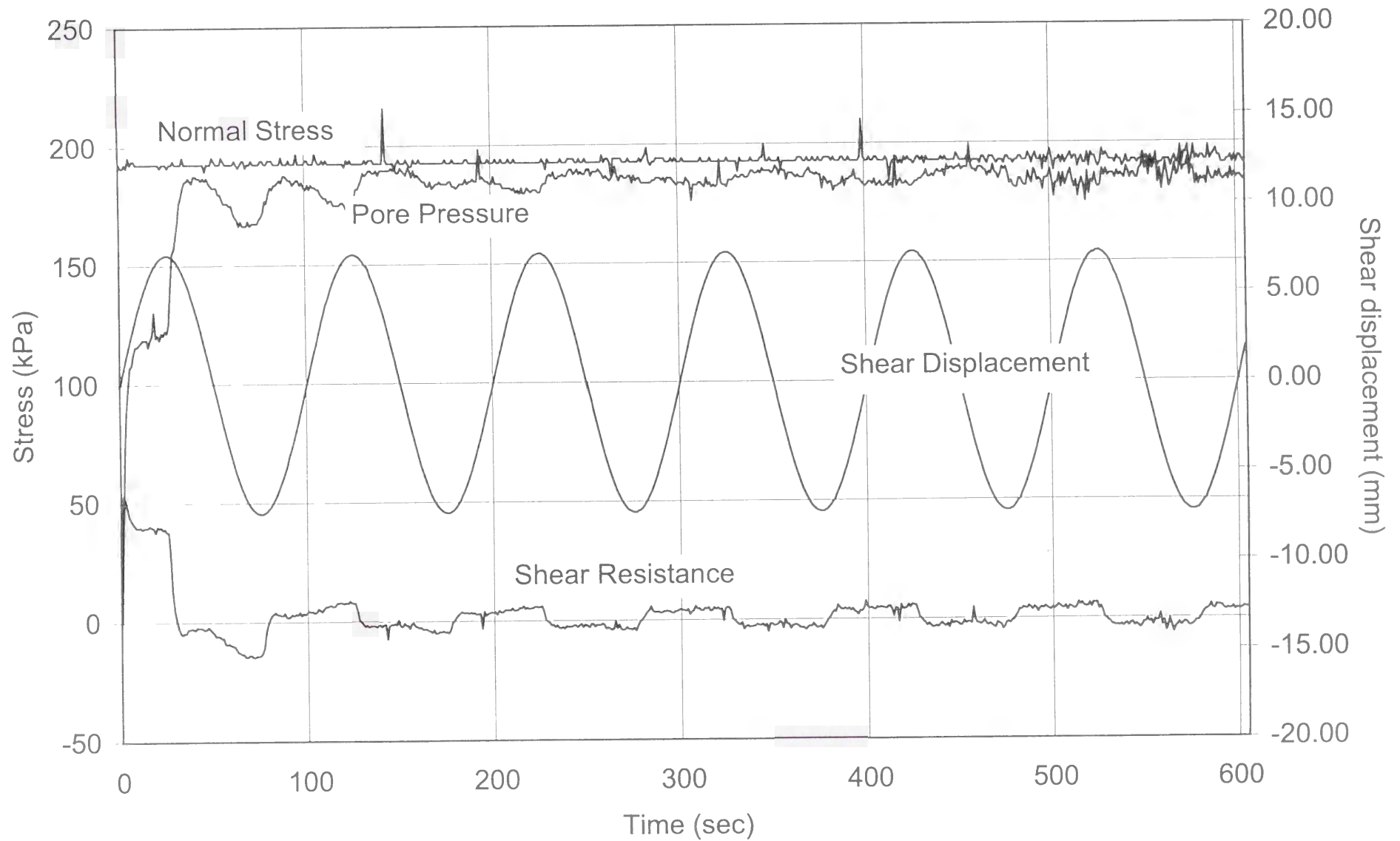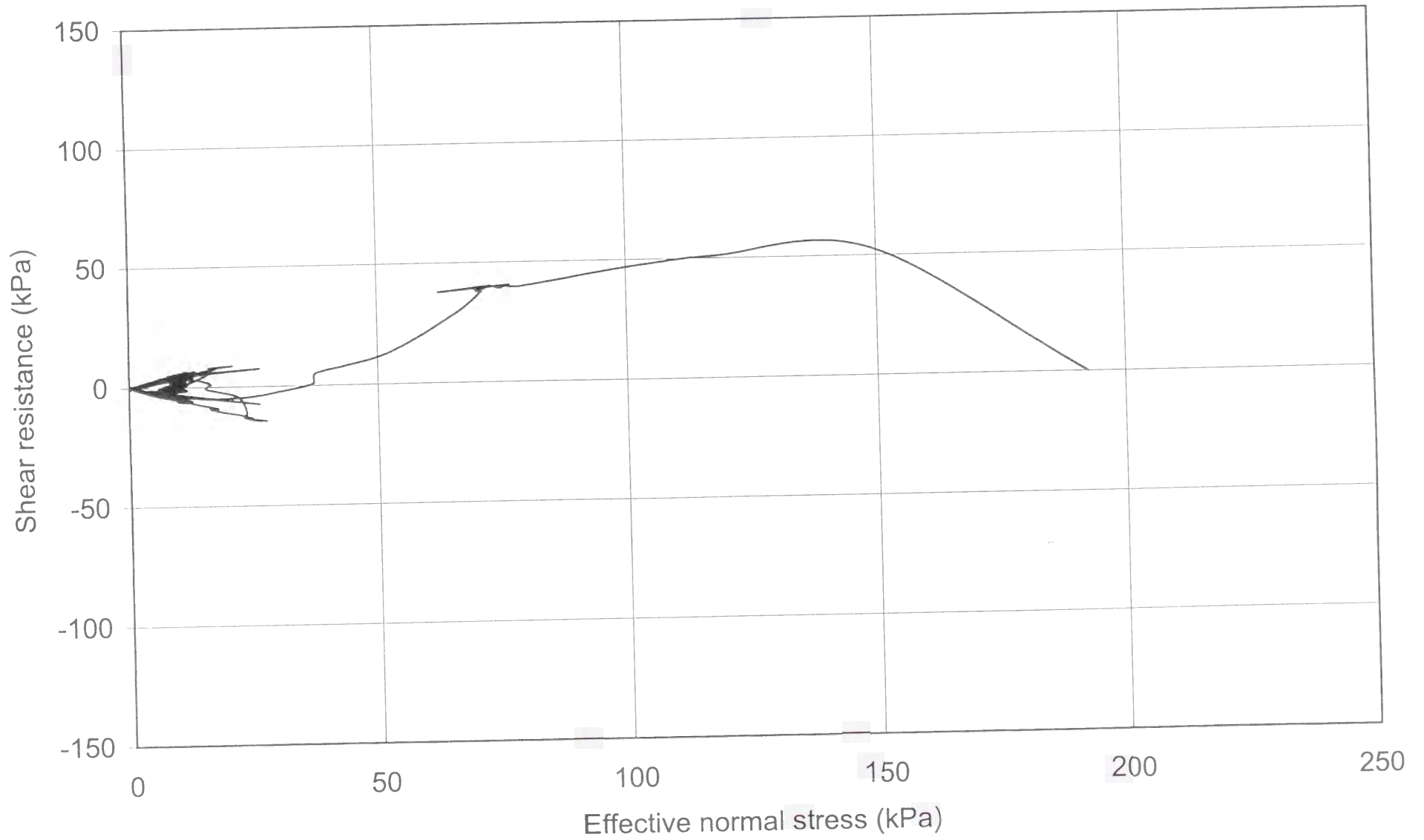| PARAMETER	UNIT	VALUE
Apparatus		Ring shear (DPRI-4)
Test type		Cyclic shear-displacement-controlled
Shear displacement amplitude	mm	7.25
Loading frequency	Hz	0.01
Data acquisition rate	point/cycle	100
Void ratio		0.59
Initial effective normal stress (σ'_{in})	kPa	193
Pore pressure coefficient B_D		0.96
Back pressure (u_0)	kPa	0

The following plots are included:

- **Plot No. 28-1**
Time series of total normal stress, shear resistance, pore pressure, and shear displacement.

- **Plot No. 28-2**
Effective stress path.

Cyclic shear-displacement-controlled test. $f=0.01$ Hz. $I_{max}=7.25$mm.

Test No.28

Plot No.28-1

Cyclic shear-displacement-controlled test. f=0.01 Hz; I_{max}=7.25mm.

Test No.28

Plot No.28-2

TEST No. 29

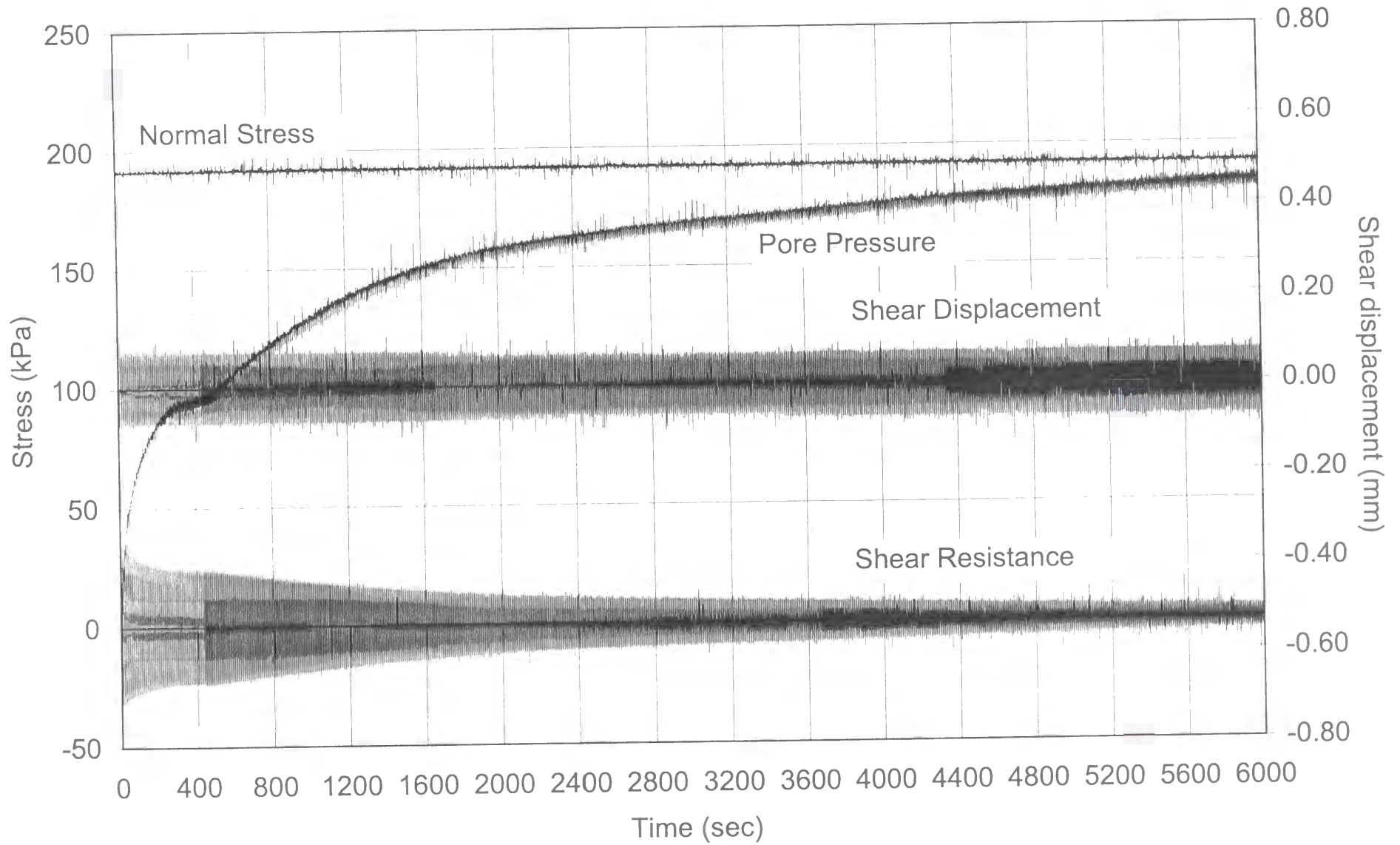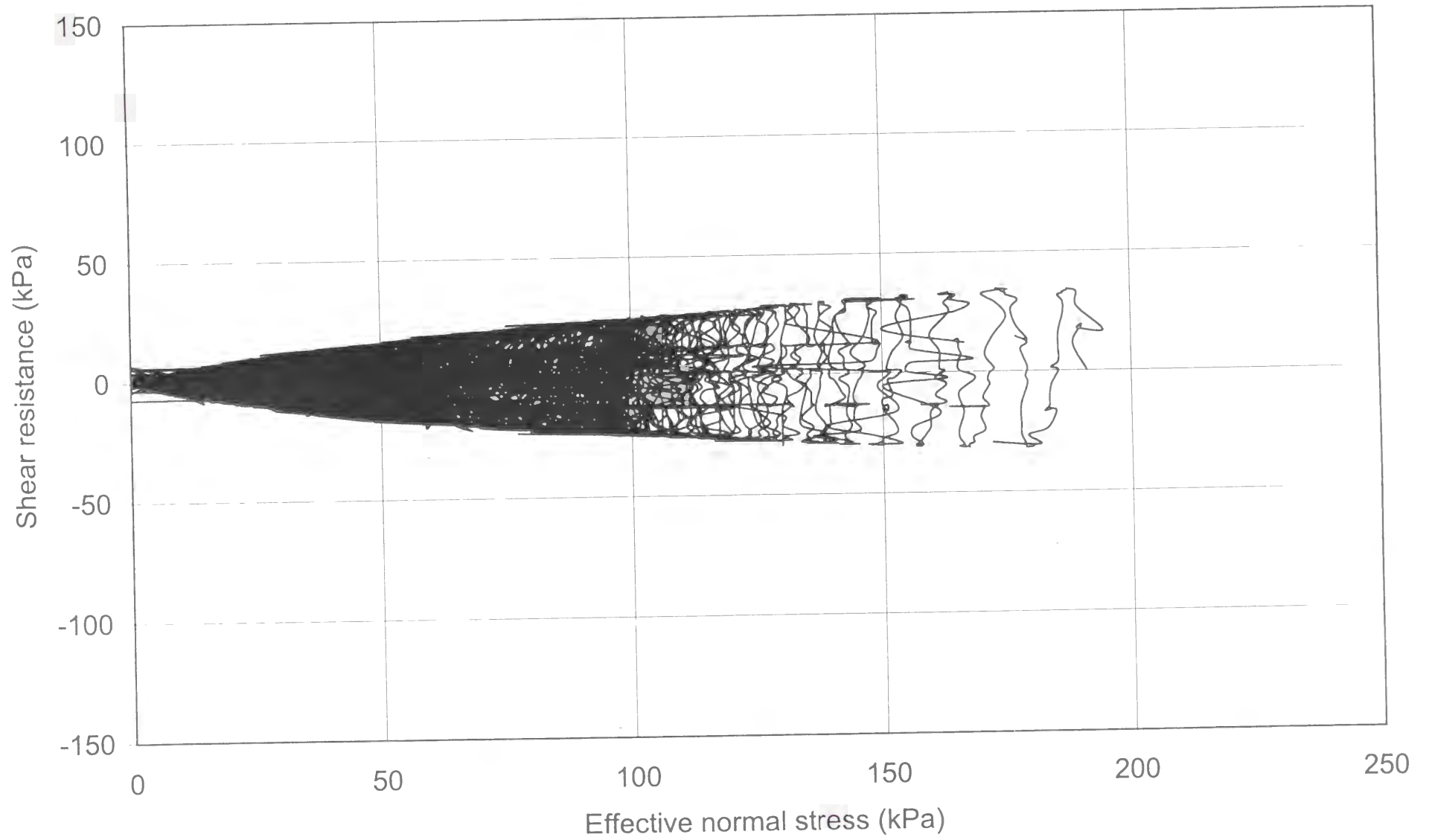| PARAMETER	UNIT	VALUE
Apparatus		Ring shear (DPRI-4)
Test type		Cyclic shear-displacement-controlled
Shear displacement amplitude	mm	0.08
Loading frequency	Hz	0.05
Data acquisition rate	point/cycle	50
Void ratio		0.62
Initial effective normal stress (σ'_{in})	kPa	191
Pore pressure coefficient B_D		0.95
Back pressure (u_0)	kPa	0

The following plots are included:

- **Plot No. 29-1**
Time series of total normal stress, shear resistance, pore pressure, and shear displacement.

- **Plot No. 29-2**
Effective stress path.

Cyclic shear-displacement-controlled test. f=0.05 Hz; l_{max}=0.08mm.

Test No.29

Plot No.29-1

Cyclic shear-displacement-controlled test. f=0.05 Hz; l_{max}=0.08mm.

Test No.29

Plot No.29-2

TEST No. 30

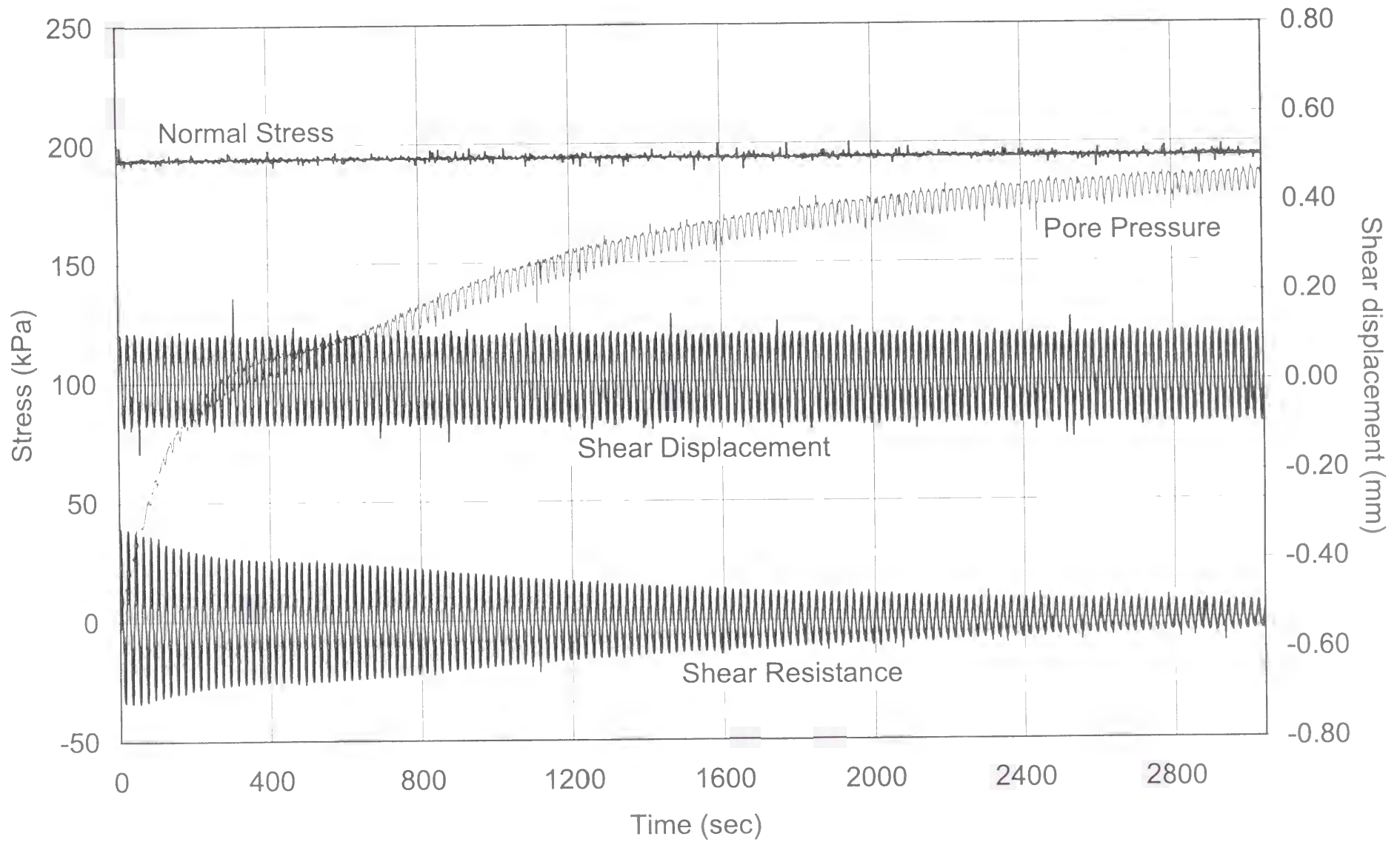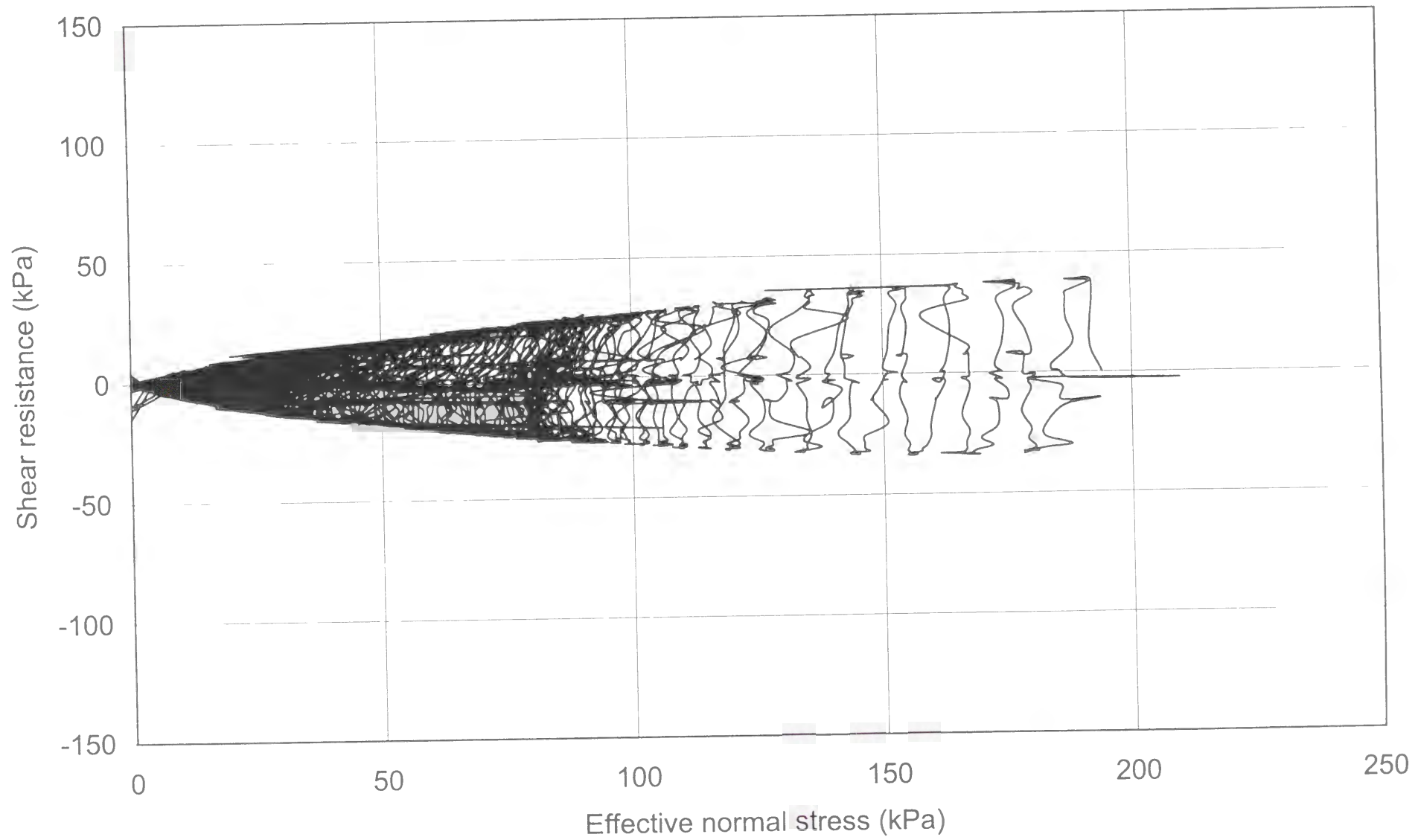| PARAMETER	UNIT	VALUE
Apparatus		Ring shear (DPRI-4)
Test type		Cyclic shear-displacement-controlled
Shear displacement amplitude	mm	0.10
Loading frequency	Hz	0.05
Data acquisition rate	point/cycle	50
Void ratio		0.61
Initial effective normal stress (σ'_{in})	kPa	194
Pore pressure coefficient B_D		0.98
Back pressure (u_0)	kPa	0

The following plots are included:

- **Plot No. 30-1**

Time series of total normal stress, shear resistance, pore pressure, and shear displacement.

- **Plot No. 30-2**

Effective stress path.

Normal Stress

Pore Pressure

Shear Displacement

Shear Resistance

Test No.30

Cyclic shear-displacement-controlled test. f=0.05 Hz; l_{max}=0.10mm

Plot No.30-1

Cyclic shear-displacement-controlled test. f=0.05 Hz; I_{max}=0.10mm.

Test No.30

TEST No. 31

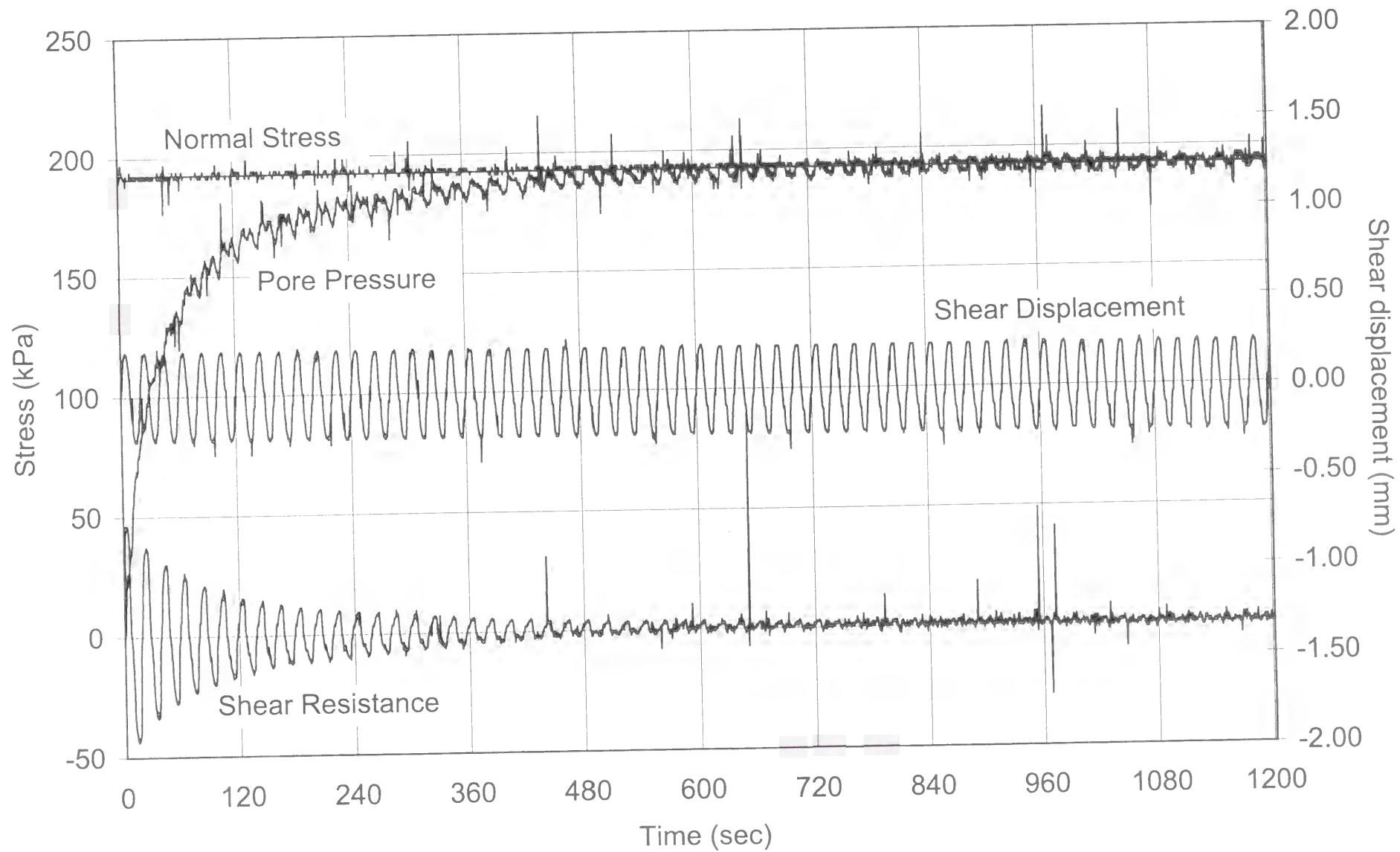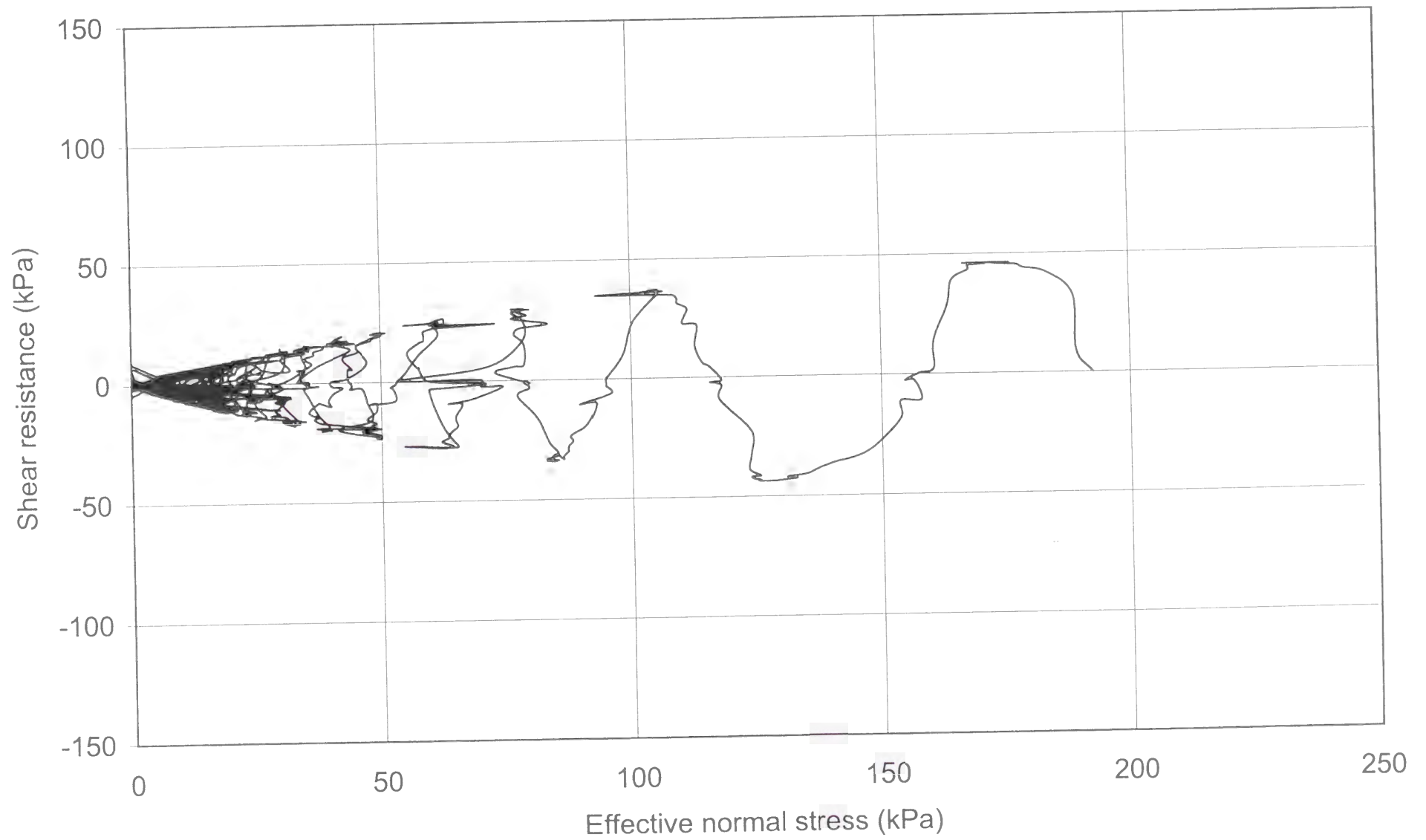| PARAMETER	UNIT	VALUE
Apparatus		Ring shear (DPRI-4)
Test type		Cyclic shear-displacement-controlled
Shear displacement amplitude	mm	0.25
Loading frequency	Hz	0.05
Data acquisition rate	point/cycle	50
Void ratio		0.62
Initial effective normal stress (σ'_{in})	kPa	193
Pore pressure coefficient B_D		0.98
Back pressure (u_0)	kPa	0

The following plots are included:

- **Plot No. 31-1**
Time series of total normal stress, shear resistance, pore pressure, and shear displacement.

- **Plot No. 31-2**
Effective stress path.

Cyclic shear-displacement-controlled test. f=0.05 Hz; I_{max}=0.25mm.

Test No.31

Plot No.31-1

Shear resistance (kPa) vs Effective normal stress (kPa)

Cyclic shear-displacement-controlled test; f=0.05 Hz; l_{max}=0.25mm.

Test No.31

Plot No.31-2

TEST No. 32

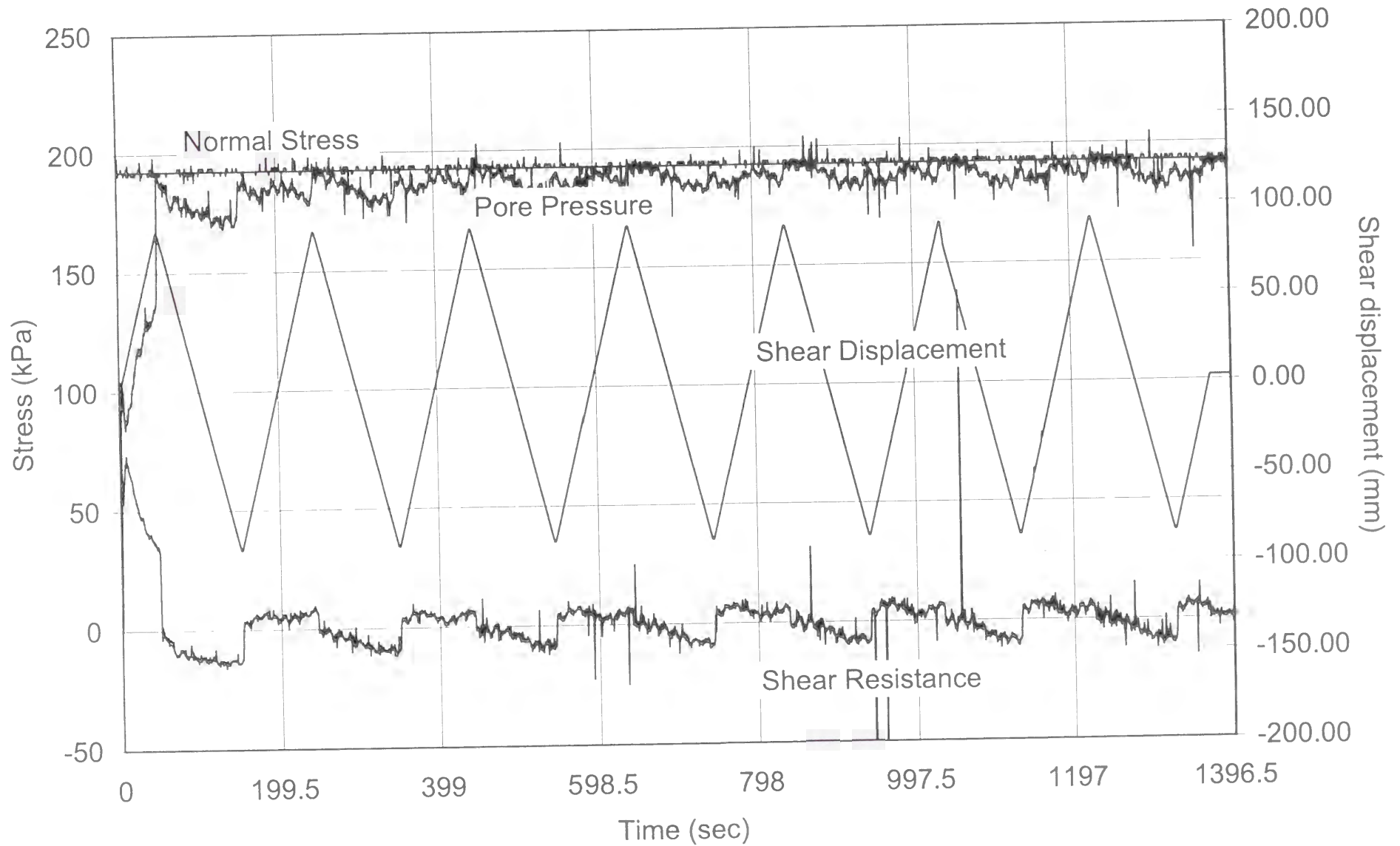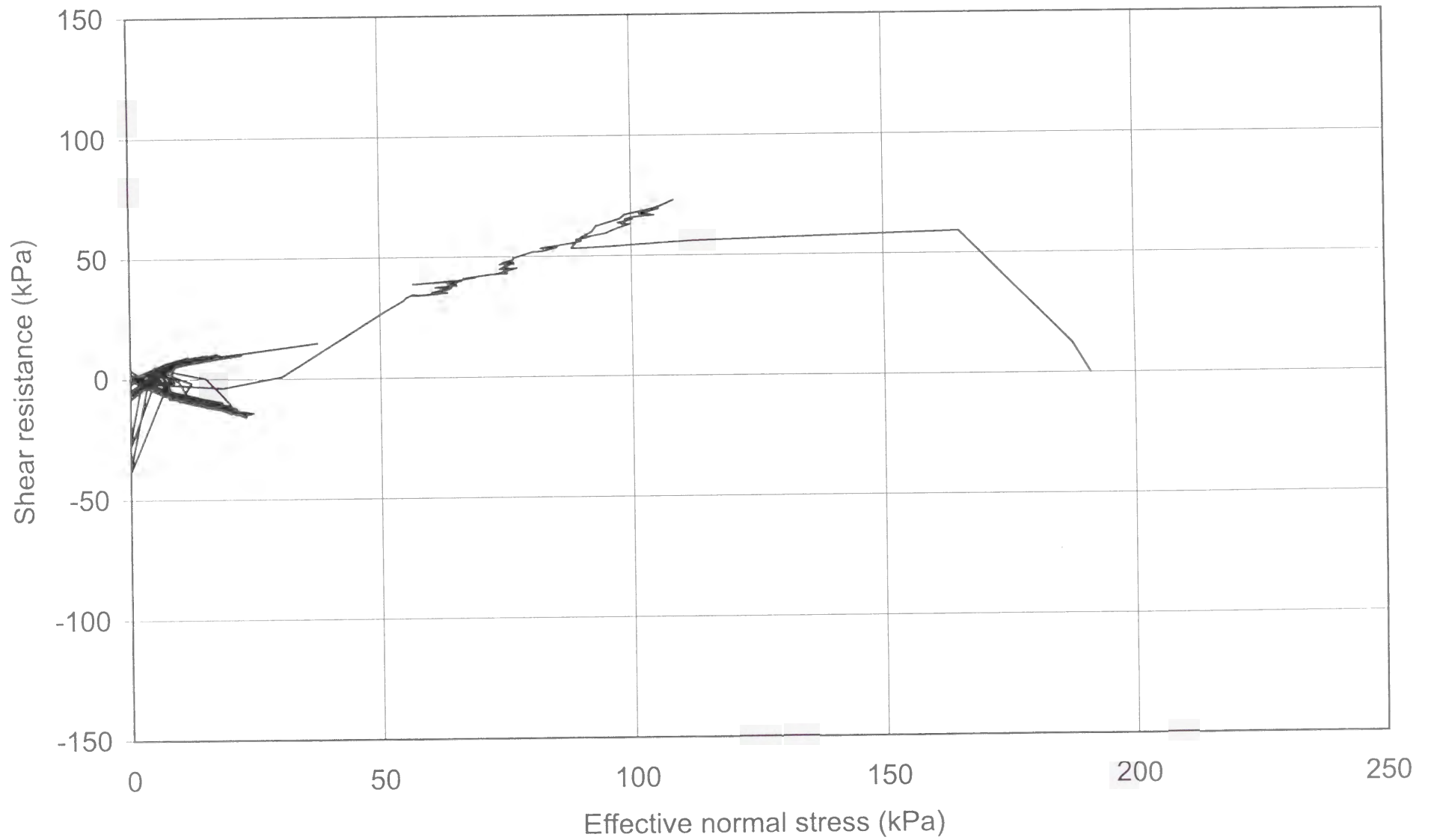| PARAMETER	UNIT	VALUE
Apparatus		Ring shear (DPRI-4)
Test type		Cyclic shear-displacement-controlled
Shear displacement amplitude	mm	89.00
Loading frequency	Hz	0.005
Data acquisition rate	point/cycle	400
Void ratio		0.63
Initial effective normal stress (σ'_{in})	kPa	191
Pore pressure coefficient B_D		0.99
Back pressure (u_0)	kPa	0

The following plots are included:

- **Plot No. 32-1**
Time series of total normal stress, shear resistance, pore pressure, and shear displacement.

- **Plot No. 32-2**
Effective stress path.

Cyclic shear-displacement-controlled test. f=0.005 Hz; l_max=89.00mm.

Test No.32

Plot No.32-1

Test No.32

Cyclic shear-displacement-controlled test. f=0.005 Hz; l$_{max}$=89.00mm

Plot No.32-2

TEST No. 33

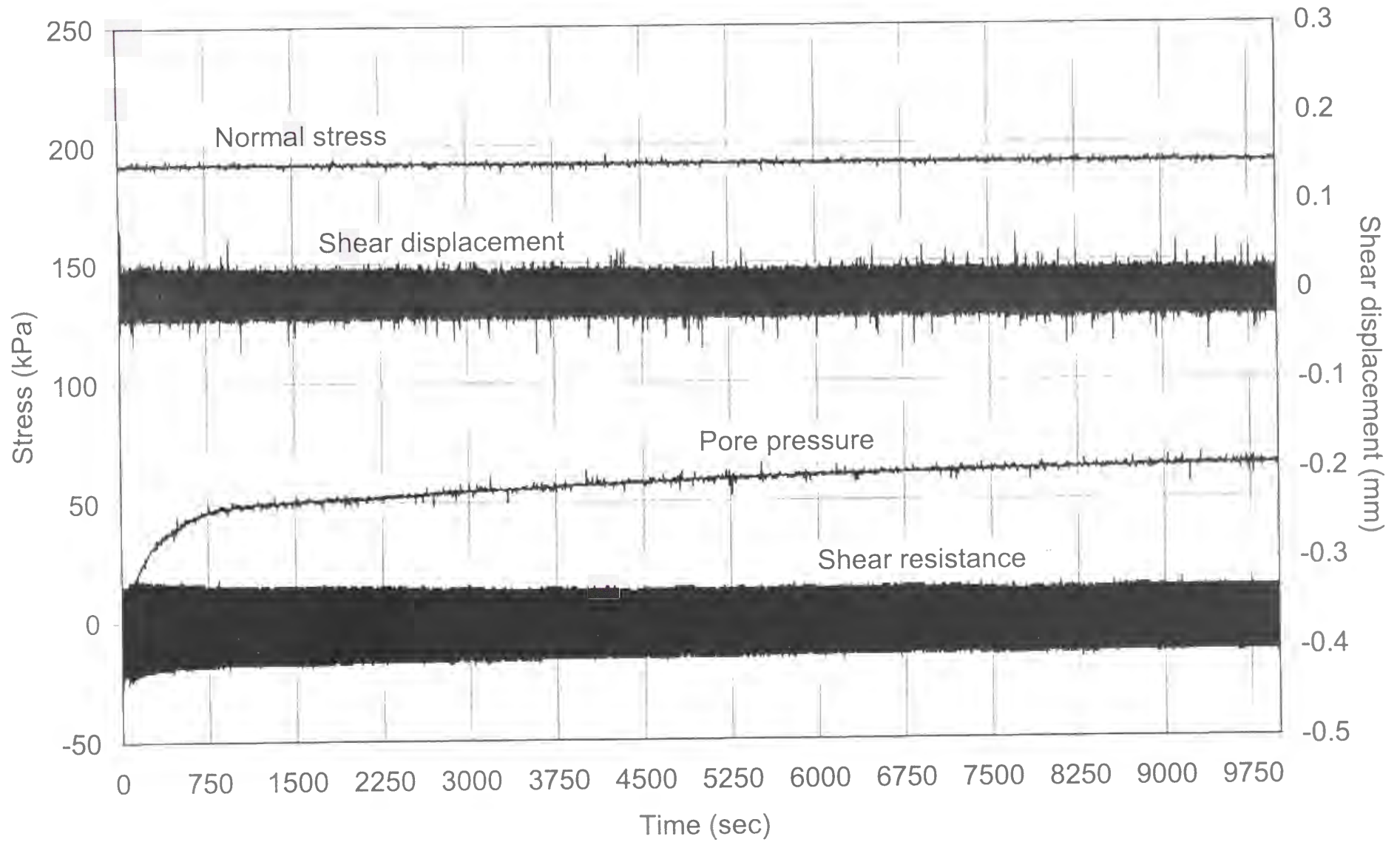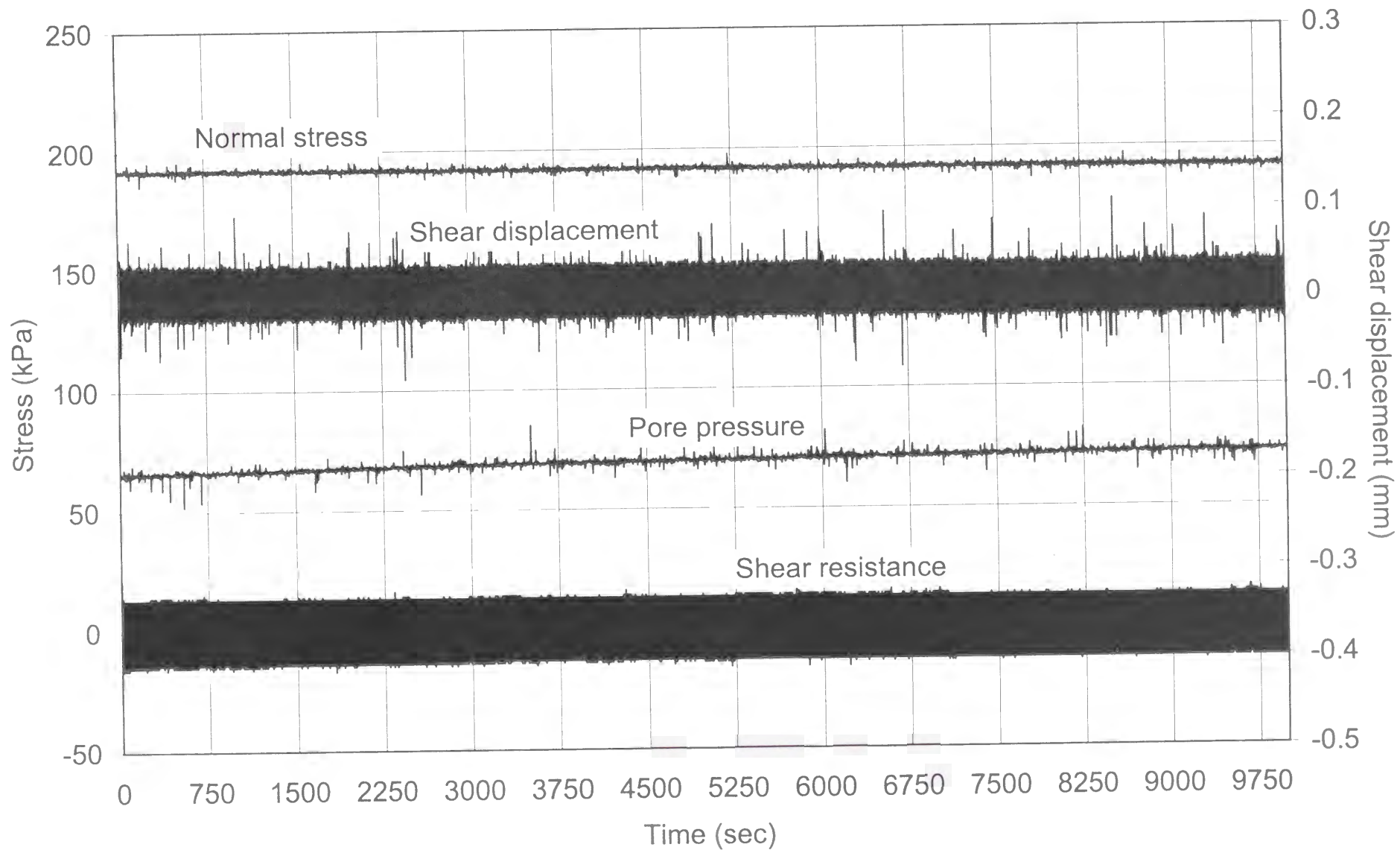| PARAMETER	UNIT	VALUE
Apparatus		Ring shear (DPRI-4)
Test type		Cyclic shear-displacement-controlled
Shear displacement amplitude	mm	0.03/0.06
Loading frequency	Hz	0.10/0.02
Data acquisition rate	point/cycle	20/25
Void ratio		0.65
Initial effective normal stress (σ'_{in})	kPa	192
Pore pressure coefficient B_D		0.98
Back pressure (u_0)	kPa	0

The following plots are included:

- **Plot No. 33-1-1, No. 33-1-2, No. 33-1-3, No. 33-1-4, No. 33-1-5, No. 33-1-6, No. 33-1-7, and No. 33-1-8**
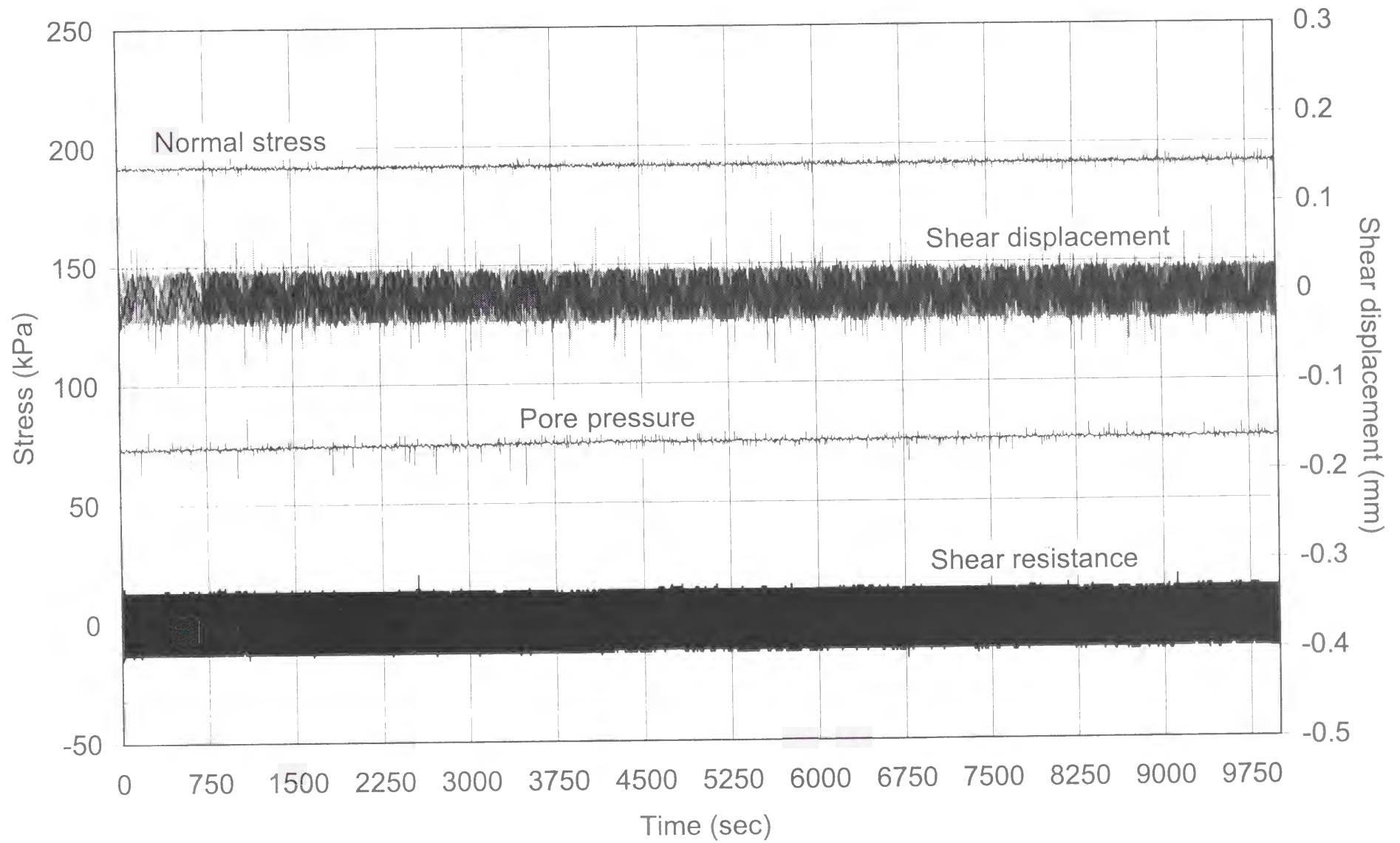*Time series of total normal stress, shear resistance, pore pressure, and shear displacement.*

- **Plot No. 33-2-1, No. 33-2-2, No. 33-2-3, No. 33-2-4, No. 33-2-5, No. 33-2-6, No. 33-2-7, and No. 33-2-8**
Effective stress path.

Cyclic shear-displacement-controlled test. f=0.10 Hz; I_{max}=0.03mm.

Test No.33 (cycles 1000-1999)   Cyclic shear-displacement-controlled test. f=0.10 Hz; l_{max}=0.03mm.   Plot No.33-1-2

Normal stress

Shear displacement

Pore pressure

Shear resistance

Stress (kPa)

Shear displacement (mm)

Time (sec)

Normal stress

Shear displacement

Pore pressure

Shear resistance

Stress (kPa)

Shear displacement (mm)

Time (sec)

Test No.33(cycles 3000-3999)   Cyclic shear-displacement-controlled test. f=0.10 Hz; l_{max}=0.03mm.   Plot No.33-1-4

Normal stress

Shear displacement

Pore pressure

Shear resistance

Stress (kPa)

Shear displacement (mm)

Time (sec)

Test No.33(cycles 4000-4999)   Cyclic shear-displacement-controlled test. f=0.10 Hz; I_{max}=0.03mm.   Plot No.33-1-5

Normal stress

Shear displacement

Pore pressure

Shear resistance

Stress (kPa): 250, 200, 150, 100, 50, 0, -50

Shera displacement (mm): 0.3, 0.2, 0.1, 0, -0.1, -0.2, -0.3, -0.4, -0.5

Time (sec): 0, 750, 1500, 2250, 3000, 3750, 4500, 5250, 6000, 6750, 7500, 8250, 9000, 9750

Test No.33(cycles 5000-5999)   Cyclic shear-displacement-controlled test. f=0.10 Hz; I_{max}=0.03mm.   Plot No.33-1-6

Normal stress

Pore pressure

Shear displacement

Shear resistance

Stress (kPa) — vertical axis (left): 250, 200, 150, 100, 50, 0, -50

Shear displacement (mm) — vertical axis (right): 0.7, 0.5, 0.3, 0.1, -0.1, -0.3, -0.5

Time (sec) — horizontal axis: 0, 4000, 8000, 12000, 16000, 20000, 24000, 28000, 32000, 36000, 40000, 44000, 48000

Test No.33(cycles 6000-6999)   Cyclic shear-displacement-controlled test. f=0.02 Hz; l_{max}=0.06mm.   Plot No.33-1-7

Cyclic shear-displacement-controlled test. f=0.02 Hz; l_{max}=0.06mm.

Test No.33(cycles 7000-7253)

Plot No.33-1-8

Shear resistance (kPa) vs Effective normal stress (kPa)

Test No.33 (cycles 1-999)

Cyclic shear-displacement-controlled test. f=0.10 Hz; l_{max}=0.03mm.

Plot No.33-2-1

Cyclic shear-displacement-controlled test. f=0.10 Hz; I_{max}=0.03mm.

Test No.33. (cycles 1000-1999)

Plot No.33-2-2

Y-axis: Shear resistance (kPa), ranging from -150 to 150

X-axis: Effective normal stress (kPa), ranging from 0 to 250

Cyclic shear-displacement-controlled test. f=0.10 Hz; l_{max}=0.03mm.

Shear resistance (kPa) vs Effective normal stress (kPa)

Test No.33(cycles3000-3999)

Cyclic shear-displacement-controlled test. f=0.10 Hz; l_{max}=0.03mm.

Plot No.33-2-4

Y-axis: Shear resistance (kPa)

X-axis: Effective normal stress (kPa)

Shear resistance (kPa) vs Effective normal stress (kPa)

Test No.33(cycles 5000-5999)　　Cyclic shear-displacement-controlled test. f=0.10 Hz; l_{max}=0.03mm.　　Plot No.33-2-6

Shear resistance (kPa) vs Effective normal stress (kPa)

Test No.33(cycles 6000-6999)   Cyclic shear-displacement-controlled test. f=0.02 Hz; I_max=0.06mm.   Plot No.33-2-7

Shear resistance (kPa) vs Effective normal stress (kPa)

Test No.33(cycles 7000-7253)   Cyclic shear-displacement-controlled test. f=0.02 Hz; I_{max}=0.06mm.   Plot No.33-2-8

TEST No. 34

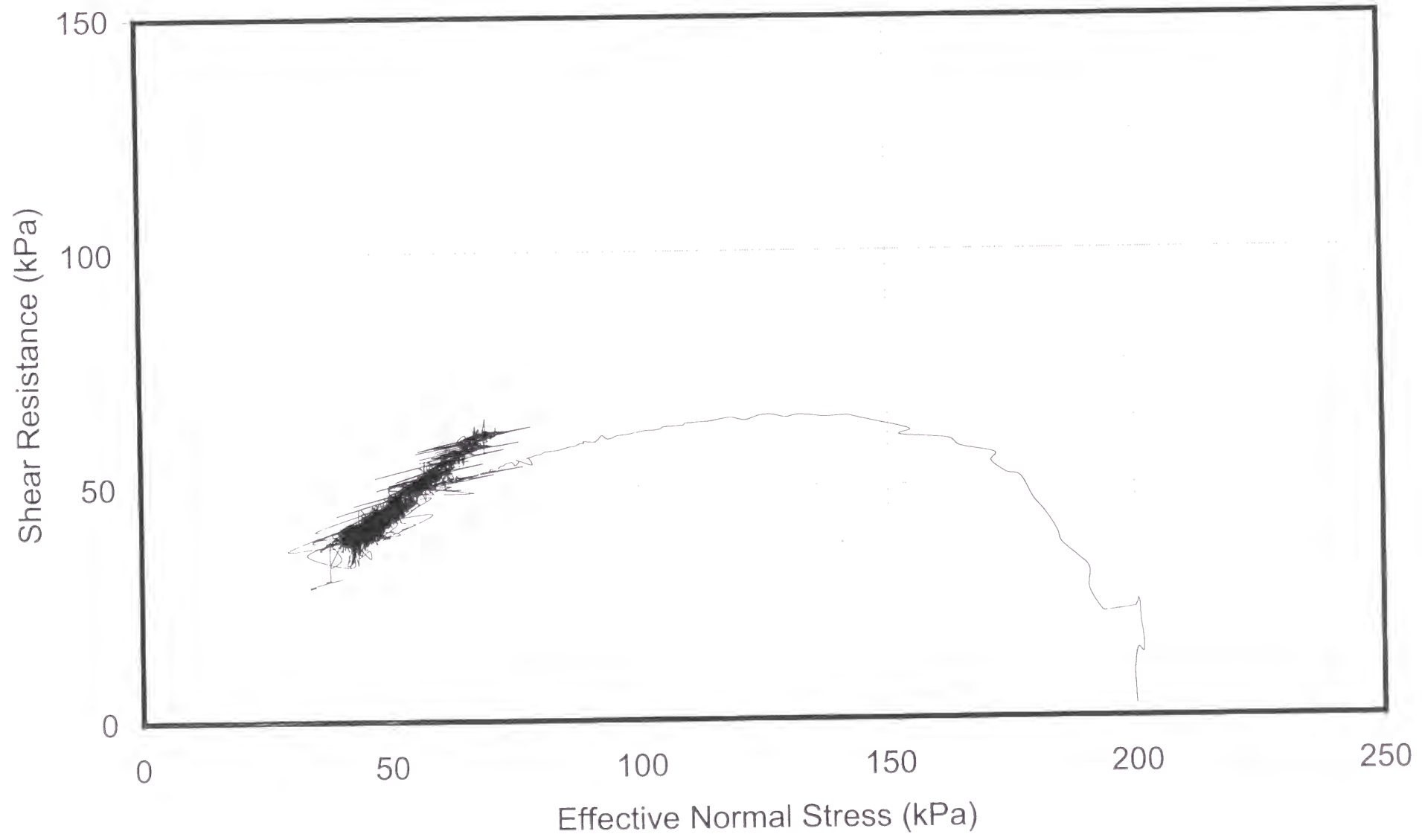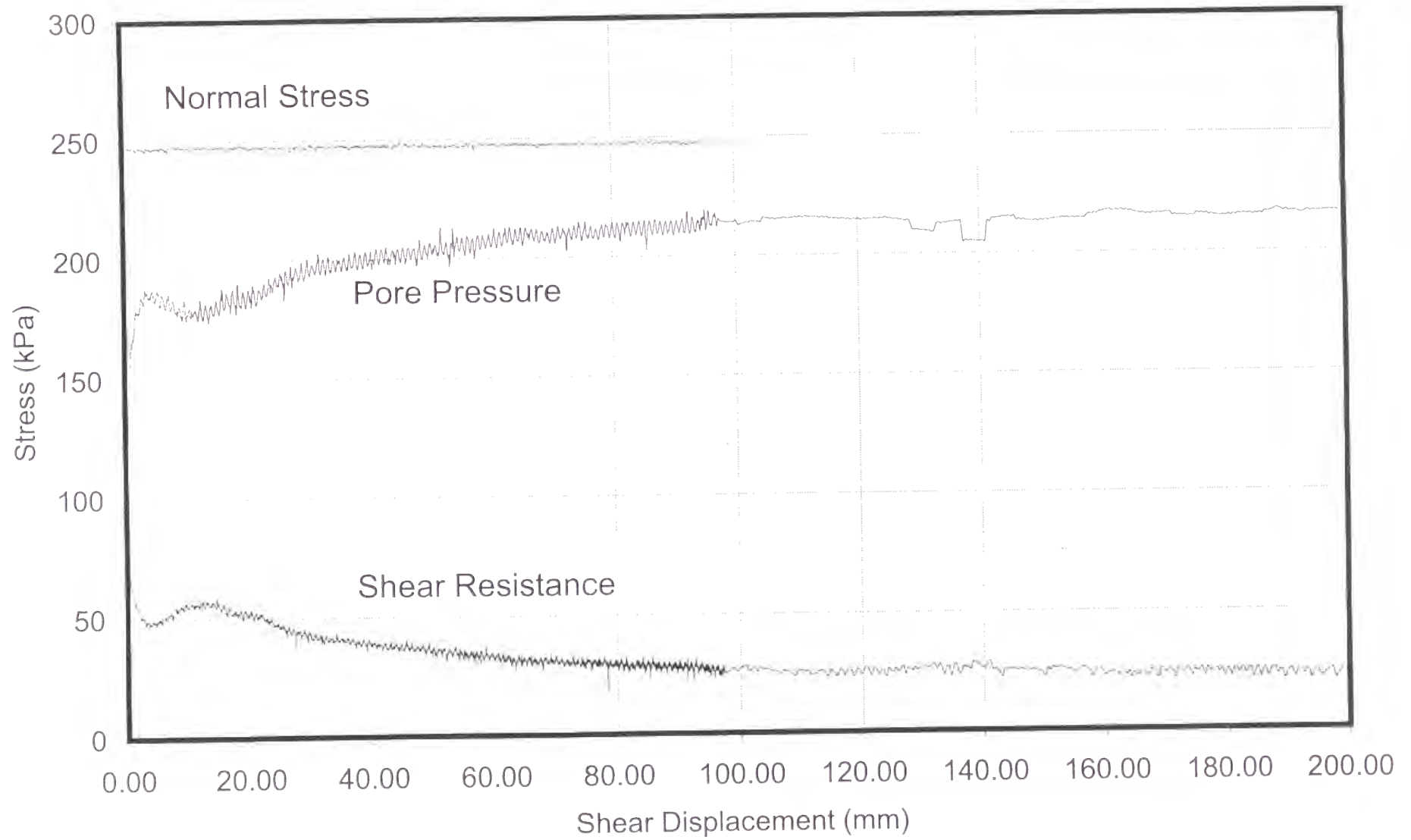| PARAMETER	UNIT	VALUE
Apparatus		Ring shear (DPRI-4)
Test type		Monotonic constant-shear-speed
Shear speed	mm/sec	0.25
Data acquisition rate	point/sec	10
Void ratio		0.60
Initial effective normal stress (σ'_{in})	kPa	200
Pore pressure coefficient B_D		0.97
Back pressure (u_0)	kPa	49

The following plots are included:

- **Plot No. 34-1**

Shear displacement series of total normal stress, shear resistance, and pore pressure.

- **Plot No. 34-2**

Effective stress path.
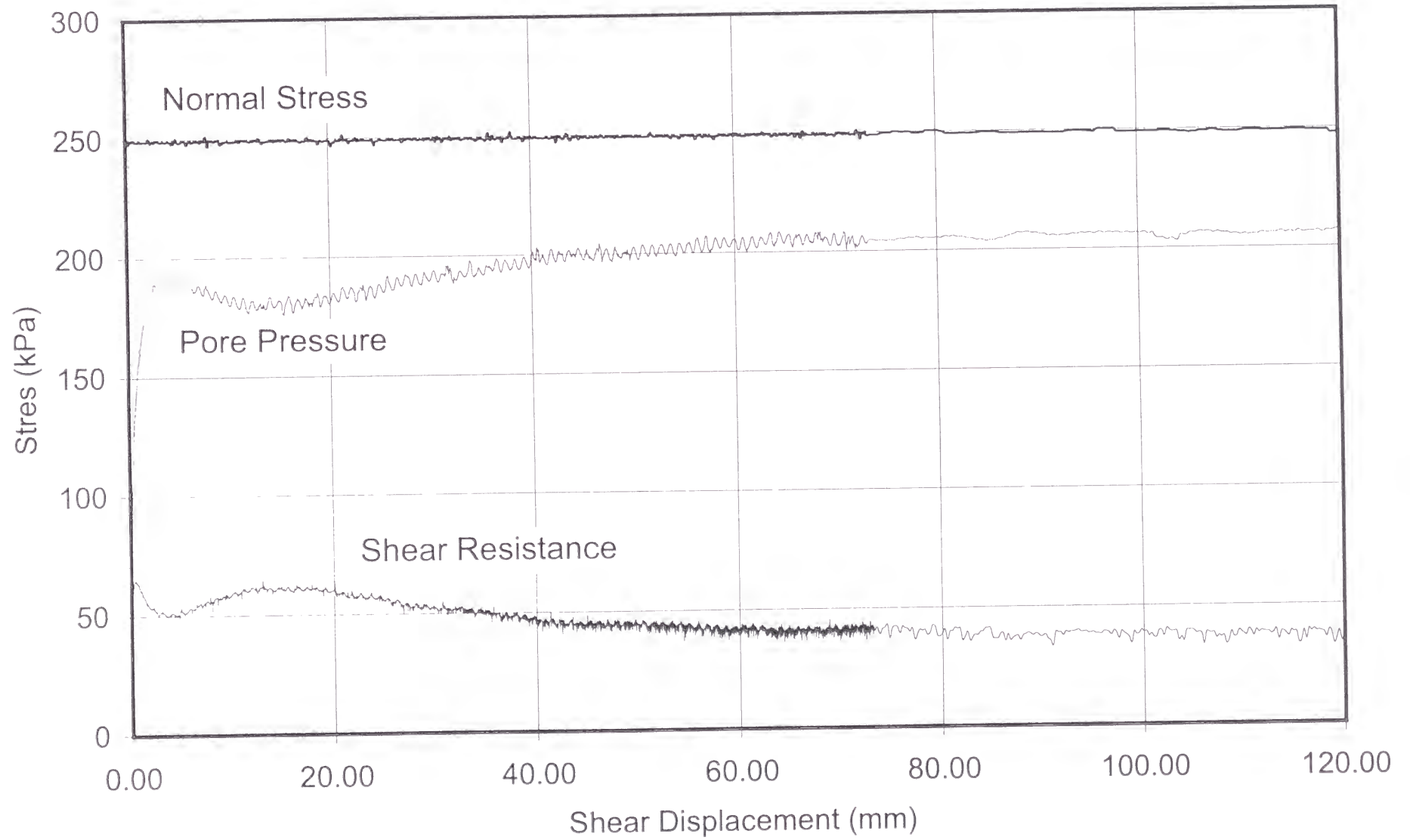
Stres (kPa) (y-axis)

Shear Displacement (mm) (x-axis)

Normal Stress

Pore Pressure

Shear Resistance

Monotonic constant-speed shear test.
Shear speed=0.26 mm/sec

Test No.34

Plot No.34-1

Y-axis: Shear Resistance (kPa) — 0, 50, 100, 150

X-axis: Effective Normal Stress (kPa) — 0, 50, 100, 150, 200, 250

Test No.34

Monotonic constant-speed-shear test.
Shear speed=0.26 mm/sec

Plot No.34-2

TEST No. 35

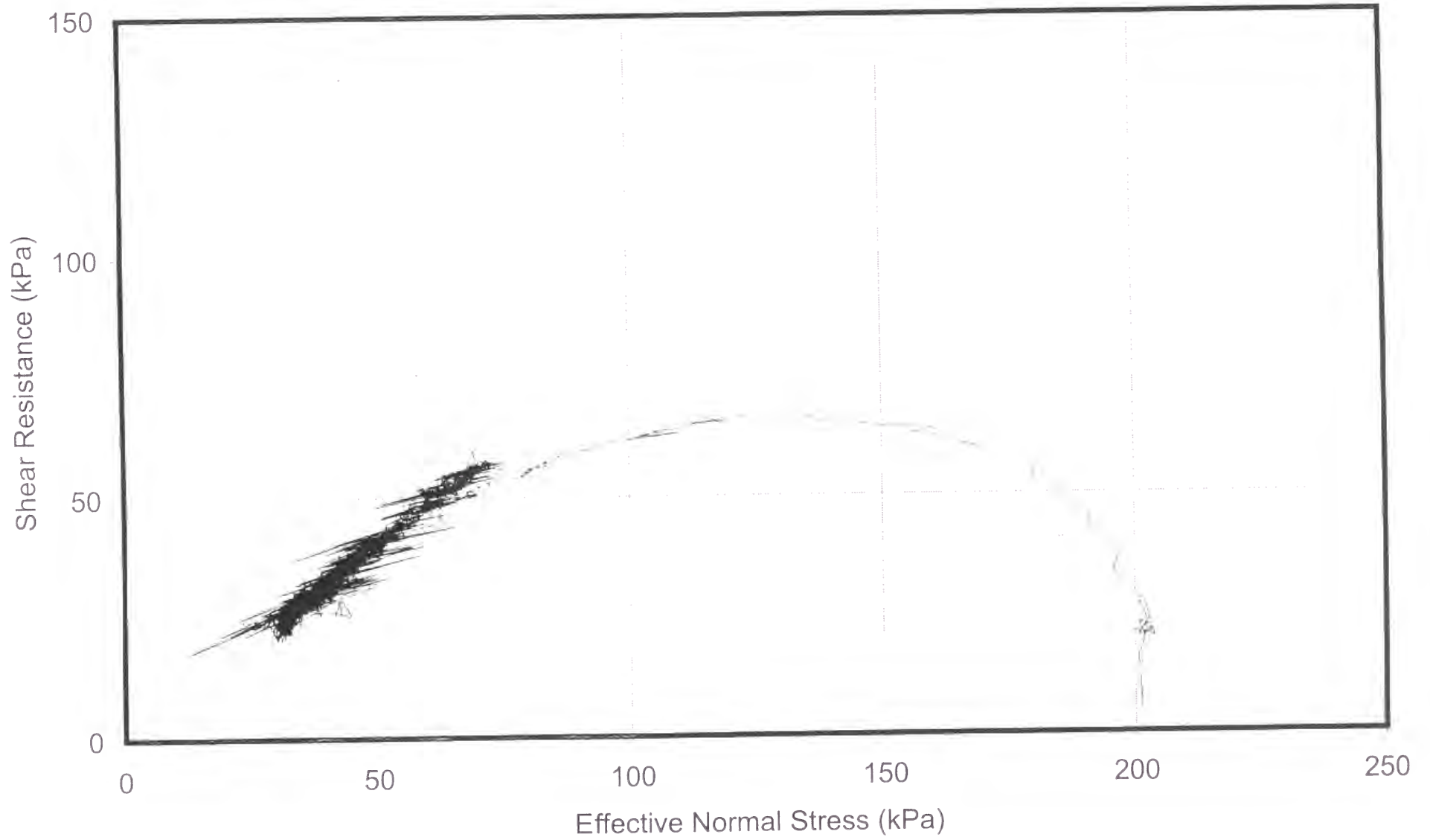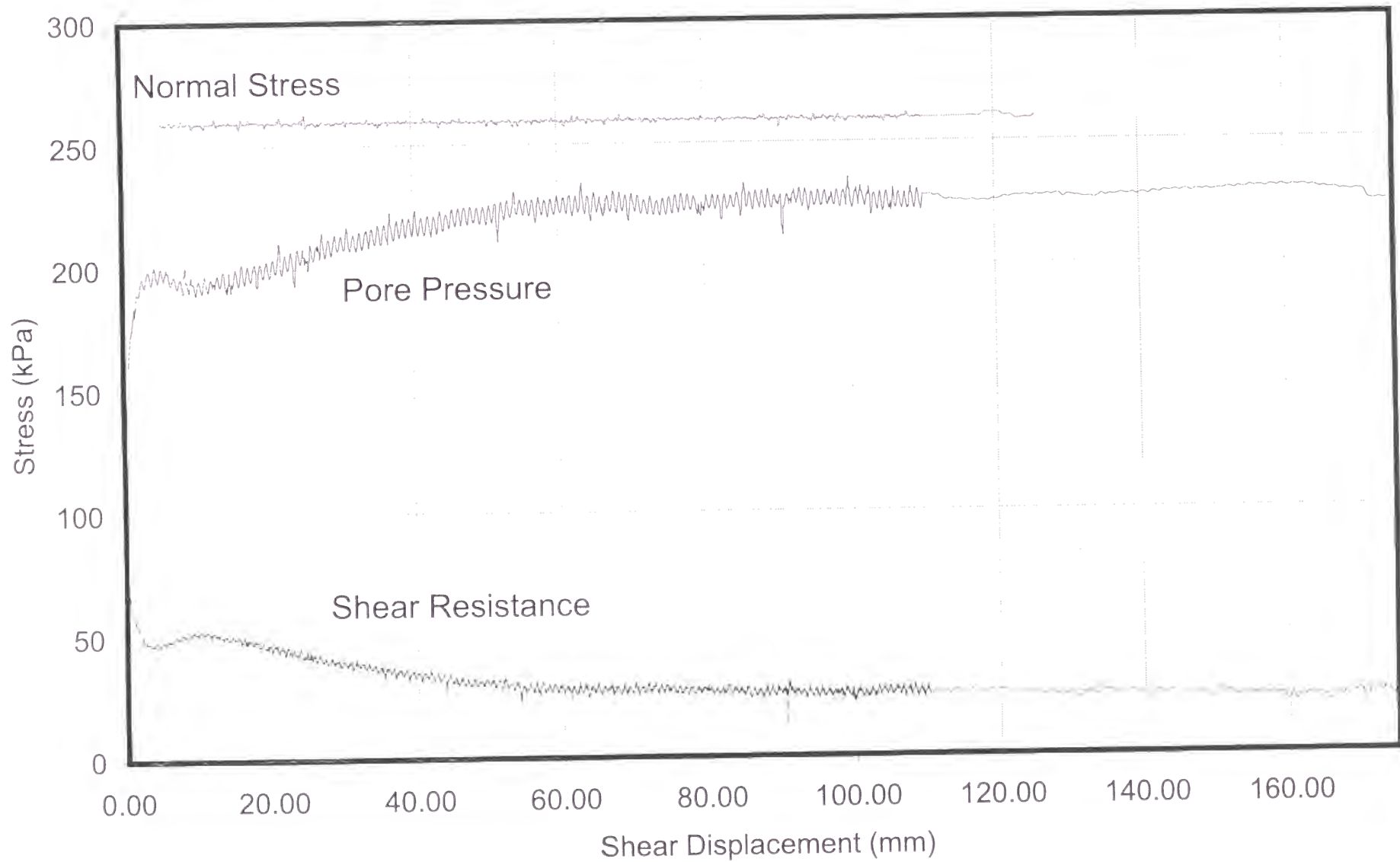| PARAMETER	UNIT	VALUE
Apparatus		Ring shear (DPRI-4)
Test type		Monotonic constant-shear-speed
Shear speed	mm/sec	0.40
Data acquisition rate	point/sec	20
Void ratio		0.67
Initial effective normal stress (σ'_{in})	kPa	201
Pore pressure coefficient B_D		0.95
Back pressure (u_0)	kPa	45

The following plots are included:

- **Plot No. 35-1**

Shear displacement series of total normal stress, shear resistance, and pore pressure.

- **Plot No. 35-2**

Effective stress path.

Normal Stress

Pore Pressure

Shear Resistance

Stress (kPa)

Shear Displacement (mm)

Monotonic constant-speed-shear test.
Shear speed=0.40 mm/sec

Test No.35

Plot No.35-1

Monotonic constant-speed-shear test.
Shear speed=0.40 mm/sec

Test No.35

Plot No.35-2

TEST No. 36

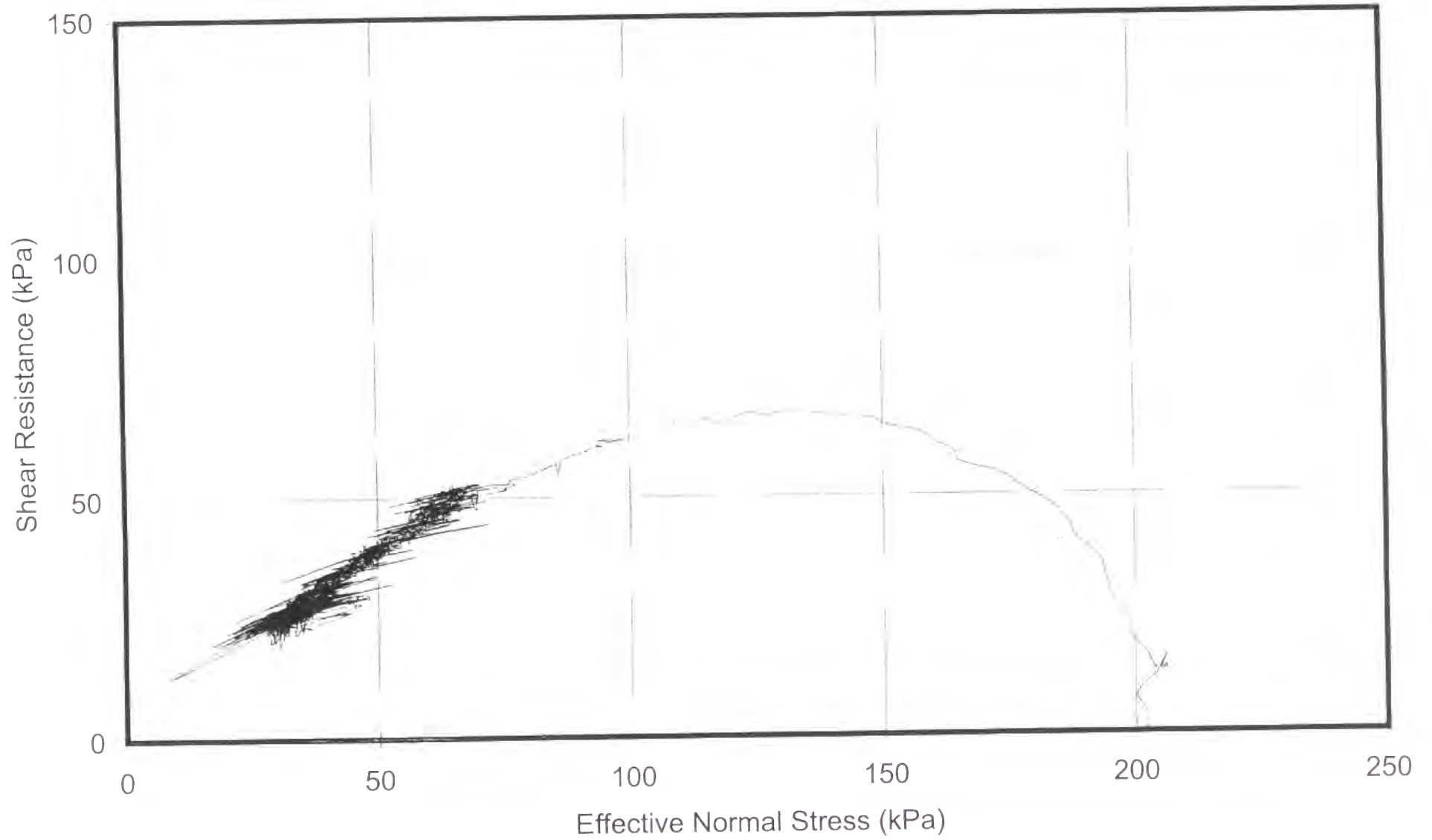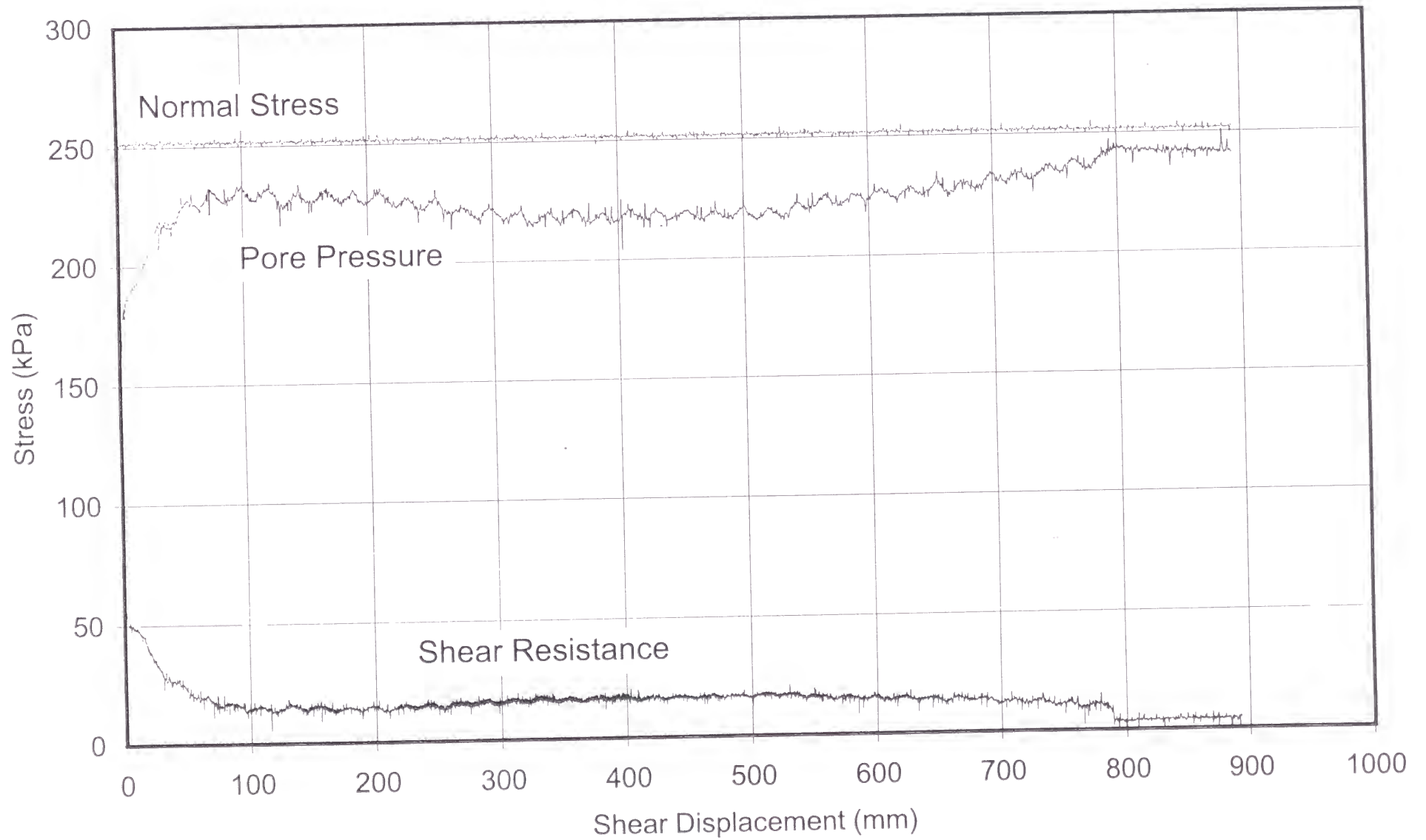| PARAMETER	UNIT	VALUE
Apparatus		Ring shear (DPRI-4)
Test type		Monotonic constant-shear-speed
Shear speed	mm/sec	0.54
Data acquisition rate	point/sec	20
Void ratio		0.68
Initial effective normal stress (σ'_{in})	kPa	202
Pore pressure coefficient B_D		0.95
Back pressure (u_0)	kPa	56

The following plots are included:

- **Plot No. 36-1**

Shear displacement series of total normal stress, shear resistance, and pore pressure.

- **Plot No. 36-2**

Effective stress path.

Normal Stress

Pore Pressure

Shear Resistance

Stress (kPa)

Shear Displacement (mm)

Monotonic constant-speed-shear test.
Shear speed=0.54 mm/sec

Test No.36

Plot No.36-1

Shear Resistance (kPa) — vertical axis (0, 50, 100, 150)

Effective Normal Stress (kPa) — horizontal axis (0, 50, 100, 150, 200, 250)

Monotinic constant-speed-shear test.
Shear speed=0.54 mm/sec

Test No.36

Plot No.36-2

TEST No. 37

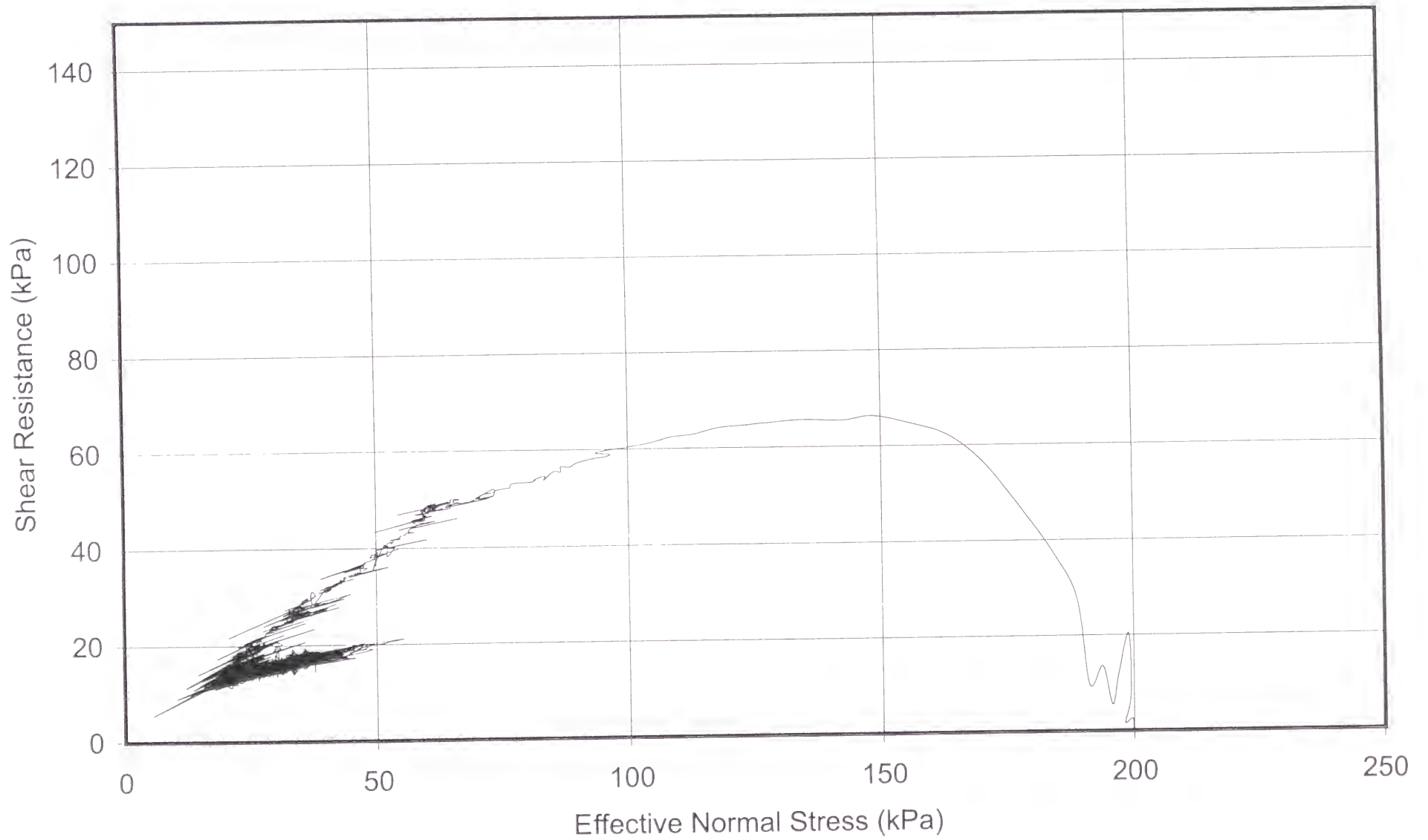| PARAMETER	UNIT	VALUE
Apparatus		Ring shear (DPRI-4)
Test type		Monotonic constant-shear-speed
Shear speed	mm/sec	8.00
Data acquisition rate	point/sec	100
Void ratio		0.69
Initial effective normal stress (σ'_{in})	kPa	200
Pore pressure coefficient B_D		0.95
Back pressure (u_0)	kPa	52

The following plots are included:

- **Plot No. 37-1**

  Shear displacement series of total normal stress, shear resistance, and pore pressure.

- **Plot No. 37-2**

  Effective stress path.

Normal Stress

Pore Pressure

Shear Resistance

Axis labels: Stress (kPa) (vertical), Shear Displacement (mm) (horizontal)

Monotonic constant-speed-shear test.
Shear speed=8.00 mm/sec

Test No.37

Plot No.37-1

Monotonic constant-speed-shear test.
Shear speed=8.00 mm/sec

Test No.37

Plot No.37-2

TEST No. 38

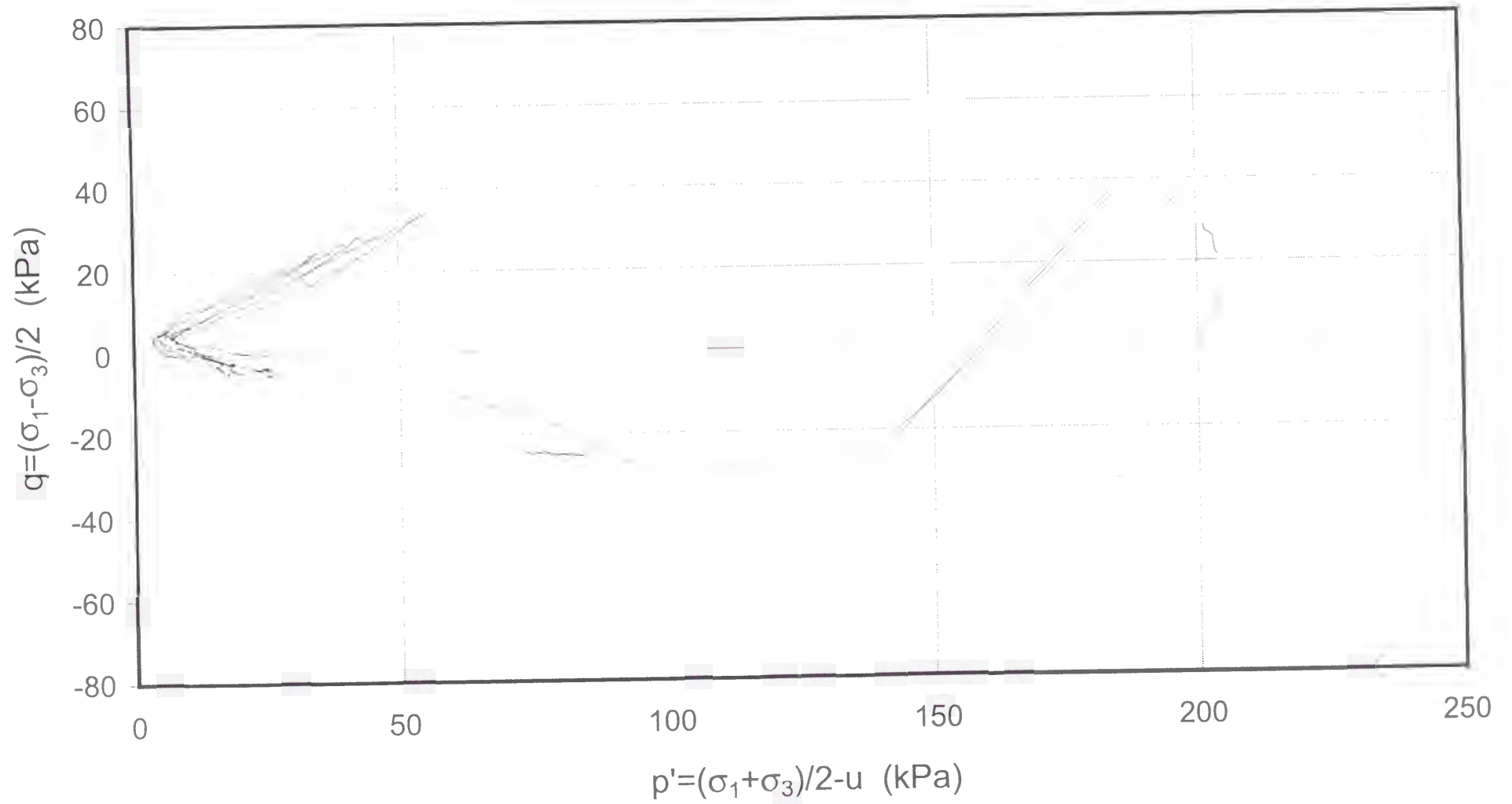| PARAMETER	UNIT	VALUE
Apparatus		Triaxial compression
Test type		Cyclic stress-controlled
Loading frequency	Hz	0.05
Data acquisition rate	point/cycle	100
Void ratio		0.65
Initial effective confining stress ($\sigma_3'_{in}$)	kPa	200
Pore pressure coefficient B		0.95
Back pressure (u_0)	kPa	98

The following plots are included:

- **Plot No. 38-1**

Time series of series of axial pressure, cell pressure, pore pressure, and axial displacement.

- **Plot No. 38-2**

Effective stress path.

Axial Pressure

Cell Pressure

Axial Displacement

Pore Pressure

Stress (kPa)

Strain

Time (sec)

Test No.38

Cyclic stress-controlled test. f=0.05 Hz.

Plot No.38-1

Axes: q=(σ₁-σ₃)/2 (kPa) versus p'=(σ₁+σ₃)/2-u (kPa)

$$q = (\sigma_1 - \sigma_3)/2 \; \text{(kPa)}$$

$$p' = (\sigma_1 + \sigma_3)/2 - u \; \text{(kPa)}$$

Test No.38

Cyclic stress-controlled test. f=0.05 Hz.

Plot No.38-2
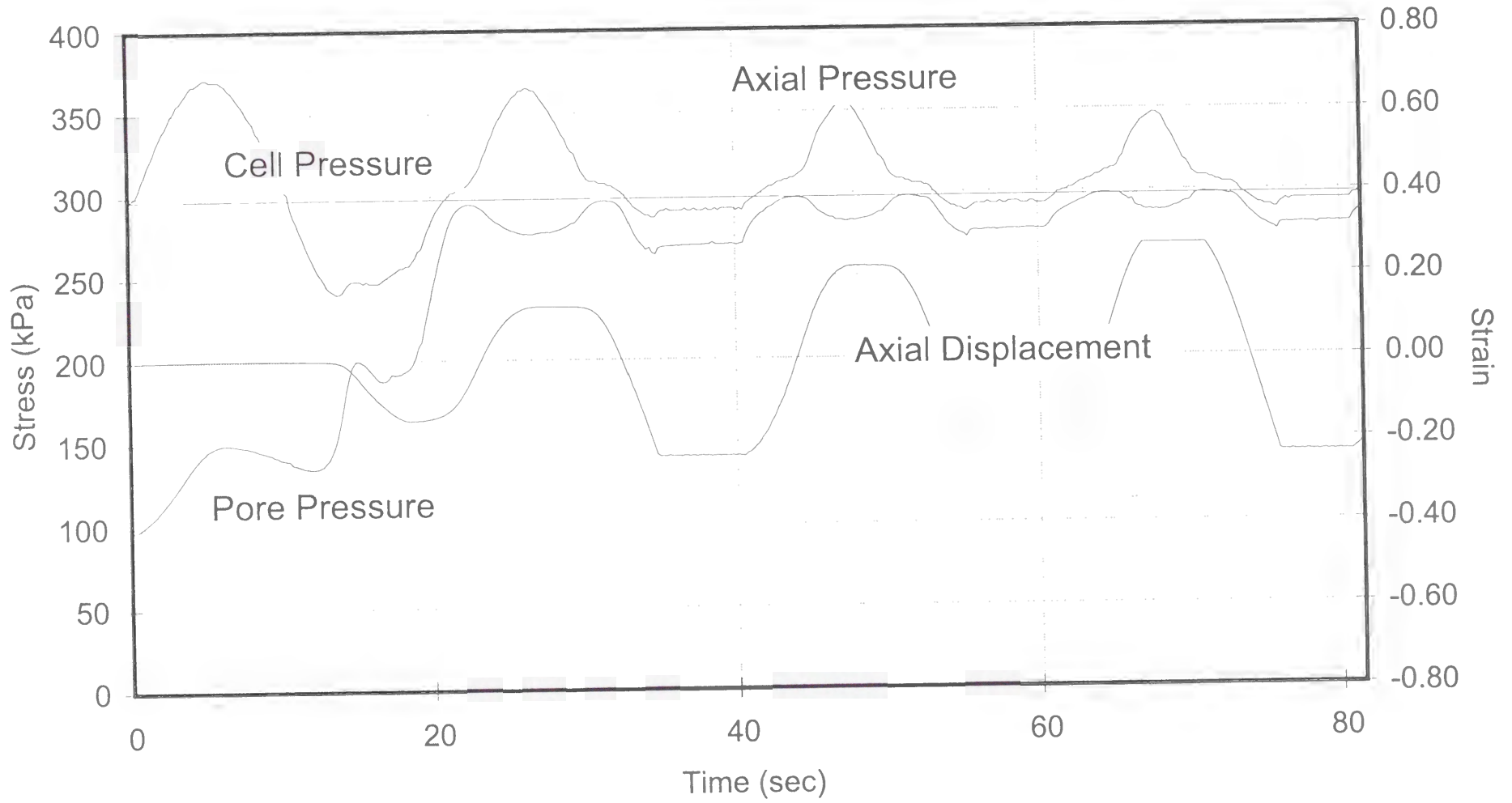
TEST No. 39

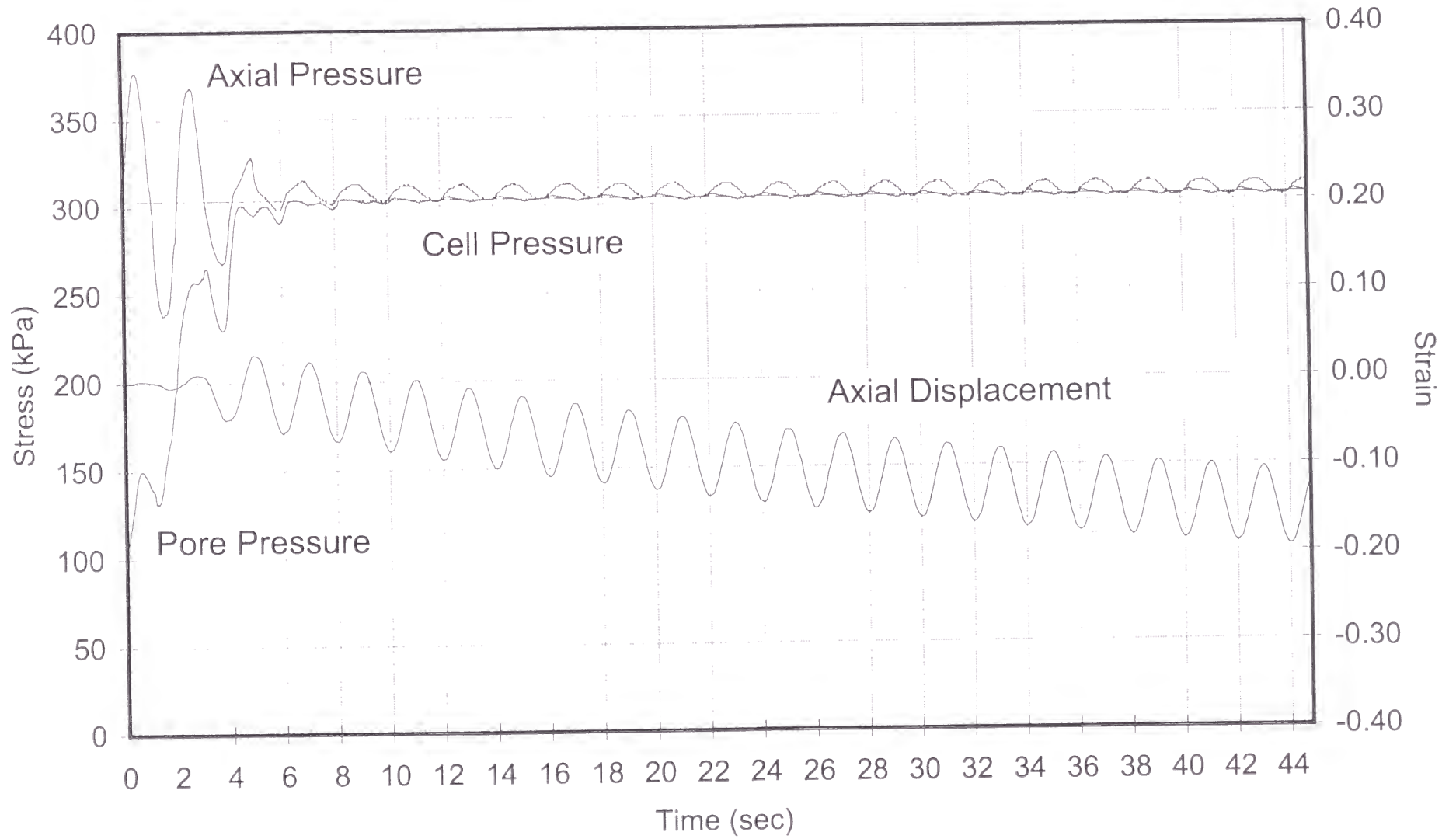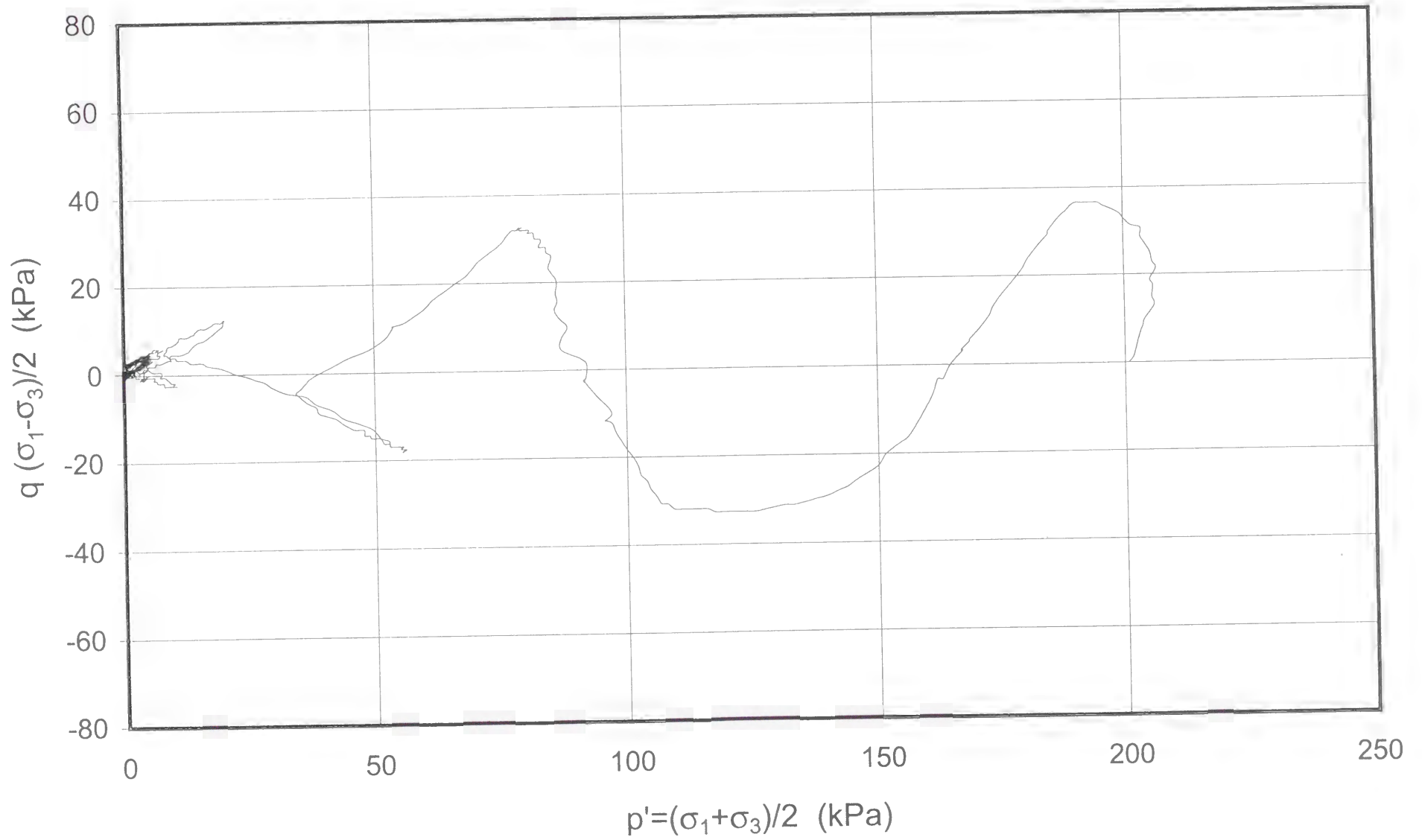| PARAMETER	UNIT	VALUE
Apparatus		Triaxial compression
Test type		Cyclic stress-controlled
Loading frequency	Hz	0.10
Data acquisition rate	point/cycle	100
Void ratio		0.62
Initial effective confining stress ($\sigma_3{'}_{in}$)	kPa	200
Pore pressure coefficient B		0.96
Back pressure (u_0)	kPa	102

The following plots are included:

- **Plot No. 39-1**

Time series of series of axial pressure, cell pressure, pore pressure, and axial displacement.

- **Plot No. 39-2**

Effective stress path.

Cyclic stress-controlled test. f=0.10 Hz.

Test No.39

Plot No.39-1
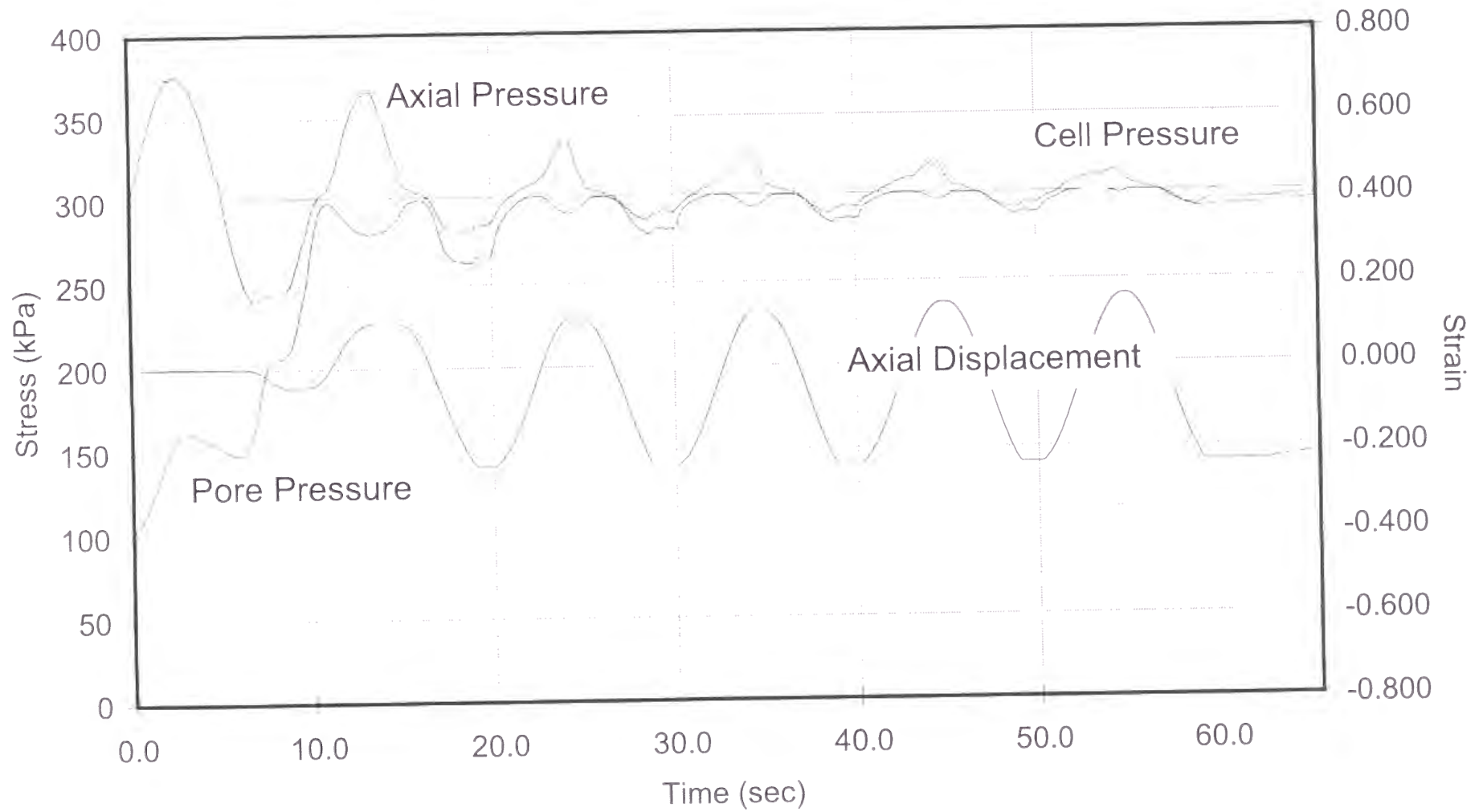
TEST No. 40

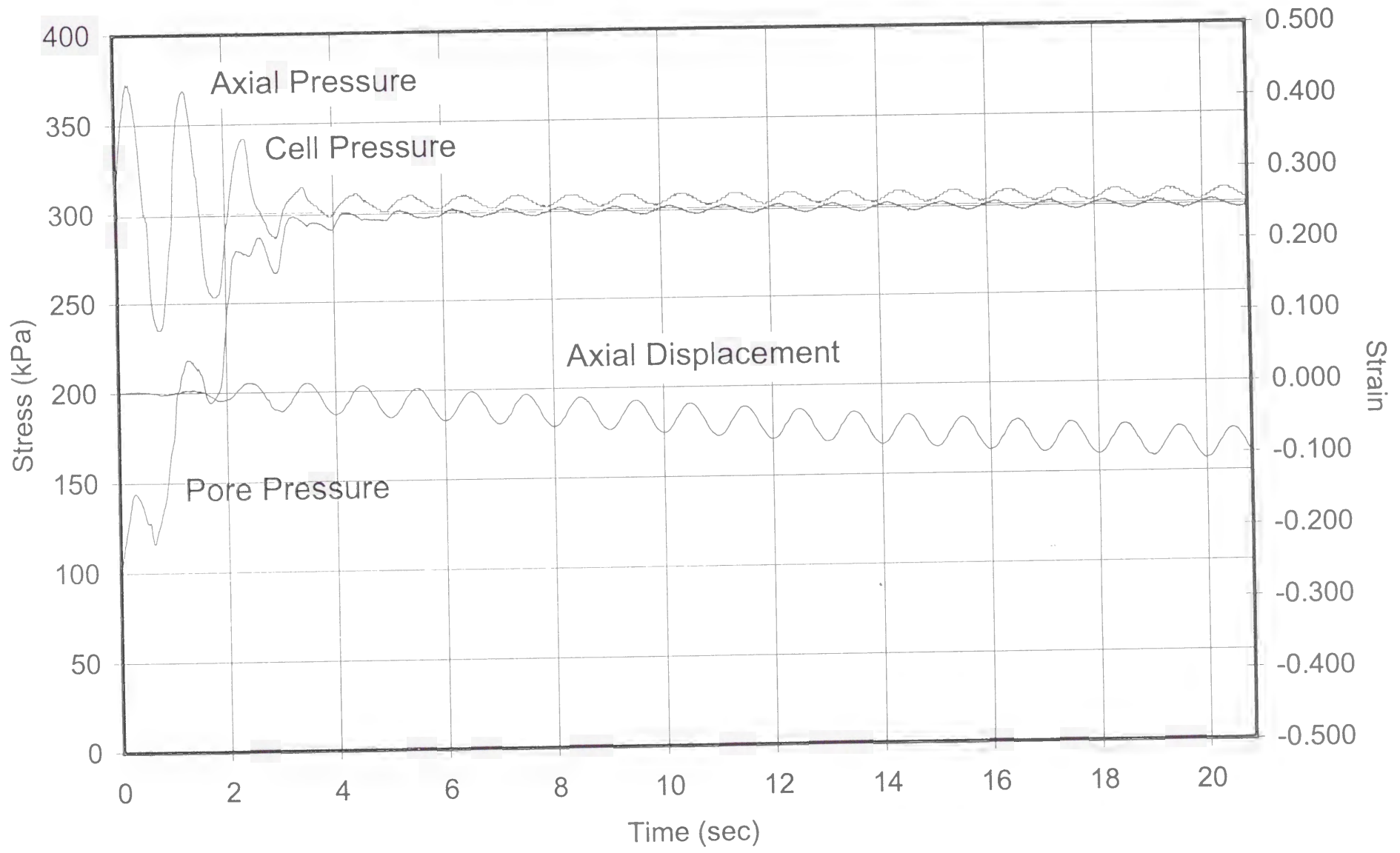| PARAMETER	UNIT	VALUE
Apparatus		Triaxial compression
Test type		Cyclic stress-controlled
Loading frequency	Hz	0.50
Data acquisition rate	point/cycle	100
Void ratio		0.64
Initial effective confining stress ($\sigma_3'{}_{in}$)	kPa	200
Pore pressure coefficient B		0.95
Back pressure (u_0)	kPa	103

The following plots are included:

- **Plot No. 40-1**
Time series of series of axial pressure, cell pressure, pore pressure, and axial displacement.

- **Plot No. 40-2**
Effective stress path.

Cyclic stress-controlled test. f=0.50 Hz.

Test No.40

Plot No.40-1

Cyclic stress-controlled test. f=0.50 Hz.

Test No.40

Plot No.40-2

TEST No. 41

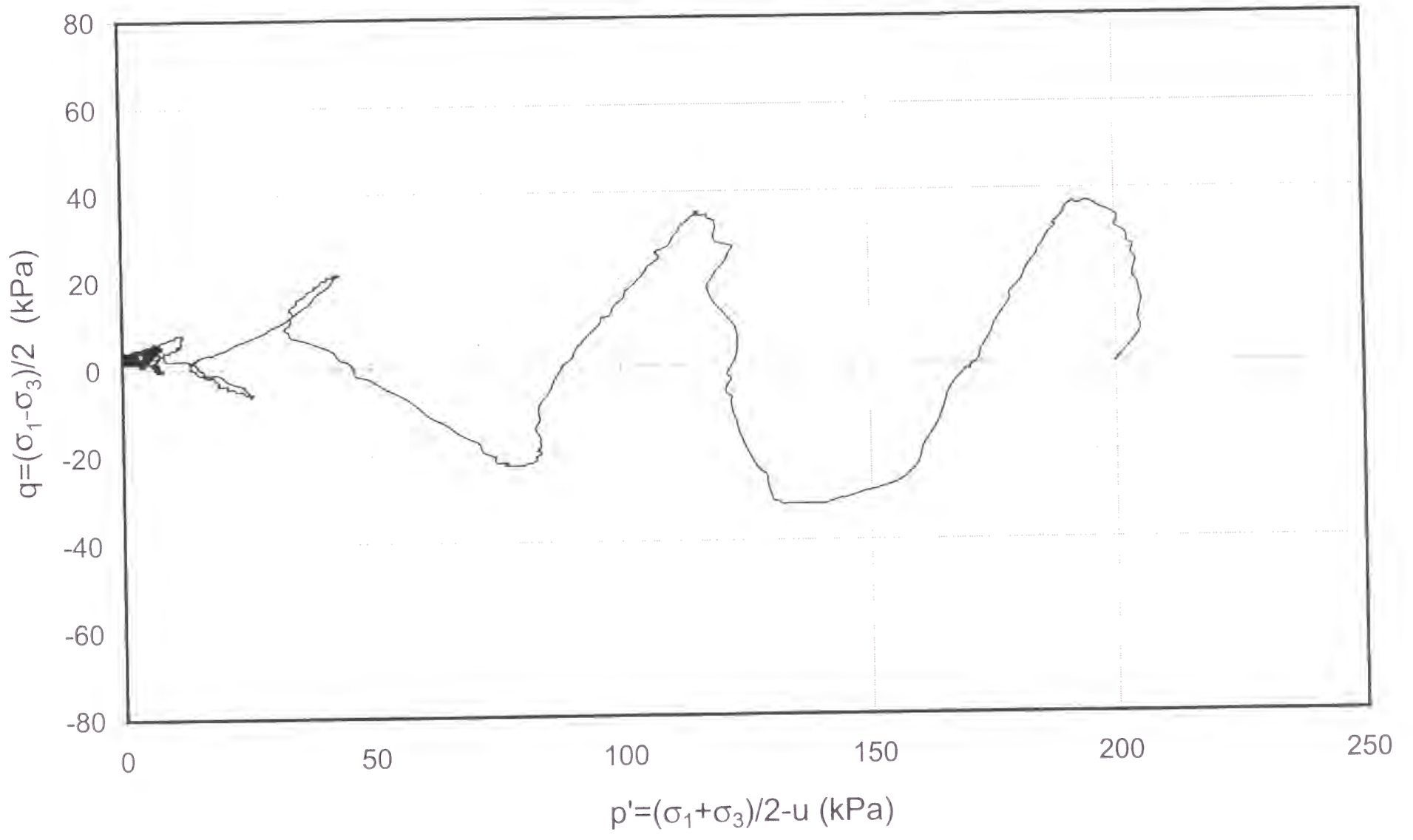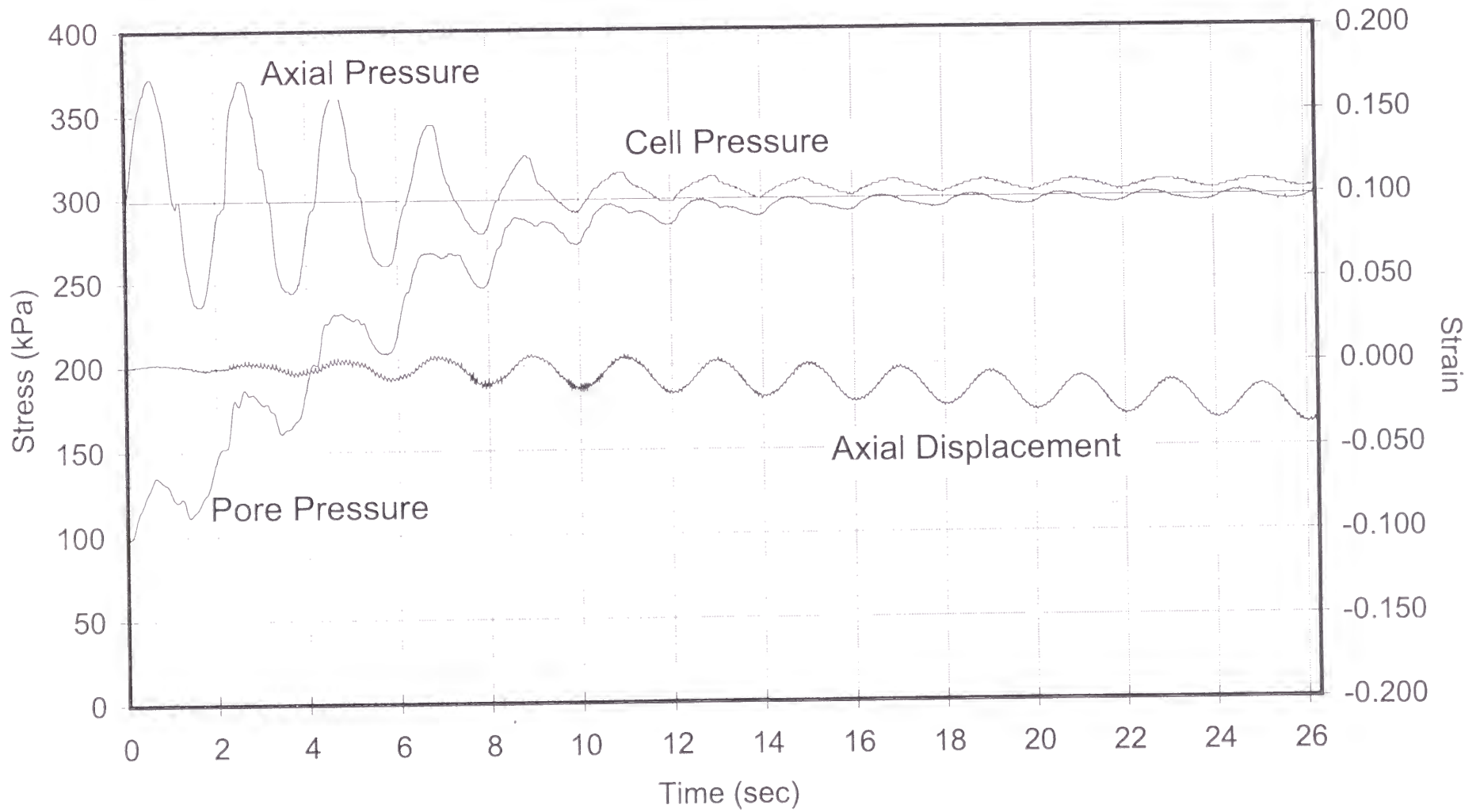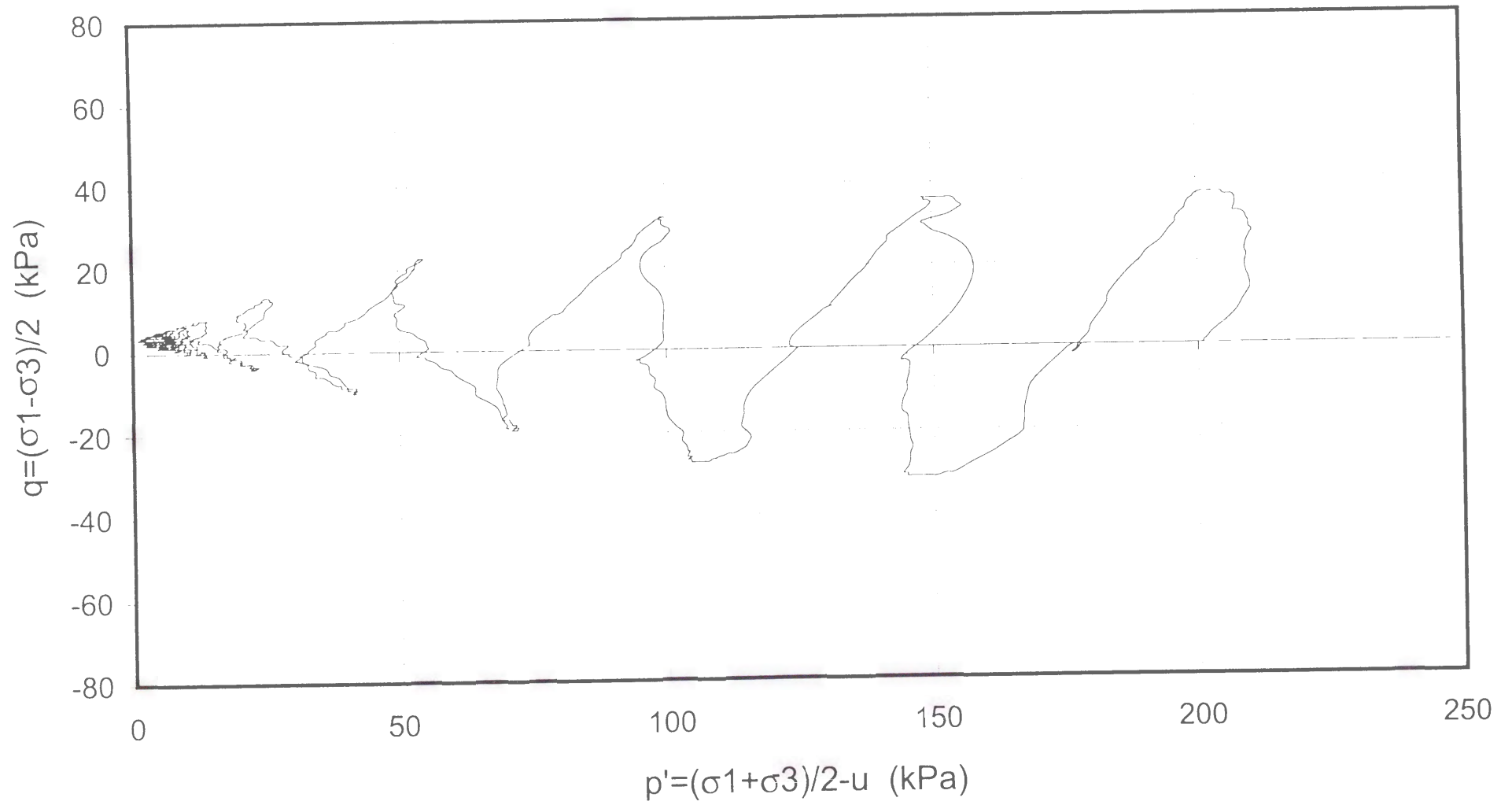| PARAMETER	UNIT	VALUE
Apparatus		Triaxial compression
Test type		Cyclic stress-controlled
Loading frequency	Hz	1.00
Data acquisition rate	point/cycle	100
Void ratio		0.64
Initial effective confining stress ($\sigma_{3}'_{in}$)	kPa	200
Pore pressure coefficient B		0.95
Back pressure (u_0)	kPa	99

The following plots are included:

- **Plot No. 41-1**

Time series of series of axial pressure, cell pressure, pore pressure, and axial displacement.

- **Plot No. 41-2**

Effective stress path.

Axial Pressure

Cell Pressure

Axial Displacement

Pore Pressure

Stress (kPa) — vertical axis: 0, 50, 100, 150, 200, 250, 300, 350, 400

Strain — vertical axis: -0.500, -0.400, -0.300, -0.200, -0.100, 0.000, 0.100, 0.200, 0.300, 0.400, 0.500

Time (sec) — horizontal axis: 0, 2, 4, 6, 8, 10, 12, 14, 16, 18, 20

Test No.41

Cyclic stress-controlled test. f=1.00 Hz.

Plot No.41-1

Axis labels:
- Y-axis: $q=(\sigma_1-\sigma_3)/2$ (kPa)
- X-axis: $p'=(\sigma_1+\sigma_3)/2-u$ (kPa)

Test No.41

Cyclic stress-controlled test. f=1.00 Hz.

Plot No.41-2

TEST No. 42

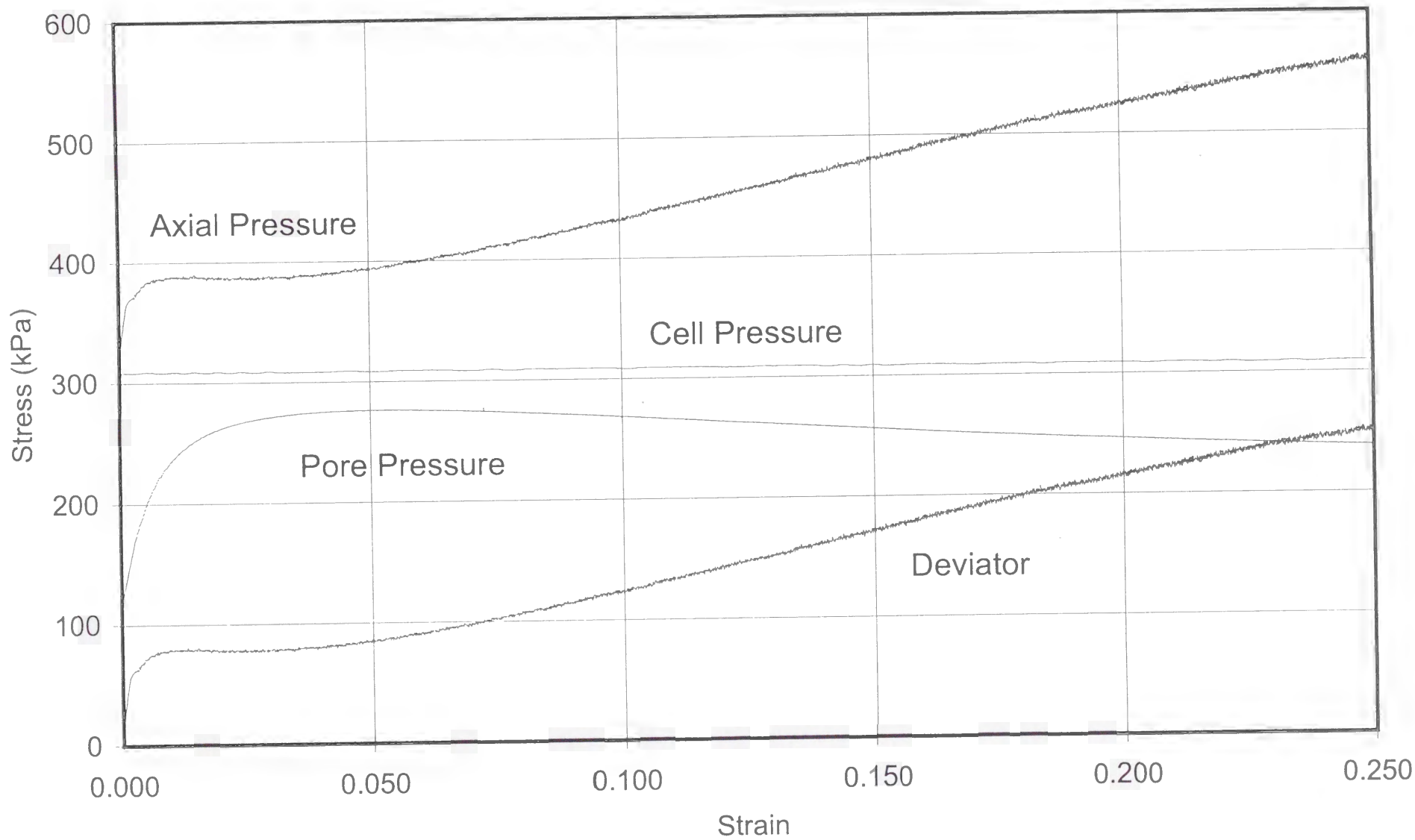| PARAMETER	UNIT	VALUE
Apparatus		Triaxial compression
Test type		Cyclic stress-controlled
Loading frequency	Hz	2.00
Data acquisition rate	point/cycle	100
Void ratio		0.63
Initial effective confining stress ($\sigma_3'{}_{in}$)	kPa	200
Pore pressure coefficient B		0.95
Back pressure (u_0)	kPa	98

The following plots are included:

• **Plot No. 42-1**
Time series of series of axial pressure, cell pressure, pore pressure, and axial displacement.

• **Plot No. 42-2**
Effective stress path.

Test No.42   Cyclic stress-controlled test. f=2.00 Hz.   Plot No.42-1

Cyclic stress-controlled test. f=2.00 Hz.

Test No.42

Plot No.42-2

TEST No. 43

PARAMETER	UNIT	VALUE
Apparatus		Triaxial compression
Test type		Monotonic constant-strain-rate
Strain rate	1/sec	0.0002
Data acquisition rate	point/sec	2
Void ratio		0.62
Initial effective confining stress ($\sigma_3'_{in}$)	kPa	200
Pore pressure coefficient B		0.96
Back pressure (u_0)	kPa	110

The following plots are included:

- **Plot No. 43-1**

Strain series of series of axial pressure, cell pressure, pore pressure, and deviator stress.
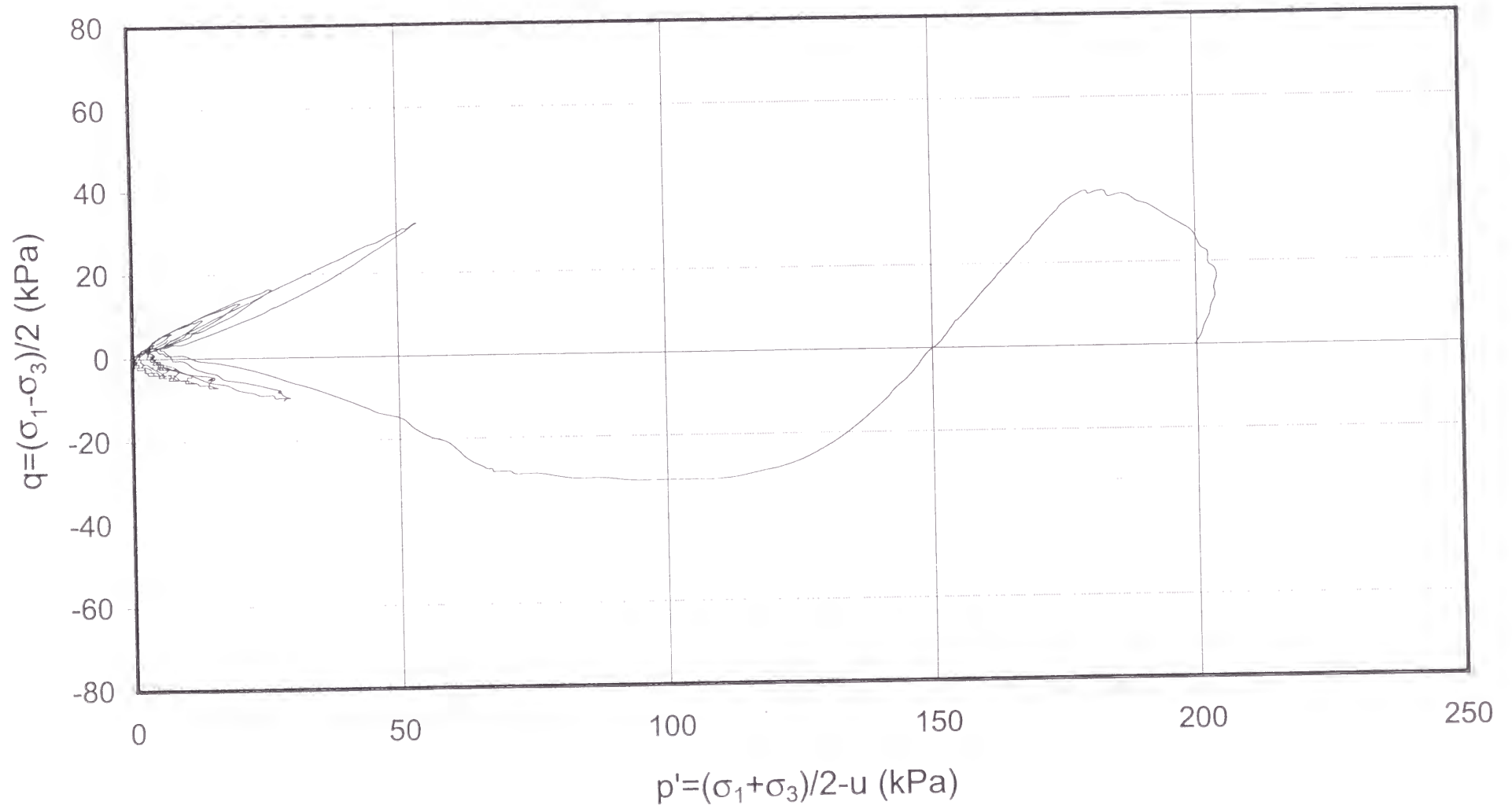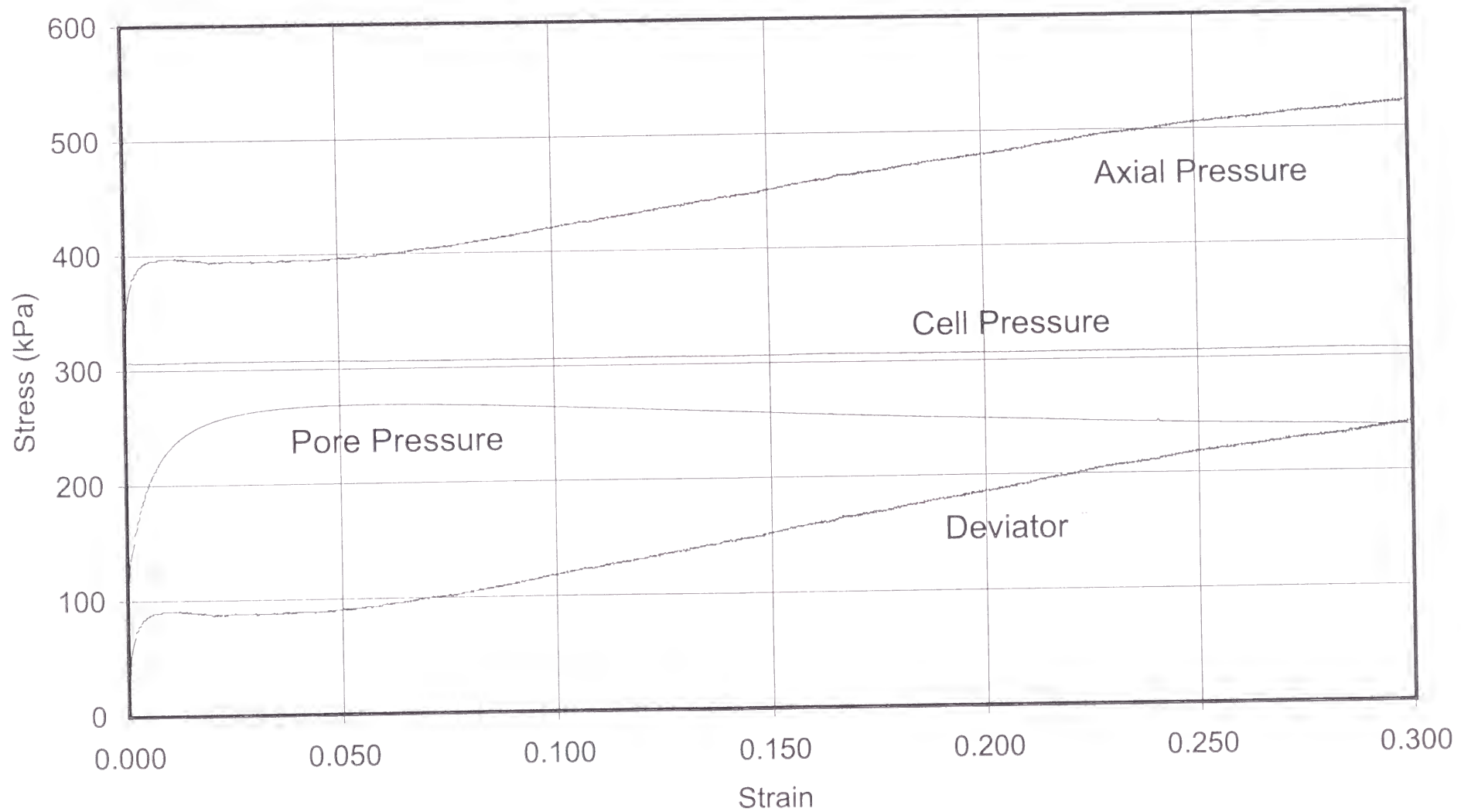

- **Plot No. 43-2**

Effective stress path.

Monotonic constant-strain-rate test.
Strain rate=0.0002 (1/sec).

Test No.43

Plot No.43-1

Y-axis: $q=(\sigma_1-\sigma_3)/2$ (kPa)

X-axis: $p'=(\sigma_1+\sigma_3)/2-u$ (kPa)

Monotonic constant-strain-rate test.
Strain rate=0.0002 (1/sec).

Test No.43

Plot No.43-2

Test No.39

Cyclic stress-controlled test. f=0.10 Hz.

Plot No.39-2
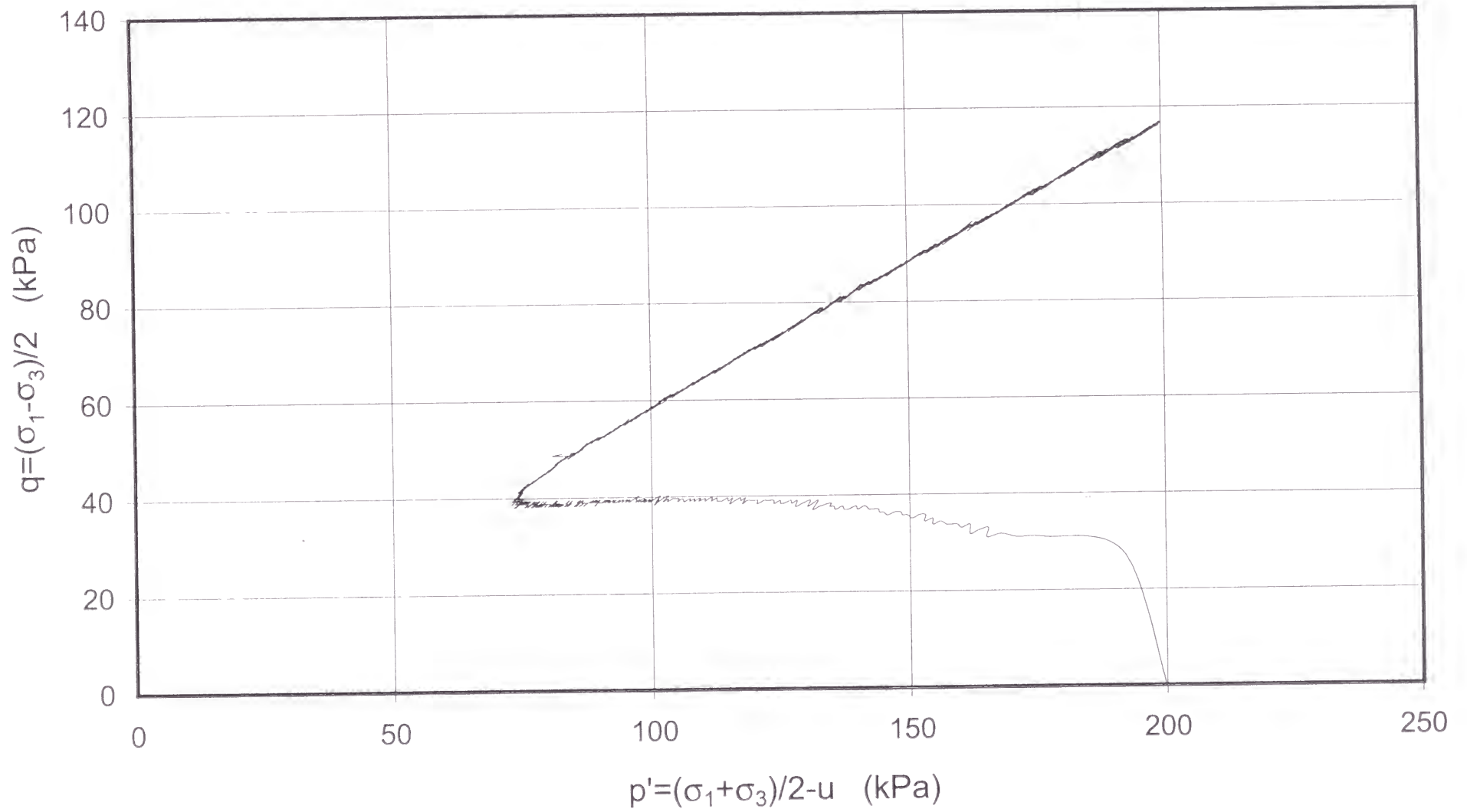
TEST No. 44

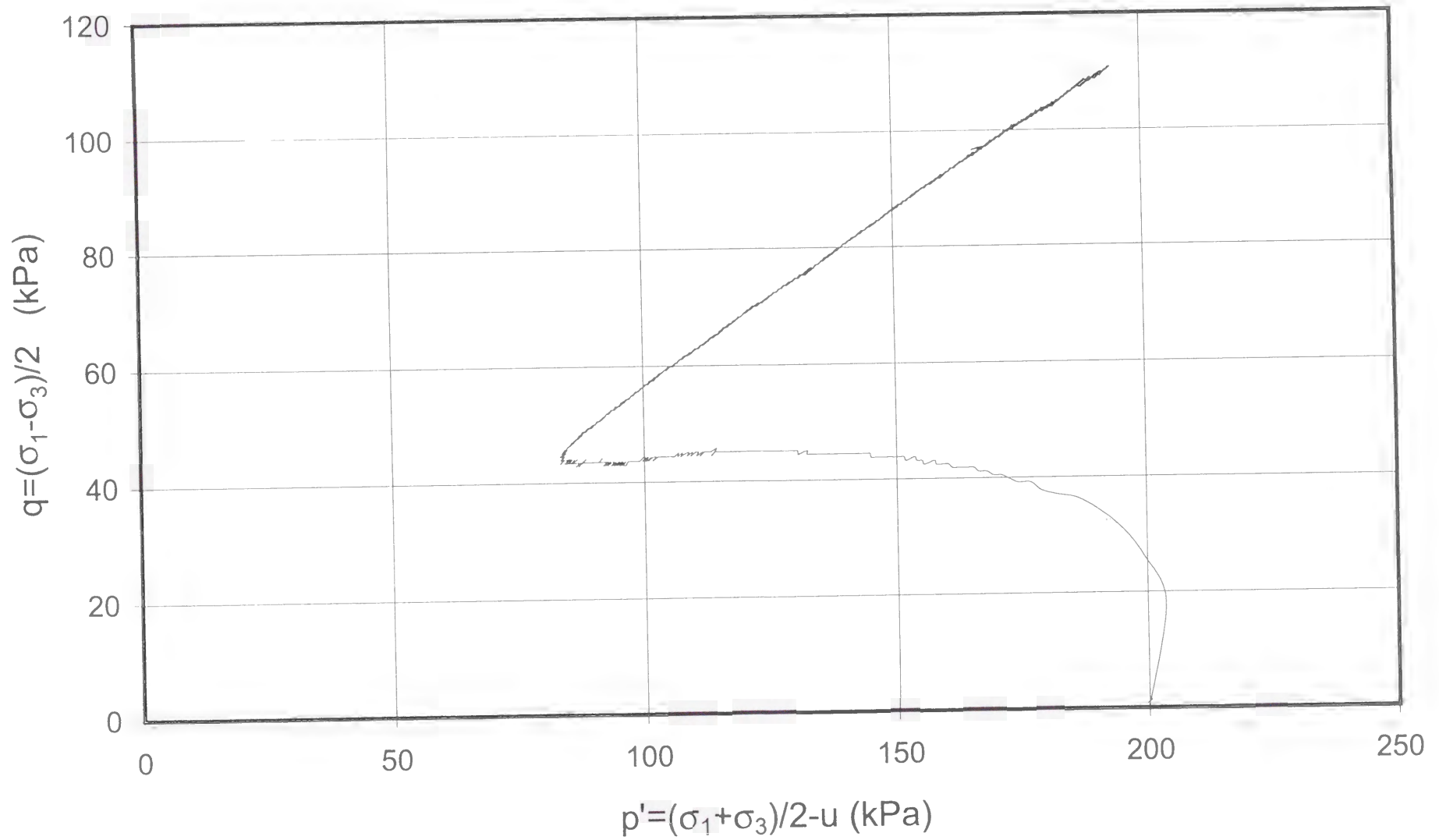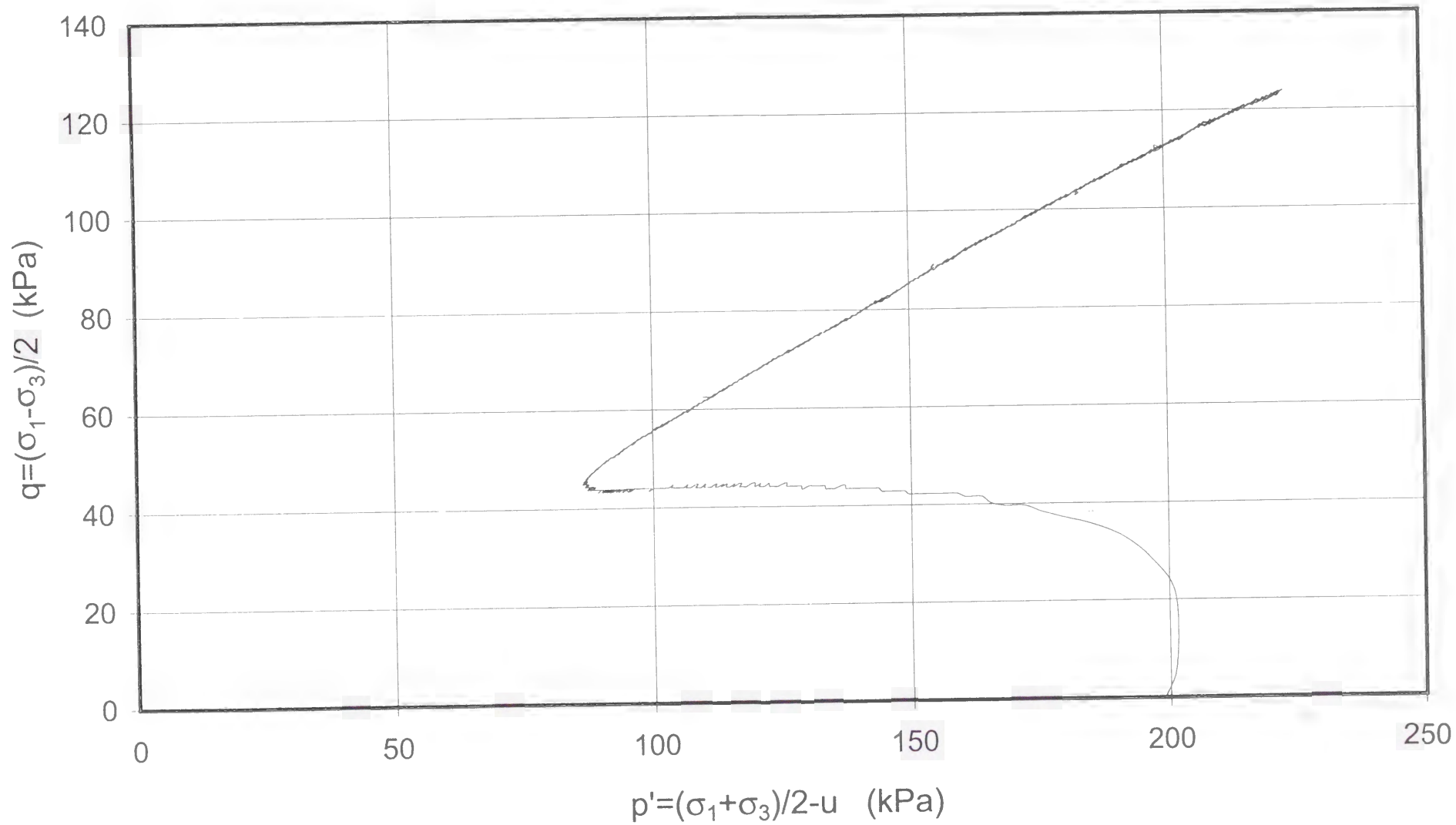| PARAMETER	UNIT	VALUE
Apparatus		Triaxial compression
Test type		Monotonic constant-strain-rate
Strain rate	1/sec	0.0010
Data acquisition rate	point/sec	10
Void ratio		0.62
Initial effective confining stress ($\sigma_{3}'_{in}$)	kPa	199
Pore pressure coefficient B		0.96
Back pressure (u_0)	kPa	107

The following plots are included:

- **Plot No. 44-1**
Strain series of series of axial pressure, cell pressure, pore pressure, and deviator stress.

- **Plot No. 44-2**
Effective stress path.

Axial Pressure

Cell Pressure

Pore Pressure

Deviator

Stress (kPa)

Strain

Monotonic constant-strain-rate test.
Strain rate=0.0010 (1/sec).

Test No.44

Plot No.44-1

Monotonic constant-strain-rate test.
Strain rate=0.0010 (1/sec).

Test No.44

Plot No.44-2

TEST No. 45

PARAMETER	UNIT	VALUE
Apparatus		Triaxial compression
Test type		Monotonic constant-strain-rate
Strain rate	1/sec	0.0020
Data acquisition rate	point/sec	20
Void ratio		0.61
Initial effective confining stress ($\sigma_3'{}_{in}$)	kPa	199
Pore pressure coefficient B		0.95
Back pressure (u_0)	kPa	107

The following plots are included:

- **Plot No. 45-1**

  Strain series of series of axial pressure, cell pressure, pore pressure, and deviator stress.

- **Plot No. 45-2**

  Effective stress path.

Cyclic constant-strain-rate test.
Strain rate=0.0020 (1/sec).

Test No.45

Plot No.45-2

Axial pressure

Cell pressure

Pore pressure

Deviator

Monotonic constant-strain-rate test.
Strain rate=0.0020 (1/sec).

Test No.45

Plot No.45-1
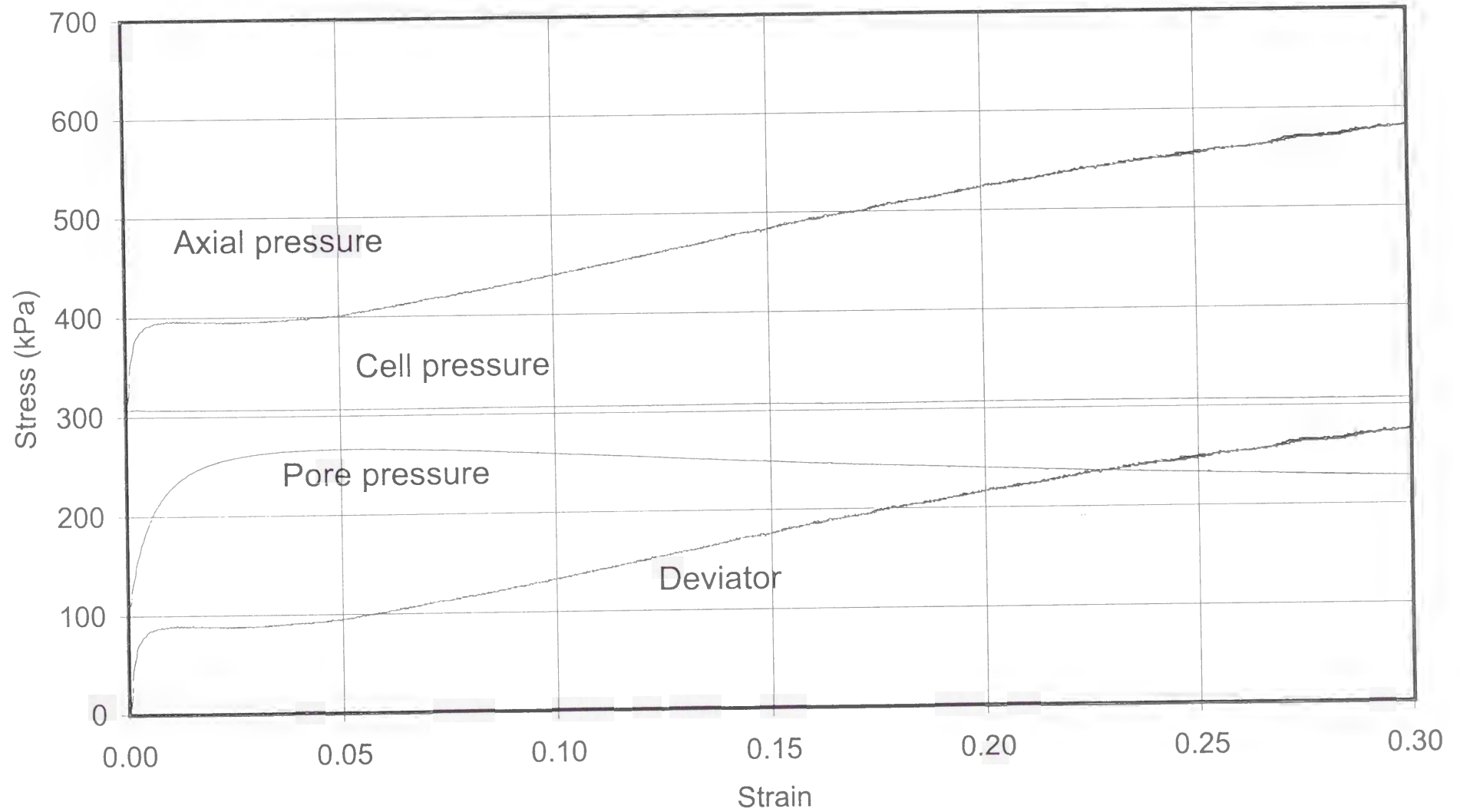
TEST No. 46

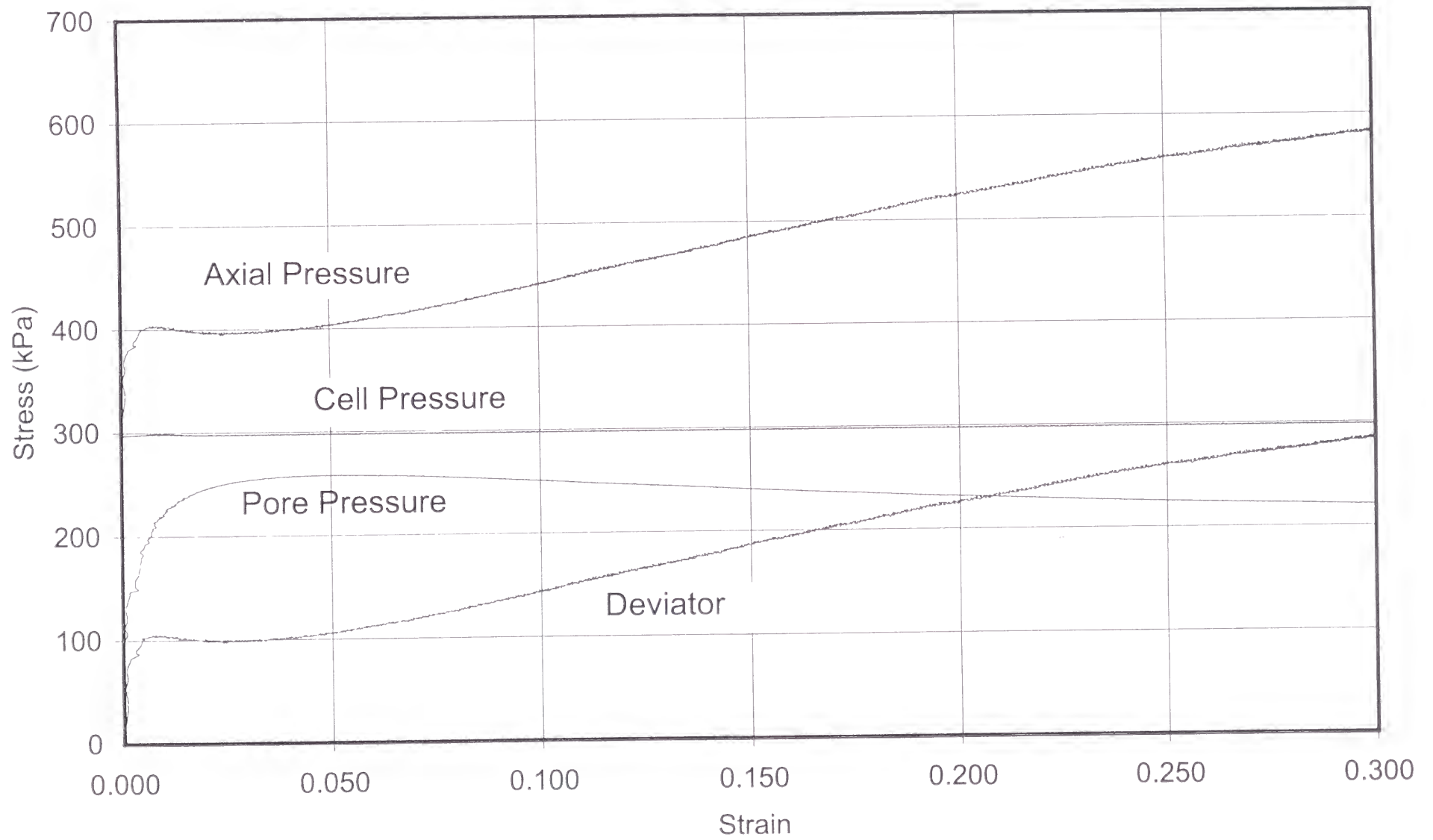| PARAMETER	UNIT	VALUE
Apparatus		Triaxial compression
Test type		Monotonic constant-strain-rate
Strain rate	l/sec	0.0102
Data acquisition rate	point/sec	100
Void ratio		0.63
Initial effective confining stress ($\sigma_3'_{in}$)	kPa	198
Pore pressure coefficient B		0.95
Back pressure (u_0)	kPa	98

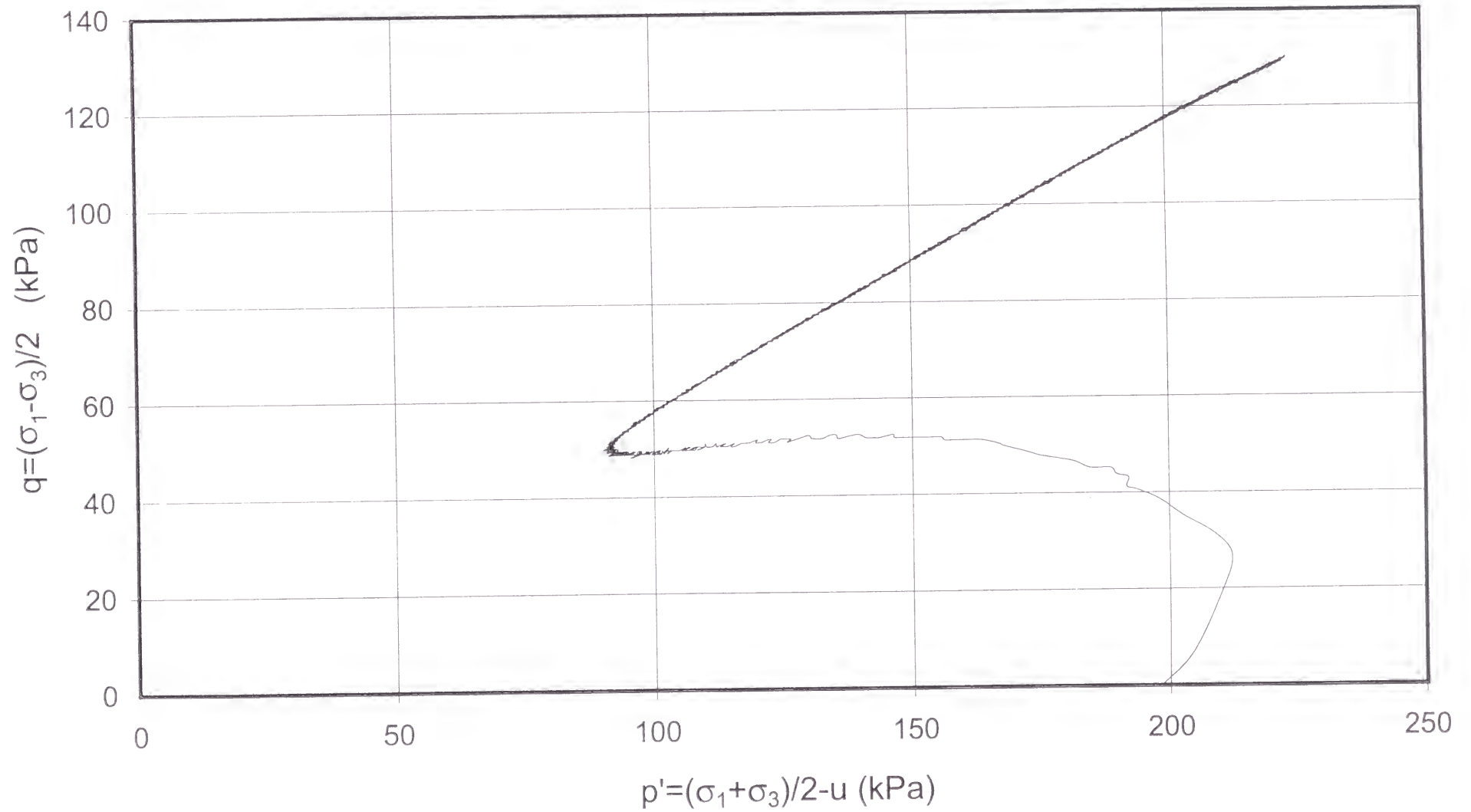The following plots are included:

- **Plot No. 46-1**
Strain series of series of axial pressure, cell pressure, pore pressure, and deviator stress.

- **Plot No. 46-2**
Effective stress path.

Monotonic constant-strain-rate test.
Strain rate=0.0102 (1/sec).

Test No.46

Cyclic constant-strain-rate test.
Strain rate=0.0102 (1/sec).

Test No.46

Plot No.46-2